DOE/MC/29248 -- 5594
(DE97002241)

Kinetic Inhibition of Natural Gas Hydrates in Offshore Drilling, Production and Processing

Annual Report
January 1 - December 31, 1994

Work Performed Under Contract No.: DE-FG21-92MC29248

For
U.S. Department of Energy
Office of Fossil Energy
Morgantown Energy Technology Center
P.O. Box 880
Morgantown, West Virginia 26507-0880

By
Center for Hydrate Research
Colorado School of Mines
Golden, Colorado 80401

Disclaimer

I. Executive Summary

Natural gas hydrates are a problem for drilling, production, and processing in cold environments. Substantial expense is incurred using thermodynamic inhibitors (such as methanol or glycol) for hydrate prevention in winter or in deep ocean operations.

In 1990 we proposed a new, kinetic means of hydrate prevention as an economical alternative to thermodynamic inhibition. We proposed to find the best kinetic inhibitors by
1. comparing rates of hydrate formation with and without kinetic inhibitors and by
2. developing a mechanism to guide selection and synthesis of kinetic inhibitors.

Seven major accomplishments for the period from January 1 - December 31, 1994 are listed below:
1. We synthesized a new type of kinetic inhibitor (e.g. poly-N-ethyl-acrylamide [PNEAM] and poly-N,N-dimethyl-acrylamide [PNNDMAM]) that has amide groups but not lactam rings.
2. We found synergistic blends of kinetic inhibitors that were effective at temperatures of 39.2°F, and pressures of 2000 psig, in combination with other kinetic inhibitors, or thermodynamic inhibitors such as salt, methanol, and monoethylene glycol.
3. We formulated a mechanism for hydrate inhibition that both explains our macroscopic data and enables a rational approach for design of inhibitors.
4. We obtained performance data for kinetic inhibitors (VC-713, PVCAP, HE-300, and PVP) on the Exxon flow loop in Houston, to determine field transferability of our laboratory data.
5. We facilitated exchange of field test information, that was reported by many member companies. We developed a model that links hydrate formation driving forces and formation rates and we analyzed field data with this model.
6. We built a visual hydrate formation/inhibition apparatus, that operates at pressures to 1,500 psig.
7. We obtained worldwide patent protection to the use of kinetic inhibitors containing lactam rings.

During 1995 we propose to do the following:
1. Finalize the mechanism for hydrate inhibition.
2. Design and synthesize inhibitors to test our mechanism.
3. Improve performance of inhibitors without salt.
4. Facilitate sharing of field and flow loop results.

During 1994, 12 member companies (Amoco, ARCO, Chevron, Conoco, DoE (U.S.), Exxon, Mobil, Oryx, Petrobras, Phillips, Statoil and Texaco) participated in the consortium, yielding a substantial leverage for each company's investment. The economics of our kinetic inhibitors was helped by a 300% increase (from $0.50 to $1.50/gallon) in the cost of methanol, the most common thermodynamic inhibitor.

II. Table of Contents

Section and Topic — Page

III. Introduction

III.A. Statement of Problem

Natural gas hydrates are crystalline materials formed of natural gas and water at elevated pressures and reduced temperatures, both above and below the ice point. Because natural gas hydrates can plug drill strings, pipelines, and process equipment, there is much effort expended to prevent their formation.

Historically four methods have been used to prevent hydragte formation:
1. Removing water, typically via contacting a hydrocarbon fluid with ethylene/diethylene/triethylene glycol or molecular sieves,
2. Increasing the system temperature above the hydrate formation point through heat exchange,
3. Reduction of the system pressure below the hydrate formation point, through pressure depletion or flaring, and
4. Injection of inhibitors such as methanol (MeOH) or mono-ethylene glycol (MEG) to shift the hydrate equilibrium, so that the system operates in the vapor-liquid region.

In deep sea operations, the ambient operating conditions (low temperature and high pressure) are very conducive to hydrate formation. In such cases, the above traditional approaches can be ineffective due to either extreme conditions or high cost. In this project, we proposed an alternate approach: to prevent plugging of flow channels by obstructing or retarding hydrate growth rate.

III.B. Goals, Objectives, and History of the Project

The goal of the project was to provide industry with more economical hydrate inhibitors. This goal was to be accomplished by the following four steps:

1. First, provide rapid screening of a large number (ca. 1000/year) of potential hydrate growth rate inhibitors.
2. Second, test the best chemicals from Step 1, in high pressure apparatuses, with simulated pipeline compositions, temperatures, and pressures.
3. Third, test those chemicals which passed inhibition conditions in Step 2 in a flow loop, at Exxon Production and Research in Houston, and
4. Finally, with cooperation of consortium member companies, field test the chemicals, and facilitate sharing of hydrate inhibition field results.

During the first 15 months of the project (9/90 -12/91) we developed a rapid screening apparatus and tested about 50

inhibitors. We also modified two high pressure apparatuses, determined their principal operating variables and established a futbaseline for comparison of experiments. Finally, using a computer, we simulated the first stages of hydrate formation as water clusters around apolar molecules.

During 1992, the second year, we tested 750 inhibitor candidates and combinations using the screening apparatus and determined transferability of screening results to the high pressure apparatuses. We applied for a chemical use patent on the two best inhibitors (PVP and HEC) with the proviso that consortium members would have royalty-free license. With the aid of computer simulation and Raman spectroscopic studies, we began to formulate a molecular inhibition mechanism. In mid-1992 Amoco, Oryx, Shell and Texaco began field tests of PVP and HEC.

In 1993 we found vastly superior inhibitors: VC-713, PVCAP, and VP/VC co-polymers, and we applied for the appropriate patents. We shifted to more stringent inhibition conditions (39.2°F and 1000 psig). We also formed two possible hypotheses for the inhibition mechanism using evidence from Raman, UV-visible spectroscopy, and molecular modeling. Having exhausted most of the commercial candidates for inhibitors, we began synthesizing inhibitors. During the 1993-94 winter almost all member companies began pilot or field tests of these chemicals.

In 1994 we proposed:
1. to define a rational approach for inhibitor design, using the most probable molecular mechanism,
2. to improve the performance of inhibitors,
3. to test inhibitors on CSM apparatuses and Exxon flow loop, and
4. to promote sharing field and flow loop results.

III.C. Organization of This Report.

This report is organized to indicate our progress on the four above-stated objectives for 1994.

- Progress in the first objective, a molecular picture of hydrate inhibition, is discussed in the following section (III.D.) because it enables comprehension of other report sections.

- Section IV.A discusses Objective 2, screening of new kinetic inhibitors and blends of inhibitors.

- The high pressure tests presented in Section IV.B indicate that the pressure range at which inhibitors can be effective has been extended and describe the limits of performance with other kinetic and thermodynamic inhibitors, addressing Objective 2 above.

• Section IV.C. presents the additional evidence determined in 1994 to support the mechanism (Objective 1) presented in III.C.

• Inhibitor test results using the Exxon Flow Loop (Objective 3) are described in Section IV.D.

• Section IV.E. describes our mathematical model that enables an analysis of the field test results to date (Objective 4).

• Section IV.F. discusses the new visual apparatus and indicates some of the results obtained with it.

• Section IV.G. indicates the current patent status of the project and provides a budget summary.

• Section V indicates work proposed for 1995 and the personnel changes necessary to accomplish these objectives.

III.D. Mechanism for Hydrate Kinetic Inhibition

While our mechanism hypothesis has progressed significantly this year, it is a logical extension of that presented in the 1993 Annual Report, to which the reader is referred for background. The 1993 report presents the basic evidence for the basic principle of cluster aggregation to hydrate masses.

Table 1 presents a summary of our current knowledge about hydrate inhibition. We have experimental evidence for each of the items in Table 1. The following mechanism accomplishes two goals. It is our best mental construct (1) to unify experimental observations, and (2) to enable more efficient experimentation.

Figure 1 **(all figures are at report's end)** depicts a mechanism for hydrate inhibition in free water. Background water molecules, which are both small and numerous, are not shown. Scattered throughout the figure are six large hydrate crystal particles, shown with pentagonal and hexagonal growth faces. Smaller hydrate particles can also be seen in the diagram.

In Figure 1, polymer strands are shown linking the larger hydrate particles, with carbon atoms represented by each vertex in the polymer backbone. Protruding from many of the polymer carbon vertices are pyrrolidone (five-membered ring) and caprolactam (seven-membered) rings (called lactam rings) that contain nitrogen (N) and carbonyl (C=O) groups. These polymer strands with protruding groups thus represent kinetic inhibitors.

The figure shows that some of the five-membered lactam rings have physically bonded (or H-bonded) to pentagonal hydrate faces, while the seven-membered lactam rings have bonded or docked to hexagonal hydrate faces. In past work we have shown that joining

hexagonal faces is an essential step in the mechanism of hydrate formation. Blocking hexagonal faces is tantamount to blocking a preferred growth site, explaining why the seven-membered caprolactam ring is one of the most effective inhibitors.

Table 1. What Do We Know About Hydrate Kinetic Inhibitors?

1. Inhibitors prevent hydrate aggregation which blocks flow channels. Inhibitors do not prevent hydrate formation. Small hydrate crystal masses form (they may be required for inhibition) - but hydrates are inhibited from growing to plug flow channels.
2. Inhibitors are effective at low concentrations (<1 wt%).
3. The best kinetic inhibitors are polymers; no low molecular weight compound has been found to be an effective inhibitor.
4. Inhibitors associate with the hydrate phase, probably through adsorption.
5. Some inhibitors alter the hydrogen bonding (H-bond) capacity of water. Yet molecules with the highest water H-bond capacity (e.g. polyvinyl alcohol and urea) are not inhibitors.
6. The best inhibitors contain an amide linkage; the nitrogen substitution pattern is influential to inhibitor performance.
7. Polymers with a caprolactam (7-member) ring are better (called primary) inhibitors, while those with a pyrrolidone (5-member) ring are labelled secondary inhibitors.
8. Blends of inhibitors can be synergistic, either performing better than either homopolymers or co-polymers of the same inhibitors. An exception is one of our best inhibitors, VC-713.
9. Inhibitor effectiveness is limited at long residence times, high pressures, and low temperatures.
10. Hydrate growth is fastest at the vapor-liquid interface; bulk growth is slow (for evidence see 1993 Annual Report pages 46-55).
11. Inhibitors cause a gel-like hydrate crystal morphology.
12. Kinetic inhibitors work best when combined with thermodynamic inhibitors like salt.
13. Performance of kinetic inhibitors varies with their concentration.
14. Mixtures of inhibitors with non-inhibitors are detrimental.
15. Polymers which increase viscosity slow growth rate.
16. Condensate and oil slow the rate of hydrate formation.

The docking phenomena occurs through both hydrogen bonding and adsorption. Docking of the polymer ring appendages to hydrate faces has two functions: (1) it serves to prevent further hydrate growth of active faces and (2) it serves to keep the polymer stabilized, or extended between hydrate crystals to form a three dimensional network.

The second function forms compartments of water between the polymer strands, so that small clusters in one compartment cannot

aggregate with clusters in other compartments. In a perturbation of Figure 1, it is not necessary to link the polymer strands; rather the strands sterically inhibit linking of hydrate particles, just as protrusions from two balls keep the balls from colliding.

When salt is placed in the solution, dissolved ions keep the polymer strands (and associated rings) dispersed. Similarly when blends of fairly soluble (e.g. five membered ring polymers like polyvinyl-pyrrolidone) polymer inhibitors are dissolved in the solution with fairly insoluble polymers (e.g. polyvinyl-caprolactam), the Hildebrand principle of "like-dissolves-like" suggests that the pyrrolidone rings keep the caprolactam rings dissolved and available for attachment to hydrate hexagonal faces.

From another perspective, the hydrate particles act as the "glue" to join the three dimensional network of polymeric inhibitors. Without the initial hydrate particles, the polymers would not be as dispersed and therefore less effective. Conversely, without the initial hydrate particles, there would be no need for inhibitors.

The inhibitors found in 1994 have a similar mechanism to that shown in Figure 1. The difference for the new inhibitors is that, while they have no ring structures, they still have the polymeric backbone and an pendant amide group. The nitrogen and the carbonyl in the amide group provide the means for polymer appendage to hydrogen bond on the hydrate face.

With the above overview of the modified mechanism (proposed in 1994) for hydrate kinetic inhibition, we now turn to a description of other 1994 accomplishments. The new experimental apparatuses, experiments, and the theoretical background determine the progress made on this project. First we consider the chemicals tested, leading to the kinetic inhibitors found, together with the evidence for the mechanism proposed above.

IV. What Was Accomplished in 1994

Our results in 1994 are discussed in the following sections:

IV.A. Screening to Find New Kinetic Inhibitors
IV.B. Pressure Limits to Inhibitor Performance, With and Without other Kinetic/Thermodynamic inhibitors (e.g. salt)
IV.C. Other Evidence to Support the Mechanism
IV.D. Exxon Flow Loop Experiments
IV.E. Field Results and an Analysis
IV.F. A New Visual Apparatus and Control System
IV.G. Patent Status and Budget Summary.

IV.A. Screening to Find New Kinetic Inhibitors

Here we present evidence for the following conclusions:

1. New polymers were synthesized and determined to be good hydrate inhibitors. These represent a new type of inhibitor.
2. Many readily available commercial polymers have been screened.

3. About ten homopolymers and five copolymers that were not commercially available were synthesized and tested.
4. Only polymers with amide groups are good inhibitors.
5. Some single polymers can inhibit, while others inhibit only when blended with another inhibitor.

We classify inhibitors as outstanding (primary) or good (secondary), with chemical structures presented in Figure 2.

Primary Inhibitors:

These chemicals include two lactam polymers reported in the 1993 annual report (VC-713 and PVCAP) and two non-lactam polymers discovered this year (poly(N-Ethyl Acrylamide) or PNEAM and poly(N,N-Dimethylacrylamide) or PNNDMAM).

Secondary Inhibitors:

These chemicals, also depicted in Figure 2, are comprised of the previously reported (1992) lactam polymer (PVP), and two non-lactam polymers containing amide groups, Poly(2-ethyl oxazoline) (P2E2OX), and poly(N-methyl-N-vinylacetamide) (PNMNVAcAM).

Blends of many non-inhibitors (those with no amide linkages) with primary inhibitors (PVCAP, VC-713) show no improved performance. However, blends of some secondary inhibitors (e.g. PVP, Poly(2-ethyl oxazoline) (P2E2OX)) with primary inhibitors (e.g. PVCAP, VC-713) show synergistically improved performance.

This section of the report is organized as follows:

IV.A.1. Screening Apparatus and Technique
IV.A.2. Chemicals Tested as Inhibitors and Results
IV.A.3. Single Polymers and Blends versus Co-Polymers

IV.A.1. Screening Apparatus and Technique. Several chemicals were tested as hydrate inhibitors in a THF-hydrate screening apparatus. Polymers which showed promising results in the THF-hydrate screening apparatus were tested in the high pressure apparatus described in Section IV.B.

The purpose of the screening apparatus was to quickly test potential hydrate inhibitors. Rapid screening was made possible by the use of tetrahydrofuran (THF), a miscible hydrate former, rather than an immiscible former such as natural gas, which can cause mass transfer and surface renewal difficulties. THF is the saturated four carbon member of the furan family. With THF, hydrate formation occurred at 4°C from a solution that was 20

weight% THF in water. At that concentration and temperature without inhibitor, all of an inhibited solution became hydrate, and the THF molecule occupied only the large cages of sII hydrate.

The screening apparatus shown in Figure 3, consisted of a motor driven rack that rotates at 15rpm. The rack held a maximum of 12 test tubes. Each test tube was charged with 6 ml of inhibitor test solution and 2 ml of THF. This provided about 20wt% THF in the solution, fulfilling the criteria of a molar ratio of 17:1 (water:THF) for hydrate formation. Mixing was achieved using a 3/8 inch 440 stainless steel ball. This type of ball also provided the best material for hydrate initiation as was found in a series of experiments reported in the 1991 annual report.

At the start of an experiment, the test tube rack was submersed in an insulated water bath that was maintained at a constant experimental temperature of 0°C. Two time-dependent measurements were made from the experiment. The start of both measurements began at the placement of the test tube rack in the constant temperature bath and the start of rotation.

The induction time (IT) is defined as the time when hydrate crystals were first visually observed in the test tube. The ball stop time (BST) is defined as the time from the start of the experiment to either the time (1) when the ball either could no longer move through the test solution, (2) when it could only move through a few centimeters in the test solution, or (3) when it moved only through a small empty pocket where there was no longer any solution. BST may be analogous to the time of pluggage in a pipeline.

Test solutions were made from a combination of chemical inhibitor solution and a sea salt solution. First, 200 grams of 5wt% concentrated solution of inhibitor was made in deionized water. Sea salt solution was also made at 5wt% concentration from ASTM synthetic sea salt and deionized water. The sea salt solution was mixed for approximately 4 hours then filtered through a 0.45 micron filter.

To make the standard inhibitor solution, the proper amount of the above 5 wt% inhibitor solution was mixed with the proper amount of 5wt% sea salt solution. Standard inhibitor concentrations were 0.5wt% inhibitor with 3.5wt% sea salt, containing 1.0 wt% methanol (methanol was present in the original inhibitor solution received from the vendor). For polymer blends, 0.25 wt% polymer and 0.125 or 0.25 wt% (PVCAP or VC-713) in 3.50 wt% SW containing 1.0 wt% methanol were used.

We used the absence of an induction time (IT) in the THF hydrate experiments as a criterion for further testing in high

pressure gas hydrate experiments. This criterion was chosen because the polymers with an absence of IT over 15 hours did not form a significant amount of hydrates in the high pressure apparatus. Experiments with polymers with no IT consumed about 0.1 mole of gas over 20 hours (PVCAP, VC-713, PNEAM, and blends) in the high pressure apparatus (Section IV.B.) at 1000 psi and 39.2°F in 3.50 wt% SW. On the other hand, polymers that had an IT of about 30 minutes had a much higher gas consumption in the high pressure experiments.

Table 2 provides a good comparison of screening and high pressure apparatus results as evidence for confidence in the screening apparatus. While the screening apparatus provided a valuable means to determine the good inhibitor performance in the high pressure apparatus, two new polymers (PNEAM and PNNDMAM) were exceptions, as indicated in the final two entries of Table 2. These exceptions (the only two of almost 1500 chemicals tested) suggested that the results from the screening apparatus, are only a good heuristic to predict results in the high pressure apparatus; the screening results are not absolute predicters.

Using 1.0 wt% methanol for the THF-hydrate screening experiments was justified by the results in Table 3. Data in Table 3 indicate than PNEAM and poly(N-methyl-N-vinylacetamide) would have been judged to be non-inhibitors if methanol was not used. The data in Table 3 also indicate that methanol is more than a thermodynamic inhibitor; it may synergistically improve performance of some inhibitors.

IV.A.2. Chemicals Tested as Inhibitors and Results. We tested a variety of chemicals, listed in Table 4, as potential inhibitors in 1994. Only the first three types (substituted poly(acrylamides), Poly(oxazolines) and poly(N-alkyl-N-vinyl amides)) are good hydrate inhibitors.

Appendix A (at the conclusion of this report) provides a listing of all chemical structures and the Table of Appendix A provides proper names of chemicals, sources, and performance ratings.

Table 2: Comparison of hydrate inhibition performances in THF-hydrate screening experiments and gas hydrate experiments at 39.2°F and 1000 psi[a].

Polymer[a]	Concentration (wt%) polymer/CH_3OH	Induction Time (min)	Ball Stop Time (min)	Gas consumption (mole, min)
PVCAP	0.50/2.0	> 24 hours	> 24 hours	~0.15, 1200
VC-713	0.50/0.8	> 24 hours	> 24 hours	~0.05, 1200
PNEAM	0.50/2.0	> 24 hours	> 24 hours	~0.12, 1200
PNEAM	0.50/0	6±3	< 40	~0.12, 1200
PVCAP	0.25/1.0	-	> 24 hours	-
VC-713	0.25/1.0	-	> 24 hours	-
PNEAM	0.50/1.0	>24 hrs	>24 hrs	-
PNNDMAM	0.50/1.0	3±2	~15	~0.15
P2E2OX	0.50/1.0	33±7	> 24 hours	~0.4, 400
HE-300	0.50/1.0	6±3	> 24 hours	~0.6, 400

[a]Structures of polymers are shown in the appendix.

Table 3: Control experiments for THF-hydrate screening of chemicals in 3.50 wt% sea water.

Polymer[a]	Concentration (wt%) polymer/methanol	Induction Time (IT, min)	Ball Stop Time (BST, min)
none	0/2.0	10±8	< 1 hour ~1cm plug in one end; ball movement is slow
none	0/1.0	4±2	< 1 hour ~ 1cm plug in both ends; ball movement is very slow
PNEAM (Mn ~30K, calc)	0.50/0	6±3	< 40
PNEAM	0.50/1.0	> 24 hours	> 24 hours
PVCAP	0.50/1.0	> 24 hours	> 24 hours
VC-713	0.50/1.0	> 24 hours	> 24 hours
PNMNVAcAM (Mn~40K, calc)	0.50/0	6±3	17±10
PNMNVAcAM	0.50/1.0	23±17	> 24 hours
PVCAP	0.125/1.0	3±2	> 18 hours (ends are plugged in 2 hours)
PNMNVAcAM/PVCAP	(0.25/0.125)/1.0	> 24 hours	> 24 hours
VC-300[b]/PVCAP	(0.25/0.125)/1.0	6±2	11±3

[a]Structures of polymers are shown in Appendix A.
[b]Caprolactam version of HE-300.

Table 4. List of Chemicals Tested in 1994

The polymers tested can be classified into the following families:

1. Substituted poly(acrylamides)
2. Poly(oxazolines)
3. Poly(N-alkyl-N-vinyl amides)
4. Polypeptides
5. Alcohols
   - Poly(vinyl alcohol)
   - Sulfonated lignin (a phenolic derivative)
6. Amines
   - Poly(ethyleneimine)-80% ethoxylated
7. Poly(vinylimidazoles) and thiazoles)
8. Epoxides
   - Poly(ethylene oxide), poly(propylene glycol, and
   - Ethylene oxide-propylene oxide-ethylene oxide tri-block copolymer (F127)
9. Polyelectrolyte
   - Poly(4-sodium styrene sulfonate)
   - Poly(diallyldimethylammonium) chloride.
10. Carbohydrates
    - Cellulose acrylamide
    - Carrageenan-contains ions-becomes gel in presence of SW.
    - Argarose- very poor water solubility
    - Chitin (a cellulosic amine, insoluble in water-not tested)
    - Chitosan (cellulosic amide, insoluble in water-not tested)

==========

In the below sections we detail the performance of the first four types of chemicals listed in Table 4. We only discuss the other types (non-inhibitors) briefly in Section IV.A.2.c due to space restrictions in this report. It should be noted that many of these chemicals had to be synthesized; those synthesized are indicated by the label "Panch" as the Source in Appendix A.

IV.A.2.a. Substituted Poly(acrylamides) Screening results for a series of poly(acrylamides) are shown in Table 5. Based on these results, the simple poly(acrylamide) which had a BST of < 30 minutes is not an inhibitor. However, poly(N-ethyl acrylamide) (PNEAM), poly(N-methyl acrylamide) (PNMAM) and poly(N,N-diethylacrylamide) (PNNDEAM) possess some inhibition efficiency as shown by the absence of BST.

It should be noted that poly(N,N-dimethylacrylamide) (PNNDMAM) show an initial BST of ~15 minutes, and thus would not be indicated as a good inhibitor - this is one of the first cases in which the screening apparatus did not give reliable predictions of performance in the high pressure apparatus.

The high pressure performance for these four acrylamide polymers are shown in Figure 4 along with PVCAP and VC-713 at 1000

psi and 39.2°F. Using predictions from the THF screening apparatus, the high pressure performance should have been PNEAM > PNMAM > PNNDEAM > PNNDMAM (read > as "better inhibition than"). However, the actual high pressure apparatus performance was PNEAM > PNNDMAM > PNMAM > PNNDEAM, a slightly different order than predicted by the screening apparatus.

Table 5: THF-hydrate screening results of polyacrylamide derivatves in 3.50 wt% sea water (polymer = 0.50 wt%, methanol = 1.0 wt%)

Polymer[a]	Induction Time (IT, min)	Ball Stop Time (BST, min)
Poly(acrylamide)	8±3	< 30
Poly(N-ethyl acrylamide)	> 48 hours	> 48 hours
Poly(N,N-diethylacrylamide)	3±2	> 19 hours
Poly(N-methyl acrylamide)	> 4 hours	> 19 hours
Poly(N,N-dimethylacrylamide)	3±2	~ 15[b]
Poly(N-isopropyl acrylamide)	Polymer precipitate by the addition of THF[c]	-
Poly(N-tertiary-butylacrylamide)	Polymer is insoluble in water	-
Poly(2-acrylamido glycolic acid)-sodium salt	Gel formation during polymerization; cannot be redissolved in water	-

[a]Structures of polymers are shown in Appendix A.

[b]test tube ends were plugged. After standing overnight the balls began moving freely.

[c]A 0.25/0.25 wt% blend with PVCAP shows comparable performance to 0.50 wt% PVCAP.

THF-hydrate screening tests for poly(N-isopropyl acrylamide) (PNIPAM) were not performed due to cloudiness that appeared when THF waus added to the aqueous polymer solution. We have previously attributed the good hydrate inhibition performance of PVCAP and VC-713 to their lower cloud point temperatures (LCST). Because of a lower LCST of 32°C for PNIPAM (comparable to VC-713), we tested PNIPAM in the high pressure at 1000 psi and 39.2°F using 0.50 wt% polymer in 3.50 wt% SW. The solution consumed ~0.5 mole of gas in < 300 minutes. However, a blend of PNIPAM with PVCAP in a 0.25/0.25 wt% ratio showed comparable performance to 0.50 wt% PVCAP (~0.15 mole gas in 1200 minutes).

The poly(tertiary butyl acrylamide) and poly(methacrylamide) were insoluble in water. Synthesis of poly(2-acrylamidoglycolic acid) and its sodium salt resulted in gel formation. The gel was not soluble in water so that hydrate inhibition tests could not be performed.

IV.A.2.b. Poly(oxazolines), poly(N-alkyl-N-vinyl amides), polypeptides: THF-hydrate screening results of some other polymers containing amide linkages are shown in Table 6. Poly(2-ethyl-2-oxazoline) (P2E2OX) and poly(N-methyl-N-vinylacetamide) showed an IT but no BST over 24 hours. Based on these observations these two polymers have some inhibition potential. On the other hand, poly(sodium-glutamate), a polypeptide, showed a short IT of 3±2 minutes and a BST of less than 20 minutes; therefore it was not listed as an individual inhibitor.

Table 6: THF-hydrate screening results of other polymers containing amide linkages in 3.50 wt% sea water.(polymer= 0.50wt%, methanol = 1.0 wt%)

Polymer[a]	Induction Time (IT, min)	Ball Stop Time (BST, min)
Poly(2-ethyl-2-oxazoline) (P2E2OX, MW= 500K)	33±7	> 24 hours
Poly(N-methyl-N-vinylacetamide)	23±17 (MW ~40K, calc) 3±2 (MW ~20K, calc)	> 24 hours
Poly(sodium-glutamate)	2±1	< 20 min. ~2 cm plug in one end of tubes
Cellulose acrylamide	3±2	< 20 min. ~2 cm plug in both ends of tubes

[a]Structures of polymers are shown in the appendix.

IV.A.2.c. Polymers with no amide linkages:

Screening results of poly(vinyl alcohol), poly(4-sodium styrene sulfonate), poly(ethyleneimine)-80% ethoxylated, poly(N-vinylimidazole, poly(diallyldimethylammonium) chloride, and lignin sulfate are shown in Table 7. All these polymers showed short IT's and BST's of less than 30 minutes. Accordingly all these polymers are not inhibitors. Inhibition tests for poly(4-methyl-5-vinylthiazole) and poly(propylene glycol) were not carried out because they are insoluble in water or form cloudiness in sea water.

Table 7: THF-hydrate screening results of other non-amide type polymers in 3.5 wt% sea water (polymer=0.50 wt%, methanol=1.0wt%).

Polymer[a]	Induction Time (IT, min)	Ball Stop Time (BST, min)
Poly(vinyl alcohol)	~5	< 30
Poly(styrene sulfonate) sodium salt	~5	< 30
Poly(ethyleneimine)-80% ethoxylated	~5	<30
Poly(N-vinylimidazole)	2±1	< 20 min. ~ 1 cm plug in one end of tubes
Poly(4-methyl-5-vinyl thiazole)	polymer is not soluble in water	-
Poly(ethylene oxide)	3±1	< 25 min. ~2 cm plug in both ends of tubes
Poly(propylene glycol)	polymer becomes cloudy in salt solutions	-
Poly(diallyldimethyl ammonium chloride)	3±1	< 20
Poly(4-pyridine-N-oxide)	3±1	< 20
Lignin sulfate (a phenolic polymer)	~5	<30

[a]Structures of polymers are shown in the appendix.

IV.A.3. Single Polymers and Blends versus Co-polymers

THF-hydrate screening results of some polymers which had an IT but no BST [PVP, P2E2OX, poly(N-methyl-N-vinylacetamide) (PNMNVAcAM), PNNDEAM, and HE-300] were blended with PVCAP, VC-713, or PNEAM. The results are shown in Table 8. The results in Table 8 indicate that these blends should perform well in the high pressure experiments. The blends of P2E2OX/PVCAP, PVP/PVCAP, HE-300/PVCAP have been tested in the high pressure reactor at 1000 psi and 39.2°F and they have shown performance comparable to 0.50 wt% PVCAP under similar conditions. The other blends will be tested in the near future. The blend compositions have not yet been optimized, yet as will be seen in the high pressure results section (IV.B.) blends seem to work better than co-polymers of the same two components.

Polymer blending studies of some chemicals which showed a ball stop time in the THF-hydrate screening experiments were also tested by blending with PVCAP or VC-713. These tests were performed to check whether the inhibition performance of these chemicals can be improved by blending with PVCAP or VC-713. Unfortunately, the results in Table 9 clearly indicate that there is no performance enhancement for any of these polymer systems.

Table 8: THF-hydrate screening results of some blends[a] in 3.50 wt sea water containing 1.0 wt% methanol.

Polymer[b]	concentration (wt%)	Induction Time (IT, min)	Ball Stop Time (BST, min)
Poly(2-ethyl-2-oxazoline) (P2E2OX)/PVCAP	0.25/0.125	> 24 hours	> 24 hours
Poly(N-methyl-N-vinylacetamide)/ PVCAP	0.25/0.125	> 24 hours	> 24 hours
PVP-K30/PVCAP	0.25/0.25	> 24 hours	> 24 hours
PVP-K30/Poly(N-ethyl acrylamide) (PNEAM)	0.25/0.25	> 24 hours	> 24 hours
P2E2OX/PNEAM	0.25/0.25	> 24 hours	> 24 hours
PVCAP/HE-300	0.25/0.25	> 24 hours	> 24 hours
Poly(N,N-diethylacrylamide)/ PVCAP	0.25/0.25	> 24 hours	> 24 hours

[a]When tested alone, the polymers used in this blending studies had an IT and no BST.
[b]Structures of polymers are shown in the appendix.

Table 9: THF-hydrate screening results of some other polymer[a] blends in 3.50 wt% sea water containing 1.0 wt% methanol.

Polymer[b]	concentration (wt%/wt%)	Induction Time (IT, min)	Ball Stop Time (BST, min)
Poly (Nvinylimidazole /PVCAP	0.25/0.125	16±7	< 1 hour
Poly(N-vinylimidazole)/ VC-713	0.25/0.125	12±5	< 1 hour
Poly(sodium glutamate)/ PVCAP	0.25/0.125	16±13	< 1 hour
Poly(diallyl dimethyl ammonium chloride)/PVCAP	0.25/0.125	40±21	49±21
Poly(diallyl dimethyl ammonium chloride)/ VC-713	0.25/0.125	9±2	> 1 hour
VC-300/PVCAP	0.25/0.125	6±2	11±3
F127/PVCAP	0.25/0.125	28±18	< 3 hours
Poly(acrylamide)/ PVCAP	0.50/0.125	4±1	> 1 hour
Poly(acrylamide)/ VC-713	0.50/0.125	9±7	17±13

IV.B. High Pressure Limits to Inhibitor Performance

In this section of the report, we present experimental evidence for three categories of conclusions and recommendations relating to polymer performance: I. new polymers, II. limits to polymer performance blended with other polymers and with thermodynamic inhibitors, and III. experimental modifications for best inhibitor evaluation.

I. New Polymers Found

A. Two non-lactam polymers (PNEAM and PNNDMAM) provided comparable inhibition to VC-713, and better than copolymers of VC/VP.

II. Limits to Polymer Performance (Recommendations for Usage)

A. Blending Polymers for High Pressure Performance

1. At 1000 psig, 39.2°F, and 3.5wt% salt, use 0.5wt% polymer, (PVCAP or VC-713 with either PVP or a new non-lactam polymer PNEAM or PNNDMAM).
2. At 1500 psig, 39.2°F, and 3.5wt% salt, use 0.75% total polymer (0.5% PVCAP blended with 0.25% PVP(K-17))
3. At 2000 psig, 39.2°F, and 3.5wt% salt, use 1.0wt% total polymer, (either a blend of 0.5% VC-713 with 0.5% PNEAM, or a blend of 0.75% PVCAP with 0.25% HE-300 .

B. Blending Polymers with Thermodynamic Inhibitors

1. At 1000 psig and 39.2°F, use 3.5% salt rather than methanol with 0.5wt% VC-713
2. At 1500 psig and 39.2°F, use 3.5% salt with >10wt% methanol and 0.5wt% VC-713
3. At 2000 psig and 39.2°F, use 3.5% salt and either:
   a. 0.5% VC-713 or PVCAP with 15wt% methanol
   b. 0.75% VC-713 or PVCAP+PVP with 15% MEG
   c. 0.75% Blend of PVCAP+PVP with 15% MEG
4. With De-Ionized Water (no salt) at 39.2°F
   a. At 1000 psig use 0.75% VC-713 or PVCAP+PVP
   b. At 2000 psig use 18.5% MeOH + 0.5 % VC-713
   c. At 2000 psig use 20% MEG + 0.75% PVCAP+PVP

C. Changing Characteristics within a Polymer Type

1. Use low MW PVCAP rather than high MW at 1000 psig, 39.2°F, and 3.5wt% salt
2. Use fresh, non-hydrolyzed PVCAP at 39.2°F at 1000 psig and 1500 psig for best performance.

III. Experimental Modifications for Best Inhibitor Evaluation

A. In our reactor, use any number of Balls with 60 g water.
B. Raising the temperature above the cloud point before redissolving the polymer does not affect performance when the polymer returns to solution.
C. While gas consumption is affected by various thermodynamic inhibitors, gas solubility alone cannot explain inhibition kinetics.

The remainder of section IV.B provides evidence for the above conclusions.

IV.B.1. Apparatus and Procedure

A schematic diagram of the High Pressure Apparatus is presented in Figure 5. The principle components of the apparatus are listed below.

1. An isothermal water bath surrounded the reactor. The temperature control of the water bath was to within 0.1°F.

2. A 300cc Autoclave reactor, with a magnetically-driven mixer rotated at 1000 rpm by a external motor.
3. A high pressure supply reservoir used to supply gas to the reactor as gas was consumed in the reactor due to the hydrate formation. Thus it was possible to run the experiments at isobaric conditions (pressure is maintained ±100 psi of the set pressure).
4. A Heise dial pressure gauge allowed pressure monitoring in the reactor.
5. A computer data acquisition system recorded the data and controls the experiment. The system was composed of a KEITHLEY Series 500 Data Acquisition System, connected to an IBM XT computer. The data recorded by the data acquisition system was temperature in the reactor, water bath temperature, high pressure reservoir temperature, high pressure reservoir pressure, and pressure in the reactor. All data were recorded in the computer for later analysis.

Data were analyzed using a computer program for gas consumption from the reservoir. The gas consumption program used the Peng-Robinson Equation of State to calculate z factors.

Operating Procedure

1. Cleaning Procedure
   a. The Autoclave reactor was disassembled and thoroughly cleaned several times with tap water.
   b. In order to eliminate any residue left from the previous run, the reactor was washed with methanol with the aid of an air driven motor for a period of about 15 minutes.
   c. After the methanol wash was completed, the reactor was rinsed several times with tap water followed by deionized water rinse.
   d. The excess water was blown from the reactor with high pressure air, and finally the reactor was well dried with Kimwipes.

2. Preparation of Test Solutions and Gases
   a. Fresh test solutions (no more than two days old) were always used in the high pressure experiments.
   b. According to the specification of the experiment, the solution make-up was as follows:
      * Concentrated solutions of the chemicals (VC-713 in 37% ethanol; PVCAP in 50% ethanol; all other polymers were in methanol) were made by dissolving the chemical in methanol, making a 20 wt% solution.
      * The concentrated (20 wt% in alcohol) solution, sea water (5 wt% salinity), and deionized water were mixed to make the final test solution.
      * Care was taken that the solution was clear and no particles are observed in solution.

c. In contrast with the THF used in screening apparatus, a synthetic gas mixture is used to form the hydrates in the high pressure apparatus. A synthetic Green Canyon Gas mixture was purchased from Matheson Gas Products, of the composition: Methane (87.2 mole%), Ethane (7.6%), Propane (3.1%), n-Butane (0.8%), i-Butane (0.5%), n-Pentane (0.2%), i-Pentane (0.2%), Nitrogen (0.4%).

3. Sealing

a. An Appropriate amount of the test solution was weighed in a beaker. For most of the kinetic and thermodynamic experiments, the amount of solution used was 120 grams. However, late in the year, translating results from Amoco experiments, we determined that using 60 grams of water decreased the experimental time required for hydrates to form, perhaps due to better mixing.
b. Sixty nine (69) stainless steel balls were placed in the reactor to provide good mixing and increase the surface area for hydrate formation
c. The weighed test solution and condensate were poured into the reactor and the reactor is sealed.

4. Start-up

a. Once sealed, the reactor was immersed in the water bath and the mixer turned on to provide faster heat transfer in bringing the solution in the reactor to thermal equilibrium with the water bath.
b. The data acquisition system was started.
c. After about 10 minutes, the mixer was turned off, and after 5 minutes the reactor was charged to operating pressure.
d. Before charging the reactor, the reactor was flushed with gas several times to eliminate the air initially present.
e. Once the reactor was charged to the operating pressure, the system was connected to the high pressure supply reservoir.
f. After the reactor reached thermal equilibrium with the water bath, all the conditions were recorded at the moment and the mixer turned on. Gas consumption measurements began from this time.

5. Running

a. The progress of the experiment is monitored every few hours for any unusual phenomena.
b. The experiment is continued for 20-22 hours.

IV.B.2. High Pressure Experimental Results

With the above apparatus and experimental procedure, we were able to measure hydrate inhibition performance of "possible kinetic inhibitors" found in the screening apparatus. The two high pressure apparatuses run continuously.

Since hydrates act to concentrate the gas inside the hydrate phase, the amount of hydrate formed was a direct function of the gas consumed in order to keep the reactor at constant pressure. Good hydrate inhibition was normally taken as a gas consumption of approximately 0.1 gmole of Green Canyon gas at 1200 minutes.

Recommendations on How to Read Section IV.B.2.

During 1994 we completed about 350 high pressure tests of about 22 hours in duration each. Due to this high volume of data, we were only able to recommend chemical inhibitor(s) for various temperature, pressure, salinity, etc. applications.

During the first quarter of 1995 (mailed prior to our March 9-10, 1995 Consortium meeting) we will send each member company a synopsis of data interpretation from both operational and mechanistic viewpoints. The review of this synopsis will be a significant portion of our March meeting.

For the present, the sheer volume of data is a overwhelming to a person with limited time to read and digest. A reader may choose to review the below summary and then to consider only the data which apply to the conclusion of immediate interest. An overview of the results from the high pressure apparatus is given below, followed by the data from the runs:

a. Sixty (60) tests were performed on 0.5wt% of new polymers at 1000 psig and 39.2°F with 3.5wt% salt:

1. Two non-lactam polymers (PNEAM and PNNDMAM) provided comparable inhibition to VC-713, and better than copolymers of VC/VP as shown in Figures 6 and 7.
2. Increasing the amount of PNNDMAM from 0.5 wt% to 1.0 wt% causes a decrease in performance, shown in Figure 8.
3. Figure 9 shows PNEAM to be sensitive to pressure so that pressure increases from 1000 to 1250psig can cause failure.

b. Eighty (80) tests were done with polymer blends.

1. At 1000 psig, 39.2°F, 0.5wt% polymer, 3.5wt% salt.
Results: at these conditions use PVCAP or VC-713 with either PVP or a new non-lactam polymer PNEAM or PNNDMAM

a.Blending PVCAP with P2E2OX provided better inhibition that either pure polymer (Figure 10)

b.Blending P2E20X with VC-713 provided equal performance to VC-713 alone (Figure 11) but perhaps at a lower cost.
c. P2E20X performed better when blended with VC-713 than with PVCAP (Figure 12)
d. Blends of PVCAP with high molecular weight (MW) HE-300 were more efficient than with low MW HE-300 (Figure 13)
e. Blends of PNIPAM and PNNDMAM with PVCAP perform better than PVCAP alone (Figure 14). However blends of PVCAP with other non-lactam rings (e.g. PAGNA and PNMAAM) promoted hydrate formation rates and amounts.
f. Blends of P2E20X with PVCAP and VC-713 worked well at 1000 psig, but failed at 1300 psig (Figures 15 and 16).

2. <u>At 1500 psig, 39.2°F, 0.75wt% polymer, 3.5wt% salt</u>
<u>Results: use 0.5% PVCAP blended with 0.25% PVP</u>
a. Blends of PVP(K-17) (Figure 17) and PVP(K-30) (Figure 18) with PVCAP provided better inhibition than PVCAP alone. The optimum ratio: PVCAP/PVP = 67/33 is almost equivalent to PVCAP/PVP = 50/50.
b. When blended with PVCAP, low MW PVP (K-17) provided better inhibition than high MW PVP (K-90) as shown in Figure 19.
c. When blended with VC-713, all MW's of PVP work better than VC-713 alone, but none were satisfactory. (Figure 20)
d. When blended with PVCAP (Figure 21) or with VC-713 (Figure 22), P2E20X provided better (although not satisfactory) inhibition than either PVCAP or VC-713 alone.
e. Figure 23 shows VC-713 to be the best candidate for a blend with P2E20X, although it doesn't perform as well as the PVP+PVCAP blend.
f. When blended with PVCAP, high MW HE-300 provided better (essentially satisfactory) performance than low MW HE-300, as shown in Figure 24.
g. High MW HE-300 provided satisfactory inhibition when blended with either VC-713 or PVCAP (Figure 25).
h. Figure 26 shows that VC-713 performed satisfactorily with HE-300 but not with HEC-100, while Figure 27 shows PVCAP yielded the same marginal performance with both (0.2gmol gas consumed).

3. <u>At 2000 psig, 39.2°F, 1.0wt% polymer, 3.5wt% salt</u>
<u>Results: at these conditions use either a blend of VC-713 with PNEAM, or a blend of PVCAP with HE-300</u>
a. Figure 28 shows PNEAM performed satisfactorily in a blend with VC-713 but PNEAM performed marginally blended with PVCAP.
b. Figure 29 shows HE-300 performed marginally with VC-713, but provided good experimental reproducability.
c. Figure 30 shows that a blend of HE-300 performed satisfactorily with PVCAP, but only marginal performance was obtained from a blend of HE-300 with either VC-713 or VC/VP.
d. Decreasing the amount (0.75wt% to 0.5wt%) of PVCAP blended

with HE-300 yielded unsatisfactory performance (Figure 31).
e. Figure 32 shows that performance of blends of PVCAP and HE-300 deteriorated in performance with age (one month).

c. Tests (130) for Mixes of Kinetic and Thermodynamic Inhibitors

1. At 1000 psig, 39.2°F, 0.5wt% polymer
Results: Use salt rather than methanol with VC-713
a. Figure 33 shows that VC-713 was more effective with salt than with an equivalent activity concentration of methanol.
b. Figure 34 indicates that PVCAP polymerized in ethanol was more effective than PVCAP polymerized in methanol with 3.5% salt, particularly when combined with 0.5%ethanol + 1.5%methanol.

2. At 1500 psig, 39.2°F, 0.5wt% polymer
Results: Use 3.5% salt with >10wt% methanol

a. Figure 35 shows that increasing the salt concentration beyond 7% will be required to provided acceptable efficiency with the use of 0.5wt% VC-713.
b. Figure 36 indicates that with 3.5 wt% salt an increase of VC-713 ().5 to 1.0 wt%) provided better (yet unsatisfactory) inhibition.
c. Figure 37 shows that 24 wt% methanol was required for satisfactory inhibition with VC-713.
d. Figure 38 indicates that salt decreased the amount of methanol required for satisfactory inhibition with VC-713; similarly methanol can decrease the salt required for effective inhibition with VC-713.

3. At 2000 psig, 39.2°F, 0.5wt% polymer, 3.5% salt
Results 1. Use 0.5% VC-713 or PVCAP with 15wt% methanol
2. Use 0.75% VC-713 or PVCAP+PVP with 15% MEG
a. Figure 39 shows that VC-713 was effective with 3.5wt% salt and 15% methanol, while PVCAP and VP/VC were less effective.
b. Figure 40 indicates that 0.5%VC-713+15% methanol provided good inhibition (better than 0.75wt%VC-713+10.5wt% methanol)
c. Figure 41 shows that decreasing either the salt or the methanol provided poorer performance, relative to VC-713 with 3.5% salt and 15% methanol
d. Figure 42 indicates the optimum conditions for 0.5wt% PVCAP was a combination of 15wt% methanol + 3.5% salt.
e. Figure 43 shows PNEAM did not work in any combination with methanol and salt as well as VC-713 did with 15% methanol and 3.5wt% salt.
f. Figure 44 indicates that increasing the concentration of vinylcaprolactam (VC) relative to vinylpyrrolidone (VP) give acceptable performance with 15% methanol and 3.5% salt.
g. Figure 45 shows that methanol is a more effective alcohol that ethanol with 0.5% VC-713 +3.5wt% salt

h. Figure 46 indicates that 15wt% MEG is not as effective as 15wt% methanol when blended with 0.5% VC-713.
i. Figure 47 shows that 15wt% MEG is effective when combined with either 0.75% VC-713 or 0.375%PVCAP+0.375%PVP. These results are comparable to 15wt% methanol with 0.5% VC-713.
j. Figure 48 indicates that increasing the concentration of MEG to 20% can provide good inhibition with a 0.75% blend PVCAP+PVP in DI water.

4. At 39.2°F in De-ionized Water at Various Pressures
Results 1. At 1000 psig use 0.75% VC-713 or PVCAP+PVP
2. At 2000 psig Use 18.5% MeOH + 0.5 % VC-713

a. Figure 49 indicates that at 1000 psig 0.75% VC-713 or a 0.75% blend of PVP/PVCAP (0.375%/0.375%) provided inhibition.
b. Figure 50 shows that at 1000 psig high molecular weight (MW) PVCAP performed better inhibition than low MW PVCAP with 3% methanol. However Figure 51 shows that different molecular weights of 0.75% copolymer of VP/VC (25/75) performed similarly (and unacceptably).
c. Figure 52 indicates that at 2000 psig 18.5% methanol was required to provide adequate inhibition with 0.5wt% VC-713, PVCAP, or a blend of PVCAP+PVP
d. Figure 53 shows that 0.75wt% polymers do not provide adequate inhibition when combined with 15% methanol.

d. Fifty (50) Tests on Changes of Polymer Type Characteristics

1. Different MW of 0.5% Polymer, 1000 psig, 39.2°F, 3.5wt% salt
Results: Use low MW PVCAP rather than High MW with salt

a. Figure 54 (in contrast to Figure 50) indicates that low MW PVCAP performed better than high MW PVCAP.
b. Figure 55 shows similar (marginal) inhibition performance for different MW of the VP/VC (25/75) co-polymer.

2. Aged and Hydrolyzed Solution of PVCAP at 39.2°F
Results: Use Fresh, nonhydrolyzed polymer.

a. Figures 56 and 57 indicate that aged 0.75% PVCAP performed worse than fresh PVCAP in DI water and in DI water+ 3% methanol, respectively at 1000 psig.
b. Figures 58, 59, and 60 show that in solutions with 3.5% salt, aged and fresh solutions of PVCAP perform similarly, both with and without methanol at 1000 psig and 1500 psig.
c. Figures 61 and 62 indicate that with 3.5% salt, hydrolyzation decreases performance of PVCAP and VP/VC polymers, respectively.

e. Forty (40) Tests Were Done to Refine Experimental Conditions

1. Changing Experimental Conditions in Hydrate Reactor.
Result: Use any number of Balls with 60 g water

a. Figure 63 shows that changing the number of balls in the

reactor does not affect the rate or amount of hydrate formation.
b. Figures 64 and 65 indicate that the amount of gas consumed (or hydrate formed) was not affected in direct proportion to the amount of total impure liquid (or the amount of agitation).
c. Figure 66 shows that the amount of gas consumption is directly proportional to the amount of DI water in the cell. To reconcile this conclusion with that in item b, see section "d" below for evidence regarding how the gas consumption is proportional to the amount of liquid with and without thermodynamic inhibitor.
d. Reducing the amount of water (120 to 60g) will:
(1)decrease the induction time (Figures 67 and 68) and
(2)reduce the amount of time required to obtain maximum gas consumption (Figures 69 and 70).
e. Figure 71 shows that, with 60 g water in cell, blending low MW PVP with PVCAP has the same qualitative increase in inhibition efficiency (compare with Figure 17 which has 120 g liquid), but both induction times in Figure 71 are quantitatively lower than those in Figure 17.

2. Surpassing the Cloud Point before Redissolving the Polymer
Result: Surpassing the Cloud Point Temperature Does Not Affect Performance if the Polymer is Redissolved.
a. A solution of VC-713 heated for 1 hour at 90°C above its cloud point (37°C) gave the same performance as fresh solution, either in DI water (with 0.75% VC-713 as in Figure 72) or in salt water (with 0.5% VC-713 as in Figure 73) at 1000 psig and 39.2°F, when it was redissolved.
b. A solution of PVCAP heated for 1 hour at 90°C above its cloud point (45°C) gave the same performance as fresh solution, either in DI water (with 0.75% PVCAP as in Figure 74) or in salt water (with 0.5% PVCAP as in Figure 75) at 1000 psig and 39.2°F, when it was redissolved

3. Gas Consumption Effects of Various Thermodynamic Inhibitors
Result: Gas Solubility Alone Cannot Explain Inhibition Kinetics
a. Figure 76 shows the total gas consumption was reduced by 20% when 3.5%salt was added to DI water.
b. Figure 77 indicates that gas solubility is identical in both methanol and ethanol.
c. Figure 78 shows that gas solubility increases slightly with a substantial increase in PVCAP concentration in water.
d. Figure 79 indicates that increasing the pressure from 1000 to 1500 psig gives a proportional increase in gas solubility.
e. Figure 80 shows that changing the salt type does not significantly affect the kinetics or amount of hydrate formation.

With these conclusions from the high pressure apparatus, and the

previous conclusions from the screening apparatus, we now turn to other pieces of evidence for the mechanism which was proposed in Section III.C.

IV.C. Other New Evidence in 1994 for the Mechanism

The principal evidence for the kinetic inhibition of hydrates was based upon three sources:
(1) experimental data from our screening apparatus and high pressure apparatus, as presented in the previous two sections,
(2) experimental data from the Exxon flow loop facility in Houston (Section IV.D) measured by one of our laboratory workers, and
(3) field tests by the members of the consortium (Section IV.E).

The last two sources are the best proof of the concept of kinetic inhibition, since they represent the reduction to field practice. Before considering the pilot plant and field studies however, we pause to consider three major conclusions which bear strongly on our mechanism for inhibition:

1. (Section IV.C.1) Hydrate adsorption of the best inhibitors is a necessary (but not sufficient) condition for inhibition. In a solution blend with PVP, twice as much PVCAP adheres to the hydrate phase as from a solution of PVCAP alone. Strong hydrate adherence of the caprolactam homopolymer (PVCAP) correlates with its being a primary inhibitor, while a pyrrolidone homopolymer (e.g. PVP) is normally a secondary inhibitor.

2. (Section IV.C.2) Light scattering explains the salt solution expanded dimensions of VC-713 relative to contracted dimensions in DI water, as compared with the effect of salt on PVCAP.

3. (Section IV.C.3) Computer simulation indicates that both good and poor inhibitors change hydrogen bond patterns in water.

The evidence for each of these conclusions is detailed in the following three sections.

IV.C.1. Adsorption of Inhibitors on the Hydrate Surface

We performed two sorts of inhibition experiments: (1) the first type was using single inhibitors, discussed in Sections IV.C.1.a and IV.C.1.b. and (2) the second type was using blends of inhibitors, discussed in Section IV.C.1.c. Single inhibitor results provide evidence for adsorption of inhibitors, while blend results provide evidence for synergism.

IV.C.1.a. Experimental Procedure for Single Inhibitors. In these experiments we measured the amount of inhibitor adsorbed to a hydrate phase relative to the inhibitor remaining in the liquid solution after hydrate formation. We used the THF hydrate

screening apparatus to generate both hydrate and solution phases to overcome the difficulties of mass transfer, pressure control, etc. inherent in the use of natural gas hydrates.

After the hydrates were formed in a solution with inhibitor, we separated the hydrate phase from the remaining liquid solution. The hydrate solution was then melted and the inhibitor concentration was determined in each phase, as an indication of the degree of attachment of inhibitor to the hydrate.

The following procedure was used in these tests:

1. We first prepared calibration curves for UV-visible absorbance versus concentration for various inhibitors. Initially this was done by complexation of a known amount of inhibitor with potassium iodide and an water evaporation was performed before the UV-Visible measurement was made at a wave length of 470nm.
   Over time both the evaporation and the complexation steps were eliminated in favor of direct measurement of solutions in the UV spectrophotometer, Typical calibration curves are presented in Appendix B.
2. We formed a substantial amount of hydrates from solutions of inhibitor in the THF screening apparatus, exactly as described in Section IV.A.1.
3. We filtered the hydrates from solution using the funnel in Figure 81, which was controlled at a temperature of 0°C to prevent THF hydrates from melting (at 4°C.)
4. We separated the filtered solution (called solution 1) from the hydrate mass. The hydrate mass was melted (solution 2). We weighed each solution for comparison with the mass of the initial solution use prior to hydrate formation.
5. We measured the concentration of inhibitor in each solution using the calibration curves prepared in step one above.
6. We calculated a mass balance as a measurement of experimental accuracy. If the mass balance was too poor (less than 80%), the experiment was repeated.

The mass balance is defined as follows:

MB = (polymer on hydrate + final liquid polymer)/(initial polymer)
Mass Balance = Abs(MB) X 100%

IV.C.1.b. Adsorption Results for Single Inhibitors. The adsorption of PVP(K17), PVP(K90), PVCAP and VC-713 is shown in Figures 82, 83, 84, and 85, respectively. These good hydrate inhibitors are about equally associated with the hydrate phase and the liquid solution.

In contrast, the adsorption of L-Tyrosine (the BP-patented inhibitor) and poly(4-sodium styrene sulfonate) are shown in

Tables 10 and 11. Both chemicals were found to be less associated with the hydrate phase than PVP, PVCAP, or VC-713. The average distribution ratio of these inhibitors (hydrate:solution) was 22%, while good inhibitors appear to be equally distributed between the hydrate phase and the solution. Both L-Tyrosine and poly(4-sodium styrene sulfonate) had previously been found to be non-inhibitors through our high pressure apparatus experiments.

Table 12 provides the adsorption results for the good single hydrate kinetic inhibitors. With two exceptions, all of the inhibitors in the table show equal concentrations of polymer in the hydrate phase and in the solution. The two exceptions are HE-300 and VC-300 (the caprolactam version of HE-300, made for us by Phillips Petroleum Company.) VC-300 did not prove to be a good kinetic inhibitor but it did adsorb (about 33wt% compared to 50wt% for the good inhibitors). However, HE-300 was found to be a good inhibitor but did not adsorb; our other work indicated that HE-300 may have a mechanism of viscous inhibition, rather than adsorption. Section IV.D discusses the performance of HE-300 in the Exxon Flow loop.

There is a third anomalous inhibitor in Table 12. The 50/50 co-polymer poly(VP/NEAM) adsorbed more strongly on the hydrate phase than any of the homopolymers that were found to be good inhibitors. The polymer concentration adhered to the hydrate was a factor of 1.6 to 3.55 times that in the remaining solution. Yet in the high pressure apparatus at 1000 psig and 39.32°C the co-polymer required less than 200 minutes to consume 0.3 gmol of gas, while both PVCAP and VC-713 never consumed that amount of gas in over 1200 minutes. It is unclear why this co-polymer works poorly with this extreme amount of hydrate adsorption, and this is currently under study.

Table 10: L-Tyrosine-Disodium Salt Adsorption Studies On THF-Hydrate; Temperature=3.9°C; 15 hours run.

Concentration (wt%)			Mass Balan.%
Initial	Hydrate Phase Solution	Liquid Phase Solution	
0.1875	0.06	0.36	79
0.1875	0.04	0.35	89
0.375	0.16	0.45	87
0.375	0.14	0.55	102
0.75	0.11	1.0	93.7
0.75	0.16	1.0	99.5

Table 11: Poly(4-Sodium Styrene sulfonate) Adsorption Studies On THF-Hydrate. Temperature=3.8°C; 15 hours run.

Concentration (wt%)			Mass Balance %
Initial	Hydrate Phase Solution	Liquid Phase Solution	
0.375	0.12	0.46a	-
0.375	0.11	0.33b	-
0.375	0.18	0.72c	108
0.375	0.17	0.53	96
0.752	0.21	0.91a	-
0.75	0.17	0.76b	-
0.75	0.38	1.20c	105
0.75	0.15	0.93	94

[a]Instead of 38 g. solution, ~43 g. solution was obtained (water leaked in).
[b]Instead of 38 g. solution, ~53 g. solution was obtained (water leaked in).
Instead of 38 g. solution, ~34.5 g. solution was obtained.

Table 12: Polymer adsorption studies of THF-hydrate

Polymer[a]	Conc. wt% polymer/wt% CH_3OH	Temp. °C	Fraction Hydrate of Tll Initl. Soln %	Concentration of (wt%)		Mass Balance	Ball Stop Time THF-Hydrate[b]
				Hydrate phase	Liquid phase		
PVCAP	0.75.0/0	1.3	18.6	0.89	0.81	90	-
	0.375/0	2.2	18	0.47	0.41	96	> 24 hours
VC-713	0.75/0	0.5	40.8	0.73	0.72	80	
	0.375/0	1.4	7.6	0.39	0.43	83.4	> 17 hours
PVPK30	0.75.0/0	2.1	38.9	0.79	0.87	98.5	-
	0.375/0	2.2	28.3	0.56	0.40	100	< 30 min.
PNEAM	0.375/1.50	1.0	46.0	0.38	0.25	81.6	-
	0.375/1.5	1.0	12.0	0.69	0.30	78.0	-
poly(VP/NEAM)	0.75/0	1.4	30.8	1.31	0.82	105	-
	0.75/0	1.4	29.5	1.41	0.83	109	-
	0.75/1.5	0.8	38.8	1.42	0.40	102	-
	0.75/1.5	0.8	33.5	1.30	0.60	100	-
	0.375/0	-	-	-	-	-	< 4 hours
PNNDMAM	0.375/1.5	2.3	48.9	n/a	n/a	-	-
PNMNVAcAM	0.37/0	2.3	60.7	0.34	0.26	95	< 30 min.
	0.375/0	2.3	70.3	0.33	0.34	91	-
HE-300	0.375/1.5	2.3	29.3	0.14	0.61	91.5	-
	0.375/1.5	2.3	27.2	0.19	0.47	94	-
VC-300[c]	0.75/1.5	2.3	48.1	0.45	0.90	76	-
	0.75/1.5	2.3	60.8	0.40	1.0	90	-

[a]Structures of polymers are shown in Appendix A.
[b]Ball stop time for 0.5wt% polymer in DI water at 2.5°C.
[c]N-Vinylcaprolactam version of HE-300.

IV.B.1.c. Adsorption Results for a Blend of PVP and PVCAP. We analyzed the adsorption of an equal mass blend of PVP and PVCAP, to determine which portion of the polymer blend adsorbed more strongly. We formed and separated the THF hydrate and solution just as before, with the apparatus and technique listed in Section IV.B.1.a above for the single polymer types.

However in this set of experiments we were forced to use another concentration measurement technique, due to the interference of the pyrrolidone (the final "P" in PVP) peak and the caprolactam peak on the UV-Visible instrument. We used Fourier-Transform Infrared (FT-IR) Spectroscopy to measure polymer concentrations in each phase. Rather than generate a calibration curve as in IV.B.1.a, we used an internal standard of PMMA in chloroform.

Figures 86, 87, and 88 provide results from the blend studies. In each figure the chemical whose peak is at 1730 cm^{-1} is the standard (PMMA), the second peak at 1680cm^{-1} represents PVP, and the final peak at 1630cm^{-1} represents PVCAP. The area under each peak is indicative of the amount of the chemical in the phase represented by the figure. Each figure is discussed in the below three paragraphs.

Figure 86 shows a 1:1:1 molar ratio of PMMA:PVP(K90):PVCAP in the initial solution. At this molar ratio the peak areas decrease in the following order PVP = PVCAP > PMMA

Figure 87 indicates the polymer concentrations on the melted hydrate phase. The peak areas decrease in the following order: PVCAP >> PVP = PMMA. PMMA is a poor inhibitor and therefore hydrate adsorption of PMMA is low. The peaks areas indicate that PVCAP is much more highly adsorbed than PVP.

Figure 88 indicates the polymer concentration in the residual solution after hydrate formation. Here the peak area decreases in the order PVP > PMMA = PVCAP. PVCAP was removed from the solution by its adsorption on the hydrate phase.

The PVCAP peak in the hydrate (Figure 87) is almost double the size of the PVCAP peak in the remaining solution (Figure 88), relative to the PMMA peak. This doubling of concentration in the hydrate phase is in sharp contrast with the equipartitioning which occurs if PVCAP alone is used as the inhibitor (see Figure 84). In contrast Figure 87 and 88 indicate that PVP remains principally in the liquid, while Figure 82 aqnd 83 indicate that PVP as a single inhibitor equipartitions.

This result suggests that the PVP/PVCAP blend is effective because PVP aids in the dissolution of PVCAP, which is the most effective due to its high degree of adsorption on the hydrate. Similarly the adsorption of PVCAP may competitively hinder the adsorption of PVP. In the mechanism evidence (Table 1 on page 7) observations 7 and 8 regarding the primacy of caprolactam rings and the synergistic effect of blends may be explained by the above "competitive adsorption" experiment.

IV.C.2. Light Scattering Shows Polymer Dimensions & Salt Effect.

During 1994 we performed two separate sets of light scattering experiments on polymers at Brookhaven Instrument Company in New York and a second set of experiments on the instrument at the Air Force Academy. These experiments were done on state-of-the-art instruments not available at the Colorado School of Mines. We list here the experimental evidence and conclusions:

1. Figure 89 shows that the PVP polymer series has an effective polymer size (through the polymer K-120) which is directly proportional to molecular weight.

2. Figure 90 indicates that PVP(K-120) has a size and dispersity which is unaffected by its concentration in solution. This lack of concentration dependence of size indicates that the polymer does not agglomerate into dimers, trimers, etc. The polydispersity portion of Figure 90 indicates that the polymers are fractionated and of relatively narrow and uniform distributions.

3. Figure 91 shows PVCAP effective size and dispersity to be unaffected by salt concentration, with a single dispersity. This may be a reason PVCAP can prove effective in the absence of salt (See IV.B.3.d).

4. Figure 92 shows that VC-713 is dramatically affected by the presence of salt. As the salt concentration increases, the small size (4-7 nm) fraction of the polymer decreases while the larger size (53-62 nm) fraction of the polymer increases. These data also indicate that VC-713 is a blend of three molecular weight distributions, rather than a single distribution such as found in PVCAP. Salt seems to be stabilizing an unfolding of this polymer, making the rings more accessible to hydrate crystal particles in salt solutions than in pure water. This information suggests both why VC-713 is one of the most effective inhibitors (observation 8 of Table 1, page 7), and why it is enhanced most by increasing the salt concentration of the solution.

5. Table 13 indicates the molecular weights and radius of gyration (or effective size) of a number of samples of PVCAP and one sample of VC-713. Two molecular weight determinations are presented: the first column was GPC data determined by ISP and the second is light scattering data. Note the PVCAP molecular weight values differ by a factor of 3-4 with the two measurement techniques.

Table 13: Molecular weight (MW) and radius of gyration (Rg) data of some lactam polymers.

PVCAP Manufacturer (Solvent)	MW[a] (x1000)	MW[b] (x1000)	Rg (nm)
ISP (CH_3OH)	20	88	23.5
BASF (C_2H_5OH)	n/a	92	24.1
BASF (CH_3OH)	n/a	120	28.0
ISP (CH_3OH)	75	246	41.8
ISP (CH_3OH)	110	318	48.2
VC-713, ISP (C_2H_5OH)	80	70	20.7

[a]GPC data supplied by ISP.
[b]Low angle laser light scattering data.

6. Figure 93 for PVCAP relates low angle laser light scattering (LALLS) data for radius of gyration (size) to number of repeat units (molecular weight). From these data R_g, the radius of gyration (in Angstroms), is related to the molecular weight by the relation $Rg = 0.40MW^{0.56}$. The value of the exponent (0.56) indicates that PVCAP is a random coil in DI water; a value of 1.5-1.8 would indicate that the polymer had a rod shape.

7. Data in Item 6 above indicate that, if the mechanism requires the complete filling of space in the solution by the polymer, then the higher molecule weight materials should be active at lower mass concentrations. However our high pressure data and data in Table 13 (Item 5) indicate that the lower molecular weight PVCAP (from BASF generated in ethanol) is most efficient. We conclude from this that the polymer does not need to completely fill every available position in solution space; instead it may form a network as in the mechanism of Figure 1.

IV.C.3. Computer Simulation of Hydrogen Bonding Patterns in Water.

Computer simulations performed during 1994 were directed at investigating the possible mechanisms of kinetic hydrate inhibition. The first hypothetical mechanism of inhibition is the adsorption of the inhibitor molecule on the growing crystal surface. This hypothesis was validated and results of this study are presented previously in this Annual Report.

The second hypothesis proposes that hydrate growth inhibition arises through changing the hydrogen bonding structure of liquid water. Water molecules are hydrogen bonded to each other in a liquid in such a way that they form a three-dimensional network of hydrogen bonds. This network of hydrogen bonds consists of polygons which are like the polygons in a hydrate lattice. However, while the hydrate lattice consists only of five- and six-membered rings, the sizes of rings in a liquid vary from three to ten or more molecules.

Adding a kinetic inhibitor into water promotes structural changes in the hydrogen bonded network of water. Upon the addition of various chemicals the number of hydrogen bonded polygons in water changes. It was shown through the computer simulations that the kinetic inhibitors which perform well in experiment have a large effect on the hydrogen bonded structure of water. The overall decrease of hydrogen bonded rings in liquid water can retard the formation of gas hydrate which is composed of five- and six- membered rings of water molecules.

We first validated the ability of our computer program to predict the properties of water through two means:

1. determining the radial distribution function (which represents the local molecular density) for water and comparing it against neutron diffraction data, and
2. comparing the number of polygonal ring structures in water against data obtained from several respected computer simulations of water.

Both of the above validations were done in 1993 and were presented in the 1993 Consortium Annual Report.

In 1994 we preformed a detailed study of how several polymers changed the structure of water. While space prevents the full explanation of the results here, we will give an abbreviated synopsis. For more complete details, the reader is referred to the Master of Science thesis of Makogon.

A summary set of studies were performed with simulated polymers of the inhibitors. The changes in the hydrogen bonding structure of water by the decamers of the six chemicals listed in

Table 14 were compared to the structure of pure water and of approximately 10 wt % aqueous methanol solution. The simulations were set up using the molar basis instead of the weight percent composition basis. All simulations were run at constant number of particles, constant volume, and at the constant temperature of 241.5 K (4 °C above ice melting). Figure 94 shows that the trend in the performance of effective versus less effective chemicals (e.g. PVA (poly vinylalcohol) and PVAM (poly vinylacrylamide)) is not pronounced.

The conclusion for these molecular simulations is an effective denial of the second hydrate inhibition hypothesis. While a decrease in the number of pentagonal and hexagonal rings in the structure of water may retard the formation of the hydrate nuclei, this decrease in the number of rings was shown to be similar for both good and less effective inhibitors.

IV.D. Exxon Flow Loop Experiments

In this portion of the report we present flow loop evidence for the following conclusions:

1. The onset temperature of hydrate formation is not a strong function of flow rate.

2. The onset temperature of hydrate formation is a strong function of inhibitor concentration.

3. PVCAP and VC-713 have similar performance and are both better than PVP.

4. Adding HE-300 to PVCAP did not significantly affect the observed onset temperature over that observed for PVCAP alone.

5. 0.125wt% HE-300 + 0.4wt% PVCAP dramatically lowers the gas consumption over that observed for PVCAP alone.

IV.D.1. Introduction. During the second quarter of 1994, we continued our collaborative research project with Exxon Production Research. The goal of this project was to investigate the transferability of PVCAP and HE-300 results between the Center for Hydrate Research hydrate formation apparatuses and the Exxon flow loop. Mr. J. P. Lederhos, one of the graduate students at the Center for Hydrate Research, went to Houston to conduct the experiments on the flow loop.

The Exxon facility was unique in that, while it represented a capital and operational investment beyond that of a normal academic institution, it was also the best pilot plant facility

Table 4. Normalized number of hydrogen bonded polygons in aqueous inhibitor solutions

Kollmann forcefield

	Number of water molecules in hydrogen bonded polygon							
Chemical	1	2	3	4	5	6	7	8
pure SPC water	0	0	0.008176	0.077673	0.242138	0.301258	0.224528	0.130189
NEA decamer in water	0	0	0.006022	0.039239	0.130342	0.167735	0.125486	0.084402
VC713 decamer in water	0	0	0.006501	0.042686	0.123524	0.142601	0.124808	0.08503
NFA decamer in water	0	0	0.004633	0.037413	0.12264	0.149213	0.120804	0.076836
NVS decamer in water	0	0	0.005996	0.042681	0.125485	0.153439	0.124074	0.081041
CH3OH ~10 wt% in water	0	0	0.005472	0.04882	0.138734	0.151931	0.107618	0.065558
PVA decamer in water	0	0	0.007143	0.038937	0.132753	0.171254	0.133275	0.081359
PVAM decamer in water	0	0	0.006206	0.041844	0.130674	0.174291	0.134486	0.08094

SPC pure water 318 molecules at 241.5 K (+4 °C above melting)

N-Ethyl Acrylamide decamer in 1144 spc waters at 241.5K (+4°C above melting)

VC713 decamer (7 VCap, 2VPy,1DMA)

N-FormAmide decamer in 1144 spc waters at 241.5K (+4°C above melting)

N-VinylSuccinimide decamer in 1134 spc waters at 241.5K (+4°C above melting)

64 CH3OH molecules in 932 spc waters at 241.5K (+4°C above melting)

PolyVinylAlcoohol decamer in 1148 spc waters at 241.5K (+4°C above melting)

PolyVinylAcrylaMide decamer in 1128 spc waters at 241.5K (+4°C above melting)

available for scale-up. The Center for Hydrate Research expresses its gratitude to Exxon for providing the opportunity to perform this research using the flow loop and for sharing the results with the consortium.

Over 50 experiments were conducted using the flow loop. All of the experiments were conducted in the presence of a structure II hydrate forming gas, synthetic sea water, and a liquid hydrocarbon. The operating pressure was maintained constant at 985 psig (except for a few tests which were run at 940 psig) resulting in a hydrate equilibrium temperature for the mixture of 64.2°F. For all tests the cooling rate was fixed at 10°F/hr; in an earlier study Reed et. al. (1993) found that varying the cooling rate between 1°F/hr and 20°F/hr had only a small effect on the observed results..

There were two different kinetic inhibitor systems tested during this project, namely PVCAP and HE-300 + PVCAP. Table 15 briefly summarizes the systems that were tested. In addition to those systems summarized in Table 15, Exxon also generously released the results for PVP and VC-713 that they had obtained prior to this project; these results are presented in Figure 99.

Table 15. Summary of systems tested using the flow loop.

PVCAP Concentration (wt%)	HE-300 Concentration (wt%)
0.05	0
0.10	0
0.20	0
0.40	0
0	0.125
0.05	0.125
0.10	0.125
0.20	0.125
0.40	0.125
0.60	0.125
0.60	0.23

IV.D.2. Exxon's Experimental Apparatus . A schematic of the Exxon flow loop is shown in Figure 95. The loop was 275 feet long, 4 inches in diameter, and of stainless steel construction. The entire loop was housed in an air cooled environmental chamber. The loop contents were circulated by a sliding vane variable speed pump capable of producing a maximum pressure rise across the pump of 200 psi. A sight glass for viewing the loop contents was located approximately 40 feet down stream of the pump.

Attached to the loop was a variable volume gas accumulator that was used to maintain a constant loop pressure. The accumulator volume was separated into two compartments by a piston. On one side of the piston was the gas that was fed to the loop and on the other side was a hydraulic fluid. As the temperature of the loop was cooled and when hydrates form, the loop pressure dropped. In response to the drop in loop pressure, the gas volume in the accumulator was decreased by pumping hydraulic fluid into to accumulator, displacing the piston and returning the loop pressure back to the set point. The gas in the accumulator was continuously mixed with the gas in the loop.

Data acquisition and control of the loop were accomplished by a PC based system located in a dedicated control room. The control room was in a separate building from the flow loop. In addition, a video camera was mounted adjacent to the sight glass on the flow loop and monitored and recorded in the control room.

Internal loop temperature measurements were accomplished by two thermal wells. One thermal well was located just upstream of the pump and one is located just downstream of the pump. These two temperatures were sensed by 100 ohm platinum resistance thermometers. In addition to the internal loop temperatures, type J thermocouple were used to measure the external temperature along the length of the pipe.

The pump inlet and differential pressure were measured by a Rosemont pressure sensor and differential sensor connected directly to the flow loop. Ports along the length of the pipe provide additional differential pressure measurements.

IV.D.3. Experimental Procedure. Prior to charging the loop, it was thoroughly washed with a detergent solution, flushed with water several times, and then vacuumed to 28 in Hg. Following this, the loop was charged with the appropriate weights of gaseous components. The heaviest component was charged first, followed by the next heaviest component, and so on. The appropriate amounts of synthetic sea water and condensate were then pumped into the loop. The condensate/gas/ synthetic sea water composition is given in Table 16 and the condensate composition is given in Table 17. The sea water was bubbled with nitrogen for several hours prior to pumping it into the loop. The entire charging process required approximately 1.5 man days.

After charging , the loop temperature was maintained at 70°F and the pump was set at a flow rate of 5.02 ft/sec for several hours prior to initiating the experimental run sequence. This ensured that the loop contents are thoroughly mixed prior to starting the run.

Table 16. Condensate/Gas/ Synthetic Sea Water mixture composition.

Component	Mole%
N_2	0.21
CO_2	0.05
C_1	9.16
C_2	2.21
C_3	2.27
$n-C_4$	1.14
$i-C_4$	0.42
Condensate	6.61
Sea Water	77.95

Table 17. Condensate composition.

Component	Mole %
$i-C_5$	17.4
$n-C_5$	13.7
C_6+	29.2
C_7+	25.8
C_8+	11.5
C_9+	2.0
$C_{10}+$	0.4

The experimental run consisted of setting the pump at the desired flow rate and then ramping the loop temperature down at 10°F/hr. At the onset of hydrate formation the loop temperature increased for a period of about 20 minutes before starting to

decrease again. The temperature ramp was continued until one of the following three conditions was met:

1.Pressure control was lost (all of the gas in the accumulator has been transferred to the loop),
2. The differential pressure across the pump exceeds 50psi (indicating the loop was plugged with hydrates), or
3. The differential temperature across the pump exceeded 4°F (indicating the loop was partially plugged with hydrates and very little liquid was passing through the pump).

In general one of these three conditions was met within 1 hour after the onset of hydrate formation. After meeting one of these three conditions, the pump was stopped and the environmental chamber temperature was increased to 80°F. After the internal loop temperature reached 80°F, the temperature was maintained at this level for additional three hours prior to starting another run. The loop temperature was held at this temperature to remove any hydrate memory (residual structure) in the subsequent run (Müller Bongartz, CSM thesis, Hydrate Research Center, 1990).

Figure 96 shows a typical pump inlet temperature versus time trace. The onset temperature is indicated by the increase in the loop temperature at about 130 minutes. The environmental chamber temperature continued to drop until about 200 minutes when the set point for the environmental chamber temperature was set to 80°F.

The best indicators of the onset of hydrate formation are a sudden increase in the loop temperature as shown in Figure 96 or a change in slope of the loop volume versus temperature trace as shown in Figure 97. Recall that the loop volume decrease is actually due to the accumulator volume decreasing.

The hydrate kinetic inhibitors are injected into the charged loop via a chemical injection pump similar to that used in the field. Before injecting the inhibitor into the loop, an aqueous liquid sample of approximately the same volume as to be injected was removed from the loop. After the first inhibitor injection, the samples were analyzed to confirm the inhibitor concentration in the loop. The inhibitors were generally diluted to 10 wt% solids with synthetic sea water before injecting into the loop. The inhibitor was injected just prior to the 3 hour hold at 80°F.

For the HE-300 inhibitor a concentration of 10 wt% solids was too viscous to inject into the loop and it was necessary to reduce the inhibitor concentration to 7 wt% solids. Even at this concentration it was very difficult to inject the inhibitor into the loop. The HE-300 solution had often blocked open the check valves on the injection pump.

IV.D.4. Experimental Results. For PVCAP the effect of flow rate on the onset temperature was investigated for two different PVCAP concentrations (0.2 wt% and 0.4wt%). The amount of subcooling was defined as:

Subcooling = Hydrate Equilibrium Temperature - Onset Temperature.

The subcooling is shown as a function of PVCAP concentrations from 0.05 wt% to 0.4 wt% in Figure 98. In addition, this figure shows the effect of flow rate at 0.2 wt% and 0.4 wt% for flow rates of 1.61 ft/sec (stratified), 5.02 ft/sec (wavy/slug), and 8.33 ft/sec (slug/dispersed). All of these experiments were conducted at 940 psig. The onset temperature of synthetic sea water(0 wt% PVCAP) is shown for comparison.

The amount of subcooling did not change appreciably with changes with the flow rate at the two PVCAP concentrations investigated. However, the amount of subcooling was observed to be a strong function of PVCAP concentration. In particular, the largest change in the amount of subcooling was observed in going from no inhibitor to 0.05 wt% PVCAP. The amount of subcooling went from about 6°F with no inhibitor present to about 12°F with 0.05 wt% PVCAP present. However, in going from 0.2 wt% PVCAP to 0.4 wt% PVCAP the onset temperature went from about 18°F to about 22°F. The effect of PVCAP concentration appears to level off at higher concentrations.

The onset temperatures for PVP, PVCAP, and VC-713 are compared in Figure 99. The flow rate for all the results in this figure was 5.02 ft/sec (wavy/slug). It is important to note that the results for PVP, VC-713, and synthetic sea water were all at 890 psig while PVCAP was at 940 psig. Even with the noted differences, the synthetic sea water results in Figure 98 at 940 psig appear identical to those in Figure 99 at 890 psig. Figure 99 indicates that the performance of PVCAP and VC-713 is similar and both are better than PVP.

In Figure 100 the results for PVCAP and PVCAP+HE300 are compared at a flow rate of 5.02 ft/sec. The amount of subcooling was not dramatically affected by adding HE-300 to PVCAP. In contrast to the subcooling results, the gas consumption results in Figures 101 and 102 show that the gas consumption of 0.125wt% HE-300 + 0.4wt% PVCAP is nearly half that of 0.4wt% PVCAP alone. Time zero in both of these figures corresponds to the onset of hydrate formation and the flow rate was held constant at 5.02ft/sec.

IV.D.5. Conclusions. The results in the Exxon flow loop pilot plant facility have shown the following to be true:
1. The onset temperature of hydrate formation is not a strong function of flow rate.

2. The onset temperature of hydrate formation is a strong function of inhibitor concentration.

3. PVCAP and VC-713 have similar performance and are both better than PVP.

4. Adding HE-300 to PVCAP did not significantly affect the observed onset temperature over that observed for PVCAP alone.

5. 0.125wt% HE-300 + 0.4wt% PVCAP dramatically lowers the gas consumption over that observed for PVCAP alone.

IV.E. Field Results and a Mathematical Analysis

IV.E.1. Introduction. In this portion of the report we present field results for kinetic inhibition of 13 wells from five companies. These data, from wells in which the kinetic inhibitor was tried with some success, represent a vital link between laboratory and field observations for hydrate formation.

Before presenting the data, we discuss our attempt to arrive at a common basis. A common basis for comparison is needed because, while we attempted to determine a common form for reporting the data, in many cases the data sets are incomplete. Field data are reported by the parameters of pressure, temperature, gas composition, along with line length, fluid velocity, mixture velocity, specific gravity and flow regime.

Neither subcooling nor overpressure are adequate bases because both measures are a function of the pressure and temperature range, respectively. For example a methane gas subcooled by 10°F at 1000 psig will have an entirely different driving force for hydrate formation that a methane+propane (95%:5%) mixture subcooled by 10°F at 2000 psig.

The model of Christiansen and Sloan (Appendix C) suggests that the best field data basis for comparison was the difference in Gibbs Free Energy of the system at operating conditions, relative to that of the system at the hydrate equilibrium conditions. The expression incorporates the effects of sub-cooling, over-pressurization, and hydrate phase composition changes. Calculation of this driving force has been incorporated into a modified version of the Colorado School of Mines hydrate prediction program (CSMHYD).

The Gibbs free energy driving force written on a basis of one mole of the hydrate phase is:

$$\Delta g^{exp}/n_w = v_w(P^{equ}-P^{exp}) + RT\left(\sum_i (n_i/n_w)\ln(f_i^{equ}/f_i^{exp})\right) + v_h(P^{exp}-P^{equ})$$

In the above expression f represents fugacity, P the pressure, n_w the moles of water, n_i the moles of each natural gas component (thus n_i/n_w is the total occupancy of gas i molecules in the hydrate phase), v_w and v_h are the molar volumes of water and the hydrate phase, R is the gas constant, T the hydrate equilibrium temperature, and the superscripts exp and equ refer to system, or experimental values and equilibrium values respectively.

Using the Gibbs free energy driving force expression calculated by the modified CSMHYD program and growth and induction time experimental data we have developed correlations for the growth rate and induction time of hydrate crystal structure. Ethane hydrate growth rate data from our laboratory (Bansal, 1994) and the data of Englezos et al.(1987) was plotted versus the Gibbs free energy driving force. A best fit was performed to determine if both sets of data could be fit in a single correlation. The following equation was found to fit the growth data reasonably well:

$$\ln r_g = -0.00614\Delta g - 17.8$$

Similarly, a good correlation for the induction time (defined as the end of the nucleation period, or the beginning of rapid hydrate growth as determined by gas consumption/pressure drop) is given by the following equation:

$$\ln t_{ind} = 0.0102\Delta g + 6.29$$

This induction time correlation has also been found to be in fair agreement with experimental induction times of a natural gas studied by Yousif (1994).

IV.E.2. Presentation and Analysis of Field Data. In a comparison of the field data we have used the Gibbs Free Energy driving force difference, expressed in Equation (1) in the previous section. In Table 18 the various temperatures, pressures, and compositions of each well were transformed to a Gibbs Free Energy driving force.

For each of the wells listed in Table 18, the driving force was also used to determine the induction time necessary for hydrate formation, using the correlation presented in Equation (3) of the last section. This induction time is physically interpreted as the time for the beginning of hydrate formation.

We compared our calculation of the induction time for the beginning of hydrate formation against the free water residence time in the pipeline from the well. The residence time was perhaps the most uncertain portion of the calculation; we simply divided the length of the pipeline by a nominal velocity of 2 ft/sec.

Figure 103 is a plot of the likelihood of hydrate formation in the 13 wells reported in Table 18. The residence time is plotted against the induction time for hydrate formation. The line at a 45° angle from the origin indicates those conditions for which the residence time is equal to the induction time. Those wells with conditions falling to the right of the line may be considered less likely to form hydrates without an inhibitor, while those to the left of the line may be considered more likely to form hydrates.

We note that several of the pipelines fall into the "less likely" hydrate formation region of Figure 103. However, we know that all of the pipelines reported required hydrate inhibition, so the graph must contain some error. One of the most probable places for the error is in the estimation of a uniform 2 ft/sec for the nominal free water phase velocity.

Our hope for 1995 is to obtain better data from Consortium members so that we can replace Figure 103 with a more accurate plot. Having a more accurate plot for the uninhibited system, it is our hope to generate a similar plot from inhibited field results.

IV.F. A New Visual Apparatus and Control System

IV.F.1. Experimental Apparatus. During 1994 we built a new sapphire screening apparatus for hydrate formation. The design of the apparatus is similar to an apparatus built by Conoco. Prior to the design and construction of our apparatus, Dr. J. P. Long and R. Miner from the Center for Hydrate Research went to Conoco's Ponca City facility to see their apparatus. Conoco supplied the Center with design specifications for their apparatus and suggestions for improvements. The Center for Hydrate Research expresses gratitude to Conoco for assisting in the design of our sapphire screening apparatus and inviting both Dr J. P. Long and R. Miner to visit their facility.

A schematic diagram of the new apparatus is shown in Figure 104. The sapphire screening apparatus consists of 10 sapphire tubes with a maximum operating pressure of 2000 psig. Each of the tubes has a nominal internal diameter of 0.42 inch and a length of 6inches. Within each tube is a stainless steel ball

that is 0.35 inch in diameter. The stainless steel ball helps to agitate the contents of the tube.

All ten sapphire tubes are mounted in a stainless steel rack that is rotated by a step motor. A manifold assembly is used to connect each of the ten tubes to a gas supply reservoir on the rack. In addition, the rack also supports 20 proximity sensors. There are two proximity sensors for each tube that are spaced 1in from each other. The proximity sensors are mounted within 0.04in from the exterior wall of the tube and are used to detect how long it takes the stainless steel bearing to travel between the two sensors. The ball travel time can be related to the viscosity of the solution in the sapphire tube. The sapphire tube rack is submersed into a temperature controlled bath.

The data acquisition and control system for the apparatus is a distributed control system by Mistic. The Mistic controller is linked to a 486 66MHz PC that records the data and displays process variables. The interface software that was used to link the Mistic controller to the PC was donated by Intellution. The donation of this package represents a $12K savings to the Center. The control system allows for the measurement of ball travel times to within an accuracy of 1 msec. In addition to the 10 ball travel time readings the control system monitors and records the bath temperature and tube pressure. Further details on the control system are available on request from the Center for Hydrate Research.

The microscope system that was purchased in 1993 for the single sapphire apparatus was relocated to the sapphire screening apparatus. This provided the ability to record visual observations as well as collect temperature, pressure and ball travel time data. The sapphire cell apparatus provided the capability of doing a large number of tests and to make visual observations similar to the THF screening apparatus. The primary differences between the sapphire screening apparatus and the THF screening apparatus is that we are now able to quickly screen inhibitors using a natural gas hydrate former. In addition, the use of the ball travel times provide more quantitative information than the THF screening apparatus. The sapphire screening apparatus has the advantages of a natural gas hydrate former, similar to the high pressure apparatus, and of visual observations, similar to THF screening apparatus.

IV.F.2. Operating Procedure. Prior to starting an experiment, the rack was flushed with 4 Liters of warm tap water and then purged with nitrogen. Methanol (approximately 0.5L) was then circulated through the rack for a period of 1 hour and then the rack is purged with nitrogen. The rack was then rinsed with 7L of deionized water, purged with nitrogen, and then evacuated for 2 hours. Each tube was then charged with 11cc of the test solution and sealed. The rack was then submersed in a

Table 18. Induction Time and Residence Time Estimates from Consortium Pipeline Test Reports.

Report	Company	Location	WHT (F)	WHP (psi)	Line Pressure (psi)	Line Inlet Temperature (F)	Line Outlet Temperature (F)	Equilibrium Pressure	Driving Force (J/mol)	Induction Time (min)	Line Length (ft)	Residence Time (min)
1	Texaco	Well 25-6	45	900				423	-200	70	120	1
		West Swan Lake, Wy.	56	1450				912	-109	177	120	1
2	Texaco	WSA Well 23-4	52	2300				679	-262	37	120	1
		West Swan Lake, Wy.										
3	Texaco	Brookland Gas Field,Tx			900	110	50	402	-198	72	42000	350
					1000	120	60	827	-45	341	42000	350
					1000		50	402	-218	59	42000	350
4	Texaco	Wilson Ranch Field, Wy.	61	660				1097	141	2280	120	1
		McNamara Well NCT 1 #2										
5	Texaco	West Swan Lake, Wy.	50	850				591	-98	199	2600	22
		State of Wyoming, V-2	50	1000				591	-137	134	2600	22
6	Texaco	Acker Field Flow Line, Tx.			300	120	50	50	-595	1	12000	100
					350		60	88	-460	5	12000	100
7	Texaco	Carter Bloxom Field, Tx.			150	100	50	55	-343	16	19000	158
					175		60	98	-202	69	19000	158
8	Texaco	Neal Field Flow Line, Tx.			300	100	50	44	-635	1	24000	200
					350		60	78	-502	3	24000	200
9	Arco	British Limited			300	43	43	303	3	554		
		Thames Alpha			600		43	303	-187	80		
10**	Amoco	Warnsutter, Wy.	54	800	800			407	-158	108	900	100
		Green River Fee #2		1000	1000			407	-194	74	900	100
11	Mobile	Harmattan, Alberta			790	66	38	194	-366	13	10560	88
					850	86	50	421	-186	81	10560	88
12	Texaco	Brookeland Gas Field, Tx.			900	110	50	401	-199	71	8800	73
		Well 4-1H Flow line			920	120	60	824	-27	410	8800	73
					920		50			539	8800	73
13	Conoco	Peco Field, Edson Alberta	54	1000				484	-173	93	75	1
		Well 10-11										
14	Conoco	Peco Field, Edson Alberta	54	1000				477	-177	89	75	1
		Well 7-23										

**For this well, a liquid velocity of 0.15 ft/s was (specified in the Amoco report) used in the residence time estimate.

temperature bath at 28°C and charged to an operating pressure of 1000psig at 28°C.

The rack was then rotated ± 30x degrees from horizonal. The bath temperature was set to a temperature 2°C above the hydrate equilibrium temperature and held at this temperature for several hours. The bath temperature was then ramped at approximately 2.5°C/hr down to approximately 2.5°C. Following the cooling ramp, the bath temperature was set to 2° C above the equilibrium and held at this temperature.

To date we have operated the system under constant volume conditions isolating each of the tubes. The pressure in each of the tubes drops as the bath temperature is lowered or when hydrates form. Since each tube is charged with 11cc of test solution, the resulting gas volume for each tube is on the order of 4cc.

IV.F.3. Initial Results. During our initial testing of the apparatus we came across a rather interesting phenomena. The ball travel time at a temperature slightly above the hydrate equilibrium temperature prior to hydrate formation differed from that observed at the same temperature after hydrate formation. In particular, the ball travel time after hydrate formation was longer than prior to hydrate formation. This is shown in Figure 105 for the Green Canyon natural gas and in Figure 106 for methane. These results appear to indicate residual structure in the water after dissociating the hydrate. In Figure 106, a gradual decrease in the ball travel time was observed over a 24 hour period. If these observations are correct, this is the first macroscopic physical property indication of residual structure.

This phenomena of residual structure is not new. Kobayashi has attributed microscopic NMR observations to residual structure. The hysterisis or memory effect (residual structure) observed for hydrate formation is well documented in the literature. Future experiments investigating the relationship of residual structure to onset temperature, degree of super heating, and the effect of the kinetic inhibitors will help to clarify the observations and possibly lead to a quantitative model for the disappearance of the residual structure.

IV. G. Patent Status and Budget Summary

IV.G.1. Patent Summary.

At the end of 1994 the patent status was as follows:

1. The CSM patent on PVP and HEC will probably be issued in February 1995.
2. The claims on the second patent application filing (lactam ring polymers) had been allowed and a patent will probably be issued in the third quarter of 1995.
3. The Shell Oil Company has assigned its European Patent Cooperation Treaty (PCT) patent application to the Colorado School of Mines.
4. A patent application has been filed on the new chemicals listed in this report.

Also at year's end royalty discussions had been initiated with BASF and ISP for PVP, PVCAP, and VC-713. It is hoped that these agreements will be firmly in place before the end of the 1994-95 hydrate season. By our contract all Consortium companies are given royalty-free license to the chemicals developed.

IV.G.2. Budget Summary

A budget summary for each of the last three years (1992, 1993, and 1994) is given in Table 19.

Table 19. Budget Summary for the CSM Hydrate Consortium

YEAR	1992	1993	1994
Salaries	$70,000	$70,000	$70,700
Faculty	14,000	14,000	14,000
Undergraduates	68,000	70,000	55,000
Graduate Students	31,000	25,000	31,000
P/T Sec. & Techcn.		37,000	52,000
Post Doctoral Fellow		11,000	14,000
Consultant			11,000
USGS (CREDA)			4,000
Carleton University			20,000
Patent			
Equipment and Supplies	30,000	30,000	83,700
Travel	12,000	12,000	9,500
Other Costs (Tuit., Fringe Copying, Official Functions)	51,000	50,000	67,000
Overhead	84,000	83,000	114,700
TOTAL	$360,000	$411,000	$526,600

V. Worked Planned for 1995

During the 1995 calendar year we plan to accomplish the following:

A. Finalize the mechanism for hydrate inhibition.

We will continue our adsorption studies with blends of polymers using FT-IR and UV-Visible spectroscopic devices. In 1994 we also initiated NMR Spectroscopy studies of inhibitor performance at the National Research Council in Canada. While the NMR results regarding the mechanism were very promising, they were too premature to report in 1994. We anticipate that this work will come to fruition in 1995.

We will continue to search for other means to modify and enhance our mechanism pictures, such as studies with blends, co-polymers, and homopolymers. For example at the end of 1994 we had contacted crystallization experts (e.g. Dr. A.S. Myerson (Brooklyn Polytechnical University)) with the idea of determining the crystallography of hydrate inhibition. We were evaluating sophisticated computer modelling programs from Molecular Simulations (e.g. Cerius^2) and from Biosym to model hydrate crystal growth and the blockage of that growth.

B. Design and synthesize inhibitors to test our mechanism.

We will continue an active synthesis effort, not only incorporating the THF screening apparatus, but also the new high pressure sapphire apparatus, discussed in detail in Section IV.F.

We will thoroughly characterize these new polymers using a new experimental device, a gel permeation chromatograph (GPC) this device will be extremely useful for measurements of molecular weights, and their distribution.

We expect that the synthesis of new chemicals will lead to better inhibitors than those currently available. Whether those inhibitors are economic relative to those available, remains to be seen.

C. Improve performance of inhibitors without salt.

Since so many field applications deal with a lack of salt, we will begin to search for inhibitors which are efficient with low ionic strength solutions. In the field, after the aqueous salt solution has been separated from the hydrocarbon fluid phase, any aqueous fluid which condenses will contain very low salt amounts; the current inhibitors will be challenged to work in this environment. Section IV.B.2.c.4 describes our success to date with polymers in de-ionized water solutions and provides our current best recommendation. A major challenge is to determine inhibitors which work at high pressure on the ocean floor, in a de-ionized water environment.

D. Act as a forum for sharing field/pilot plant results.

It is our intention to continue to provide as much as one day during our consortium meetings for the sharing of field results. We will also provide an analysis of these results for determination of the practical limits of the inhibitors. A graduate student in Petroleum Engineering may participate in field tests (both onshore and offshore) to gather data.

VI. A Word of Appreciation

The Center for Hydrate Research is grateful for the support of its member companies and hopes that the translation of this research to the field will be of economic use in the prevention of hydrate plugs. Without question, the twelvefold leverage of funds provided by each company has enabled both a substantially greater research effort, and the education of several students (and faculty) who will extend their efforts in the industry.

APPENDICES

Lactam Polymers

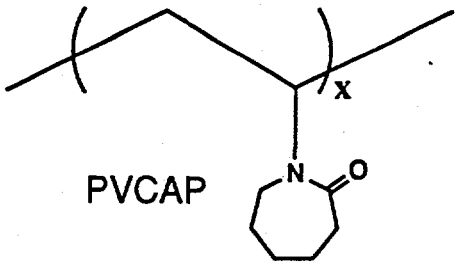

Poly(N-vinylcaprolactam)

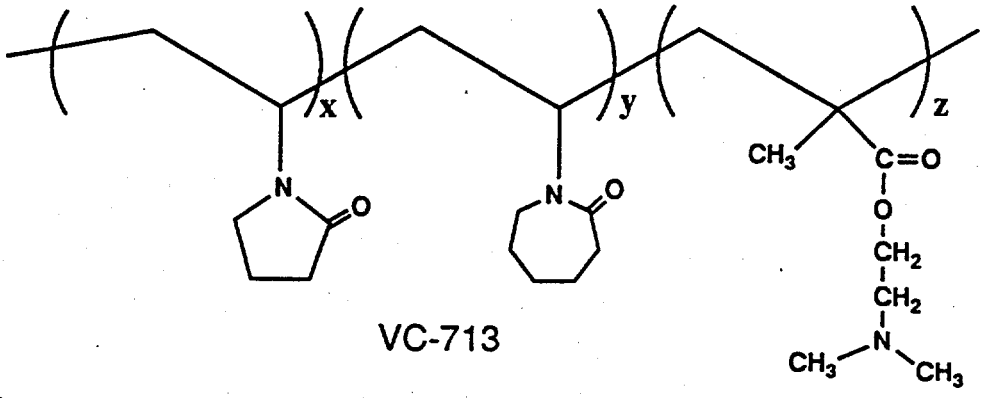

Terpolymer N-vinypyrrolidone/N-vinylcaprolactam/N,N-dimethylaminoethyl methacrylate

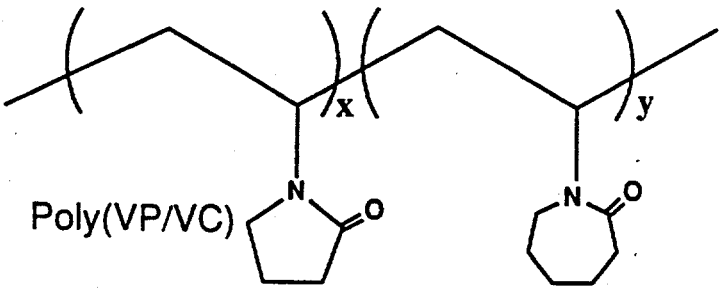

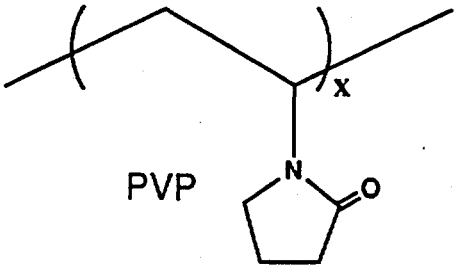

Poly(N-vinylpyrrolidone)

Poly(N-vinylpyrrolidone-co-N-vinylcaprolactam)

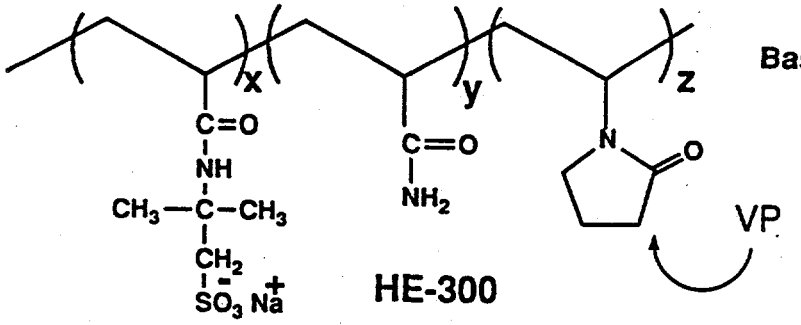

Based on THF- hydrate inhibition

VC-300 =-change caprolactam for VPcomonomer

Appendix: Structures of substituted poly(acrylamides)

(1)

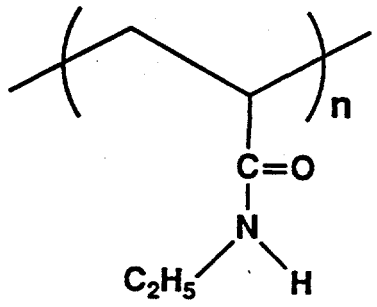

Poly(N-Ethyl Acrylamide)
(PNEAM)

(2)

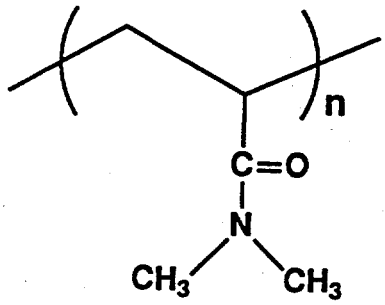

Poly(N,N-Dimethylacrylamide)
(PNNDMAM)

(3)

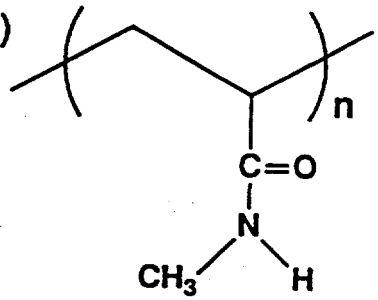

Poly(N-Methyl Acrylamide)
(PNMAM)

(4)

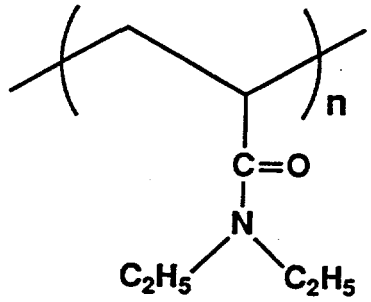

Poly(N,N-Diethylacrylamide)
(PNNDEAM)

(5)

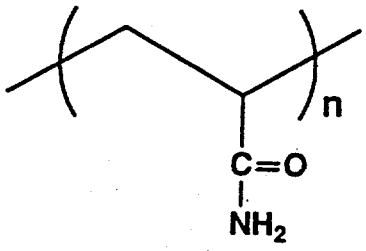

Poly(Acrylamide)
(PAM)

Appendix- continued

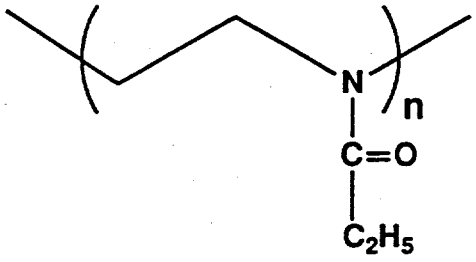

Poly(2-Ethyl-2-Oxazoline)

(P2E2OX)

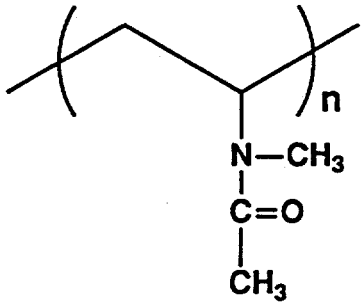

Poly(N-Methyl-N-Vinylacetamide)
(PNMNVAcAM)

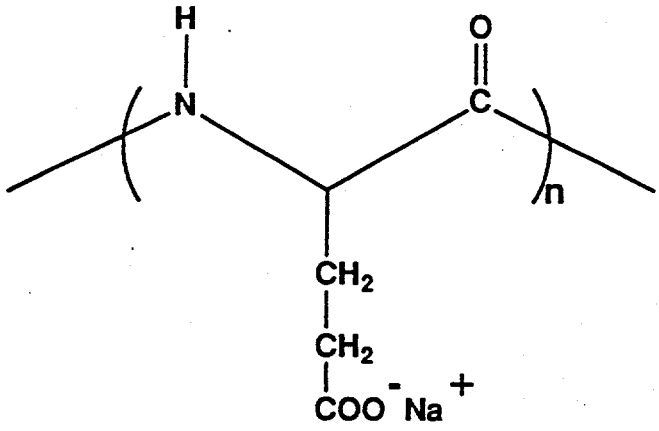

Poly(Sodium-glutamate) - A polypeptide

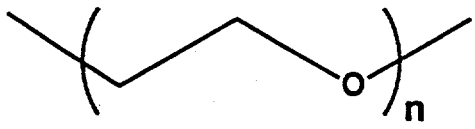

Poly(Ethylene oxide) (PEO)

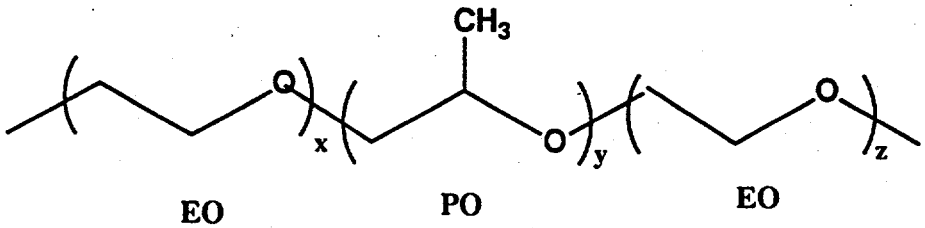

Ethylene oxide-propylene oxide-ethylene oxide tri-block copolymer (F-127)

Appendix-(continued)

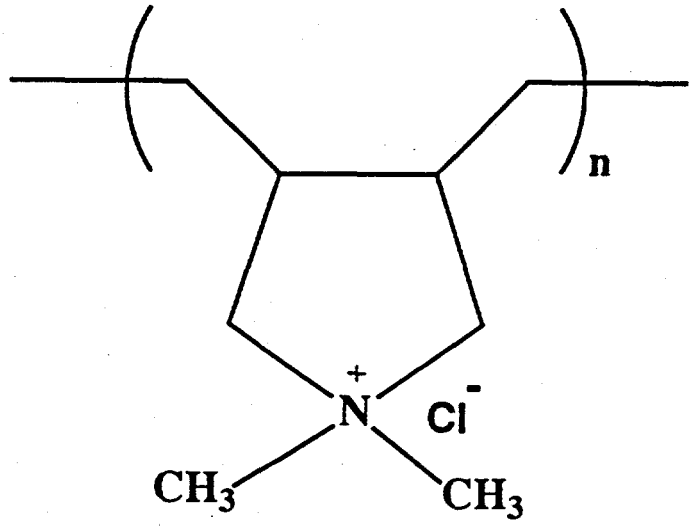

Poly(Diallyldimethylammonium chloride)

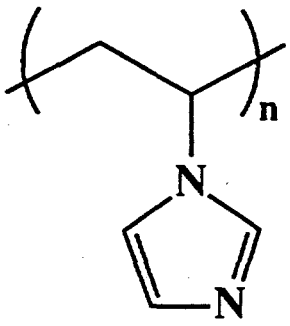

Poly(N-vinylimidazole)

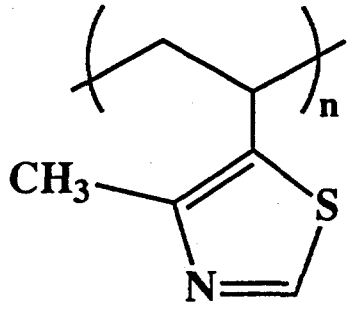

Poly(4-methyl-5-vinylthiazole)

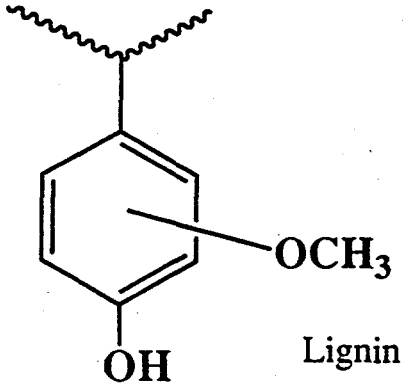

Lignin

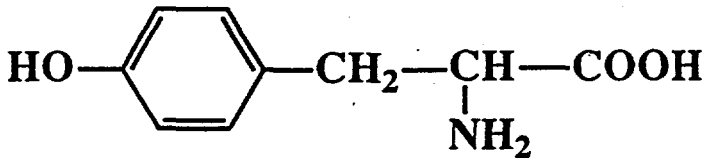

L-Tyrosine

Other Acrylamide Polymers Tested As Inhibitors

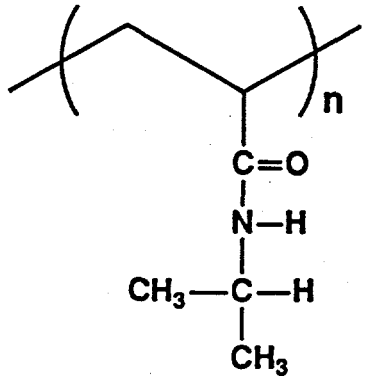

Poly(N-Isopropyl Acrylamide)

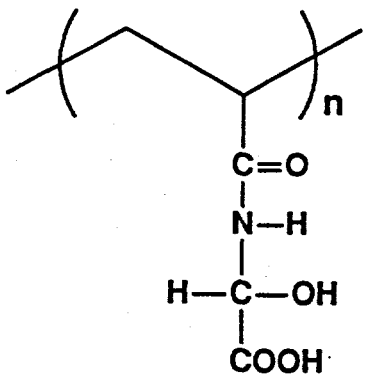

Poly(2-Acrylamidoglycolic Acid) or its sodium salt (PAGANa)

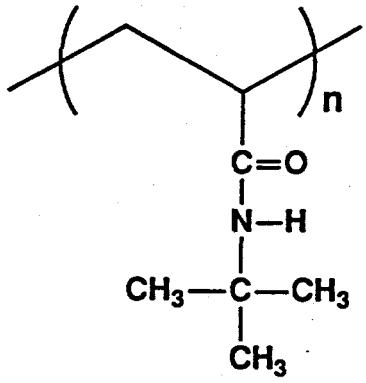

Poly(*t* -Butyl Acrylamide)

Appendix-(continued) Other poly(acrylamides)

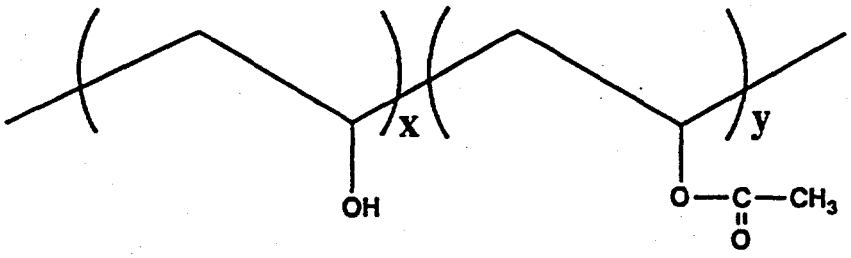

Poly(vinyl alcohol-co-vinyl acetate)

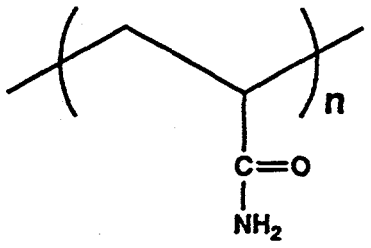

Poly(acrylamide)

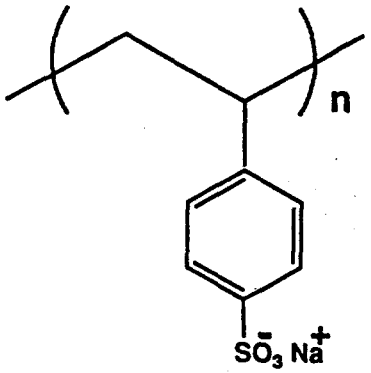

Poly(styrene sulfonate)

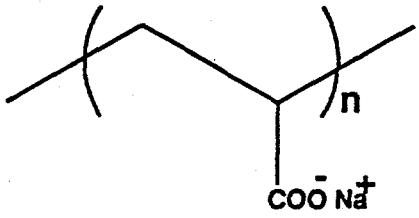

Poly(sodium-acrylate)

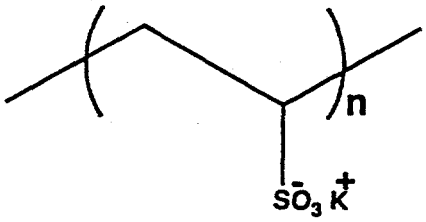

Poly(potassium-vinylsulfonate)

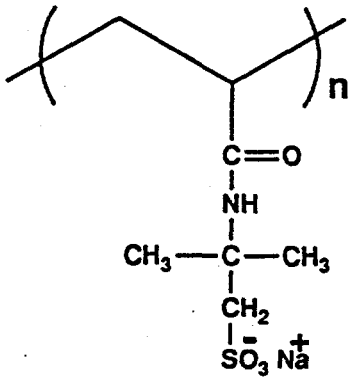

PNaAMPS

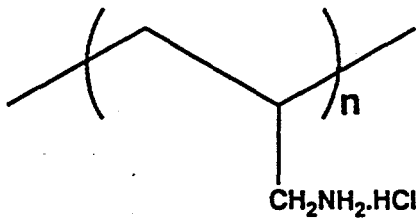

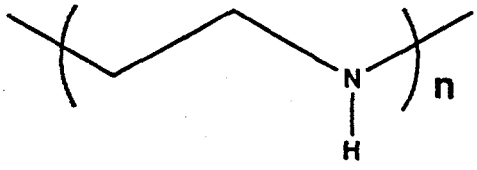

Poly(ethyleneimine)

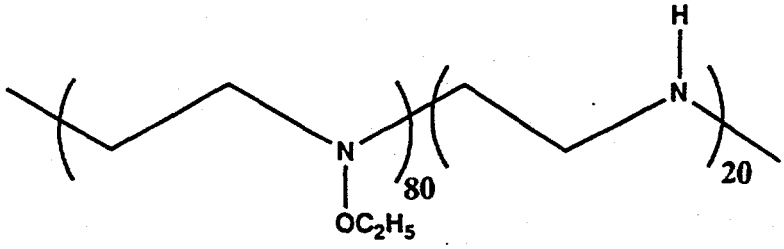

Ethoxylated PEI

Appendix- (Continued)-Common hydrophilic polymers

Polymers Tested As Gas Hydrate Inhibitors

Chemical	Source	THF/Natural Gas (NG)
Alcohols		
1. Poly(Vinyl Alcohol)	Aldrich	Non-Inhibitor
2. Poly(Phenol)-Sulfonated lignin	Arco	Non-inhibitor
Polysaccharides		
3. Methyl Cellulose	Aldrich	Non-Inhibitor
4. Carrageenan-A Polysaccharide	Sigma Chemicals	Non-Inhibitor
5. Argarose	Aldrich	Not soluble in water
Amines/Polyelectrolytes/Ammonium salts		
6. Poly(ethyleneimine)	BASF	Non-Inhibitor
7. Poly(ethyleneimine)-hydrochloride	BASF(+HCl)	Non-Inhibitor
8. Poly(allylamine)-hydrochloride	Aldrich	Non-Inhibitor
9. Poly(Styrene Sulfonate)-Sodium Salt	Aldrich	Non-Inhibitor
10. Poly(Acrylic Acid)-Sodium Salt	Aldrich	Non-Inhibitor
11. Poly(Vinyl Sulfonic Acid)-Potassium salt	Aldrich	Non-Inhibitor
12. Poly(2-Acrylamido-2-methyl Propane Sulfonate)-Sodium Salt [PAMPS]	Aldrich	Non-Inhibitor
13. Sodium dodecyl sulfate (SDS)	Aldrich	No improvement to the KI
14. Dodecyltrimethyl ammonium bromide	Aldrich	No improvement to the KI
15. Tetrabutylammonium fluoride)	Aldrich	THF-hydrate/promoter
16. Tetrabutyl ammonium-PAMS (PAMS is a polymeric anion)	Panch	Non-inhibitor
17. Tetrabutyl ammonium bromide	Chem. Dept.	Non-inhibitor
Amino acids/Polypeptides		
18. L-Tyrosine (mono sodium salt)& (disodium salt)	Fluka/NaOH	Non-Inhibitor
19. L-Tyrosine methyl ester	Fluka	Non-inhibitor
20. Poly(Sodium Glutamate)	Gelest	Non-Inhibitor (THF)
21. Gelatin (Knox brand)	King Soopers	Non-Inhibitor
22. PolyPep-An enzyme digested Calogen	Sigma Chemicals	Non-Inhibitor

Poly(Acrylamides)

23. Urea	Aldrich	Improve the performance of PVCAP (THF Hyd)
24. Poly(Acrylamide) (200K & 10K)	Aldrich (200K) Polysciences (10K)	Non-Inhibitor Non-Inhibitor
25. Poly(Methyl Methacrylamide)	Polyscience	Insoluble In Water
26. Poly(N-Ethyl acrylamide)	Panch	Inhibitor
27. Poly(N, N-dimethylacrylamide)	Panch	THF (X), NG-inhibitor
28. Poly(N, N-Diethylacrylamide)	Panch	Better than PVP
29. Poly(N-Methyl acrylamide)	Panch	Better than PVP
30. Poly(N-Isopropyl acrylamide)	Polyscience	Inhibitor by blending with PVCAP
31. Poly(Tert. butyl acrylamide)	Panch	Insoluble in water
32. Poly(allylurea)	Panch	polymerization in progress

Copolymers

33. Poly(N-vinylpyrrolidone/vinyl acetate) Copolymer (60/40, 50/50, 30/70)	Aldrich	Non-Inhibitor
34. Poly(N-vinylpyrrolidone/styrene) Copolymer (40/60, 30/70)	Aldrich, Monomer-Polymer & Dajack	THF (OK), NG (X)
35. Poly(Tert. butyl acrylamide/N-vinylpyrrolidone) Copolymer (30/70)	Panch	Insoluble in water
36. Poly(2-acrylamidoglycolic acid)-sodium salt	Panch	Gel formation prevent water solubility
37. Poly(N-Vinylcaprolactam/N,N-dimethylacrylamide) Copolymer	Panch	THF(OK), NG (No)
38. Poly(N-Vinylpyrrolidone/N-Ethyl acrylamide) Copolymer (50/50)	Panch	THF(OK), NG (No)
39. poly(N-Vinylcaprolactam/acrylic acid) copolymer	panch	Non-inhibitor
40. Poly(N-Vinylcaprolactam/styrene sulfonate) copolymer	Panch	Non-Inhibitor
41. Poly(N-Vinylcaprolactam/2-acrylamido-2-methyl propane sulfonate-sodium salt) copolymer	Panch	Non-Inhibitor

42. Poly(N-Vinylcaprolactam/acrylamide) copolymer	Panch	Non-Inhibitor (THF)
43. Poly(N, N-Dimethylacrylamide/diacetone acrylamide) copolymer	Panch	Non-Inhibitor (THF)
44. HE-300 (N-vinylpyrrolidone/acrylamide/ 2-acrylamido-2-methyl propane sulfonate sodium salt)	Phillips 66 (Dr. Parrish)	Inhibitor as a blend

Oxazolines

45. Poly(2-Ethyl-2-oxazoline)	Aldrich	Inhibitor as a blend
46. Poly(2-Methyl-2-oxazoline)	Panch	?

Poly(N-Alkyl-N-Vinyl Acetamides)

47. Poly(N-Methyl-N-vinylacetamide)	Panch	Inhibitor as a blend
48. poly(N-vinylformamide)	?	?

Epoxides

49. Poly(ethylene oxide)	Union Carbide	Non-Inhibitor
50. Poly(propylene glycol)	Aldrich	Non-Inhibitor
51. Ethylene oxide-propylene oxide-ethylene oxide terpolymer	BASF	Non-Inhibitor

Other Polymers & small Organics

52. Poly(N-Vinylimidazole)	Panch	THF hyd. Non-Inhibitor
53. Styrene/Maleic Anhydride Copolymer	Aldrich	Non-Inhibitor
54. Poly(N-Vinyl carbozole)	Monomer-Polymer	Insoluble in water
55. Poly(N-Vinyl succinimide)	-	Insoluble in water
56. Poly(4-Methyl-5-vinylthiazole)	Panch	Insoluble in water
57. Cyanuric acid	Aldrich	Not soluble in water
58. Babituric Acid (similaar to cyanuric acid)	Aldrich	Non-Inhibitor
59. Murexoide (similaar to cyanuric acid)	Aldrich	?
60. 1,3-Dimethylbabituric acid (similaar to cyanuric acid)	Aldrich	limited solubility Non-Inhibitor
61. Poly(pyridine -N-oxide)	Aldrich	Non-Inhibitor

Modified Polymers

62. Partially hydrolyzed PVCAP	Panch	Reduced Inhibition than PVCAP
63. Partially hydrolyzed poly(2-ethyl-2-oxazoline)	Panch	No enhancement in performance compared to virgin material
64. Protonated VC-713	Panch	decreased performance compared to virgin material (THF-hyd.)
65. Partially acetylated poly(ethyleneimine)	Panch	Performance Improved than virgin material

UV-Vis. Calibration Curve For Poly(VP/NEAM) Copolymer at 220 nm

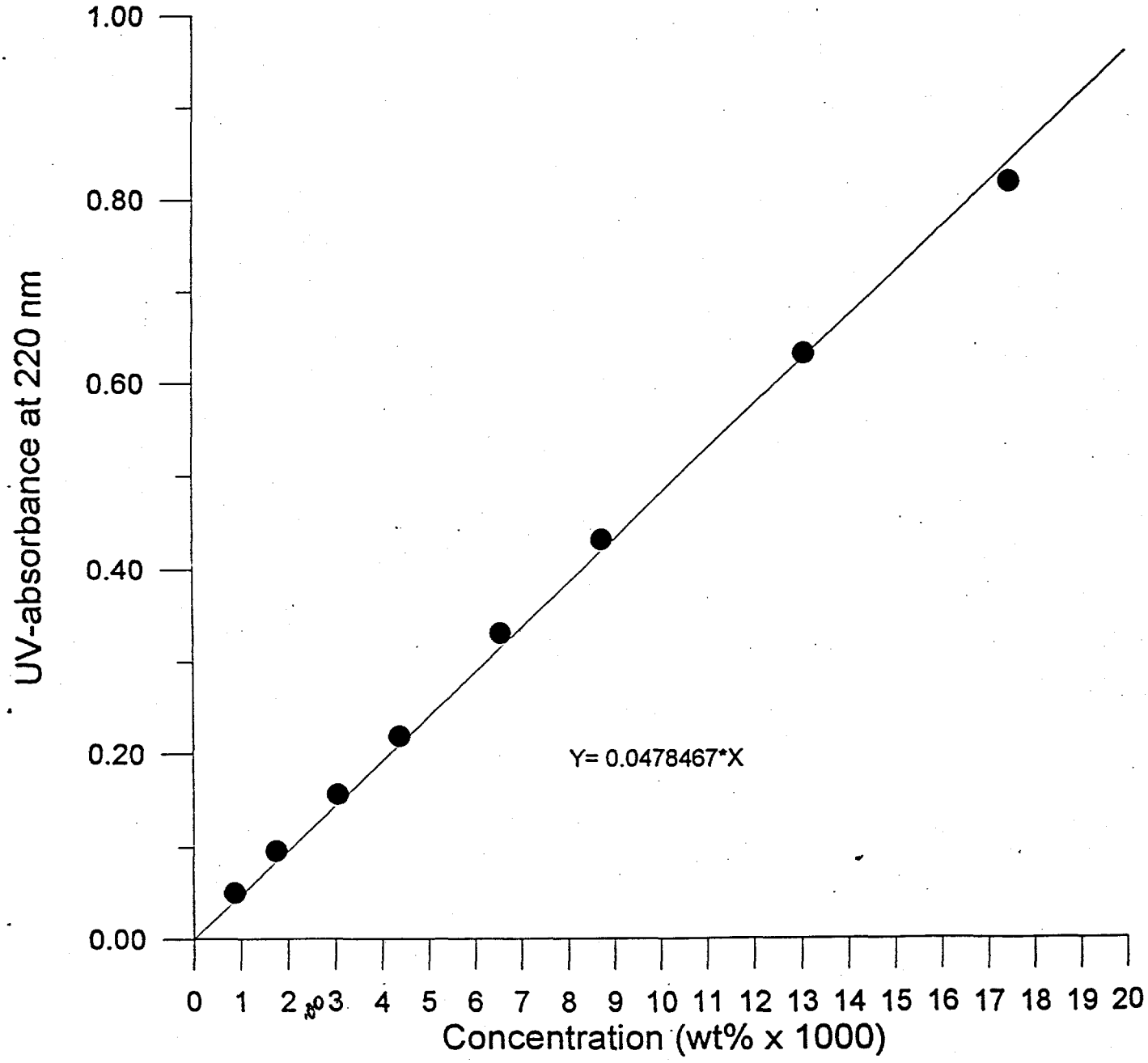

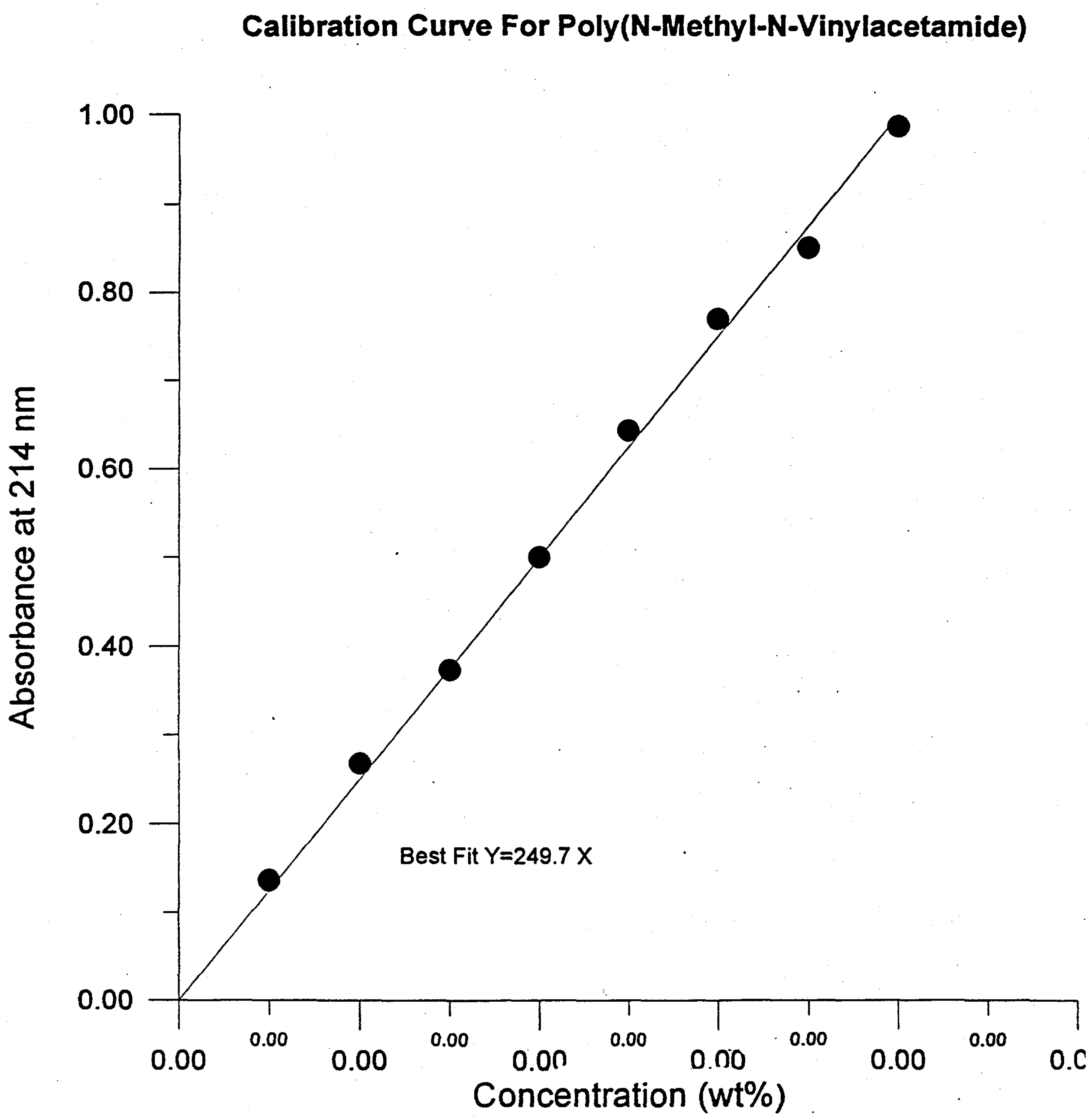
Calibration Curve For Poly(N-Methyl-N-Vinylacetamide)
Absorbance at 214 nm
1.00
0.80
0.60
0.40
0.20
0.00
Best Fit Y=249.7 X
0.00
0.00
0.00
0.00
0.00
0.00
0.00
0.00
0.00
0.00
0.00
0.00
0.00
0.00
0.0
Concentration (wt%)

Poly(Styrene Sulfonate)-Sodium salt; 254 nm, DI Water

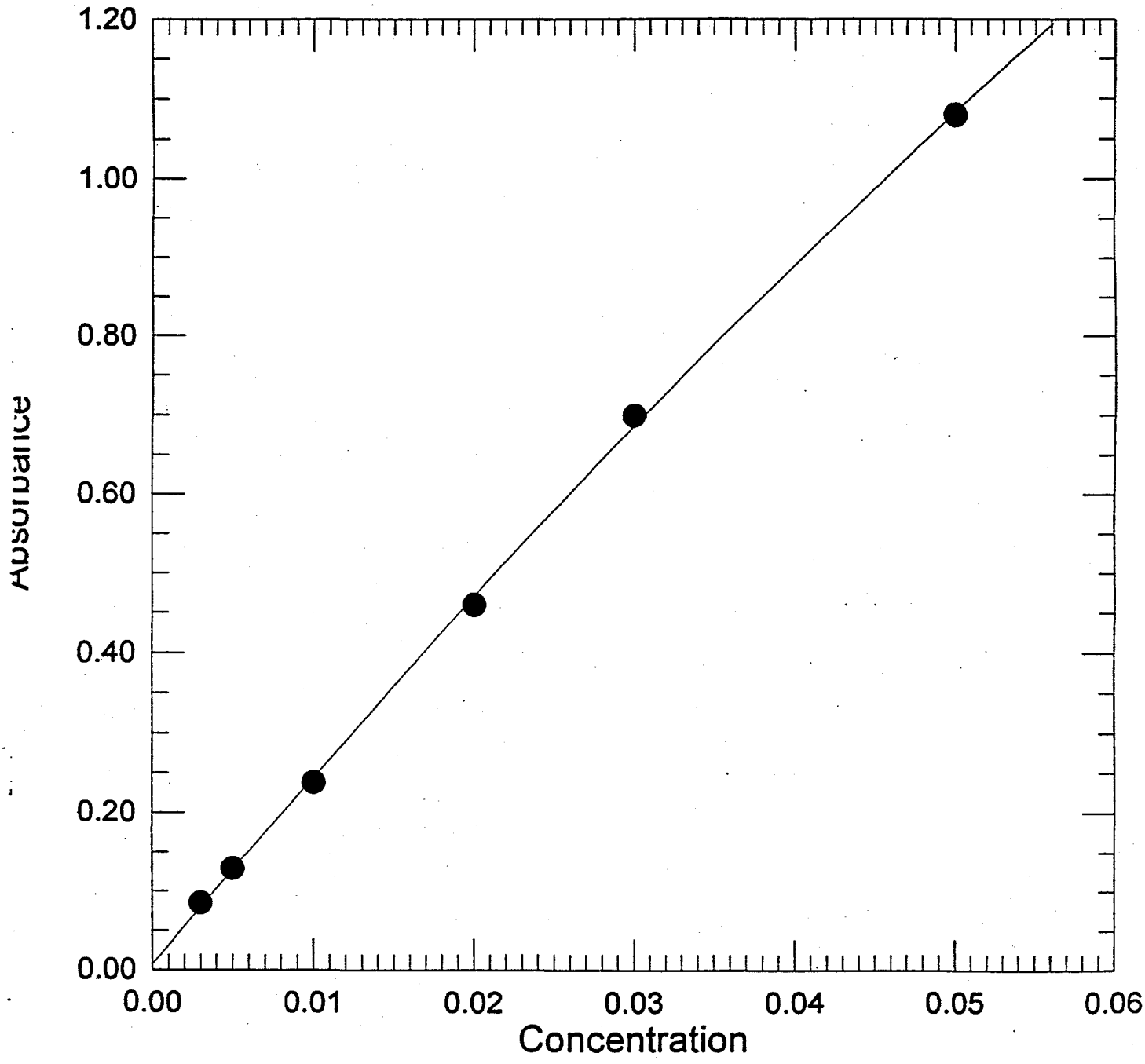

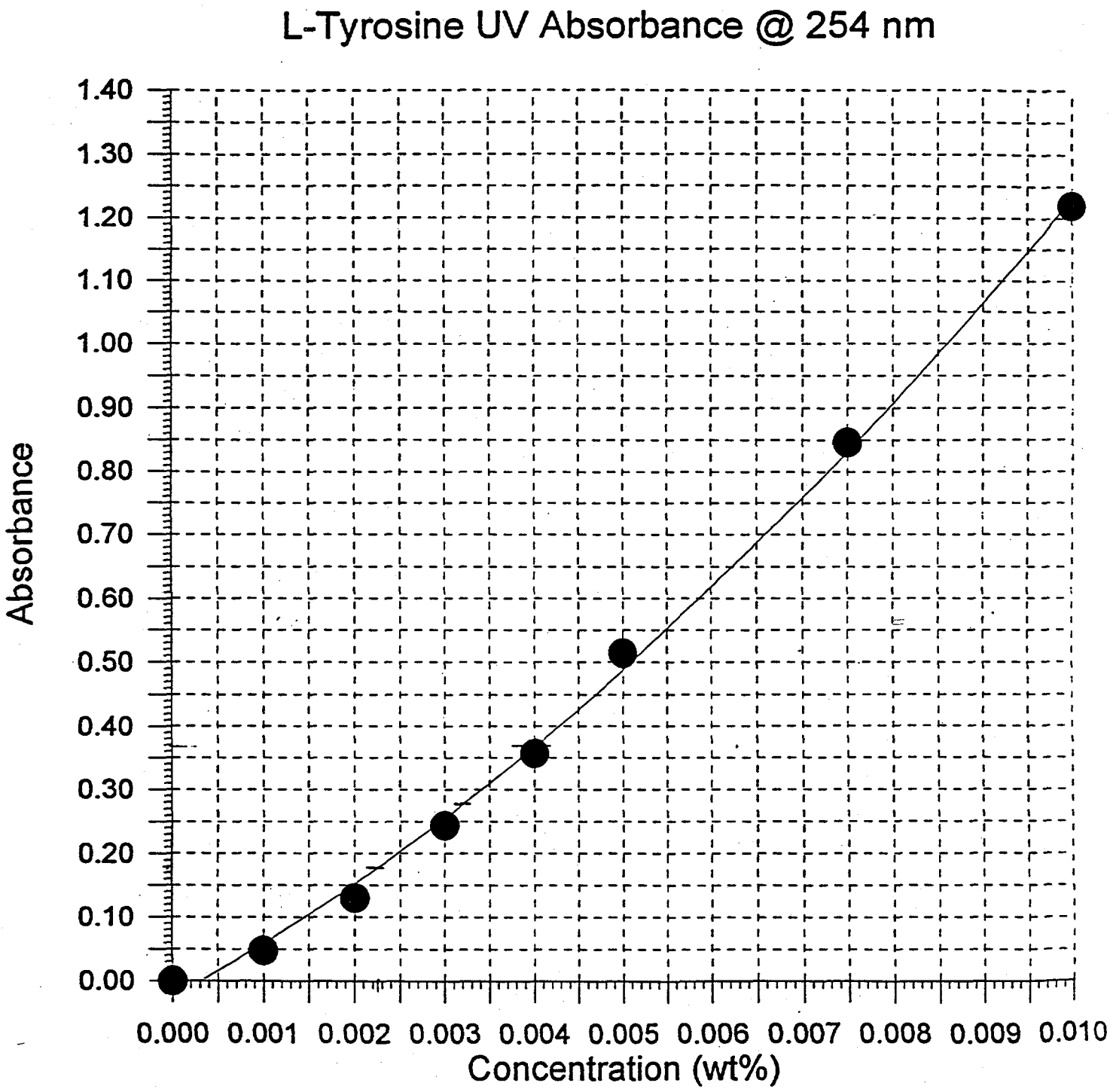
L-Tyrosine UV Absorbance @ 254 nm
Absorbance
1.40
1.30
1.20
1.10
1.00
0.90
0.80
0.70
0.60
0.50
0.40
0.30
0.20
0.10
0.00
0.000 0.001 0.002 0.003 0.004 0.005 0.006 0.007 0.008 0.009 0.010
Concentration (wt%)

Appendix C.

A Compact Model for Hydrate Formation

Richard L. Christiansen and E. Dendy Sloan, Jr.
Center for Hydrate Research
Colorado School of Mines
Golden, Colorado 80401

Abstract

Quiescent drop ethane hydrate growth rate data from this laboratory are shown to be comparable with stirred growth data from Bishnoi's laboratory, when compared on the basis of gas-liquid interfacial area. The specific Gibbs free energy change (Δg) is shown to correlate the hydrate growth rate data from both laboratories. In addition, Δg correlates data for induction times, both for ethane and for natural gas data from a third (Yousif's) laboratory. These correlations form the basis for a simple hydrate formation model which may be suitable for incorporation in a pipeline simulator. The macroscopic model reflects a molecular mechanism proposed earlier.

1. Introduction

The formation of hydrates is of central interest to the energy industry because these compounds can plug transmission channels. Cubic structure I (CSI) and cubic structure II (CSII) hydrates (Dyadin et al., 1991) are found in both the laboratory and in industrial practice, but the more recently discovered structure H (HSIII) hydrate (Ripmeester et al., 1987) has been limited to date to the laboratory. Consequently the present work deals with the former two structures. The time-independent, thermodynamic nature of CSI and CSII hydrates have been quantified with acceptable accuracy for industrial applications. The last decade has witnessed a change in the state-of-the-art to a study of the time-dependent, kinetic nature of hydrate formation.

Typical data for hydrate nucleation and growth are shown in Figure 1. In the figure the fraction of water converted to hydrate is shown as a function of time, with the induction time (the end of the nucleation period) marked as the time of data departure from the abscissa, and the growth rate typically taken as the most linear portion of the water conversion curve.

Macroscopic models for hydrate growth rate have been generated by the group of Bishnoi (see for example, Englezos et al. 1987; Dholabhai et al. 1993). However due to its stochastic nature, only a few attempts have been aimed at modeling the nucleation rate (Bishnoi et al. 1994).

Two microscopic mechanisms have been proposed, each having some elements in common. The mechanism of Lekvam and Ruoff (1993) is an autocatalytic model based on instability theory.

Recently Christiansen and Sloan (1994) proposed a mechanism extending similar mechanisms from this laboratory (Sloan, 1990a; Sloan and Fleyfel, 1991; Müller-Bongartz, et al., 1992). We proposed that the following steps, shown in Figure 2, were essential to nucleation and growth:

1. Labile clusters of water molecules with particular coordination numbers exist around dissolved apolar natural gas molecules.
2. Hydrate formation consists of joining these clusters together.
3. Clusters may transform from one coordination number to another upon joining.
4. While CSI has no distinguishing alternatives for joining hexagonal faces, CSII has two alternatives, which leads to many competing structures and slows hydrate nucleation and growth.

From the perspective of the above four elements, induction times for hydrate nucleation of methane, ethane, propane, carbon dioxide, and blends of these species of natural gas were qualitatively predicted, and then confirmed experimentally (Bansal, 1994; Christiansen and Sloan, 1994).

In Section 2 we present some experimental observations about common aspects of hydrate formation and growth. In Section 3 an exposition of the driving force for hydrate formation is shown to correlate growth rates and induction times. Sections 4, 5, and 6 respectively present the model, its implications, and a method for its use.

2. Observations on Kinetics of Hydrate Growth

When small aggregates of hydrate exceed a critical size, then the aggregates begin to grow. Although hydrate nucleation is probably not heat or mass transfer limited, growth is limited by both transfer processes. The rate of growth of a hydrate crystal surrounded by liquid is severely limited by diffusion of dissolved gas species. But growth is quite rapid where the gas phase, the aqueous phase, and the hydrate phase are in intimate contact (Long, 1994).

Bansal (1994) measured growth rate of ethane hydrate from an aqueous drop (1-2 mm diameter) resting on a metal pedestal as shown in Figure 3. Interested readers are referred to the thesis of Bansal for detailed experimental information. Surprisingly, the growth rates per unit surface area of the drop are comparable o rates measured in a vigorously stirred (400 rpm) reactor, as reported by Englezos et al. (1987). For the drop, the growth rates ranged from 2×10^{-8} to 2×10^{-6} moles/cm^2/s. In the stirred reactor, the ethane hydrate growth rates ranged from 7×10^{-8} to 2×10^{-7} moles/cm^2/s, based upon the cited gas-liquid surface area of 128 cm^2.

In Bishnoi's laboratory, Dholabhai et al. (1993) and Englezos et al. (1987) reported that stirring eliminates mass

transfer resistance around particles of hydrate dispersed in the aqueous phase. The approximate equivalence of rates from the small drop reactor and the vigorously stirred reactor suggests a different explanation. Perhaps, stirring breaks up the hydrate particle-layer at the gas-liquid interface such that intimate contact of the three phases (hydrate, aqueous phase, and gas) is maximized.

3. Driving Force for Hydrate Formation

In the next section we formulate a kinetic model for the rate of hydrate formation in which rate is a function of driving force and resistance. Before that model can be formulated, a quantitative description of the driving force is needed. A satisfactory driving force should correlate the experimentally observed growth rates and nucleation rates (or induction times).

Some researchers (Englezos et al. 1987) have chosen to use the extent of overpressure, defined as either the pressure (or fugacity) above the equilibrium value at a given temperature, as a measure of the driving force. Others (Yousif, 1994) have chosen the extent of subcooling (below the equilibrium temperature at a given pressure) as the driving force. Bishnoi et al. (1994) chose to use the ratios of fugacities ($f_i^{exp}/f_i^{equ} -1$) as a driving force. Here, we propose a description of driving force as the change in Gibbs free energy when hydrates form.

Change in Gibbs free energy is often used for indicating direction of movement toward equilibrium. Under the constraints of constant temperature and pressure, processes move toward a minimum value of Gibbs free energy. Thus we propose a driving force for hydrate formation in terms of Gibbs free energy change.

To describe the Gibbs free energy change for hydrate formation, a procedure is recognized from chemical reaction equilibrium (Kyle, 1992). The procedure is outlined in Figure 4. The value of ΔG^{exp} represents the change in Gibbs free energy at experimental conditions. The change in Gibbs free energies can be written as

$$\Delta G^{exp} = \Delta G_R + \Delta G_P \qquad (1)$$

with

$$\Delta G_R = \sum_{i=1}^{N} (\mu_i^{equ} - \mu_i^{exp})\, n_i \qquad (2)$$

and

$$\Delta G_P = \sum_{i=1}^{N} (\mu_i^{exp} - \mu_i^{equ})\, n_i \qquad (3)$$

Excess water, excess gas, or other chemicals in a reaction vessel that do not participate in hydrate formation in an

experiment are not included in the summations of Equations (2) and (3).

For any species i experiencing a change at constant temperature from some condition 1 to some condition 2, the change in chemical potential is

$$\mu_i^2 - \mu_i^1 = \mathcal{R}T \ln \left(\hat{f}_i^2 / \hat{f}_i^1 \right) \qquad (4)$$

Expressions of the form of Equation (4) can be substituted for each species in Equations (2) and (3). But for the essentially incompressible liquid water and solid hydrates, it is more convenient to use the Poynting correction

$$\mu_i^2 - \mu_i^1 \cong v_i \, (P^2 - P^1) \qquad (5)$$

The molar volumes v_i in Equation (5) are average values for the pressure considered. The molar volume of hydrate v_h is defined as the volume of hydrate per mole of water in the hydrate. Combining Equations (1) through (5), the total change of Gibbs free energy in an experiment is

$$\Delta G^{exp} \cong n_w v_w (P^{equ} - P^{exp}) + \mathcal{R}T \sum_{i=1}^{N} n_i \ln(\hat{f}_i^{equ}/\hat{f}_i^{exp}) + n_w v_h (P^{exp} - P^{equ}) \qquad (6)$$

On a basis of a mole of water consumed, the expression for the change of specific Gibbs free energy Δg ($= \Delta G^{exp}/n_w$) may be written as

$$\Delta g = \Delta G^{exp}/n_w \cong v_w (P^{equ} - P^{exp}) + \mathcal{R}T \sum_{i=1}^{N} (n_i/n_w) \ln(\hat{f}_i^{equ}/\hat{f}_i^{exp}) + v_h (P^{exp} - P^{equ}) \qquad (7)$$

As a simple example of the use of Equation (7), consider the application to an experiment in which pure water and pure ethane are converted to CSI hydrate. For that case,

$$\Delta g^{exp} \cong v_w (P^{equ} - P^{exp}) + (n_{ethane}/n_w) \mathcal{R}T \ln (f_{ethane}^{equ}/f_{ethane}^{exp}) + v_h (P^{exp} - P^{equ}) \qquad (8)$$

The ratio n_{ethane}/n_w may be calculated at the equilibrium condition using the van der Waals and Platteeuw (1959) model with the computer program CSMHYD (Sloan, 1990b). The ratio of

fugacities can be estimated with an equation of state. An example calculation with Equation (8) is shown in Table 1. The fugacities are estimated with the Peng-Robinson equation of state.

The first and third term (to the right of the equal sign) in Equation (8) are of equal magnitude but opposite sign, so their sum is approximately nil. The second term in Equation (8) is an order of magnitude higher than either of the others, so that it is the most significant contributor to the total change in the Gibbs free energy. The change in Gibbs free energy per mole of consumed water is negative, indicating that the hydrate is thermodynamically favored at experimental conditions.

Table 1. Driving Force for Ethane Hydrate Formation at 277.8 K

Press kPa	Fugacity kPa	Terms in Equation (8), J/mol Term 1	Term 2	Term 3	Δg J/mol
848(equl)	776	0.0	0.0	0.0	0.0
1148	1018	-5.4	-81.2	6.3	-80.3
1448	1242	-10.8	-140.9	12.6	-139.1
1748	1448	-16.2	-187.2	18.9	-184.5
2048	1638	-21.6	-224.2	25.2	-220.6
2348	1811	-27.0	-254.3	31.5	-249.8

Figure 5 shows the ethane hydrate growth rate plotted against the driving force for the quiescent drop data (open triangles) from this laboratory (Bansal, 1994) and for the data (filled triangles) of Englezos et al. (1987), which were obtained in an agitated (400 rpm) cell. A single correlation which provides a reasonable fit to both sets of growth data is given by

$$\ell n\ r_g = 0.00614\ \Delta g - 17.8 \qquad (9)$$

Equation (9) shows the specific rate (r_g) and driving force (Δg) explicitly; resistances are incorporated in the constants.

Similarly, Figure 6 shows ethane hydrate nucleation induction time (defined in the Section 1 and in Figure 1) to be well correlated by the Δg driving force:

$$\ell n\ t_{ind} = -0.0102\ \Delta g + 6.29 \qquad (10)$$

It is surprising that Equation (10) also correlates the induction time of the natural gas mixture studied by Yousif (1994) as shown in Figure 7. Yousif's natural gas had the composition: 0.39 mol% N_2, 87.26% CH_4, 7.57% C_2H_6, 3.10% C_3H_8, 0.49% i-C_4H_{10}, 0.79% n-C_4H_{10}, 0.20% i-C_5H_{12}, 0.20% n-C_5H_{12}.

One might ask if Equation (8) can be related to the driving force used by Bishnoi et al. (1994). Because the second term in Equation (8) dominates, then

$$\Delta g^{exp} \cong (n_{ethane}/n_w)\ RT\ \ell n\ (f^{equ}_{ethane}/f^{exp}_{ethane}) \quad (11)$$

The logarithm term can be approximated by the first term in an infinite expansion

$$\ell n\ x = (x - 1) - \ldots \quad (12).$$

When the fugacity ratio of Equation (11) is taken as x in Equation (12), one recognizes the driving force of Bishnoi, shown to be a good approximation for fugacity ratios less than 1.3. Figure 8 indicates other possible driving force definitions, shown as approximations to the logarithm term.

4. Model Development

We consider the rate of hydrate formation to be a linear combination of the nucleation rate R_n and the growth rate R_g:

$$dn_h/dt = R_n + R_g \quad (13)$$

where

n_h = moles of water in the hydrate phase.

In the present model we take the process of nucleation to be a volume-controlled phenomenon, with the rate written as the product of the moles and volume of water in the aqueous phase, $n_w v_w$, multiplied by a nucleation rate per unit volume of water, r_n:

$$R_n = n_w v_w\ r_n \quad (14)$$

where

n_w = moles of water in the aqueous phase, and
v_w = partial molar volume of aqueous phase water.

Other choices for nucleation rate are possible, but Equation (14) is both simple and convenient for the model.

While nucleation appears to be volume-controlled, hydrate growth requires several orders of magnitude more gas and water than are soluble in either the bulk gas or liquid phases. Microvideo recordings of experiments in our laboratory (Bansal, 1994; Long, 1994) indicate that hydrate growth occurs at the gas-water interface.

Growth in either bulk phase is severely hindered by mass transfer; hydrate formation at the interface acts as a barrier to the transport of each fluid phase. In addition, the concentration of gas in the aqueous phase (and that of water in the gaseous phase) is much lower than that required for hydrate formation.

Our experimental results indicate that growth rate is proportional to the area A_{gwh} of "intimate contact" between gas, aqueous, and hydrate phases multiplied by the growth rate per unit area, r_g:

$$R_g = A_{gwh}\, r_g \tag{15}$$

If a hydrate particle is separated from the gas phase by an aqueous film that is 0.1 cm thick the characteristic time for diffusion through the film ($t = \Delta\ell^2/\mathcal{D}_{\mathcal{AB}}$) is on the order of 1000 seconds; for a film 0.01 cm thick the characteristic time is on the order of 10 seconds. From these estimates, it seems clear that rapid hydrate growth would occur for a film thickness of 0.01 cm and smaller.

We approximate A_{gwh} as the product of A_{gw}, the surface area between the gas and aqueous suspension, times the bulk mole fraction of hydrate and water:

$$A_{gwh} = A_{gw}(n_h n_w / n_{wT}^2) \tag{16}$$

where

n_{wT} = total moles of water present ($n_h + n_w$), a constant.

Combining equations (1) through (4), we obtain:

$$\frac{d}{dt}\left(\frac{n_h}{n_{wT}}\right) = v_w r_n \left(\frac{n_w}{n_{wT}}\right) + \frac{A_{gw} r_g}{n_{wT}} \left(\frac{n_h}{n_{wT}}\right)\left(\frac{n_w}{n_{wT}}\right) \tag{17}$$

where both sides have been divided by a constant, n_{wT}.

Equation (17) has a form that resembles a rate expression for a first order reaction in parallel with a second order autocatalytic reaction, producing species B from species A:

First Order: $\mathcal{A} \rightarrow \mathcal{B}$ (18)

Second Order Autocatalytic: $\mathcal{A} + \mathcal{B} \rightarrow 2\mathcal{B}$ (19)

where A and B might represent concentrations of labile clusters and hydrate aggregates respectively, as shown in Figure 2.

If k_n and k_g are rate constants for the two above equations, then the rate of production of B is:

$$\left(\frac{d\mathcal{B}}{dt}\right) = -\left(\frac{d\mathcal{A}}{dt}\right) = k_n\, \mathcal{A} + k_g\, A\, \mathcal{B} \tag{20}$$

The steps in the development of Equation (17) were chosen so as to produce similarity with Equation (20). Equation (20) is the simplest equation which can represent the behavior shown in

Figure 1.

At the same time, the model of Equation (17) is only as complex as the quality and quantity of data permit. Although other expressions than Equation (17) for the combined rate of nucleation and growth are possible, the expression is likely the simplest which embodies the two essentials of hydrate formation: induction time followed by rapid growth.

Equation (17) can be integrated to obtain

$$\frac{n_h}{n_{wT}} = \frac{1 - \exp[-k_n(1+\beta)t]}{1 + \beta \exp[-k_n(1+\beta)t} \qquad (21)$$

where the constants k_n, k_g, and β are defined as

$$k_n = v_w r_n, \qquad (21a)$$

$$k_g = A_{gw} r_g / n_{wT}, \text{ and} \qquad (21b)$$

$$\beta = k_g/k_n = A_{gw} r_g/(v_w r_n n_{wT}). \qquad (21c)$$

5. Implications of Model

An essential feature in the development of Equation (21) is that growth of hydrate dominantly occurs at the area of intimate contact between the gas, aqueous, and hydrate phases. If hydrate formation nucleates in the bulk aqueous phase, initial hydrate growth will be severely limited by mass transfer. Hydrate growth in the bulk liquid is not modeled by Equation (21). The model described by Englezos et al. (1987) is more appropriate for describing hydrate formation in the bulk phase.

Figure 9 shows the relationship between conversion and time in Equation (21), with somewhat arbitrarily chosen values for k_n and k_g, where $n_{wT} = 1$. Such behavior reflects the experimental observations reported by Bansal (1994) and by Christiansen et al. (1994).

The maximum growth rate predicted by Equation (21) occurs at 50% conversion. The induction time is defined as the intersection of the maximum growth rate line with the abscissa. For values of rate constants in the range of those used in Figure 9, the induction time (t_{ind}) is given as:

$$t_{ind} = (\ell n\ \beta - 2)/k_g \qquad (22)$$

Substituting the definition for β in Equation (21), we obtain a relation between induction time and the specific nucleation and growth rates, k_n and k_g:

$$t_{ind} = (\ell n\ k_g - \ell n\ k_n - 2)/\ k_g \qquad (23)$$

Equation (23) clearly shows that the induction time is inversely proportional to the specific growth rate, while t_{ind} is a weaker (logarithmic) function of the nucleation rate. For the values used in Figure 9, doubling k_g will decrease the induction time by about 50%, while doubling k_n will decrease induction time by less than 5%. The k_n must be multiplied by about 4000 in order to decrease the induction time by 50%.

Induction times are often considered an indication of nucleation rate. However, according to Equation (23), induction time is much more sensitive to growth rate than to nucleation rate. Poor reproducibility of induction times may indicate variations in growth rates rather than nucleation rates.

If we solve Equation (23) for k_n and substitute the definitions of k_n and k_g, an expression for nucleation rate per unit volume is obtained:

$$\ell n\ r_n = \ell n \frac{A_{gw}\ r_g}{n_{wT}\ v_w} - \frac{A_{gw}\ r_g\ t_{ind}}{n_{wT}} - 2 \qquad (24)$$

Equation (24) provides a means for calculating the rate of nucleation from growth rate and induction time data. Equation (24) is the last expression needed to relate experimental observations to the parameters of the hydrate formation model given in Equations 21, 21a, 21b, and 21c.

Figure 9 also shows the result of increasing the driving force. An increase in the driving force increases the growth rate, and decreases the induction time, as predicted earlier by inspection of Equations (9), (10), and (23). The model thus indicates that high growth rates will cause the rapid growth of nuclei, and shorten the induction time.

6. Method for Model Use

Using the model given above one may determine the growth of hydrate as a function of time. One might generate a curve similar to that shown in Figure 9 in order to determine when a fraction of the water would be converted, as a beginning indication of flow channel blockage. The steps to such a process are as follows:

1. Calculate the driving force, Δg as shown in Section 3 with Equation (7).

2. Use the correlation of Equation (10) to determine the induction time (t_{ind}) before hydrate growth begins. This value provides an estimate of when hydrate formation will begin; no further calculation may be needed for some process engineers.

3. Use the correlation of Equation (9) to determine the growth rate r_g from the Δg value calculated in Step 1.

4. Calculate the growth rate parameter kg from Equation (21b) using rg, an estimate of the vapor-liquid surface area, and the total moles of water.

5. With t_{ind} and r_g calculate the specific nucleation rate r_n using Equation (24). Calculate k_n via Equation (21a).

6. Using Equation (21), calculate the fractional conversion of total water to hydrate as a function of time.

7. Conclusion

A thermodynamic driving force has been proposed that correlates both hydrate induction time and growth rate. The driving force correlates data from quiescent and stirred reactors. The similarity of growth rates in quiescent and stirred reactors reflects the dominance of hydrate growth at the gas-liquid interface.

The two correlations fit kinetic data from three laboratories, for ethane hydrates and natural gas hydrates. With the two correlations, a compact model is proposed which may be used in pipeline simulators. The model reflects molecular mechanisms for hydrate formation.

8. Acknowledgments

The Gas Research Institute (Contract No. 5091-260-2124) and the Gas Processors Association supported the hydrate data gathering portion of this work. Ms. Vibha Bansal, Mssrs. Jim McCulloch and Kevin Wagner performed the measurements.

10. References

Bansal, V.: Kinetic Study of Clathrate Hydrates, M.S. Thesis T-4545, Colorado School of Mines, (January 1994)

Bishnoi, P.R., Natarajan, V., and Kalogerakis, N., "A Unified Description of the Kinetics of Hydrate Nucleation, Growth, and Decomposition," Proceedings of the First International Conference on Hydrates, *Annals of the New York Academy of Science*, 715, 311 (1994)

Christiansen, R.L. and Sloan, E.D., Jr.: "Mechanisms and Kinetics of Hydrate Formation," Proceedings of the First International Conference on Hydrates, *Annals of the New York Academy of Science*, 715, 283 (1994)

Dholabhai, P.D., Kalogerakis, N., and Bishnoi, P.R.: "Kinetics of Methane Hydrate Formation in Aqueous Electrolyte Solutions," Can. J. Chem. Eng., 71, 68 (1993)

Dyadin,Y.A., Bondaryuk, I.V., Shurko, F.V., "Clathrate Hydrates at High Pressures," Inclusion Compounds, v.5, pg 213, Atwood, et al., eds., Oxford Univ. Press, (1991)

Englezos, P., Kalogerakis, N., Dholabhai, P., and Bishnoi, P.R.: "Kinetics of Formation of Methane and Ethane Gas Hydrates," Chem. Eng. Sci., 42, 2647 (1987)

Kyle, B.G., Chemical and Process Thermodynamics, 2nd Ed., 342-344, Prentice Hall, Englewood Cliffs (NJ), 1992

Lekvam, K. and Ruoff, P.: "A Reaction Kinetic Mechanism for Methane Hydrate Formation in Liquid Water," J. Am. Chem. Soc., 8565, 115, (1993)

Long, J.P.: Gas Hydrate Formation Mechanism and Kinetic Inhibition, Ph.D. Thesis T-4265, Colorado School of Mines, (April 1994)

Müller-Bongartz, B., Wildeman, T.R., and Sloan, E.D., Jr.: "A Hypothesis for Hydrate Nucleation Phenomena," Proc. 2nd Int. Offshore and Polar Eng. Conf., 628, San Francisco, June (1992)

Ripmeester, J.A., Tse, J.S., Ratcliffe, C.I., Powell, B.M., "A New Clathrate Hydrate Structure," Nature, 135, 325 (1987)

Sloan, E.D., Jr.: "Hydrate Nucleation from Ice," Proc. 69th Ann Gas Proc. Conv., 8, Phoenix, AZ, March (1990a)

Sloan, E.D., Jr.: Clathrate Hydrates of Natural Gases, Appendix B and accompanying software, Marcel Dekker, New York (1990b).

Sloan, E.D.,Jr. and Fleyfel, F.: "A Molecular Mechanism for Gas Hydrate Nucleation from Ice," AIChE Journal, 1281, 37, (1991)

van der Waals, J.H. and Platteeuw, J.C.: "Clathrate Solutions," Adv. Chem. Phys., 1, 2 (1959)

Yousif, M.H.: "The Kinetics of Hydrate Formation," SPE 28479, presented at SPE Annual Technical Conference and Exhibition, New Orleans, 25-28 September 1994.

11. Nomenclature

A = area, cm^2
$\mathcal{A}$ = moles of species $\mathcal{A}$
$\mathcal{B}$ = moles of species $\mathcal{B}$
$\mathcal{D}$ = Diffusivity, cm^2/s
$\hat{f}$ = fugacity of a component in a mixture, kPa

G = Gibbs free energy, J
g = specific Gibbs free energy, J/mol
k_n = nucleation rate constant, sec^{-1}
k_g = growth rate constant, $(mole \cdot sec)^{-1}$
ℓ = stagnant film thickness, cm
N = number of components
n = number of moles
P = pressure, kPa
R = rate, mole/s
r_g = growth rate per unit area, $mole/(cm^2-s)$
r_n = nucleation rate per unit volume, $mole/(cm^3-s)$
$\mathcal{R}$ = universal gas constant, J/(mol-K)
T = Temperature, K
t = time, min
v = volume, cc
x = dummy variable in Equation (12)

Greek Letters

β = rate constant ratio, k_g/kn
μ = chemical potential, kcal
Δ = change in state of the following variable

Superscripts
equ = equilibrium conditions
exp = experimental conditions

Subscripts
g = growth
gw = gas+water
gwh = gas+water+hydrate phases
h = hydrate
i = component index
ind = induction
n = nucleation
nT = total moles of water present
P = product in phase equilibria reaction
R = reactant in phase equilibria reaction
w = water

12. List of Figures

Figure 4. Formulation of Gibbs Free Energy Driving Force for Hydrate Formation

Figure 5. Growth Rate per Unit Area as a Function of Gibbs Free Energy Driving Force. (Closed Triangles = present work; Open Triangles = Englezos et al. (1987)

Figure 6. Nucleation Induction Time as a Function of Gibbs Free Energy Driving Force

Figure 7. Nucleation Induction Time for the Natural Gas Data of Yousif (1994) as a Function of Proposed Gibbs Free Energy Driving Force

Figure 8. Various Approximations g(x) of the Logarithm of Fugacity Ratio

Figure 9. Model Predictions as a Function of Gibbs Free Energy Driving Force

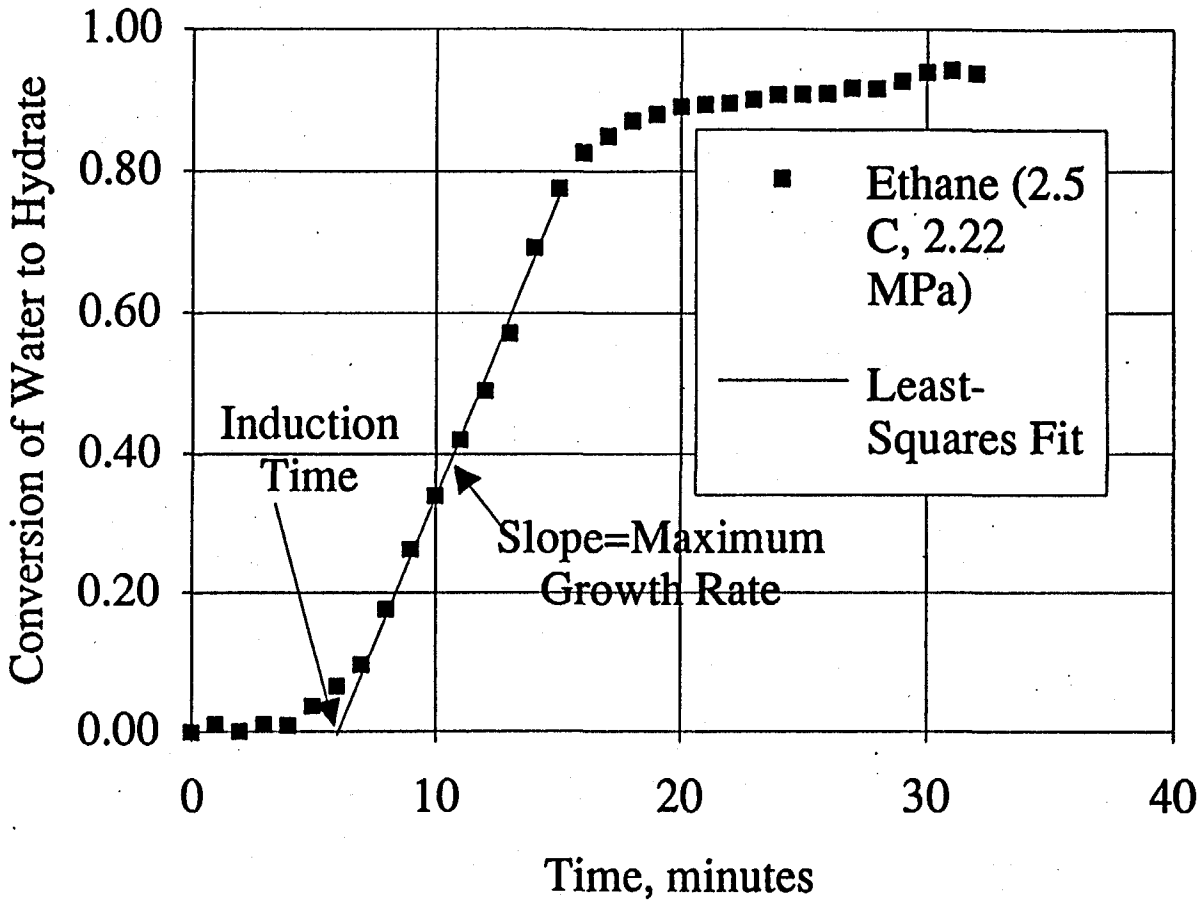
1.00
0.80
0.60
0.40
0.20
0.00
Conversion of Water to Hydrate
0
10
20
30
40
Time, minutes
Induction Time
Slope=Maximum Growth Rate
Ethane (2.5 C, 2.22 MPa)
Least-Squares Fit

Figure 1

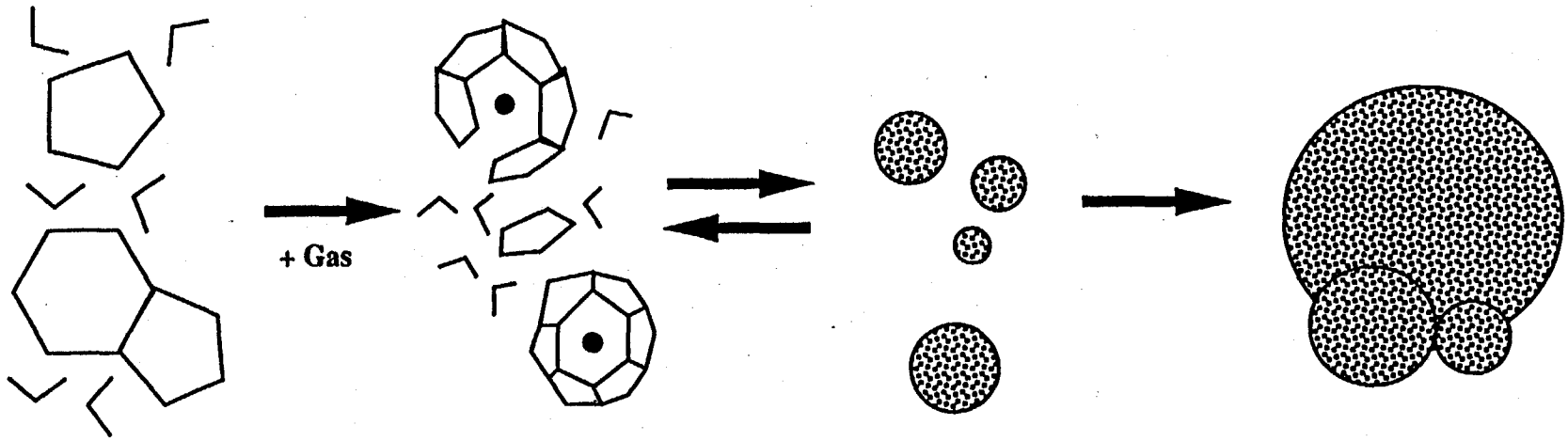

A. Initial Condition
Pressure and temperature in hydrate forming region, but no gas molecules dissolved in water

B. Labile Clusters
Upon dissolution of gas in water, labile clusters form immediately.

C. Agglomeration
Labile clusters agglomerate by sharing faces, thus increasing disorder.

D. Primary Nucleation and Growth
When the size of cluster agglomerates reaches a critical value, growth begins.

Figure 2

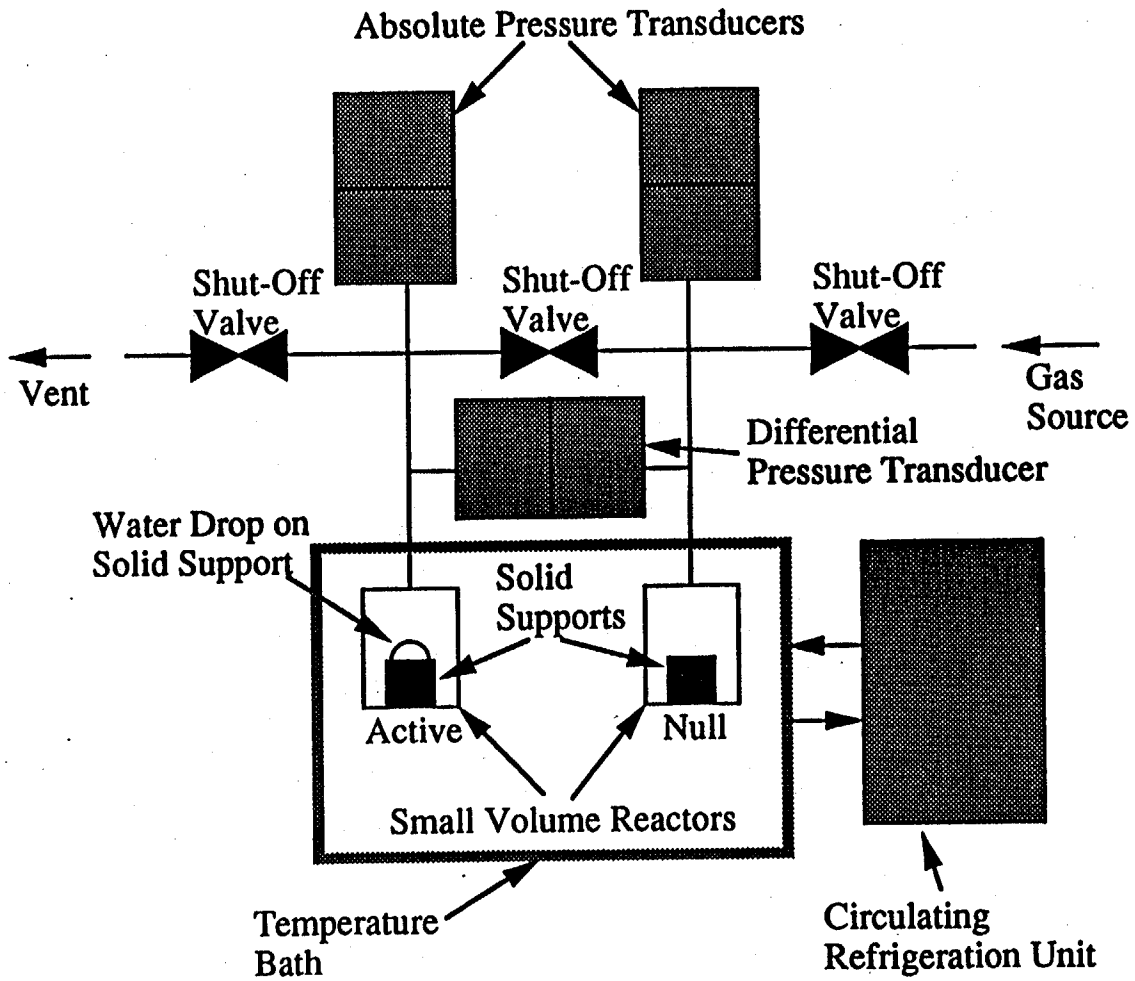
Absolute Pressure Transducers
Shut-Off Valve
Shut-Off Valve
Shut-Off Valve
Vent
Gas Source
Differential Pressure Transducer
Water Drop on Solid Support
Solid Supports
Active
Null
Small Volume Reactors
Temperature Bath
Circulating Refrigeration Unit

Figure 3

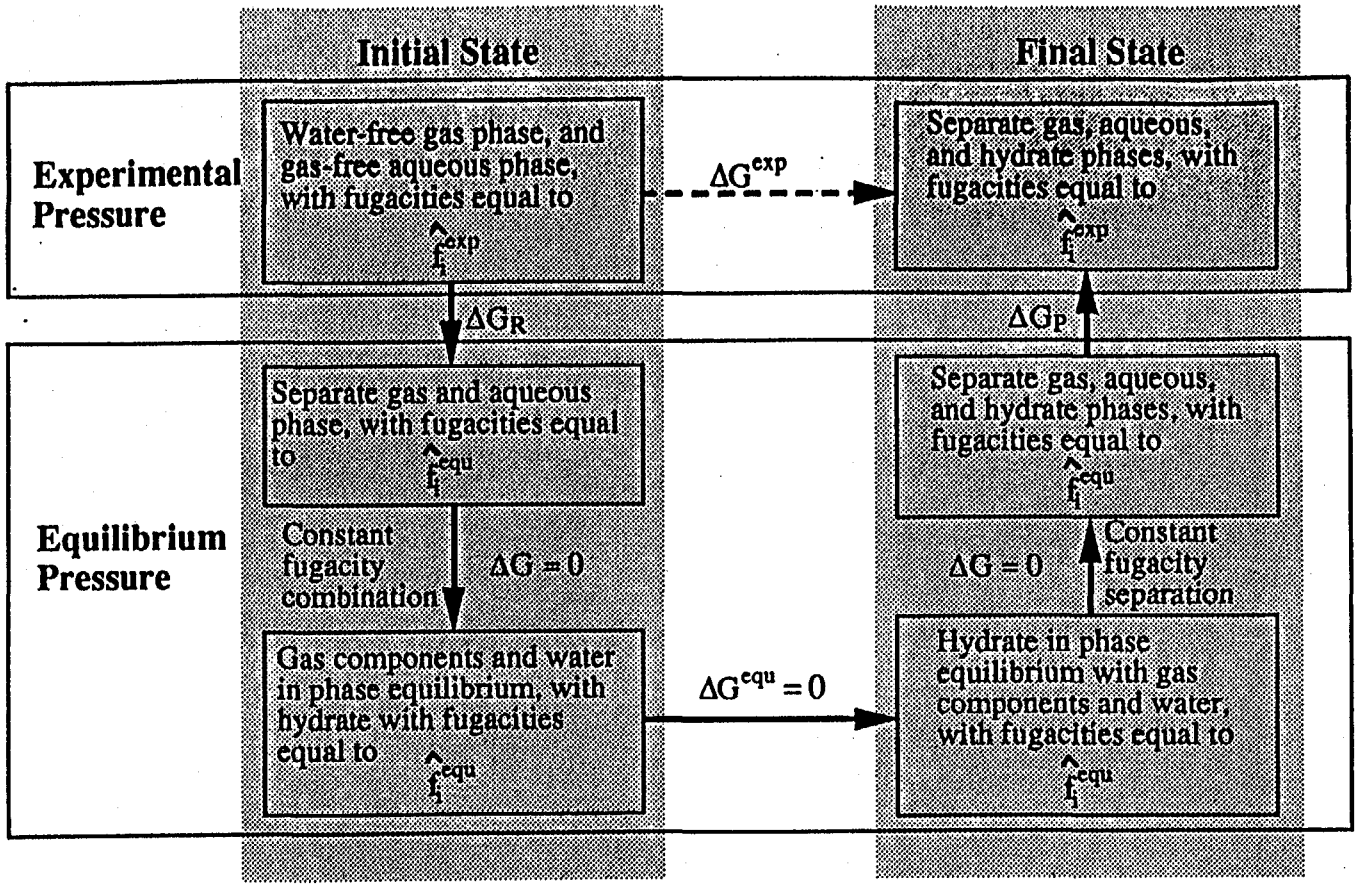

Hypothetical Process for Estimating Driving Force for Hydrate Formation at a Constant Temperature.

Figure 4

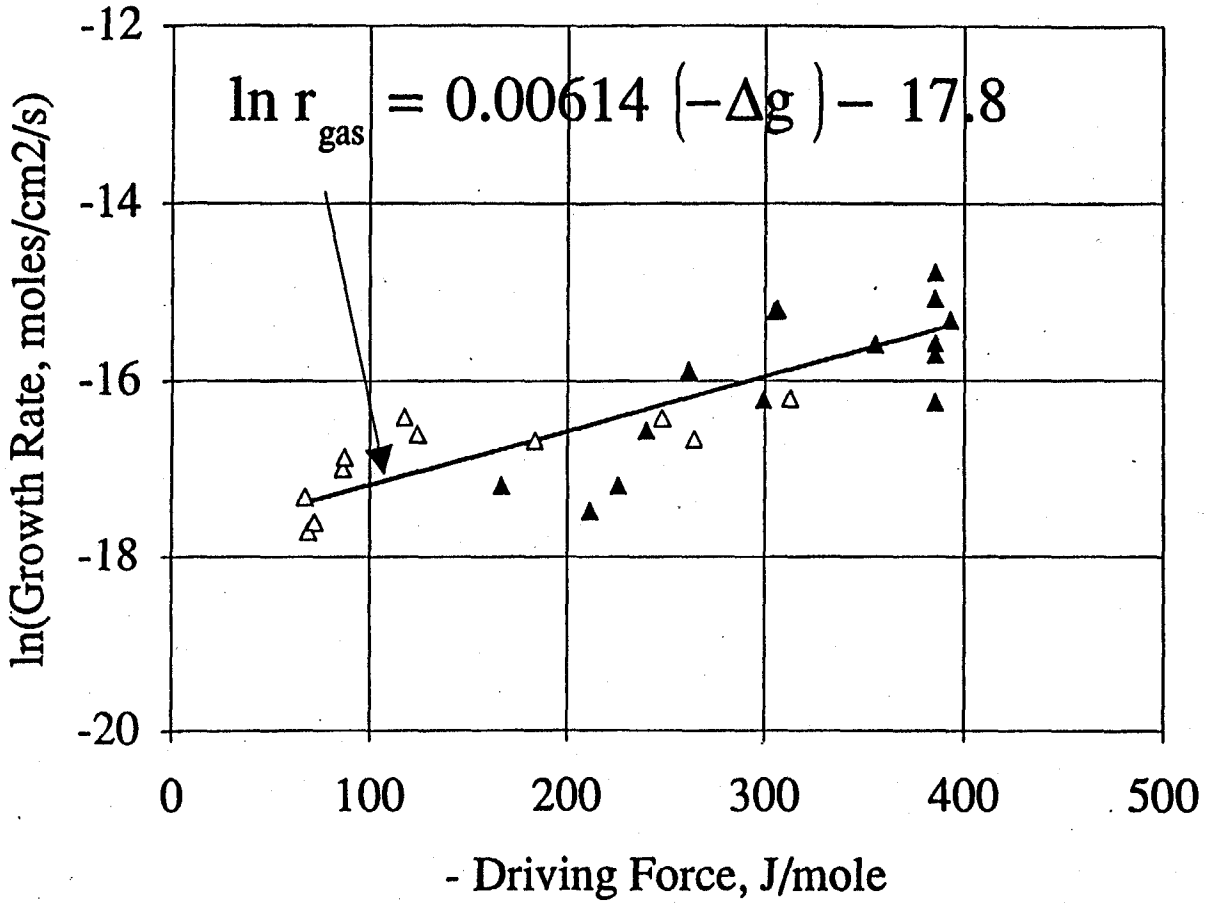
ln r gas = 0.00614 (−Δg) − 17.8
-12
-14
-16
-18
-20
0
100
200
300
400
500
ln(Growth Rate, moles/cm2/s)
- Driving Force, J/mole

Figure 5

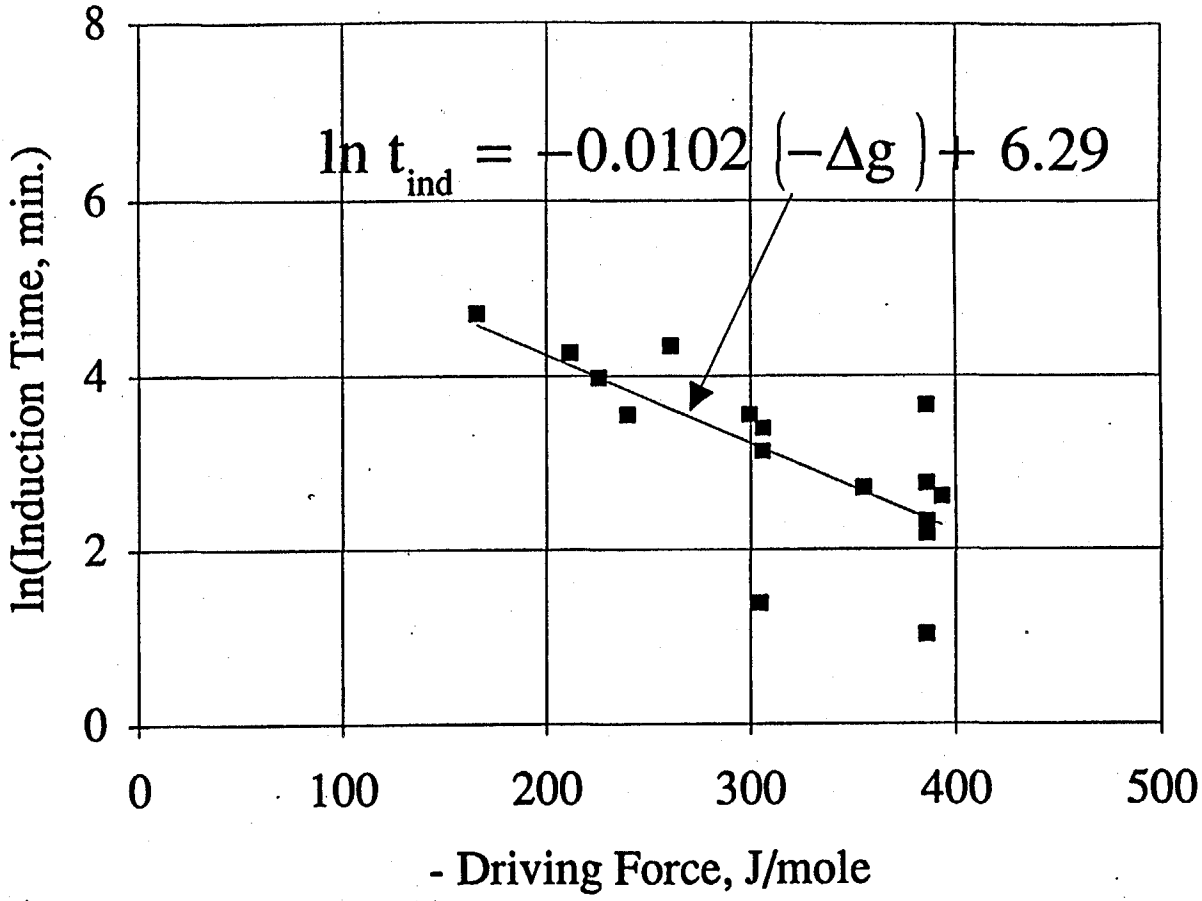
ln t_ind = −0.0102 (−Δg) + 6.29
ln(Induction Time, min.)
8
6
4
2
0
0
100
200
300
400
500
- Driving Force, J/mole

Figure 6

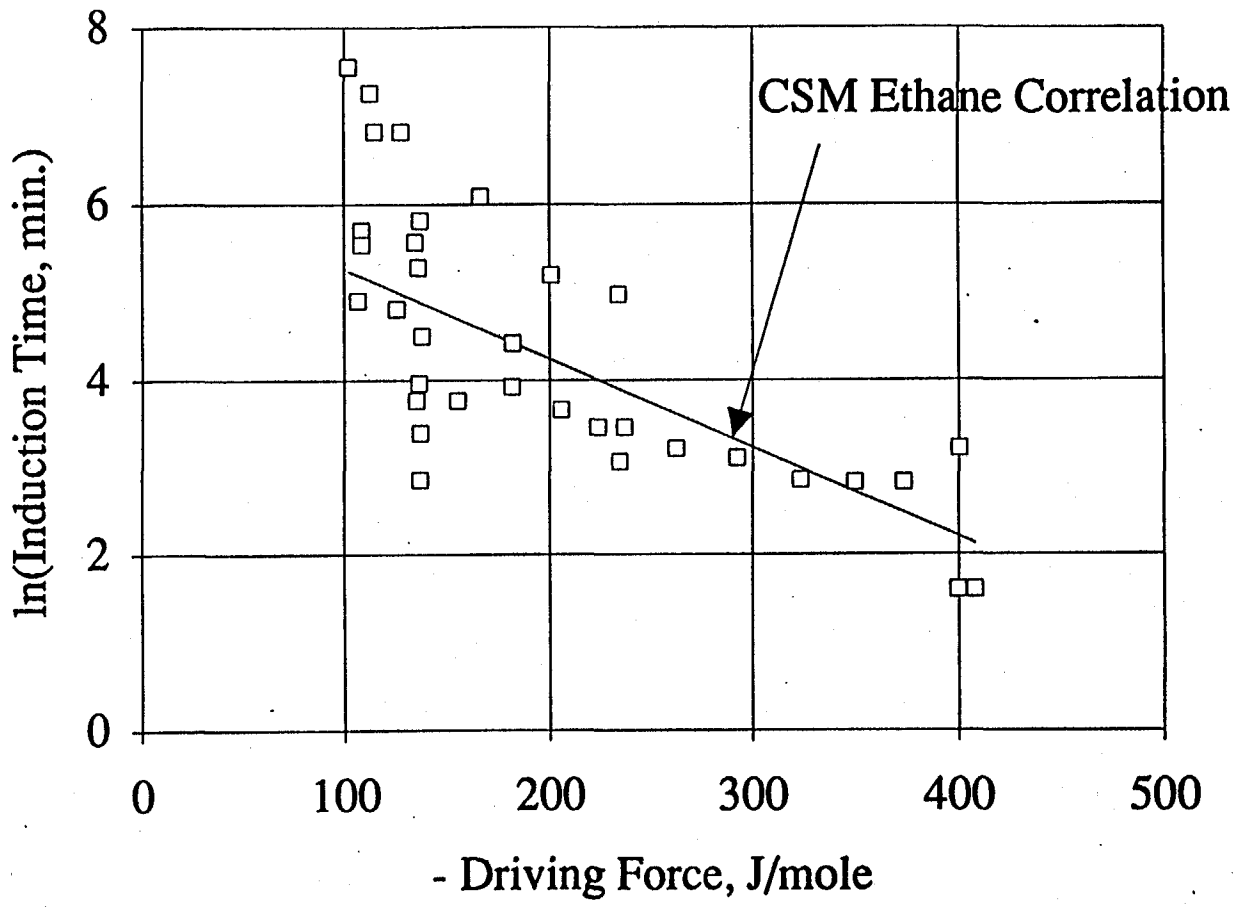
CSM Ethane Correlation
ln(Induction Time, min.)
8
6
4
2
0
0
100
200
300
400
500
- Driving Force, J/mole

Figure 7.

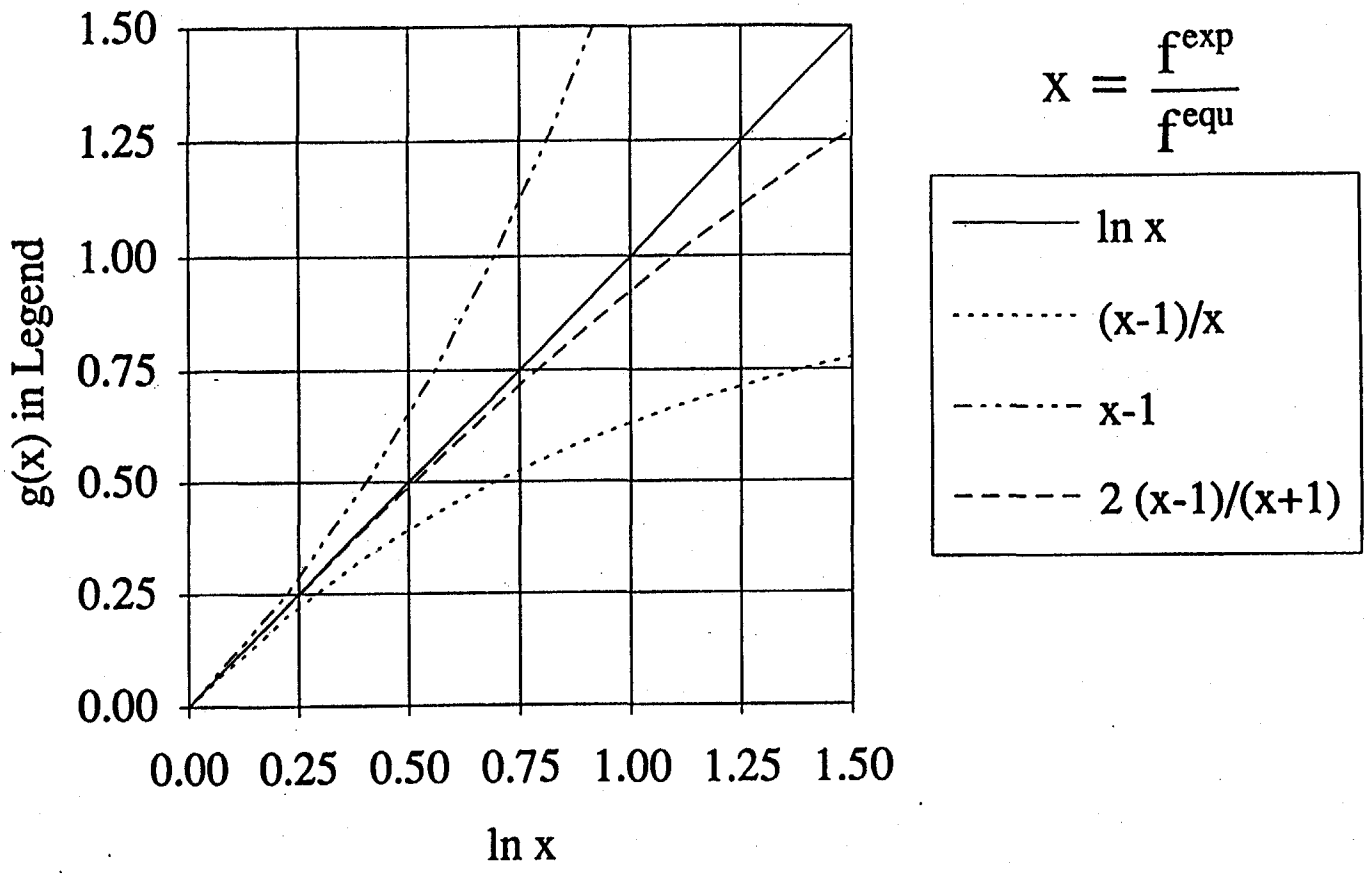
1.50
1.25
1.00
0.75
0.50
0.25
0.00
g(x) in Legend
0.00 0.25 0.50 0.75 1.00 1.25 1.50
ln x
$x = \frac{f^{exp}}{f^{equ}}$
ln x
(x-1)/x
x-1
2 (x-1)/(x+1)

Figure 8

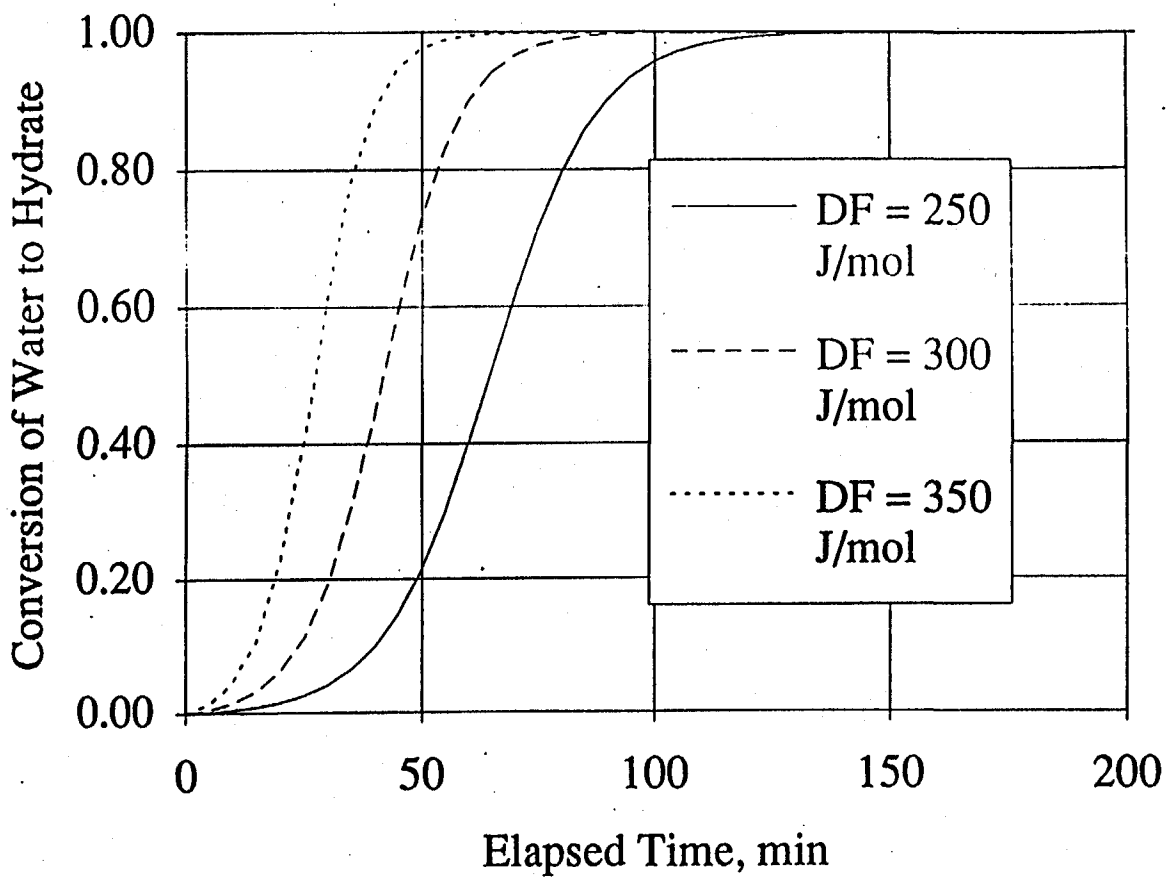
1.00
0.80
0.60
0.40
0.20
0.00
Conversion of Water to Hydrate
0
50
100
150
200
Elapsed Time, min
DF = 250 J/mol
DF = 300 J/mol
DF = 350 J/mol

Figure 9

FIGURES

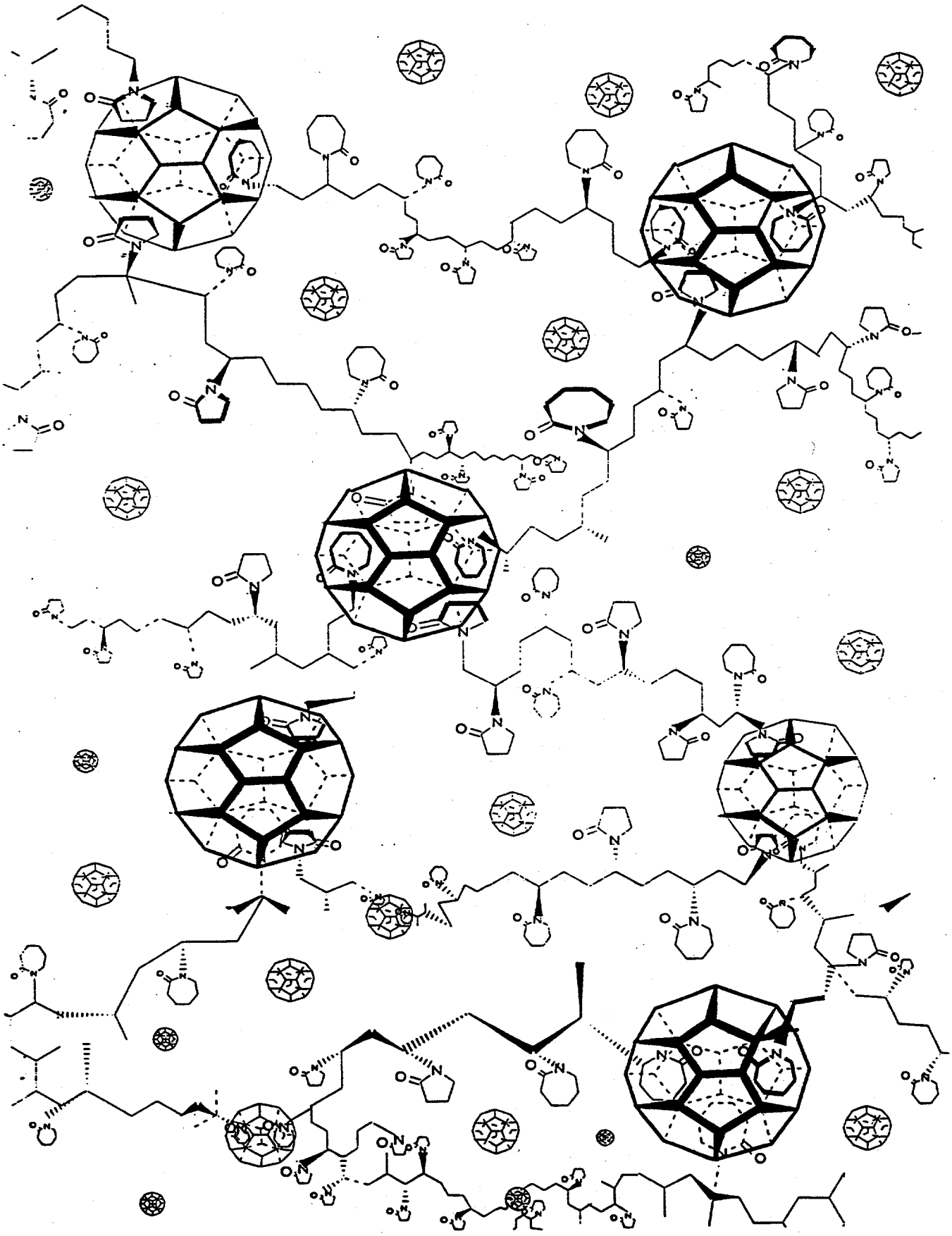

Figure 1. Schematic of our hydrate inhibition mechanism.

Primary Inhibitors

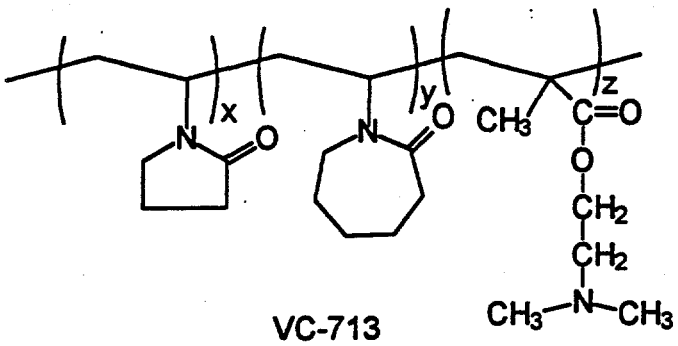

VC-713

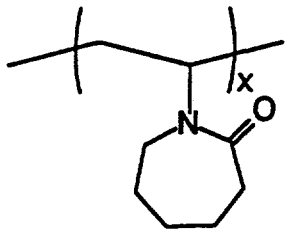

PVCAP

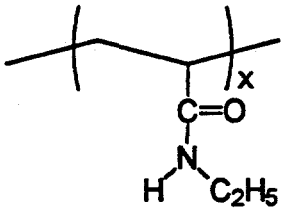

Poly(N-Ethyl Arylamide) (PNEAM)

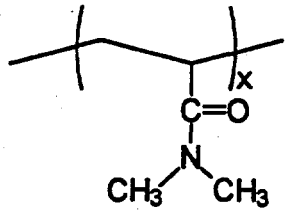

Poly(N,N-Dimethylacrylamide) (PNNDMAM)

Secondary Inhibitors

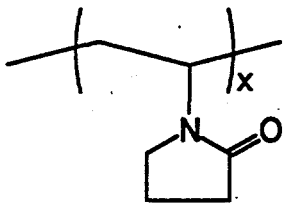

PVP

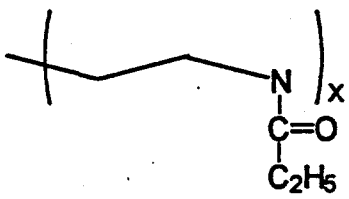

Poly(2-Ethyl-2-Oxazoline) (P2E2OX)

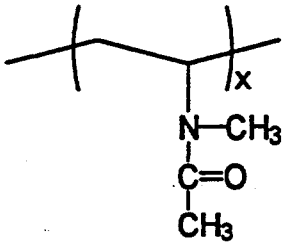

Poly(N-Methyl-N-Vinylacetamide) (PNMNVAcAM)

Figure 2. Chemical structures for hydrate inhibitors.

Schematic Diagram of THF Hydrate Multiple Screening Reactor

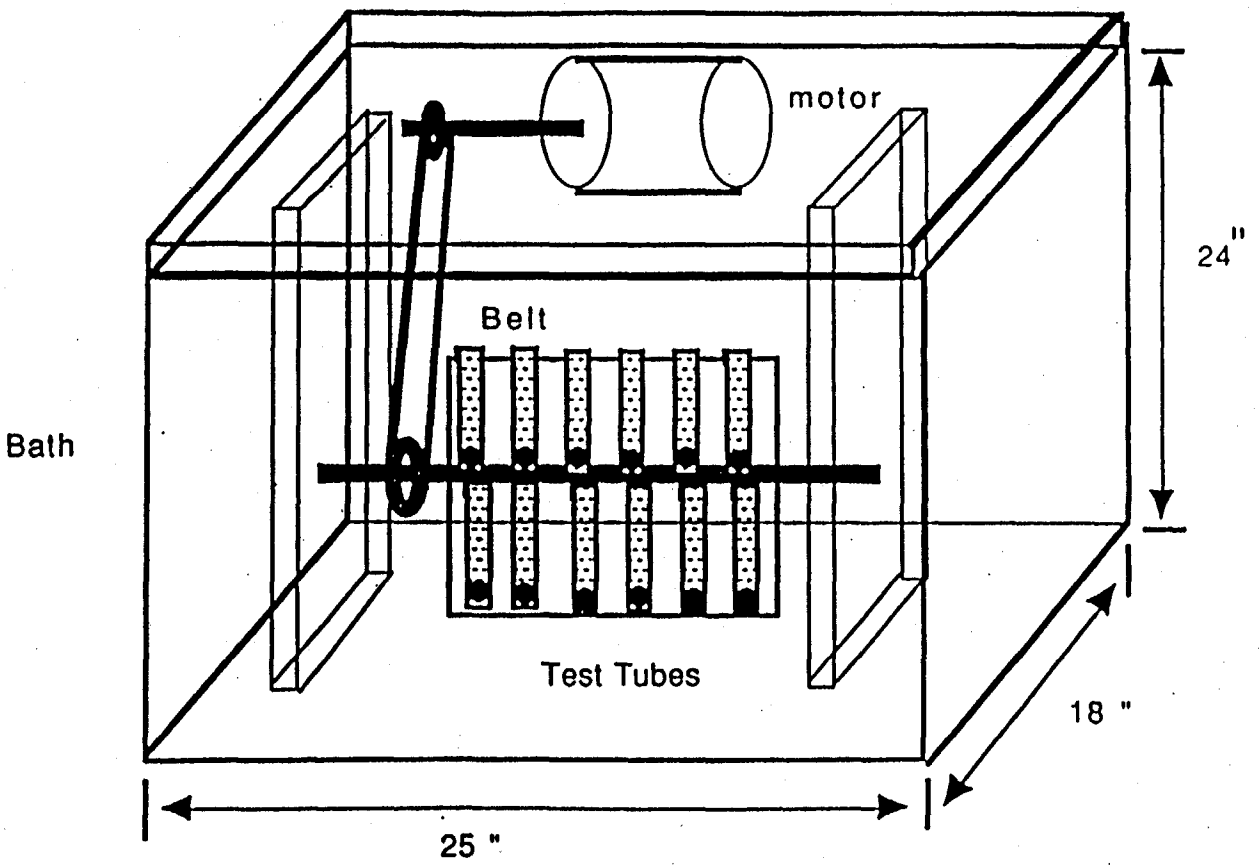

Figure 3. Schematic diagram of the THF screening apparatus.

Figure 4.

Two New Non-Lactam Polymers Perform Similar to PVCAP and VC-713

0.5wt% Polymer + 3.5wt% Sea Salt ,
P = 1000 psig, and T = 39.2°F

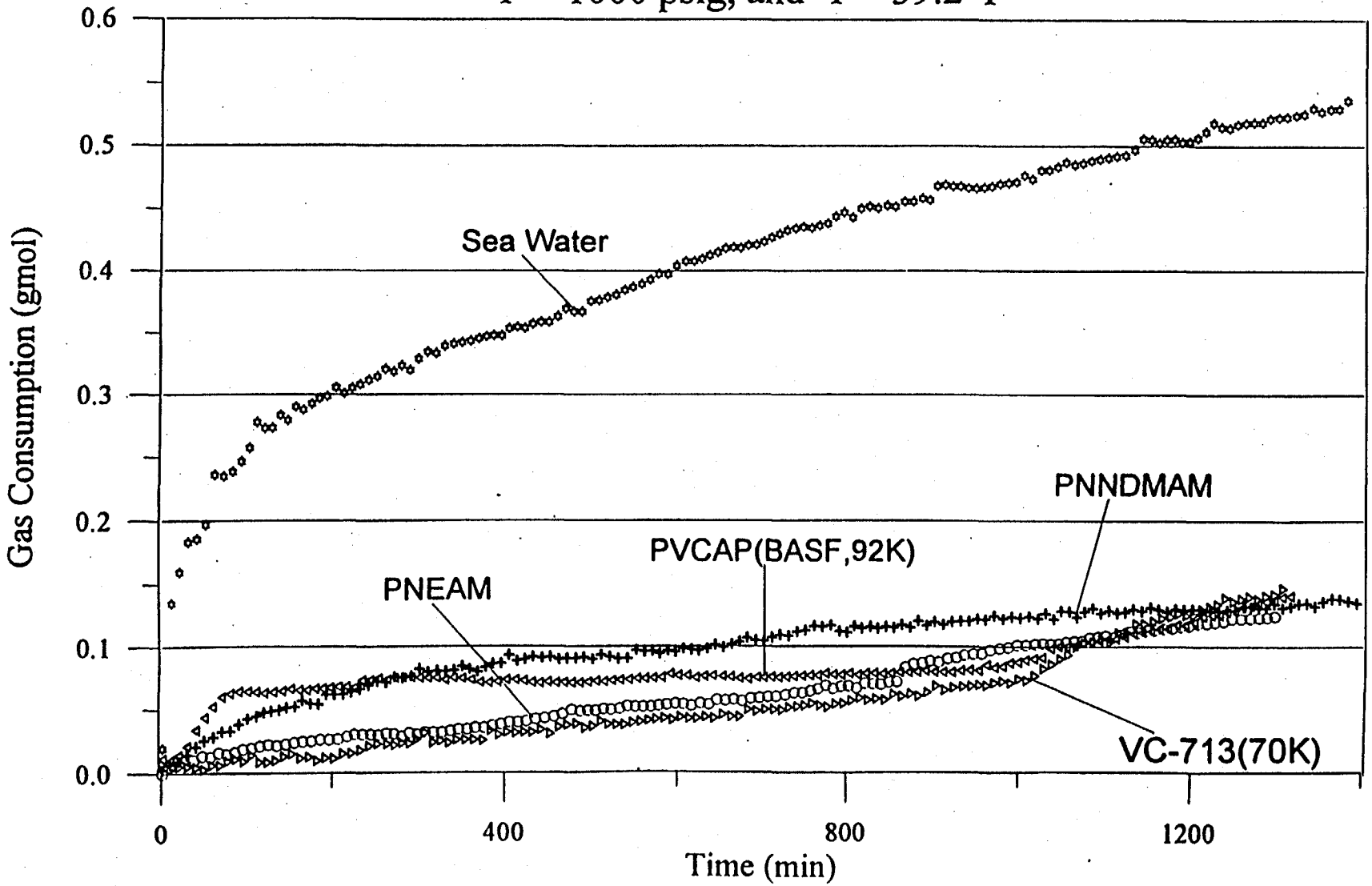

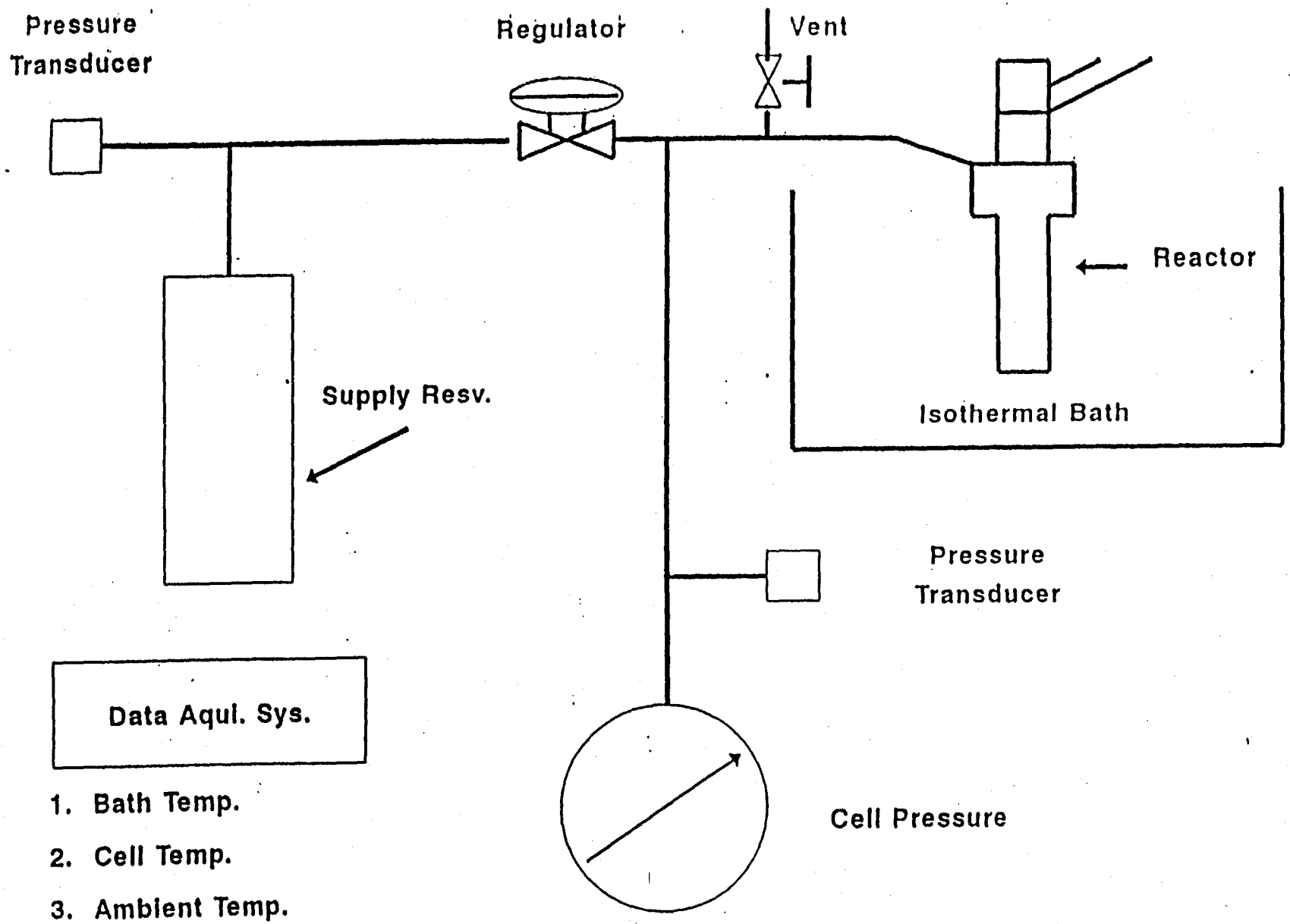

Figure 5. Schematic diagram of the high pressure apparatus.

Figure 6.

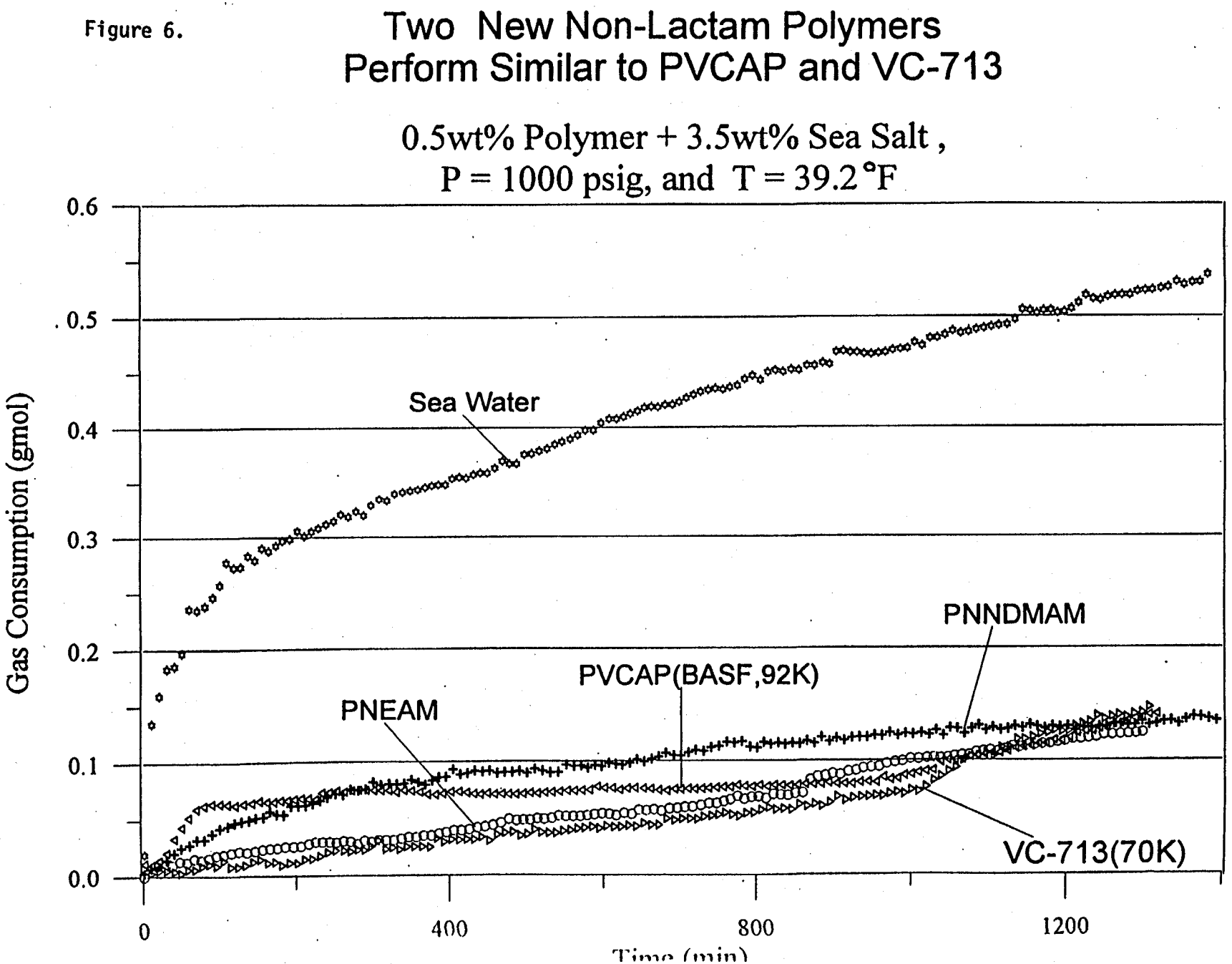
Two New Non-Lactam Polymers
Perform Similar to PVCAP and VC-713
0.5wt% Polymer + 3.5wt% Sea Salt ,
P = 1000 psig, and T = 39.2 °F
Gas Consumption (gmol)
0.0
0.1
0.2
0.3
0.4
0.5
0.6
0
400
800
1200
Time (min)
Sea Water
PNNDMAM
PVCAP(BASF,92K)
PNEAM
VC-713(70K)

Figure 7.

PNEAM Performs Similar to VC-713 And PNNDMAM Performs Similar to PVCAP(BASF3)

0.5wt% Polymer+ 3.5wt% Sea Salt
P = 1000 psig and T = 39.2°F

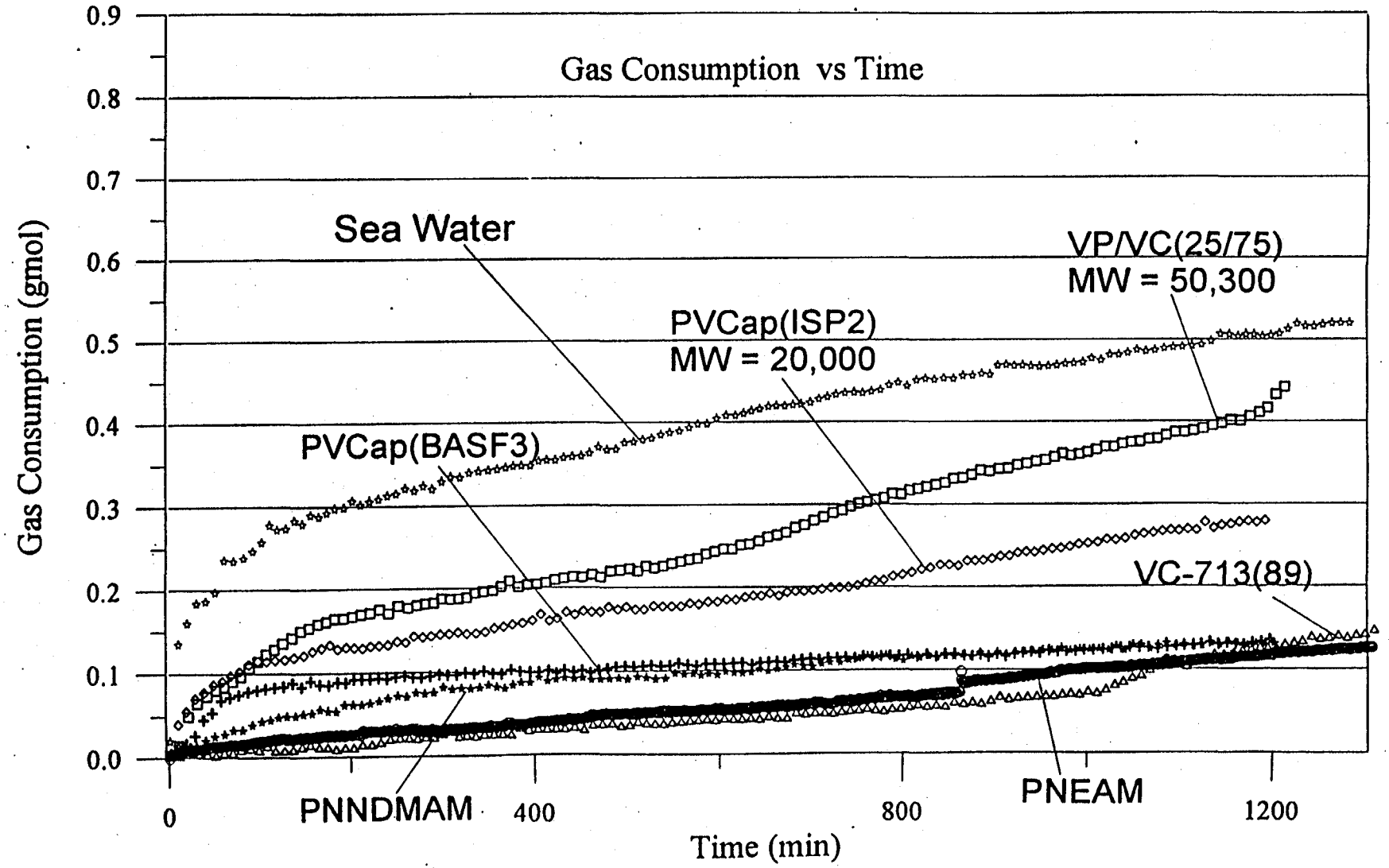

Figure 8. 0.5wt% PNNDMAM Performs Better Than 1.0wt% PNNDMAM at The Conditions of 3.5wt% Salt, P = 1000 psig, and T = 39.2°F

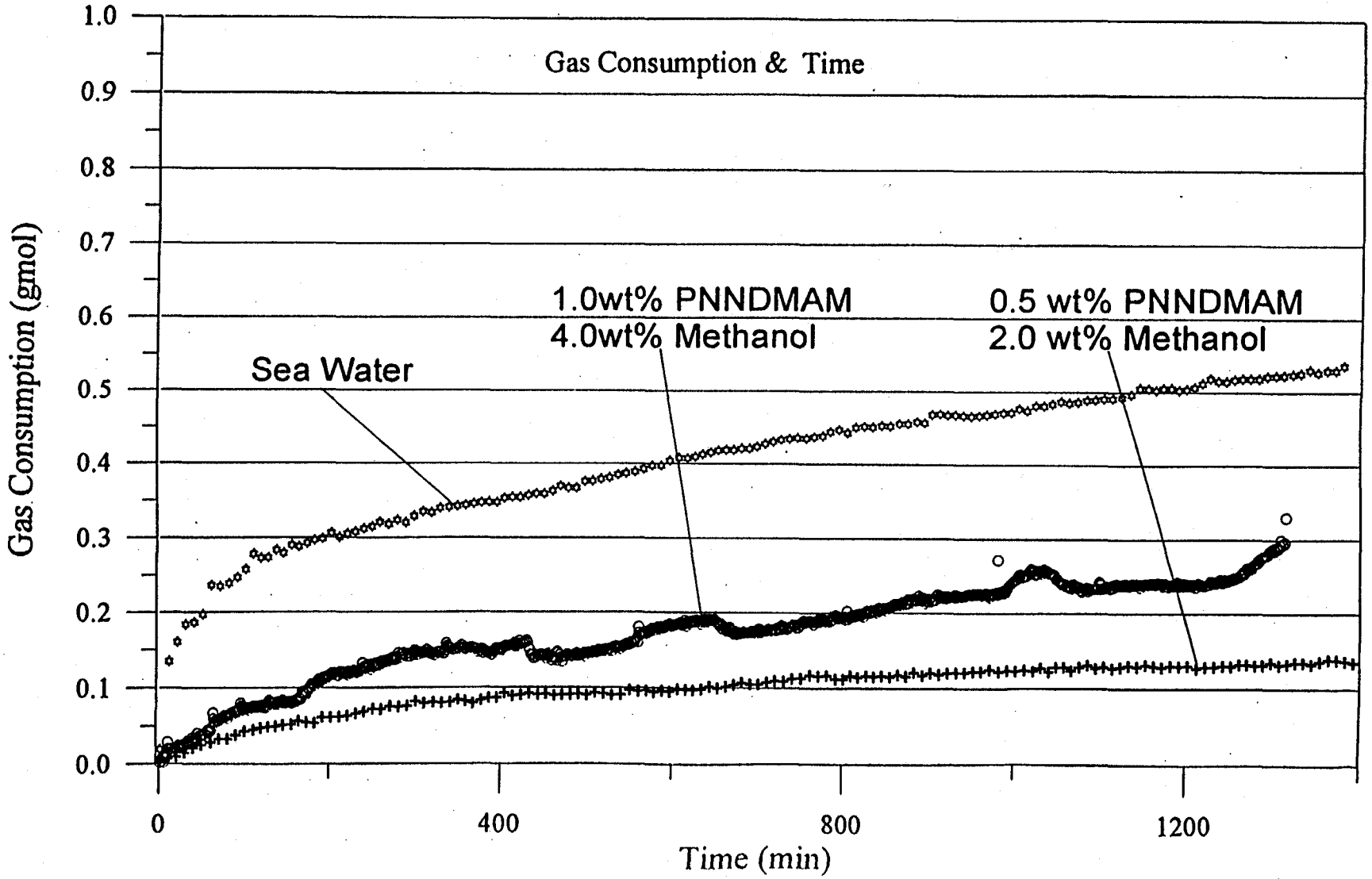

Figure 9. When Increased The Pressure from 1000 psig to 1250 psig, The Gas Consumptions of 0.5wt% PNEAM in Sea Water Did Not Change Very Much at 39.2°F

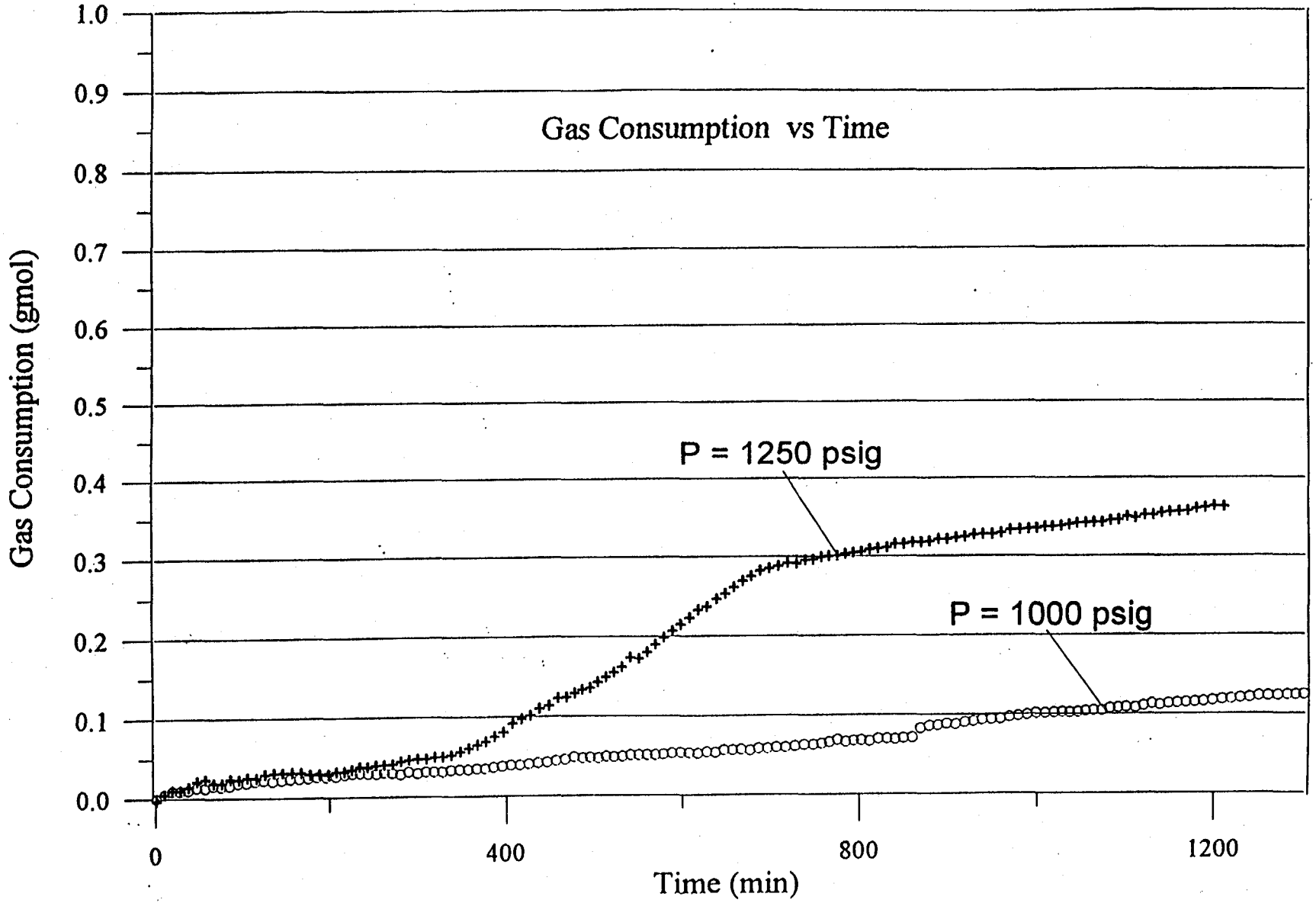

Figure 10 Blending PVCap(ISP3) with P2E2OX(MW=500K) Performs Better Than Using PVCap or P2E2OX Alone at The Conditions of 1000 psig, 39.2°F and 3.5wt% Salt

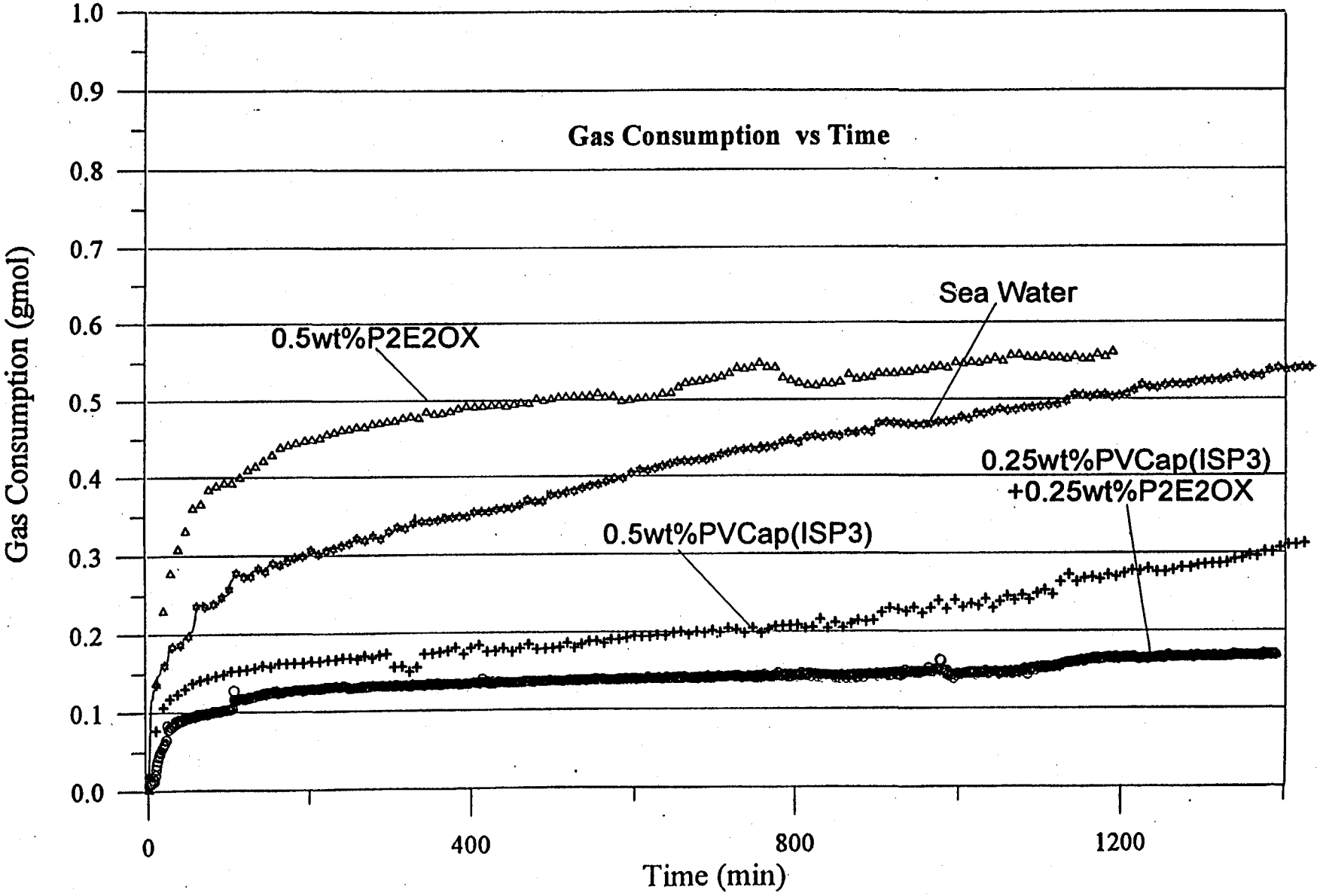

Figure 11.

Blending 0.25 wt% P2E2OX with 0.25wt% VC-713 Performs as Well as 0.5wt% VC-713 in Sea Water at 1000 psig and 39.2° F

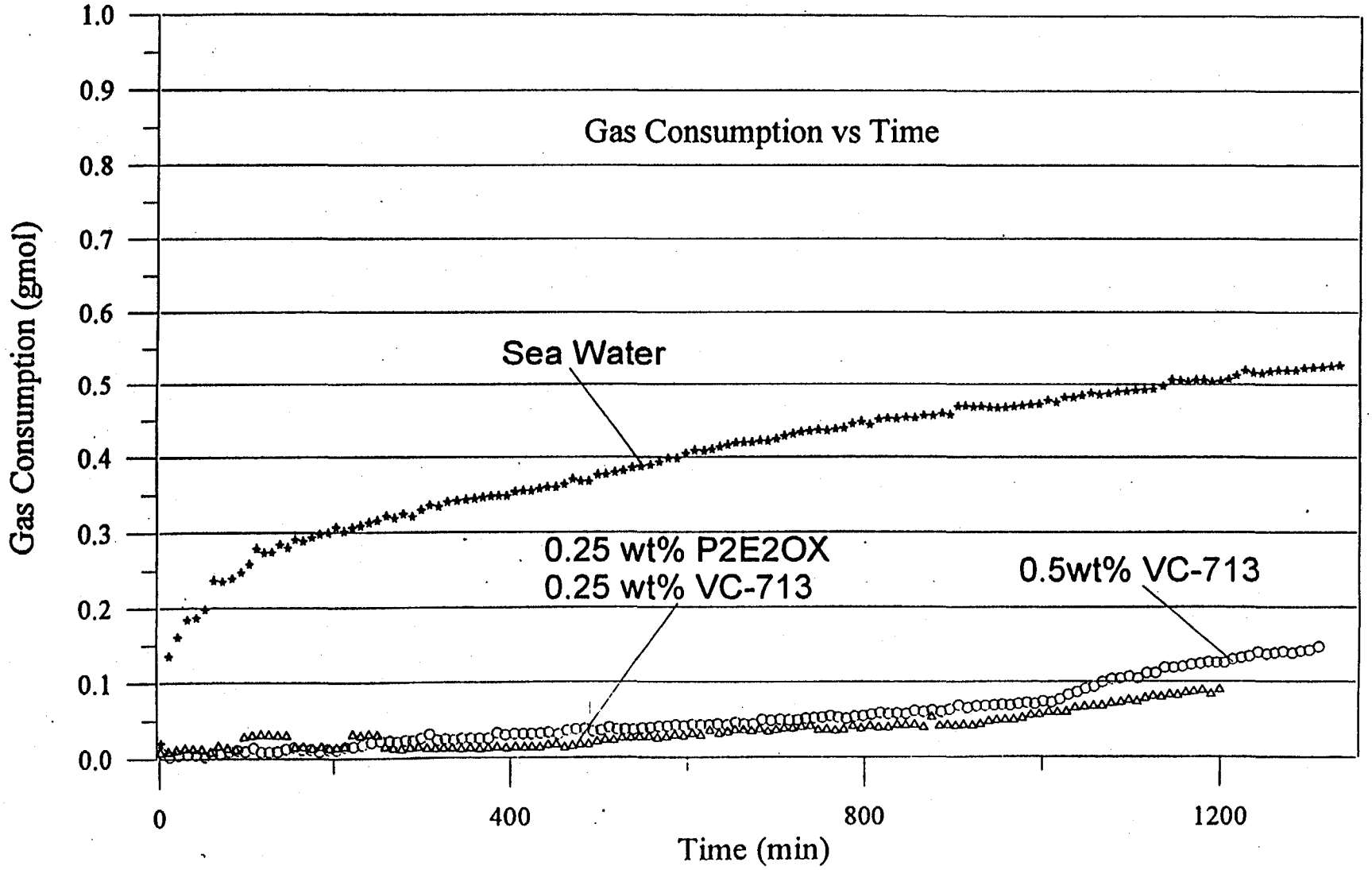

Figure 12. 0.25wt%VC-713(89) + 0.25wt%P2E2OX Works Better Than 0.25wt%PVCap(ISP3) +0.25wt%P2E2OX at The Conditions of 3.5wt% Sea Salt , P = 1000 psig and T = 39.2°F

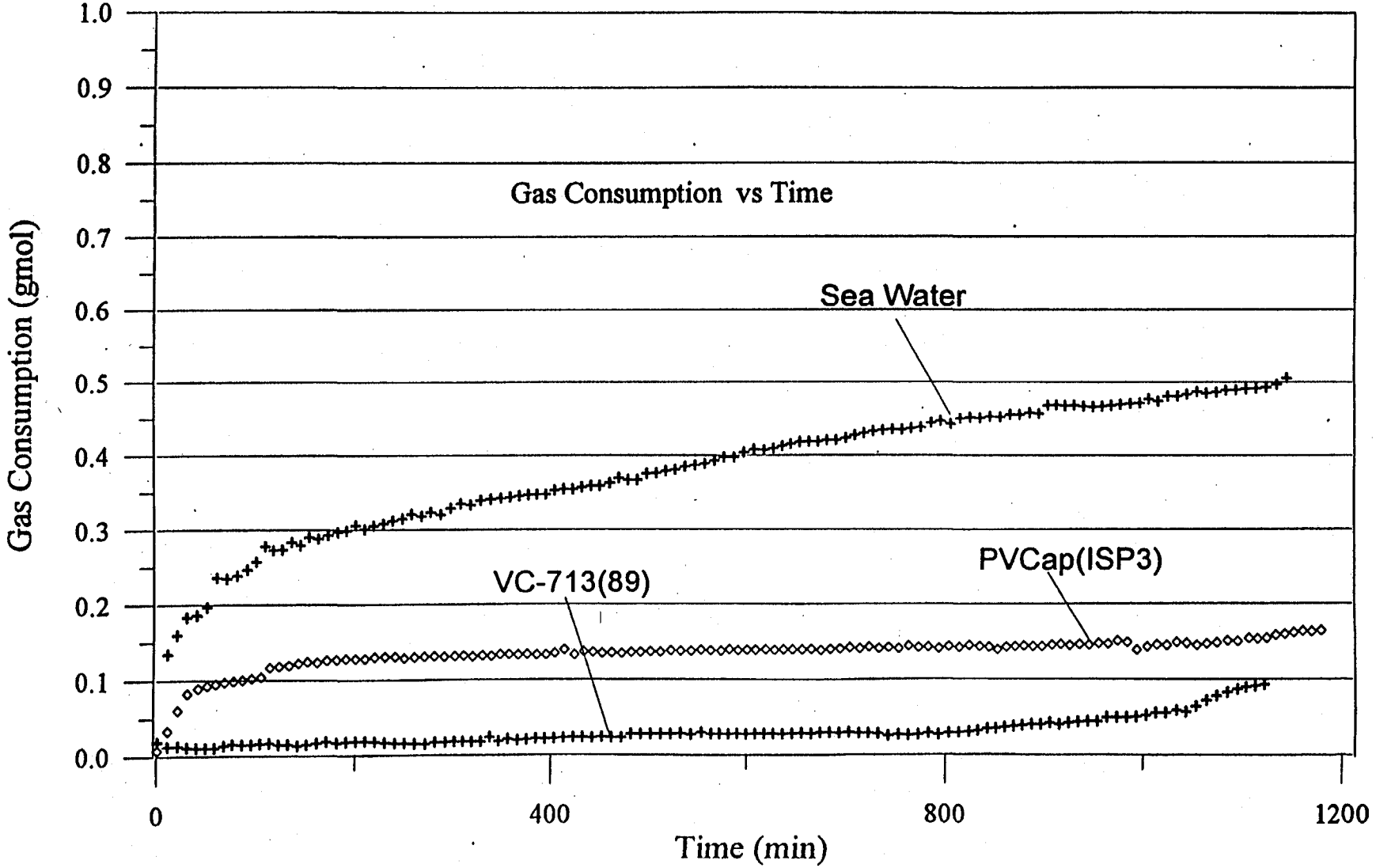

Figure 13.

Low MW HE-300 Consumes More Gas Than High MW HE-300 When Combined with PVCAP at The Conditions of 3.5wt% Salt, P = 1000 psig, and T = 39.2°F

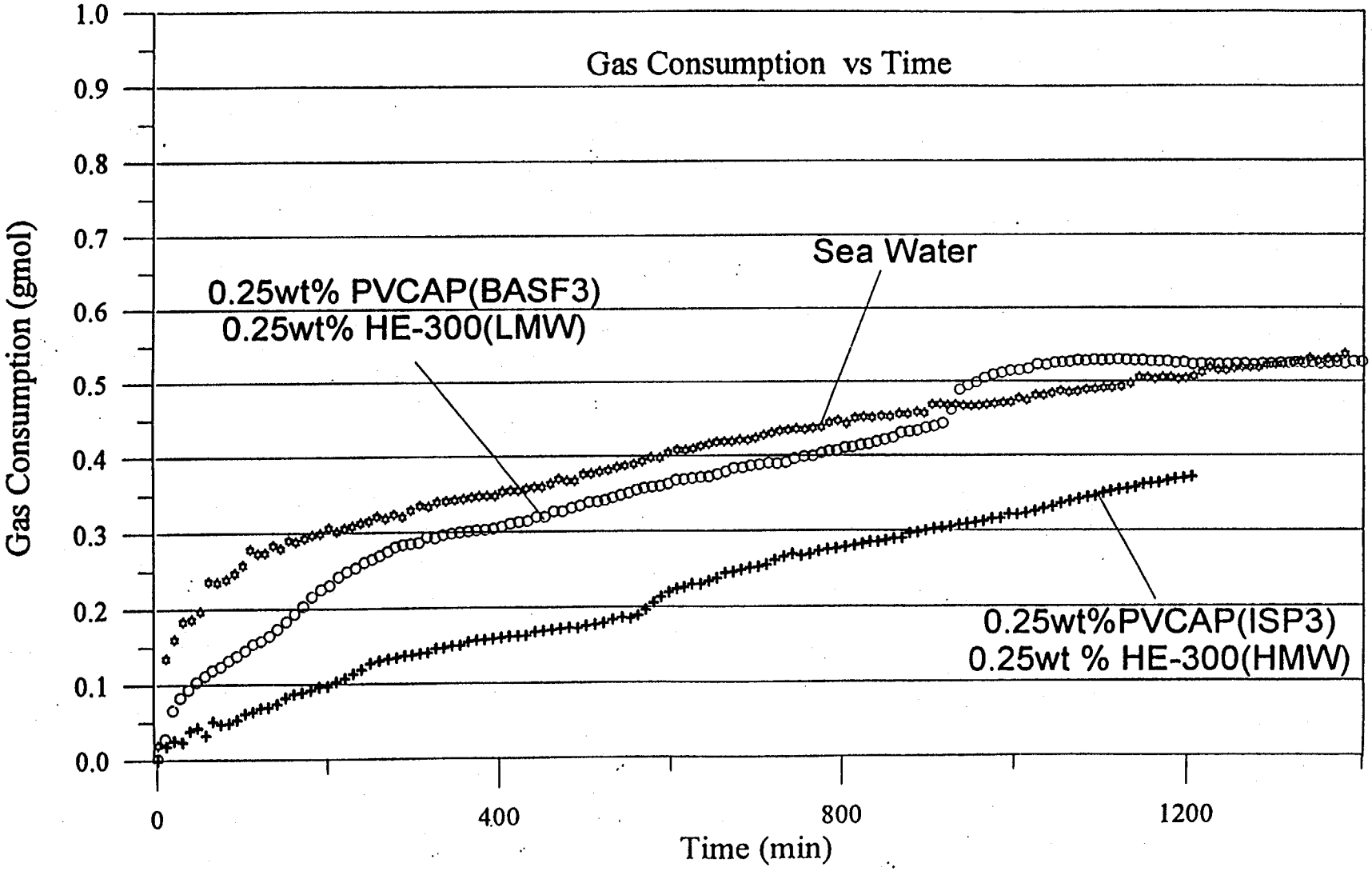

Figure 14. Compare The Perfomance of Blending Different New Polymers with PVCAP at The Conditions of 0.25wt% New Polymer + 0.25wt% PVCap (ISP2) + 3.5wt% Sea Salt+2.0wt% MeOH P = 1000 psig and T = 39.2°F

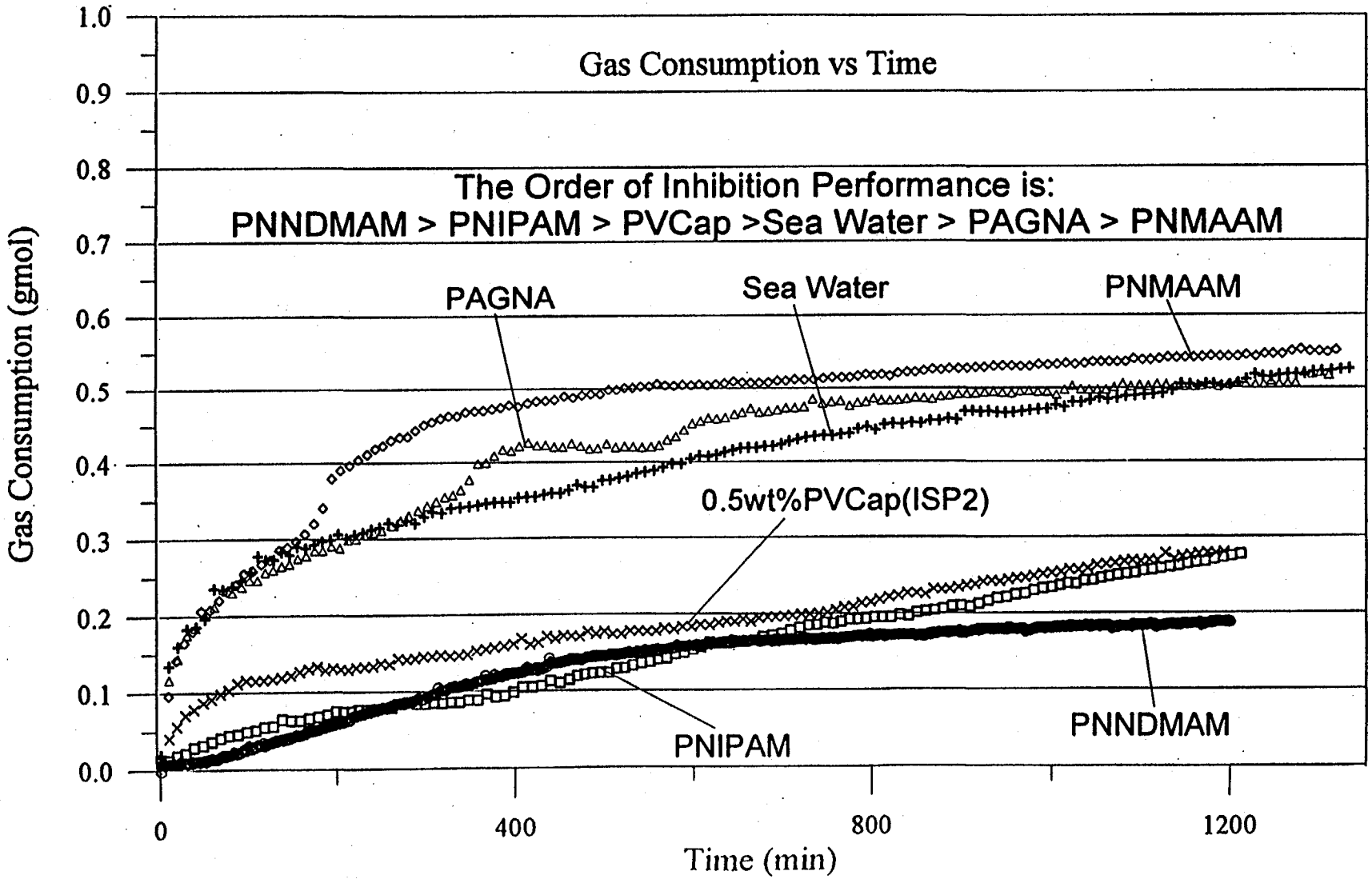

Figure 15. 0.25% PVCAP(ISP3) + 0.25wt% P2E2OX Works at 1000 psig, But It Does Not Work at 1300 psig (3.5wt% Sea Salt + 2.0 wt% Methanol, T = 39.2°F)

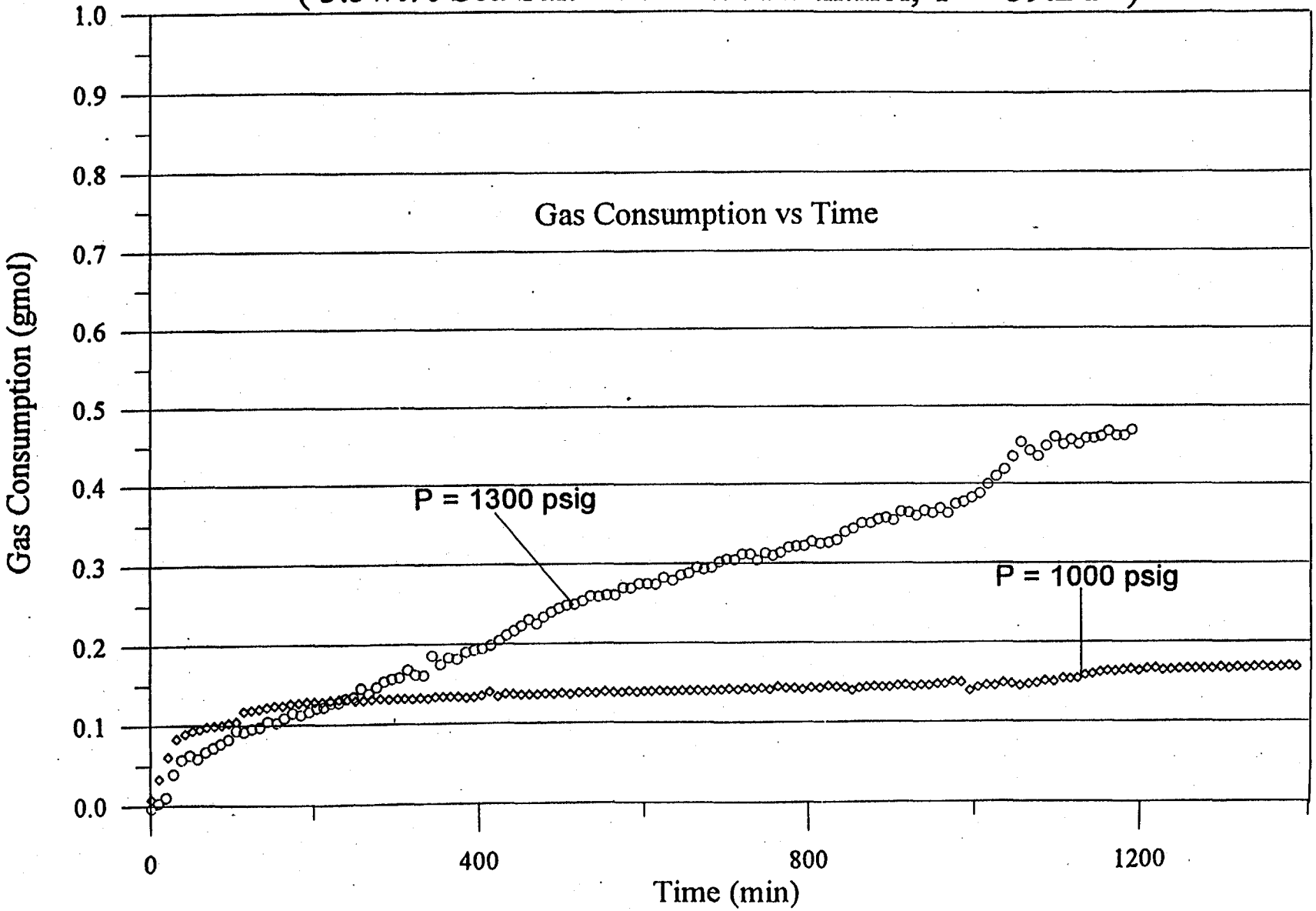

Figure 16. The Solution of 0.25wt%VC-713(89) + 0.25wt%P2E2OX +3.5wt% Sea Salt Works Well at P = 1000 psig , But It Does Not Work at P = 1300 psig (T = 39.2°F)

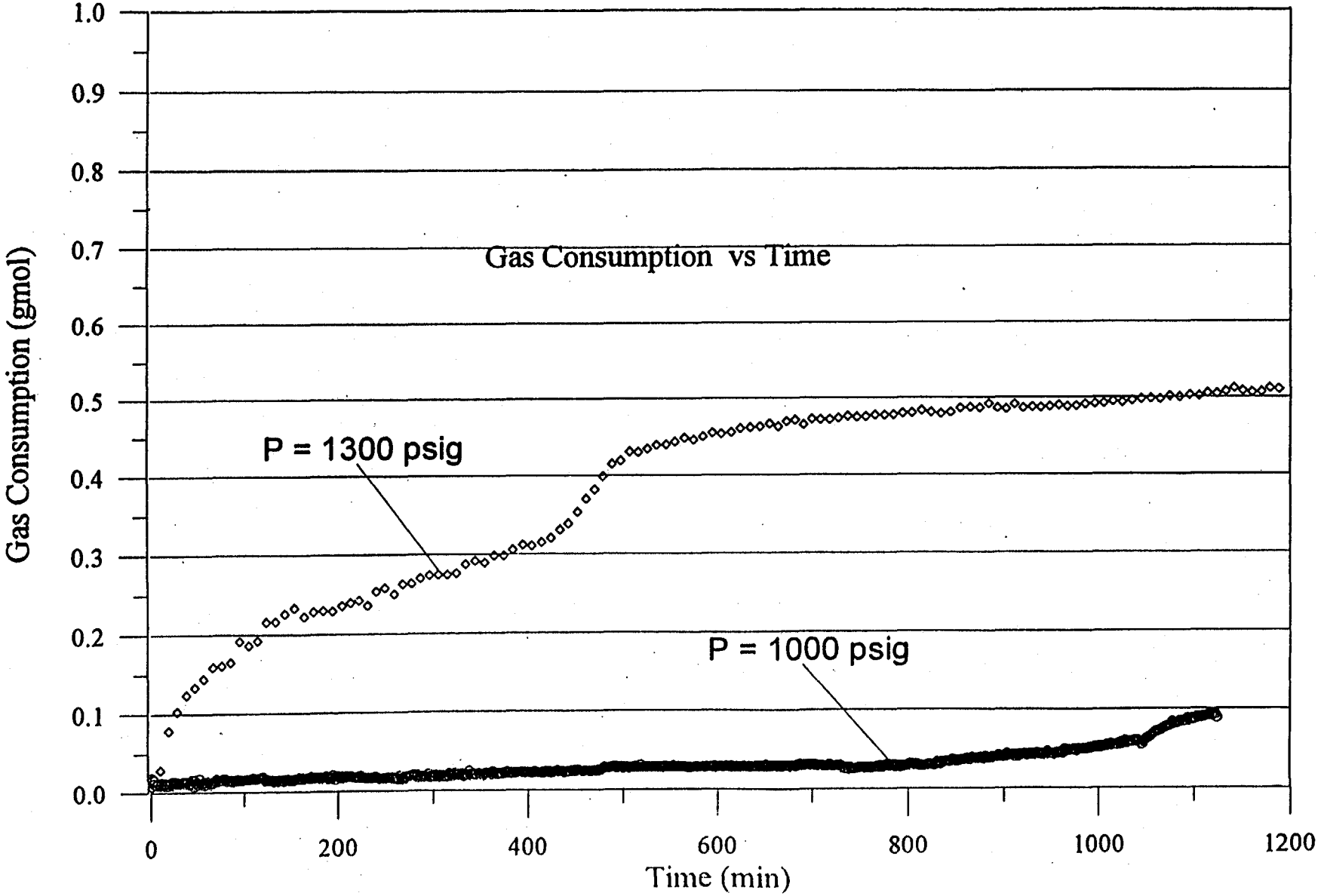

Figure 17.

Blending PVP(K-17) with PVCAP(BASF,92K) Provides Better Performance Than Using PVCAP(BASF,92K) Alone

3.5wt% Salt, P = 1500 psig, and T = 39.2 °F

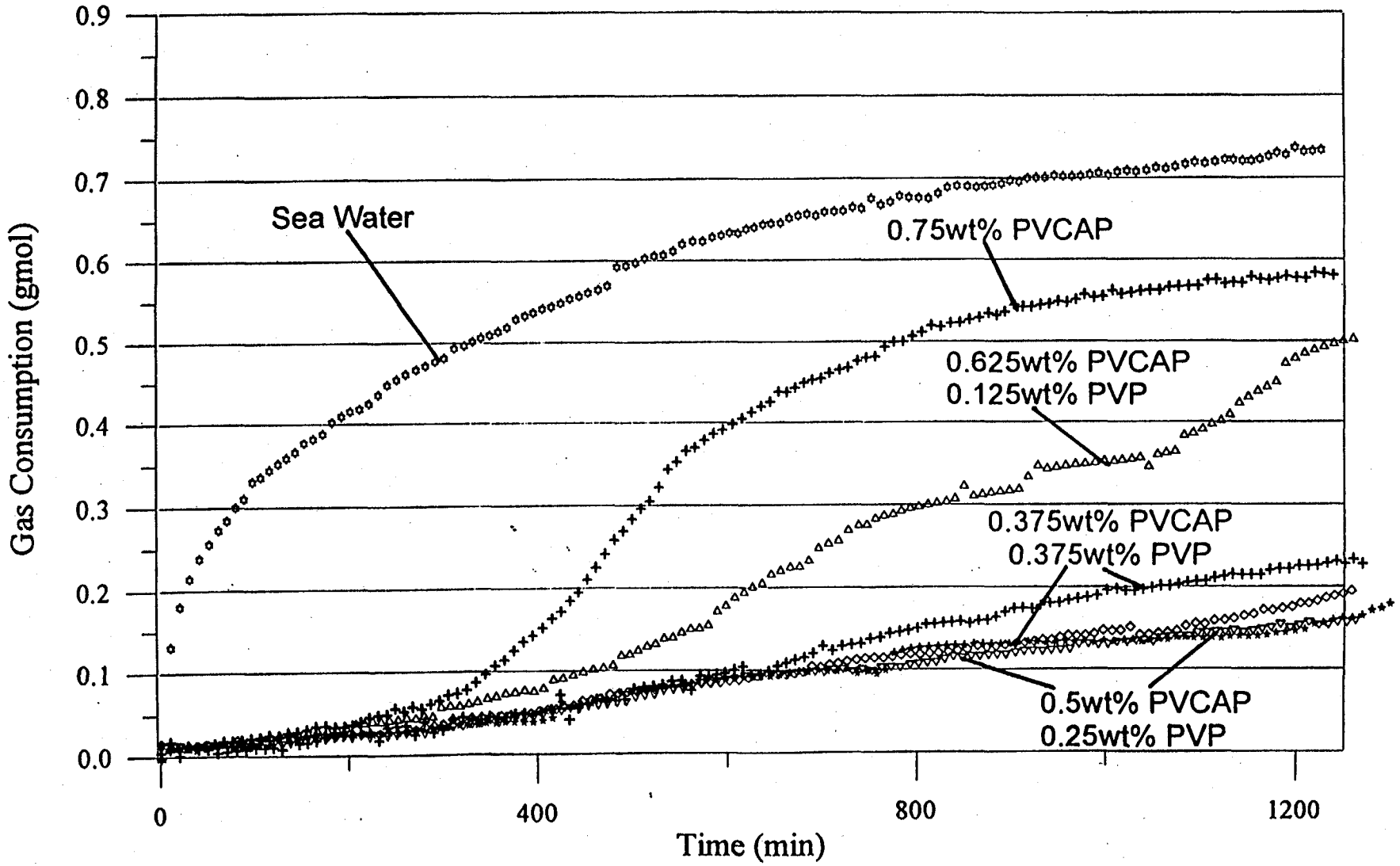

Figure 18.

Combining PVP(K-30) with PVCAP(BASF,92K) Provides Better Performance Than Using PVCAP(BASF,92K) Alone

3.5wt% Salt, P = 1500 psig, and T = 39.2°F

No. 7

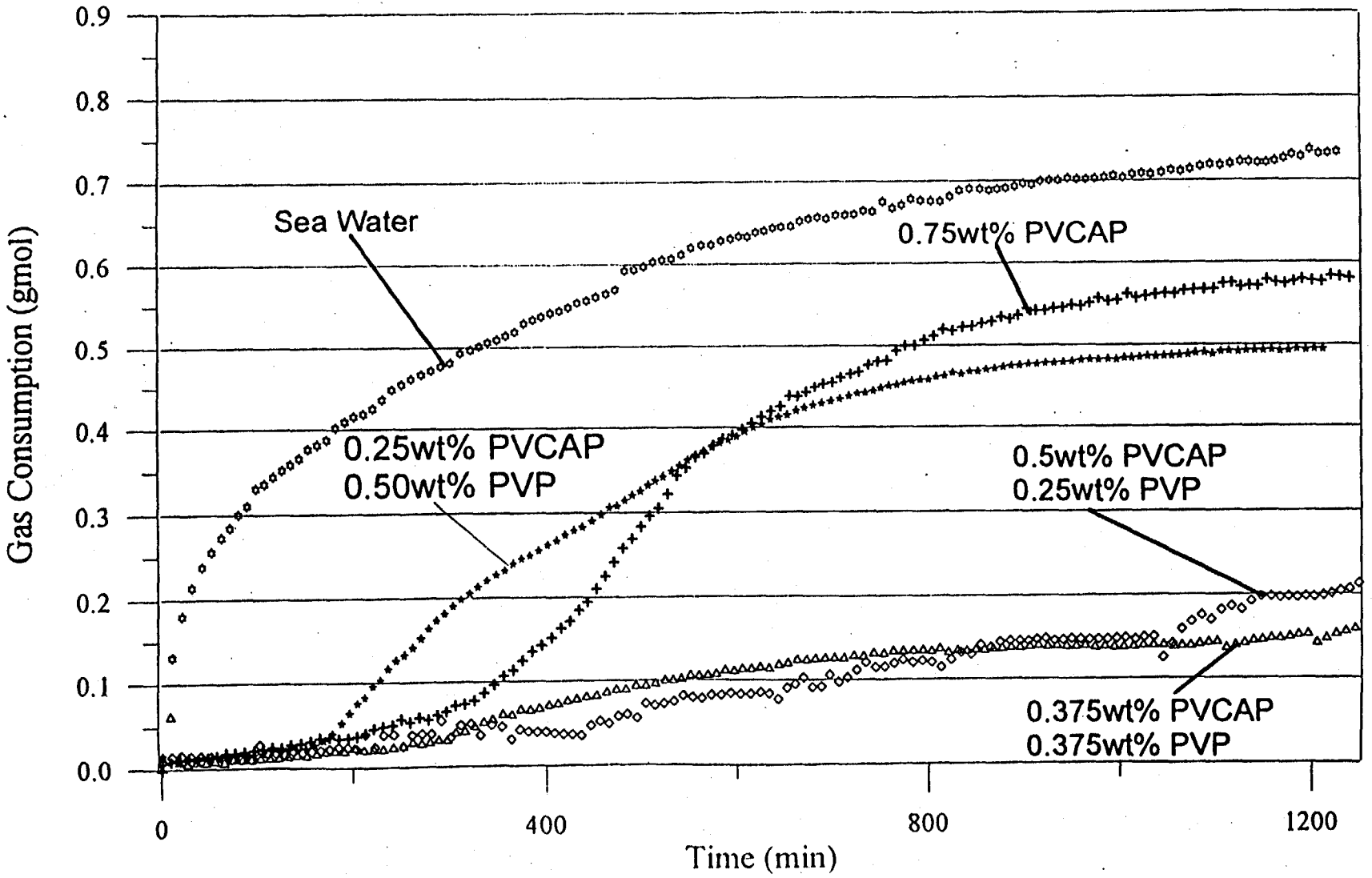

Figure 19.

When Combined with PVCAP, Low MW PVP Performs Better Than High MW PVP

3.0wt%Methanol + 3.5wt% Salt,
P = 1500 psig, and T = 39.2°F

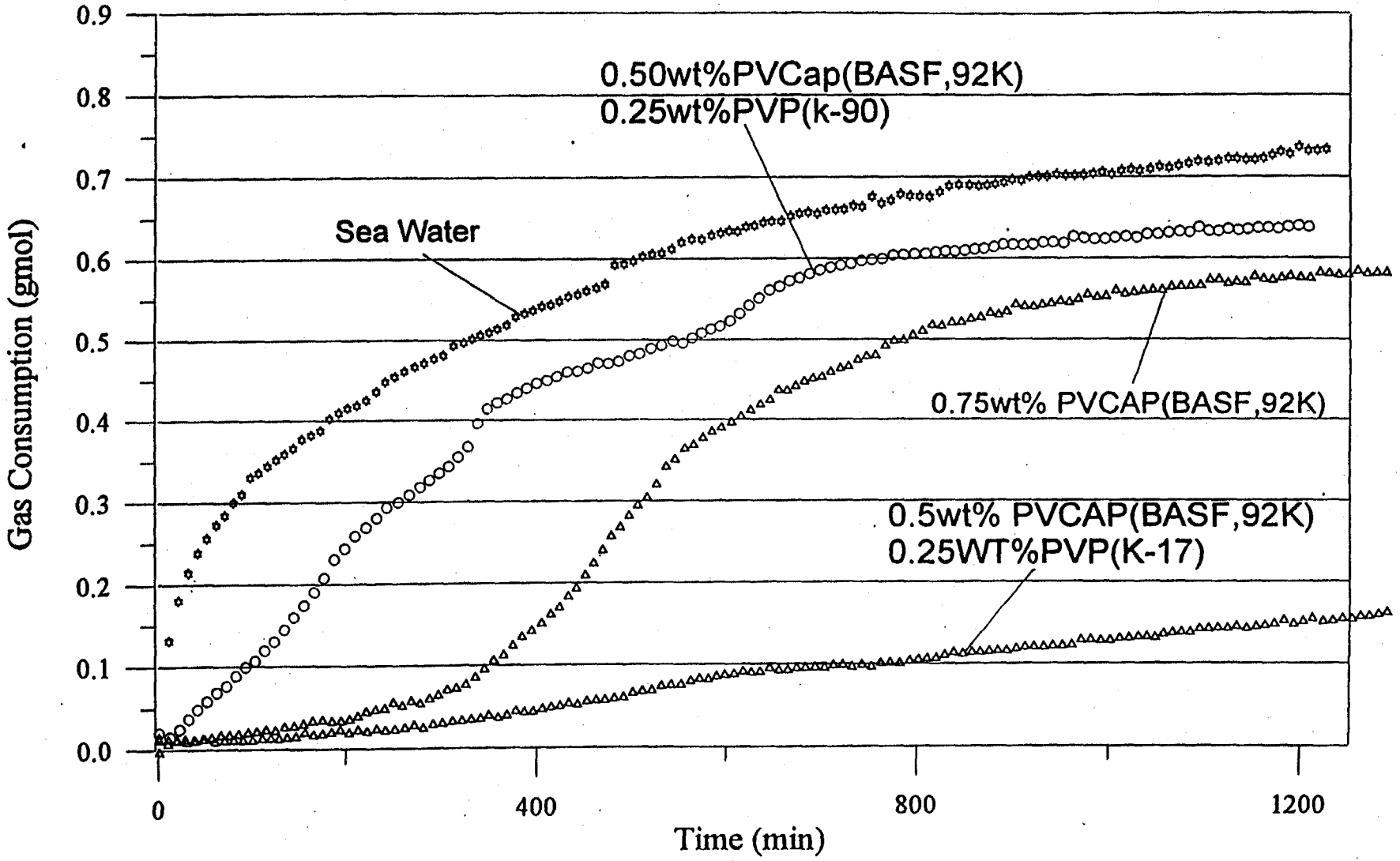

Figure 20.

Combining PVP(K-30) or PVP(K-17) with VC-713(70K) Gives Better Performance Than Using VC-713(70K) Alone

3.5wt% Sea Salt, P = 1500 psig, and T = 39.2°F

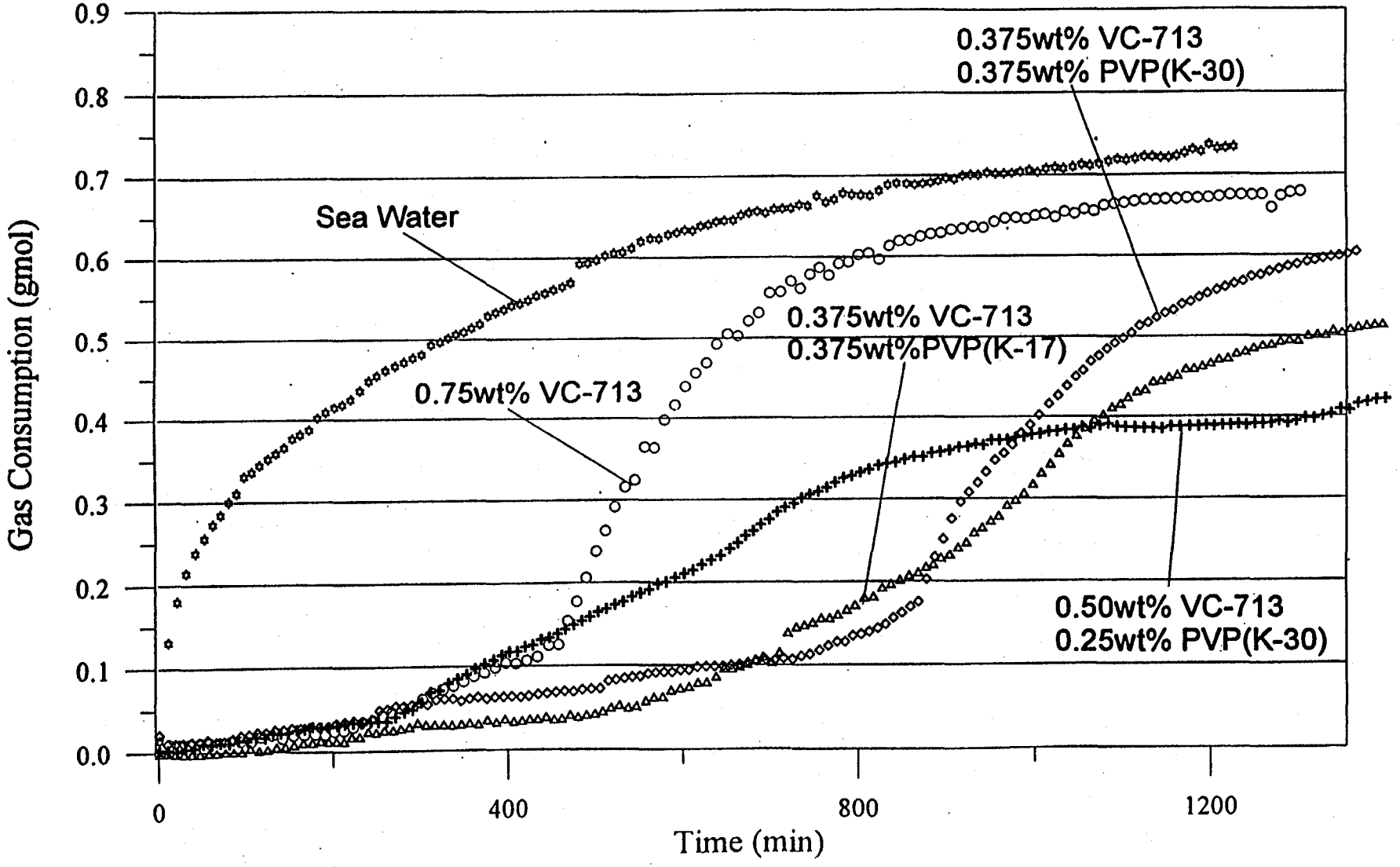

Figure 21.

Combining P2E2OX(500K) with PVCAP(BASF,92K) Provides Better Performance Than Using PVCAP(BASF,92K) Alone

3.5wt% Salt, P = 1500 psig, and T = 39.2°F

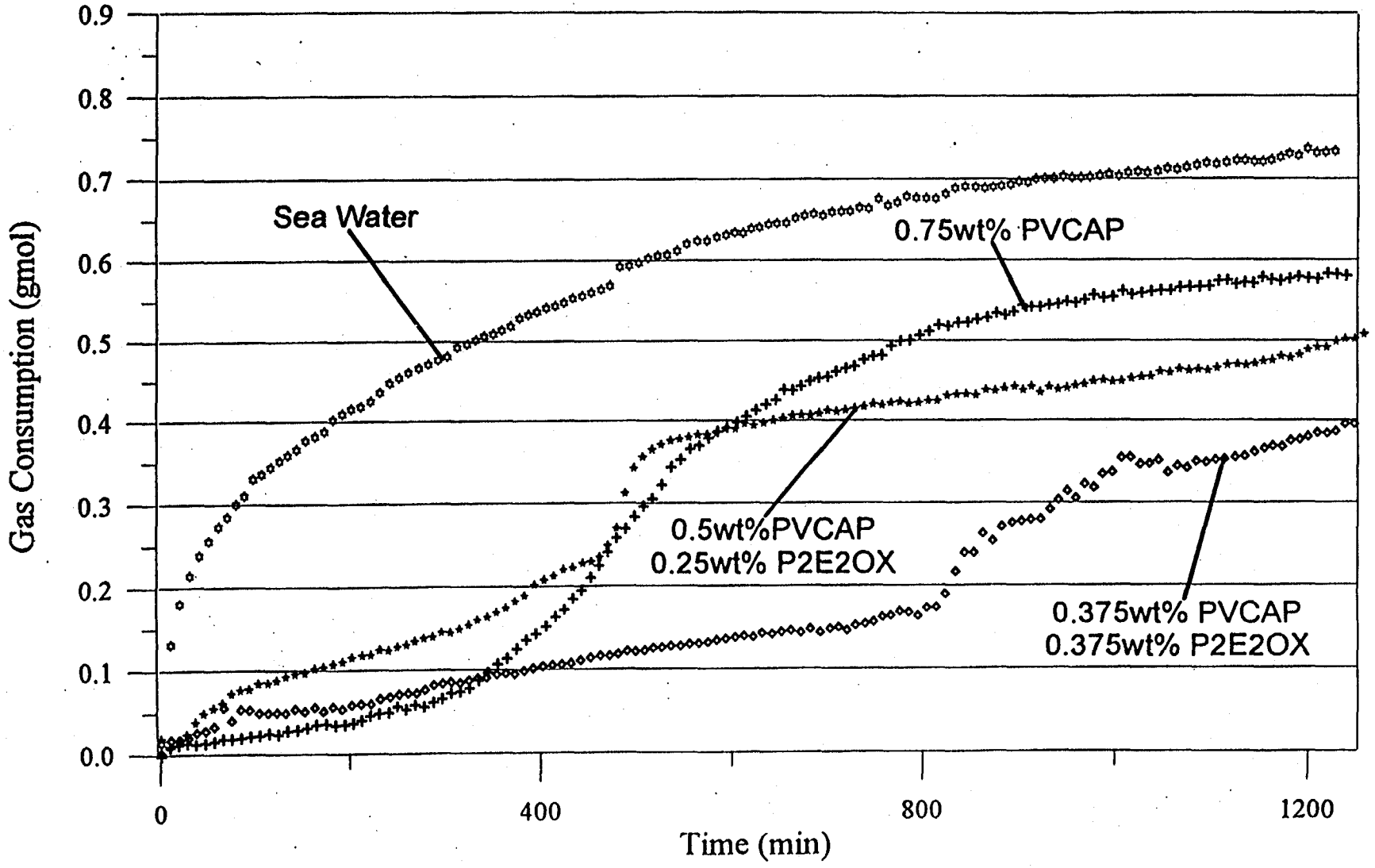

Figure 22.

Combining P2E2OX(500K) with VC-713(70K) Gives Better Performance Than Using VC-713 (70) Alone

3.5wt% Sea Salt, P = 1500 psig, and T = 39.2°F

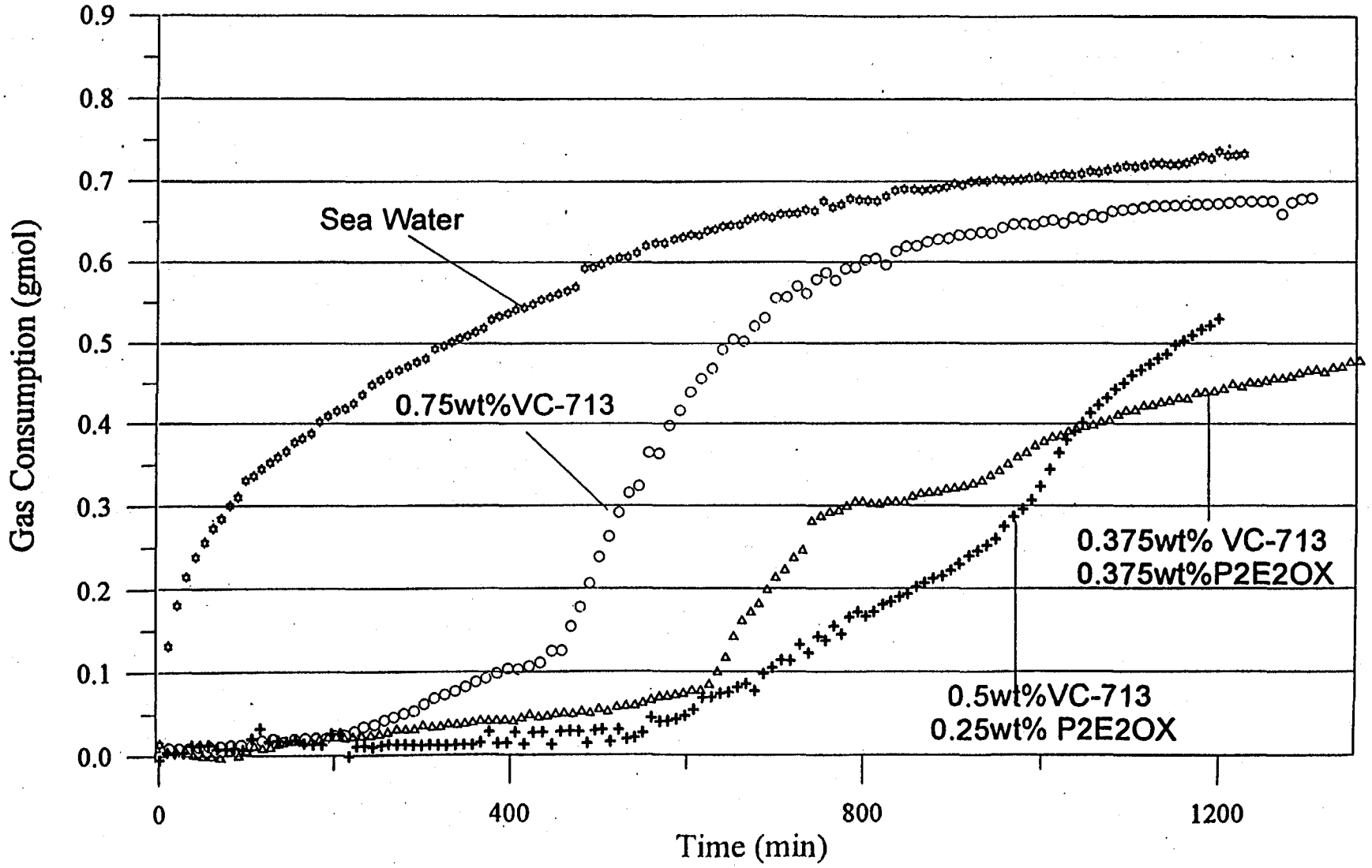

Figure 23.

Blending 0.25wt% P2E2OX with 0.5wt% Different Polymers, VC-713 Performs Best at The Conditions of 3.5wt% Salt , P = 1500 psig and T = 39.2°F

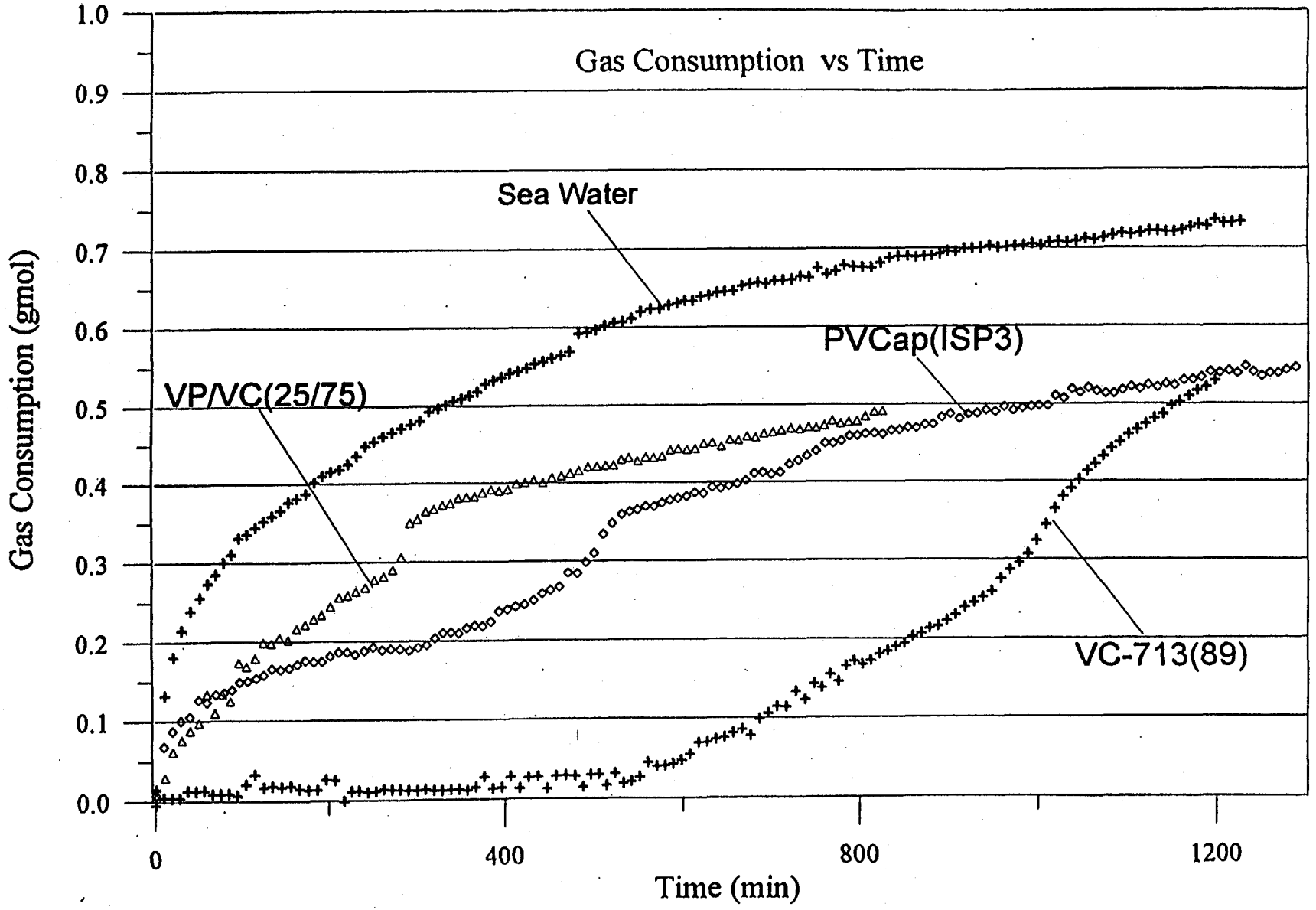

Figure 24. Low MW HE-300 Consumes More Gas Than High MW HE-300 When Combined with PVCAP at The Conditions of 3.5wt% Salt, P = 1500 psig, and T = 39.2°F

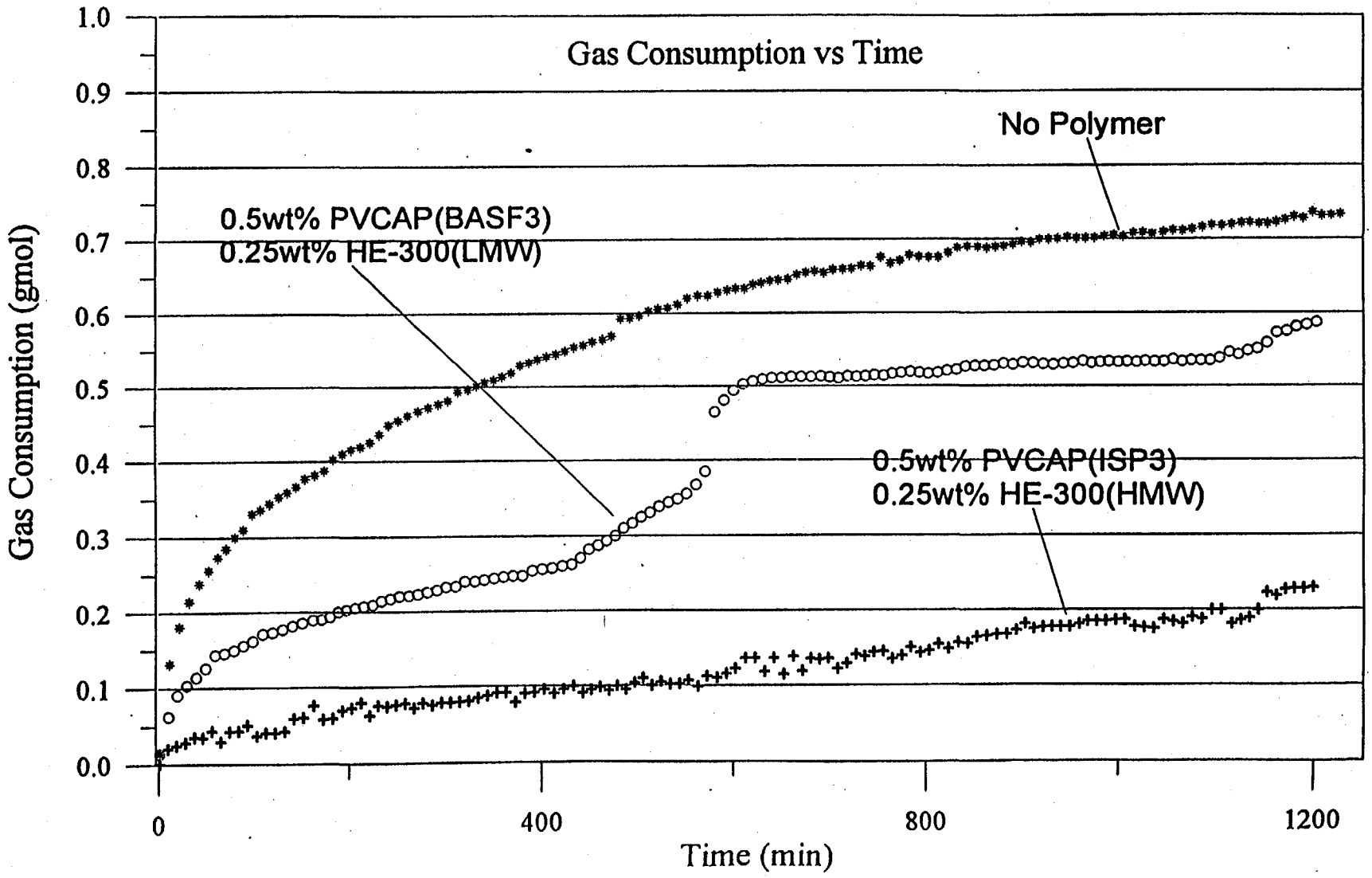

Figure 25..

Combining Both 0.5wt% PVCap(ISP3) and 0.5wt% VC-713(89) with 0.25wt% HE-300 Provide Hydrate Inhibition at The Conditions of P = 1500 psig and T = 39.2°F (Old Batch HE-300)

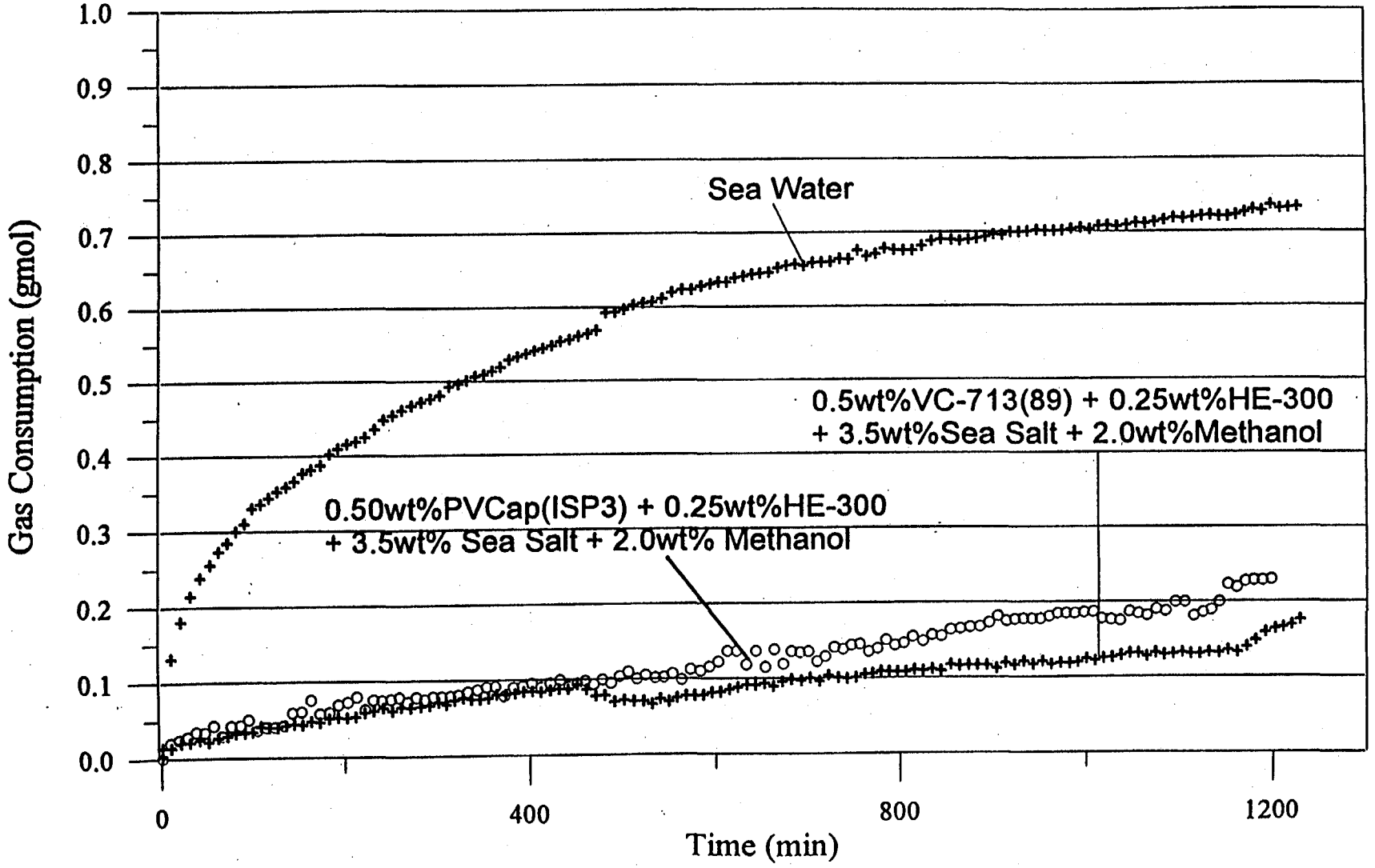

Figure 26. Blending VC-713 with HE-300 Performs Better Than with HEC-100 at The Conditions of 3.5wt% Sea Salt P = 1500 psig and T = 39.2°F

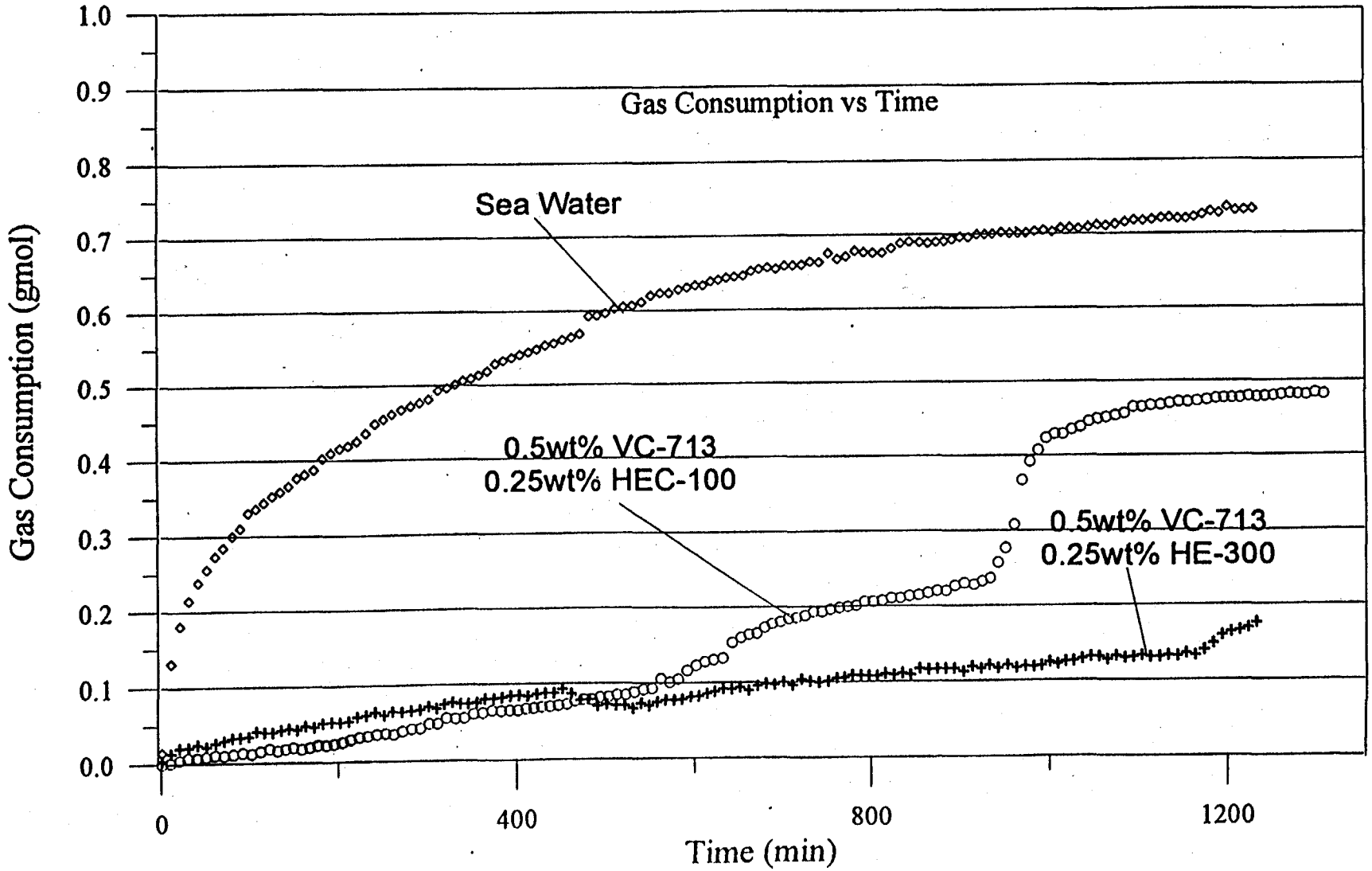

Figure 27.

Blending PVCAP(ISP3) with HE-300 Performs Similar to Blending PVCAP(ISP3) with HEC-100 at The Conditions of P = 1500 psig , T = 39.2°F and 3.5wt% Salt

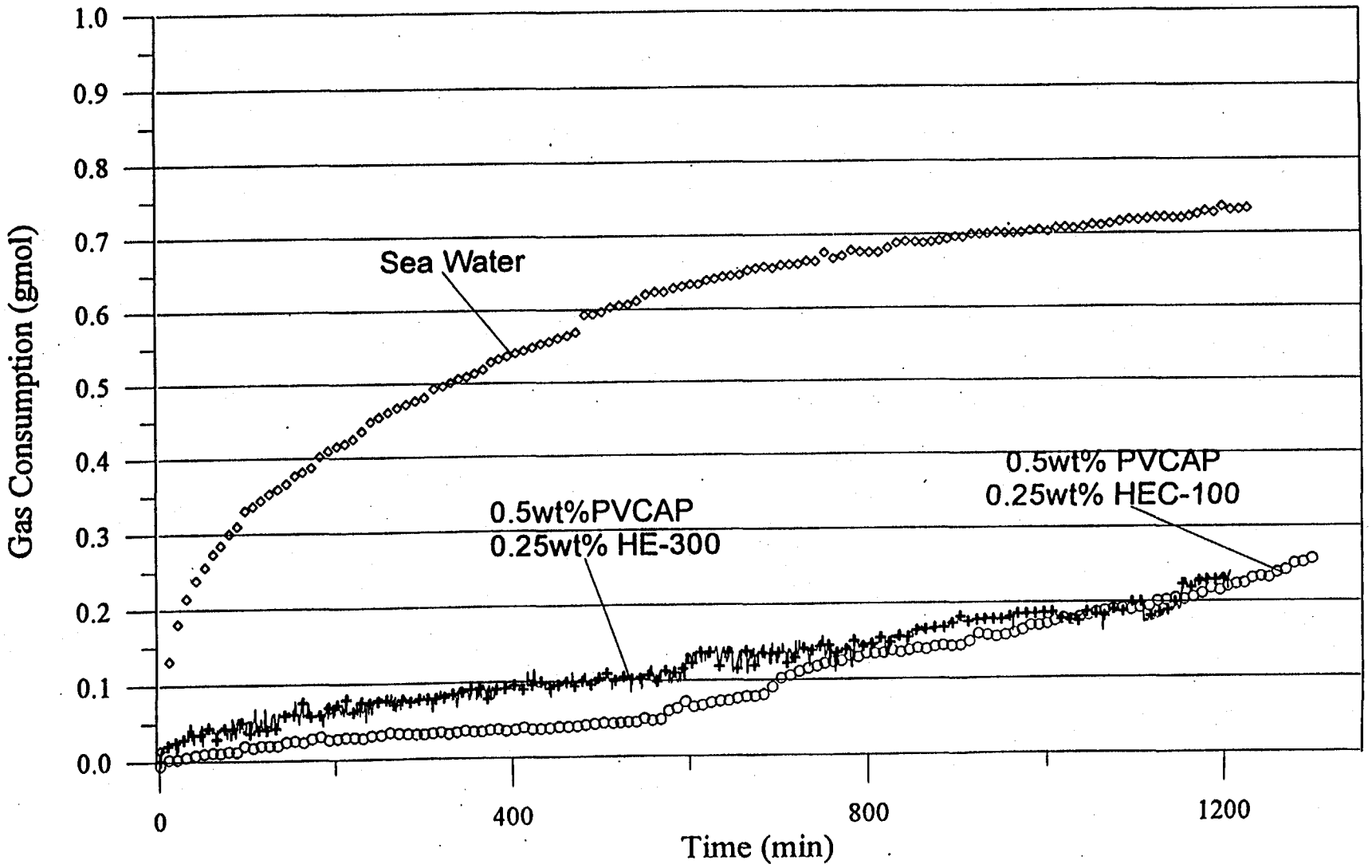

Figure 28.

Blending 0.5wt% PNEAM with 0.5wt% VC-713 Works at 2000 psig, But Blending PNEAM with PVCAP at The Same Conditions Does Not Work Well ,

Test Conditions are: 0.5wt% Polymer + 0.5wt%PNEAM + 3.5wt% Salt
P = 2000 psig and T = 39.2°F

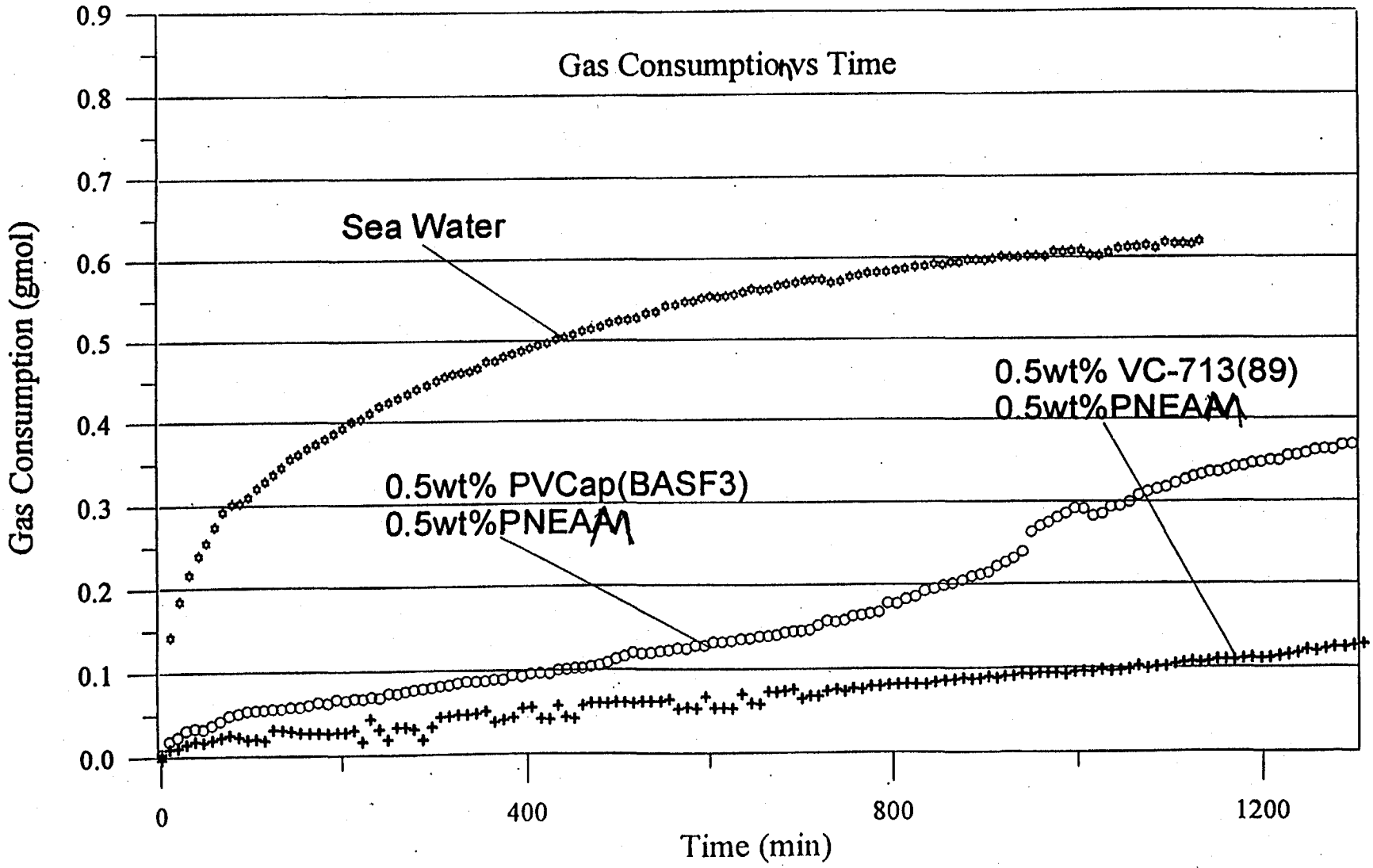

Figure 29.

The Solution 0.75wt%VC-713(89) + 0.25wt%HE-300 + 3.5wt% Sea Salt, Provides Hydrate Inhibition and Has Good Reproducibility at P = 2000 psig and T = 39.2 F

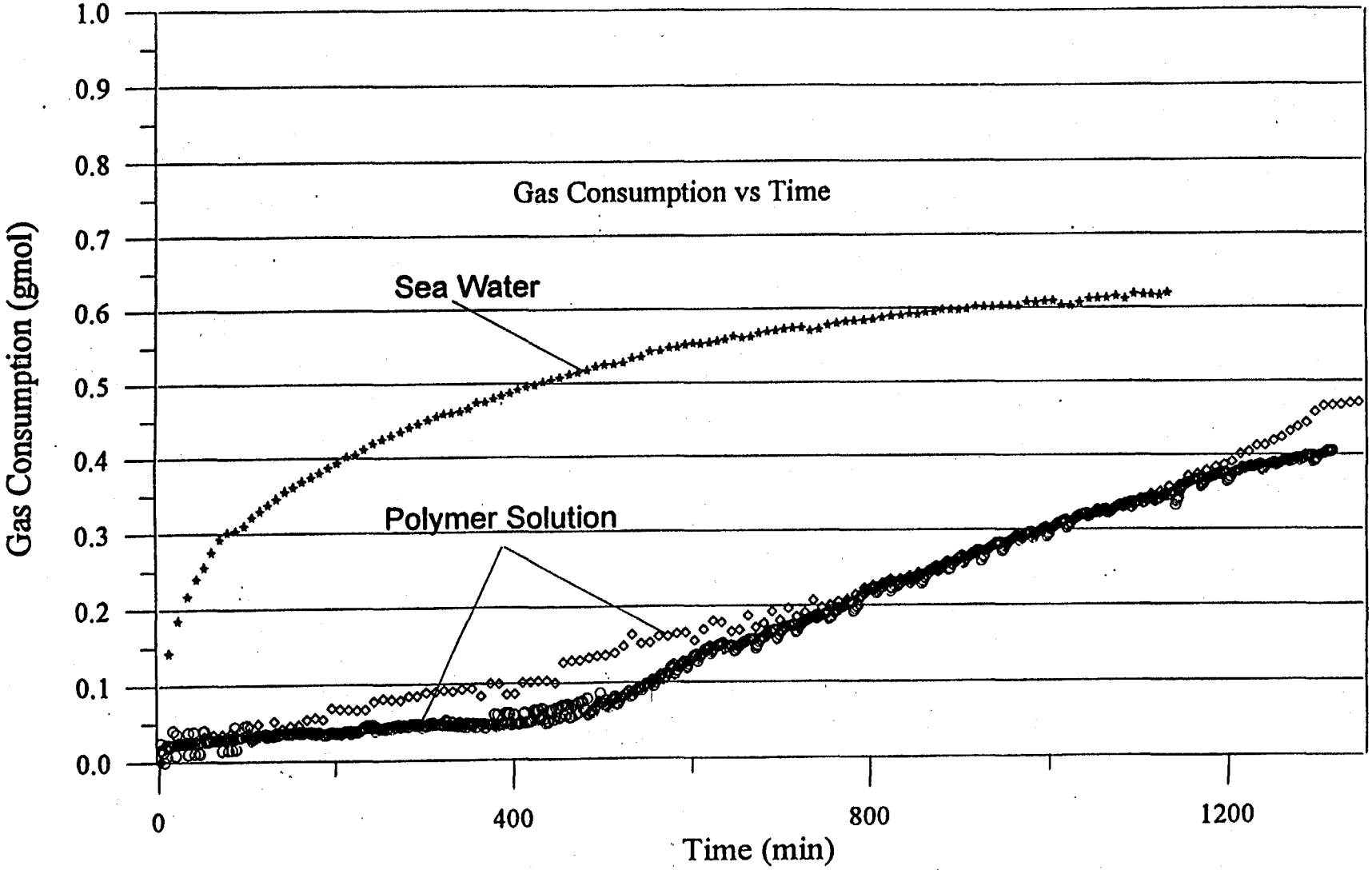

Figure 30.

When Blended with HE-300, PVCap(ISP3) Works,
VC-713(89) and VP/VC(25/75) Do Not Work
at the Conditions of 0.75wt% Polymers + 0.25wt% HE-300
+3.5wt% Salt + 3.0wt%Methanol , P = 2000 psig and T = 39.2 F
(Old Batch HE-300)

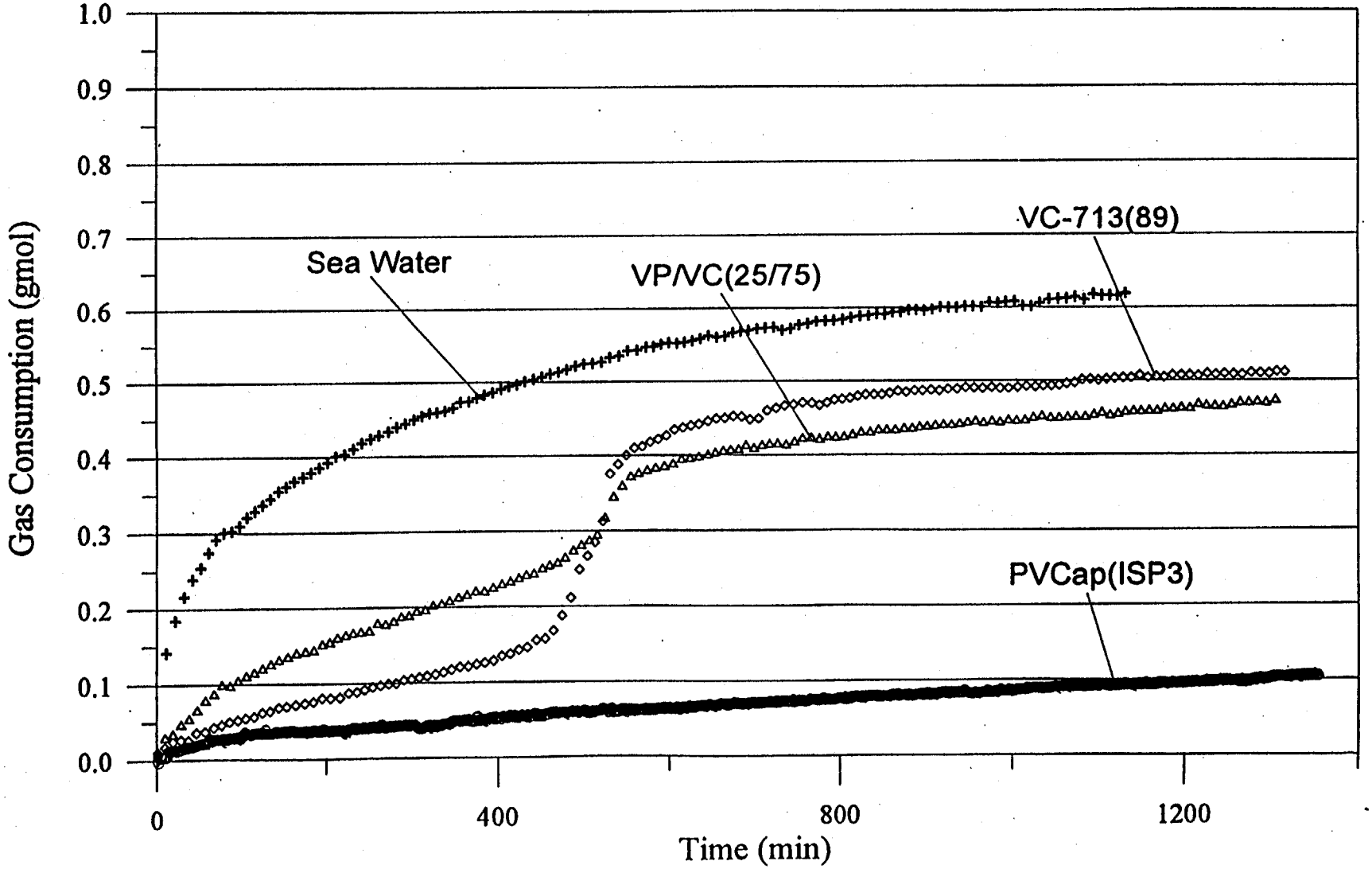

Figure 31.

0.75wt% PVCap(ISP3) + 0.25wt% HE-300 Works Well,
0.50wt% PVCap(ISP3) + 0.25wt% HE-300 Does Not Work at
The Conditions of 3.5wt% Sea Water ,P = 2000 psig and T= 39.2°F
(Old Batch HE-300)

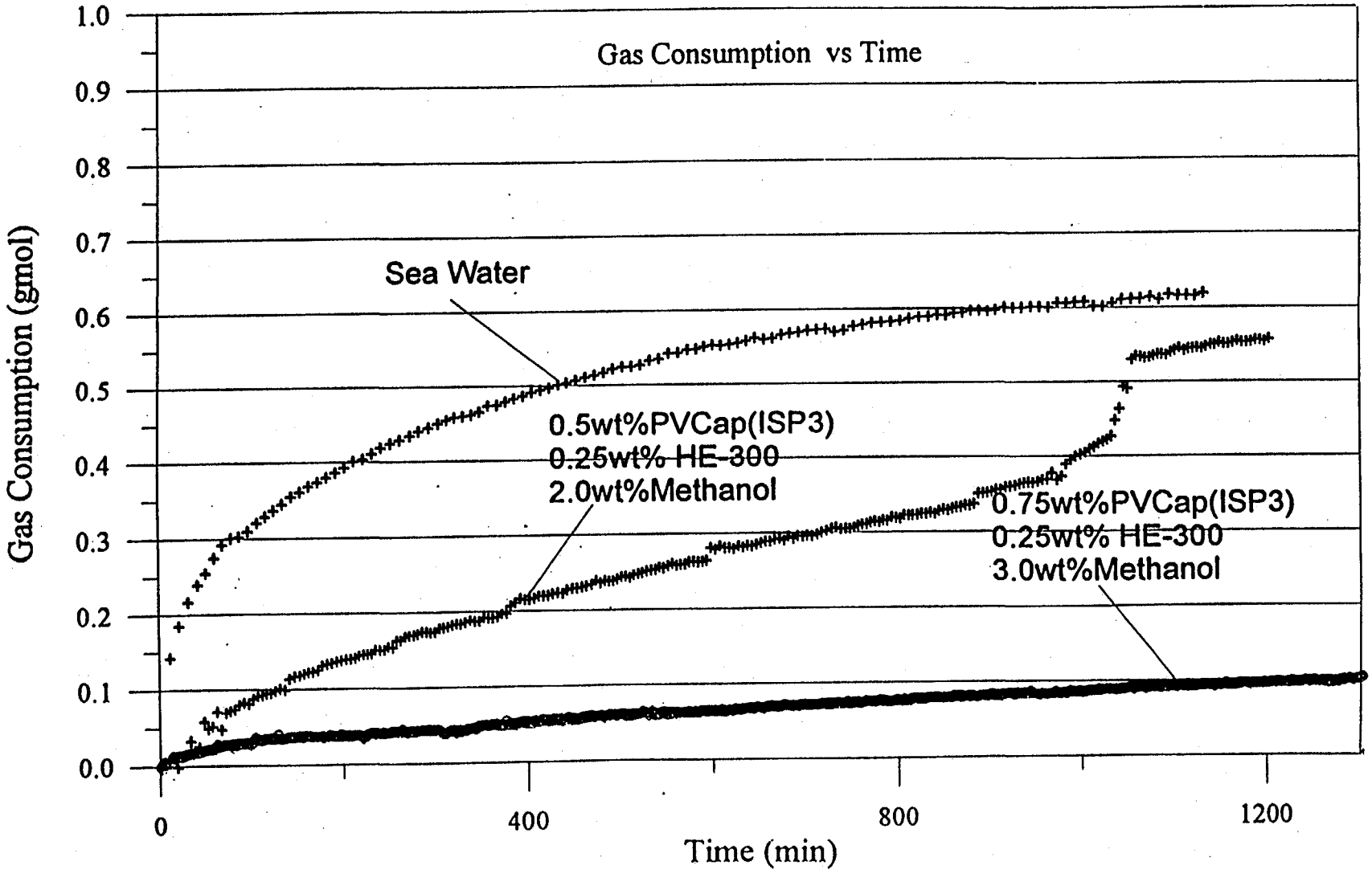

Figure 32.

0.75wt%PVCap(ISP3) + 0.25wt% HE-300 + 3.5wt% Sea Salt
The Fresh Solution Worked Well, After one Month,
The Aged Solution Does Not Work. (Old Batch HE-300)
at 2000 psig and 39.2°F

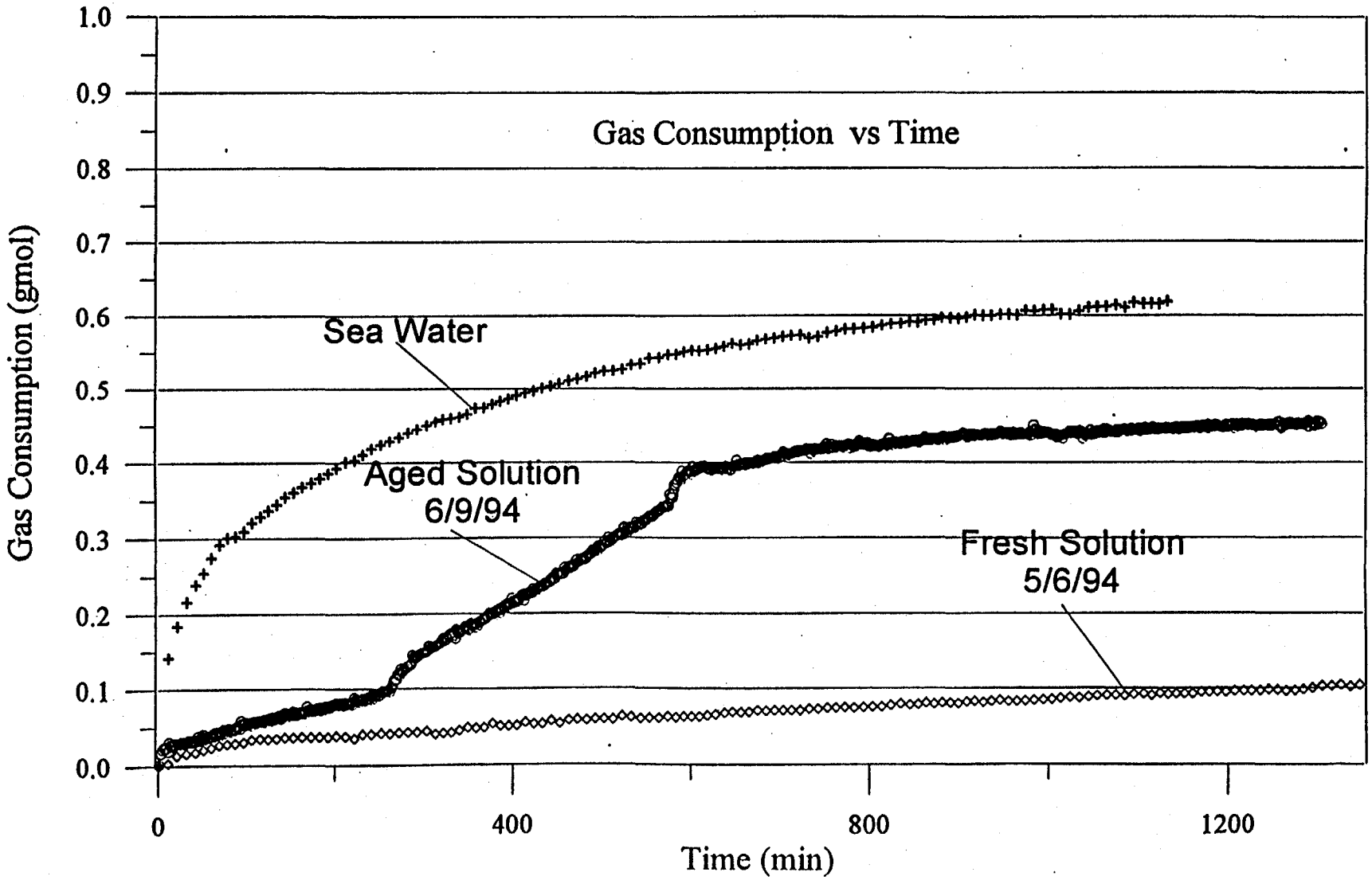

Figure 33.

Combine 0.5wt%VC-713(89) with 3.5wt% Salt Works Well, But Combine 0.5wt% VC-713(89) with 3.4wt% or 8.0wt% Methanol Does Not Work at P = 1000 psig , T = 39.2°F

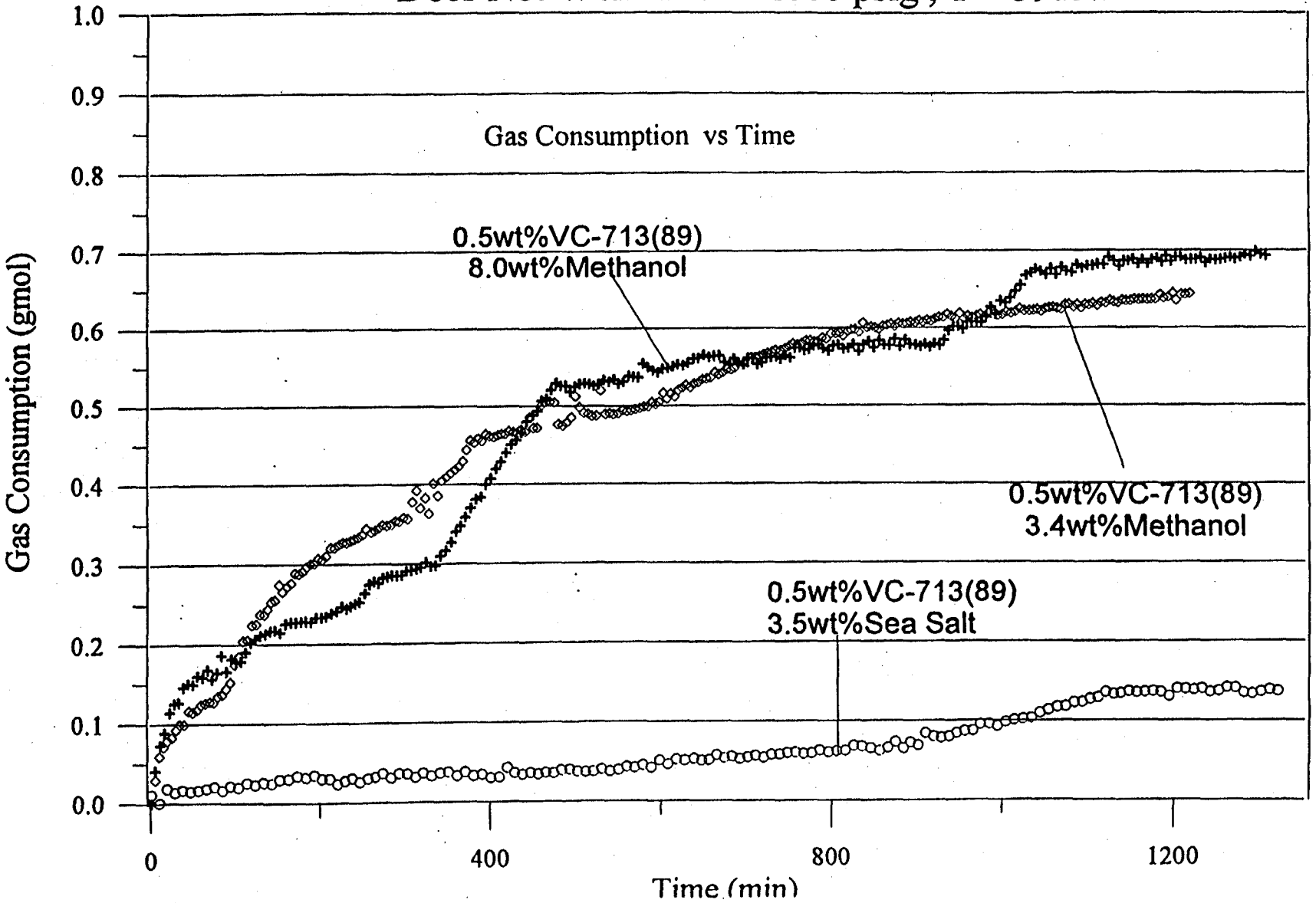

Figure 34.

PVCAP(BASF3, 50wt% Solids in Ethanol) Performs Better Than PVCAP(BASF4, 50wt% Soliods in Methanol) at The Conditions of 0.5wt%PVCAP + 3.5wt% Sea Salt, P = 1000 psig and T = 39.2°F

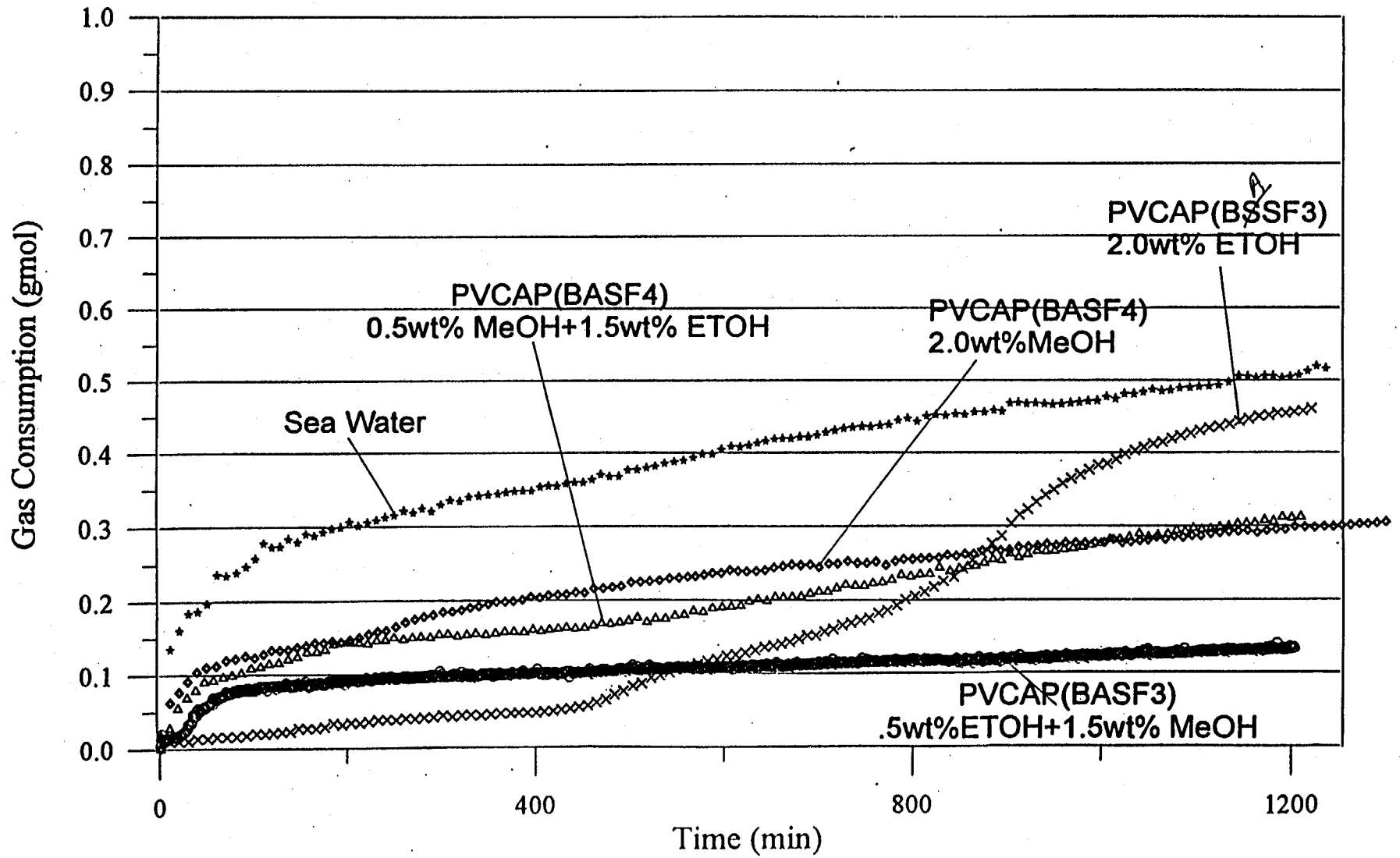

Figure 35.

High Concentrations of Sea Salt in the Solutions Containing 0.5wt%VC-713(89) Provides Inhibition Performance at P = 1500 psig and T = 39.2°F .

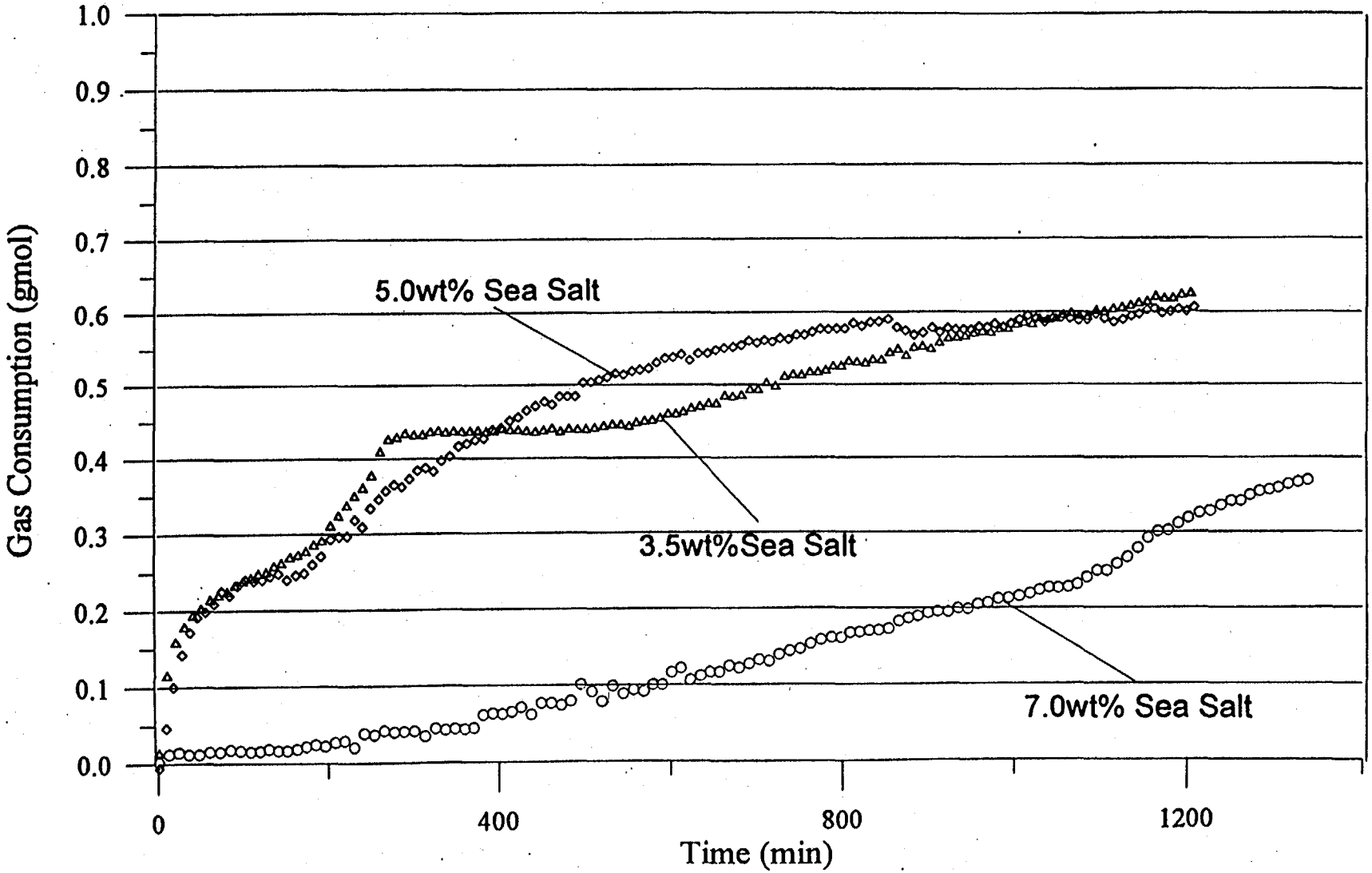

Figure 36.

Increasing The Concentration of VC-713 Can Improve The Inhibition Performance in 3.5wt% Salt Solution at P = 1500 psig, and T = 39.2°F

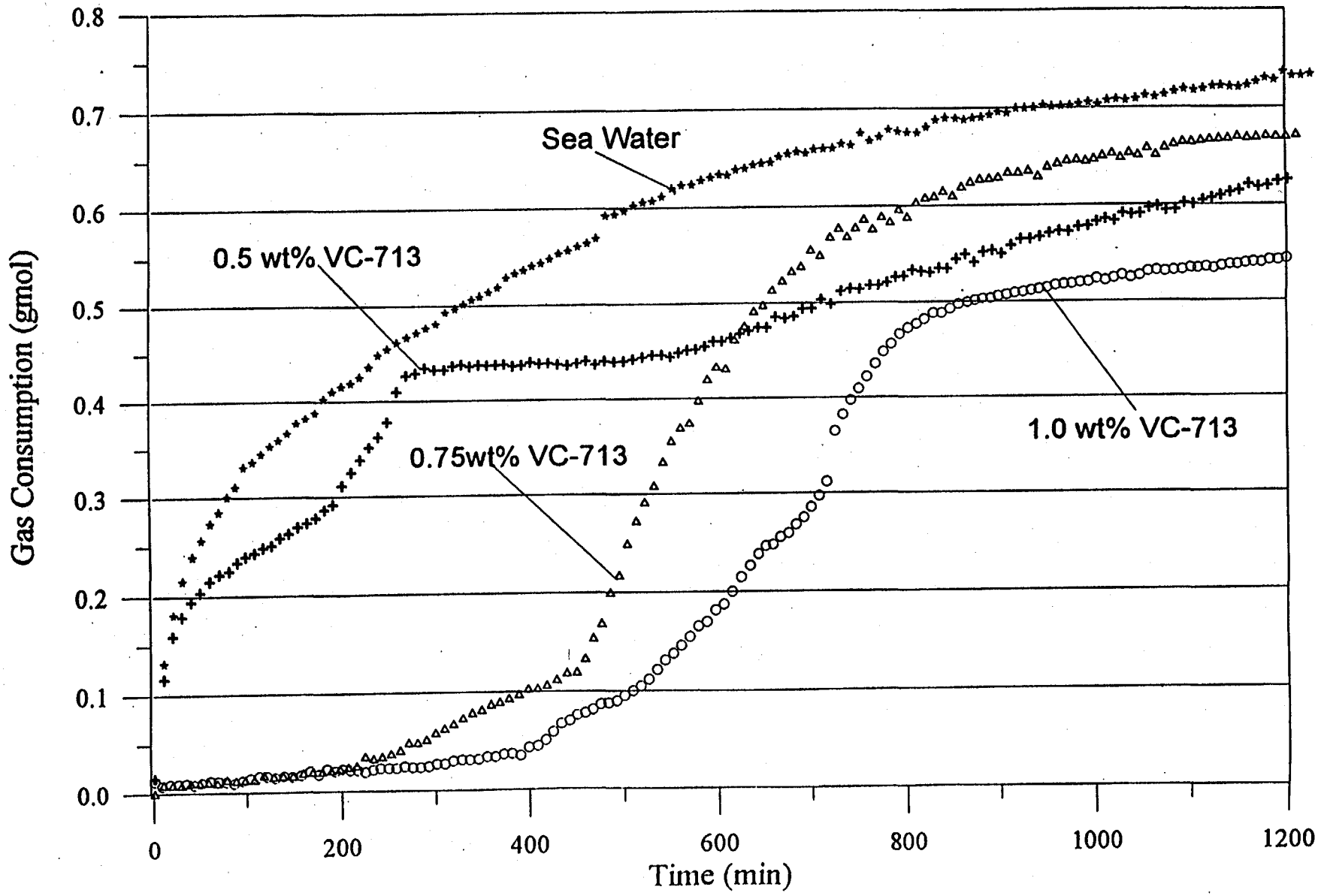

Figure 37.

When Combined with 0.5wt% VC-713, Increasing The Concentration of Methanol Can Improve Hydrate Inhibition in DI Water at 39.2 °F

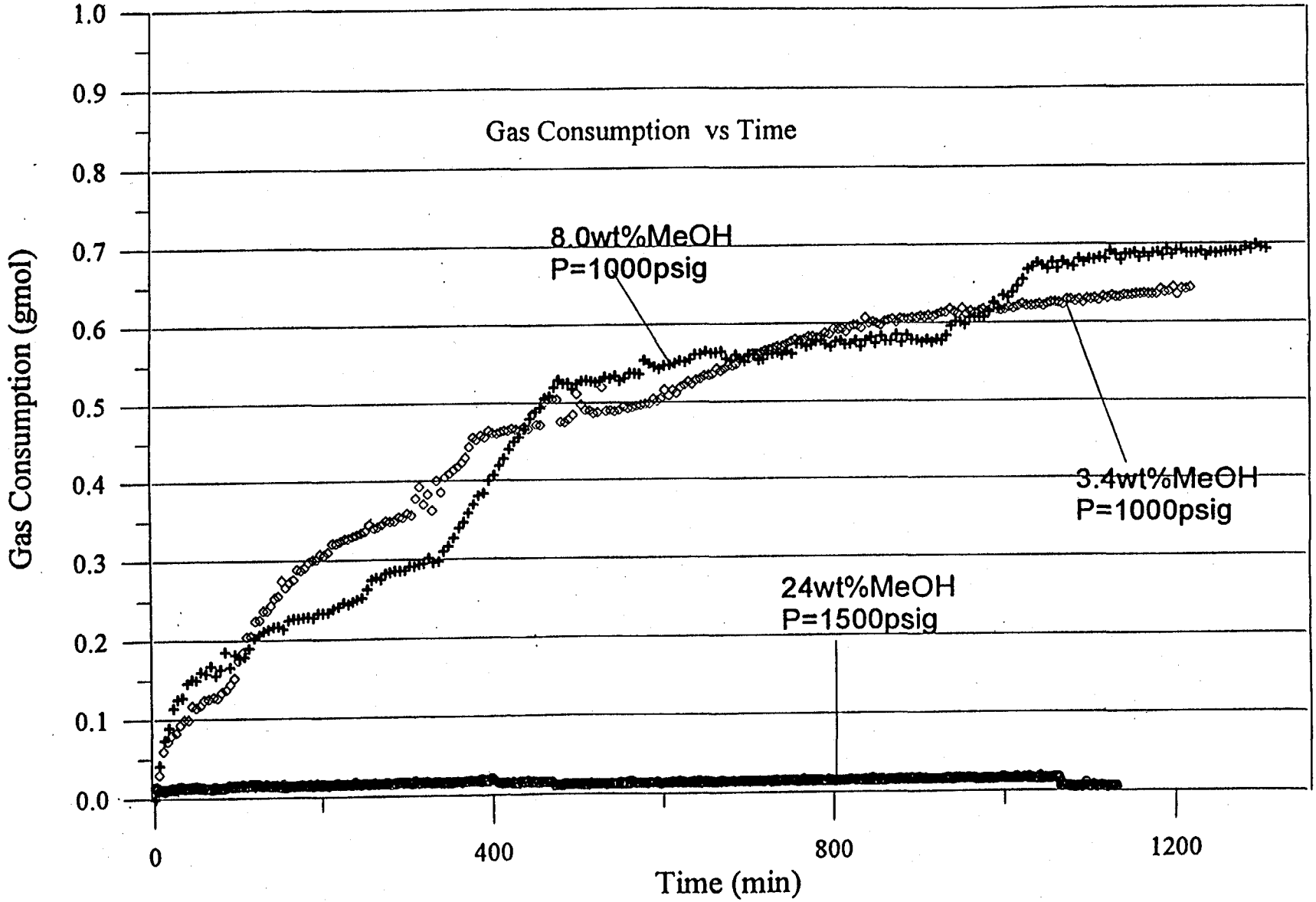

Figure 38.

Increasing The Concentration of Thermodynamic Inhibitors
Can improve Inhibition Performance When Combined
with 0.5wt% VC-713 at 1500psig and 39.2° F

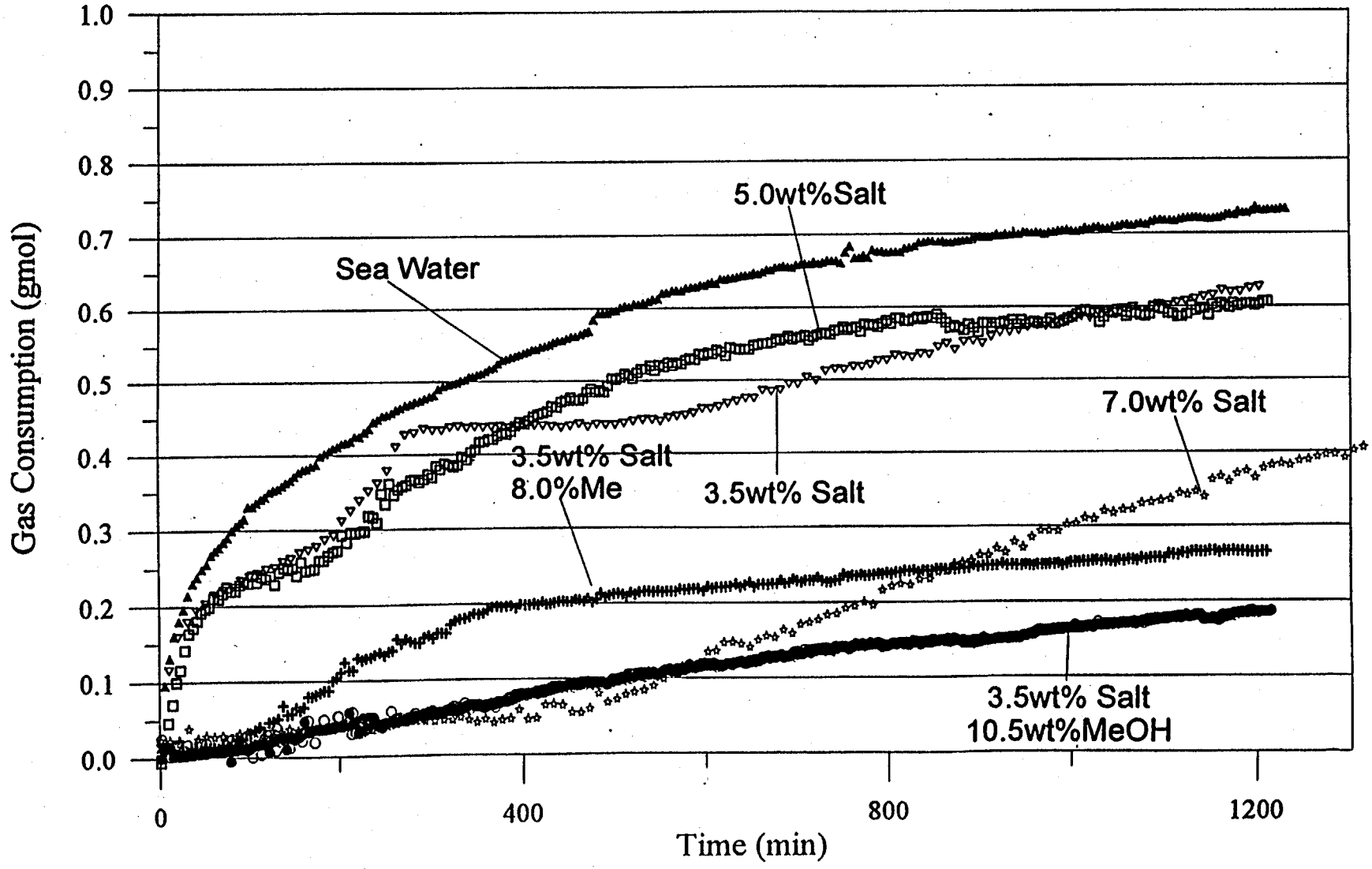

Figure 39.

Hydrate Inhibition at 2000 psig and 39.2°F Can Be Achieved by Combining Kinetic and Thermodynamic Inhibitors

0.5wt% Polymer + 3.5wt% Salt + 15.0wt% Methanol

No. 13

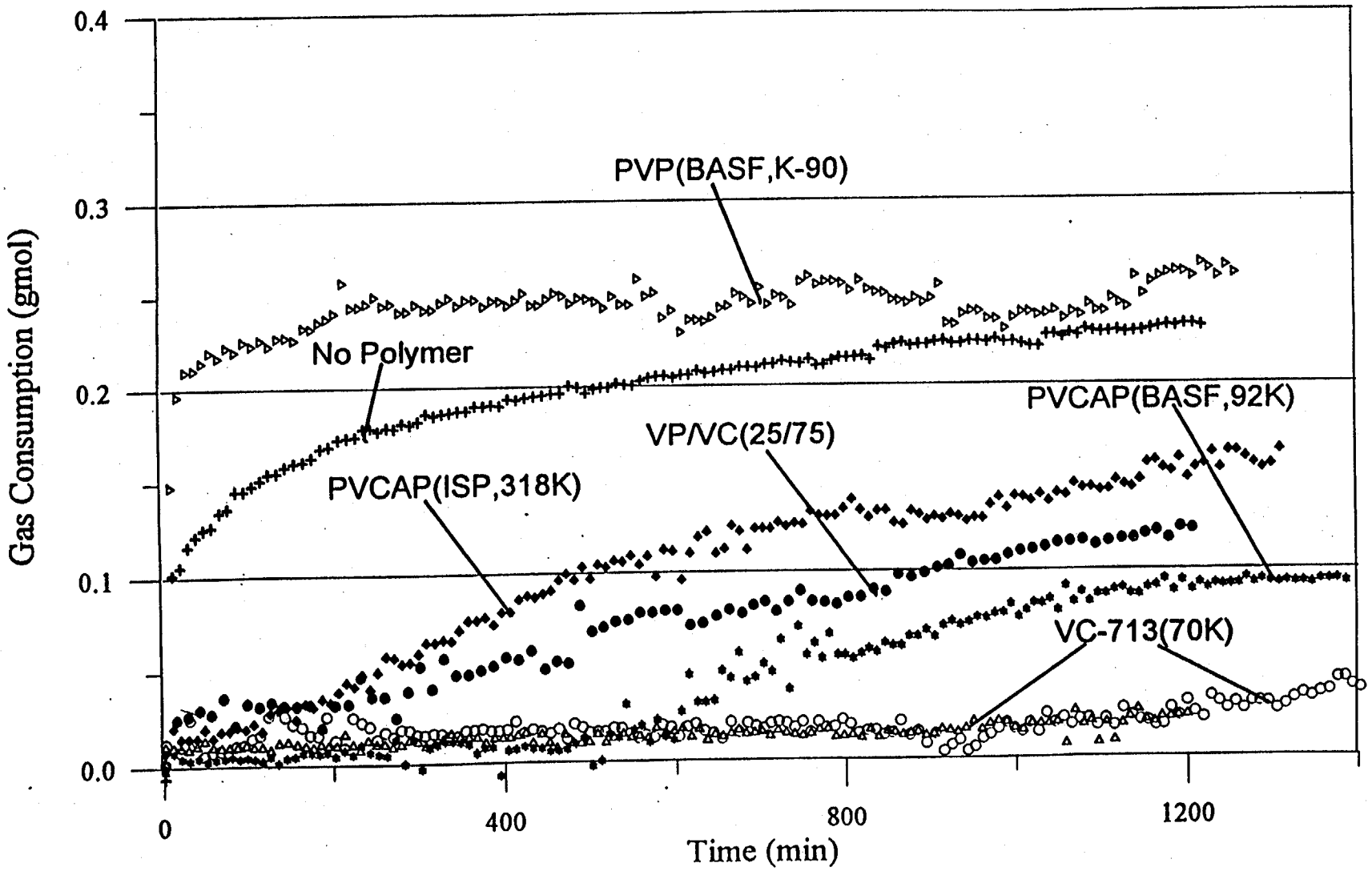

Figure 40.

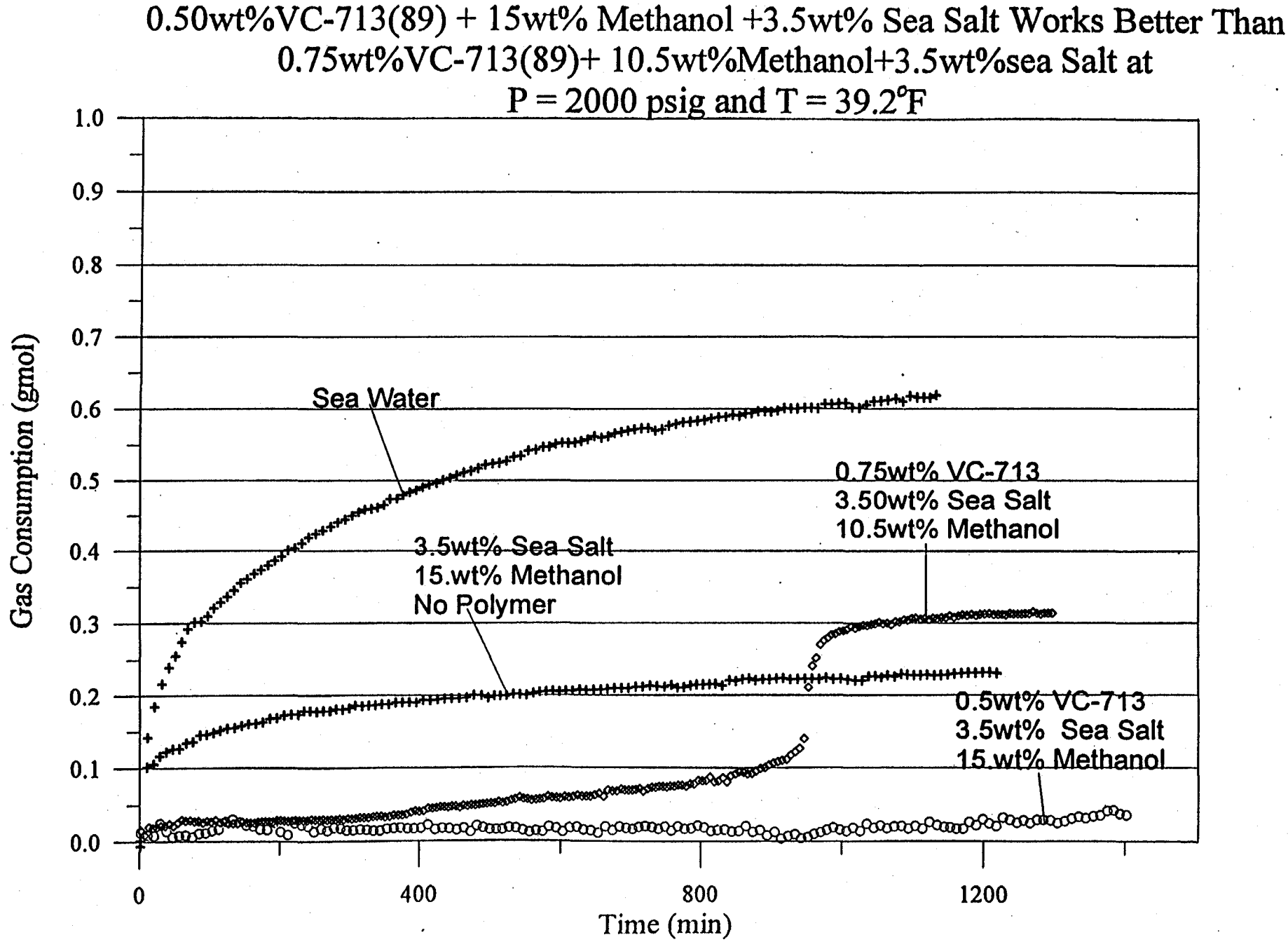
0.50wt%VC-713(89) + 15wt% Methanol +3.5wt% Sea Salt Works Better Than
0.75wt%VC-713(89)+ 10.5wt%Methanol+3.5wt%sea Salt at
P = 2000 psig and T = 39.2°F
Gas Consumption (gmol)
1.0
0.9
0.8
0.7
0.6
0.5
0.4
0.3
0.2
0.1
0.0
0
400
800
1200
Time (min)
Sea Water
0.75wt% VC-713
3.50wt% Sea Salt
10.5wt% Methanol
3.5wt% Sea Salt
15.wt% Methanol
No Polymer
0.5wt% VC-713
3.5wt% Sea Salt
15.wt% Methanol

Figure 41.

Reducing Salt or Methanol in The Solution of 0.5wt% VC-713 + 15wt% Methanol + 3.5wt% Salt, The Gas Consumption Will Increase at P = 2000 psig and T = 39.2°F.

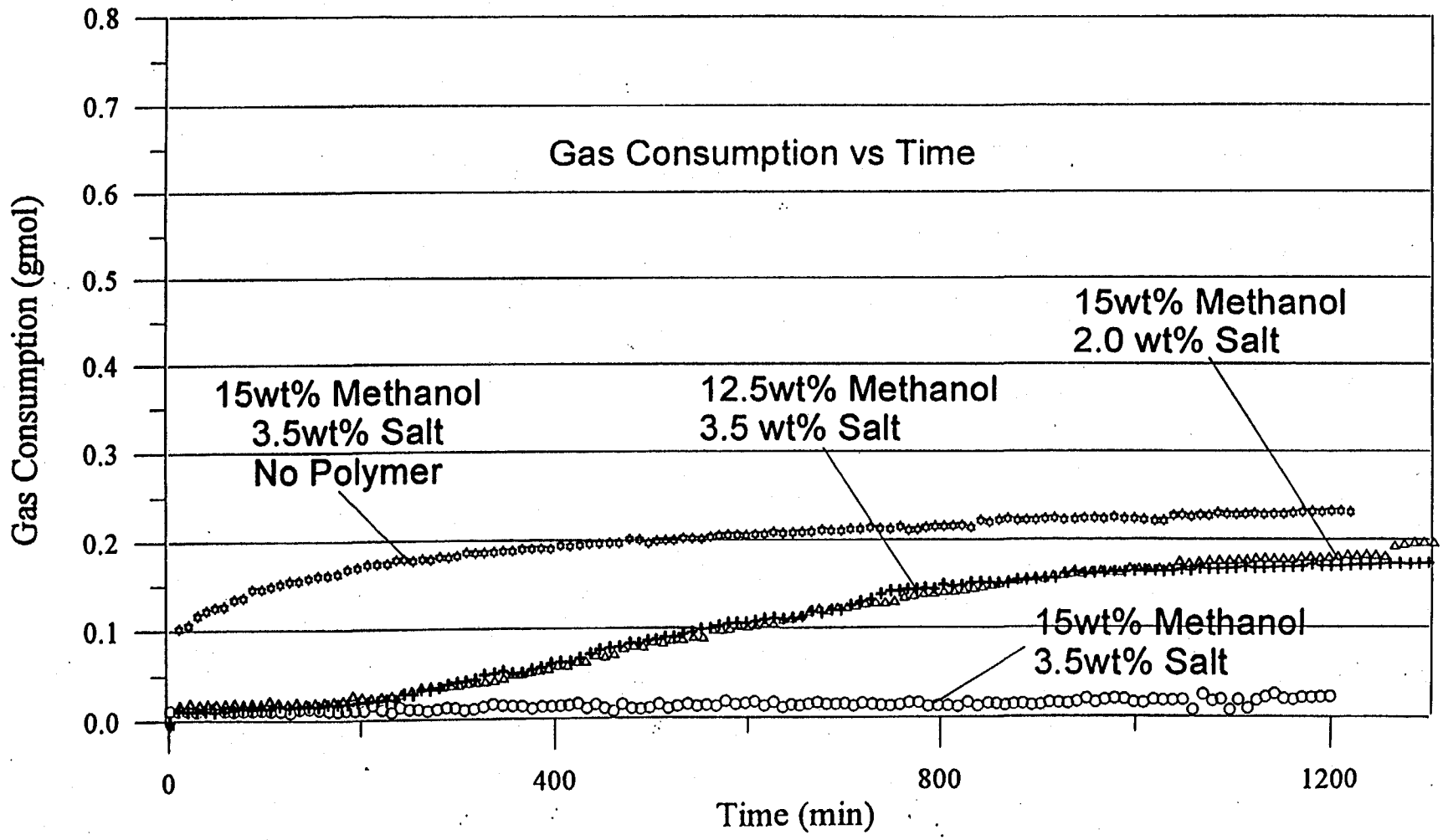

Figure 42.

Reducing Salt or Methanol in The Solution of 0.5wt% PVCAP (BASF3) +15.wt% Methanol + 3.5 wt% Salt, The Gas Consumption Will increase at P = 2000 psig, T = 39.2°F

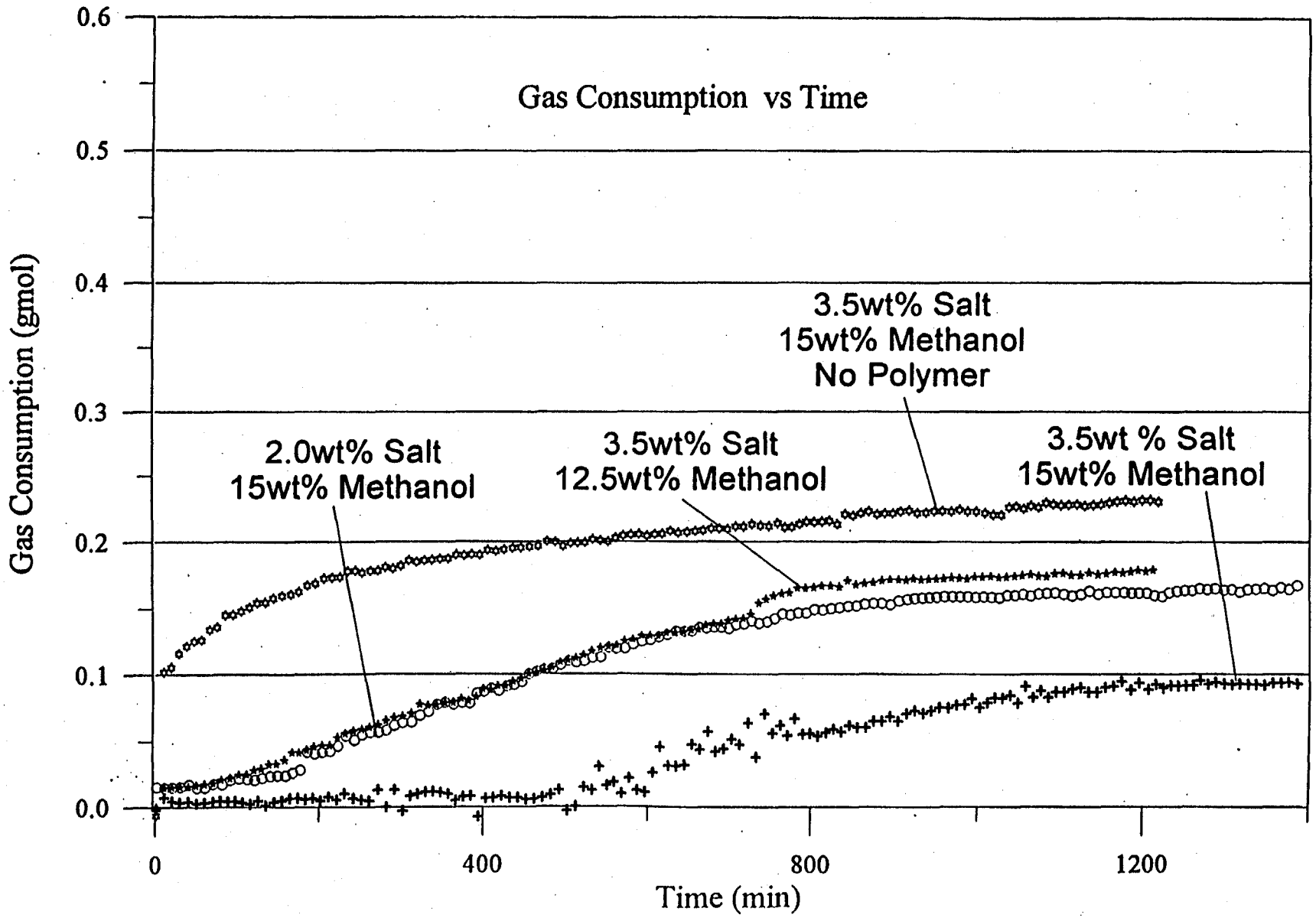

Figure 43.

At 2000 psig and 39.2°F, Combing 15wt% Methanol with 0.5wt% VC-713 Works Well in Sea Water, at The Same Conditions, PNEAM Does Not Work

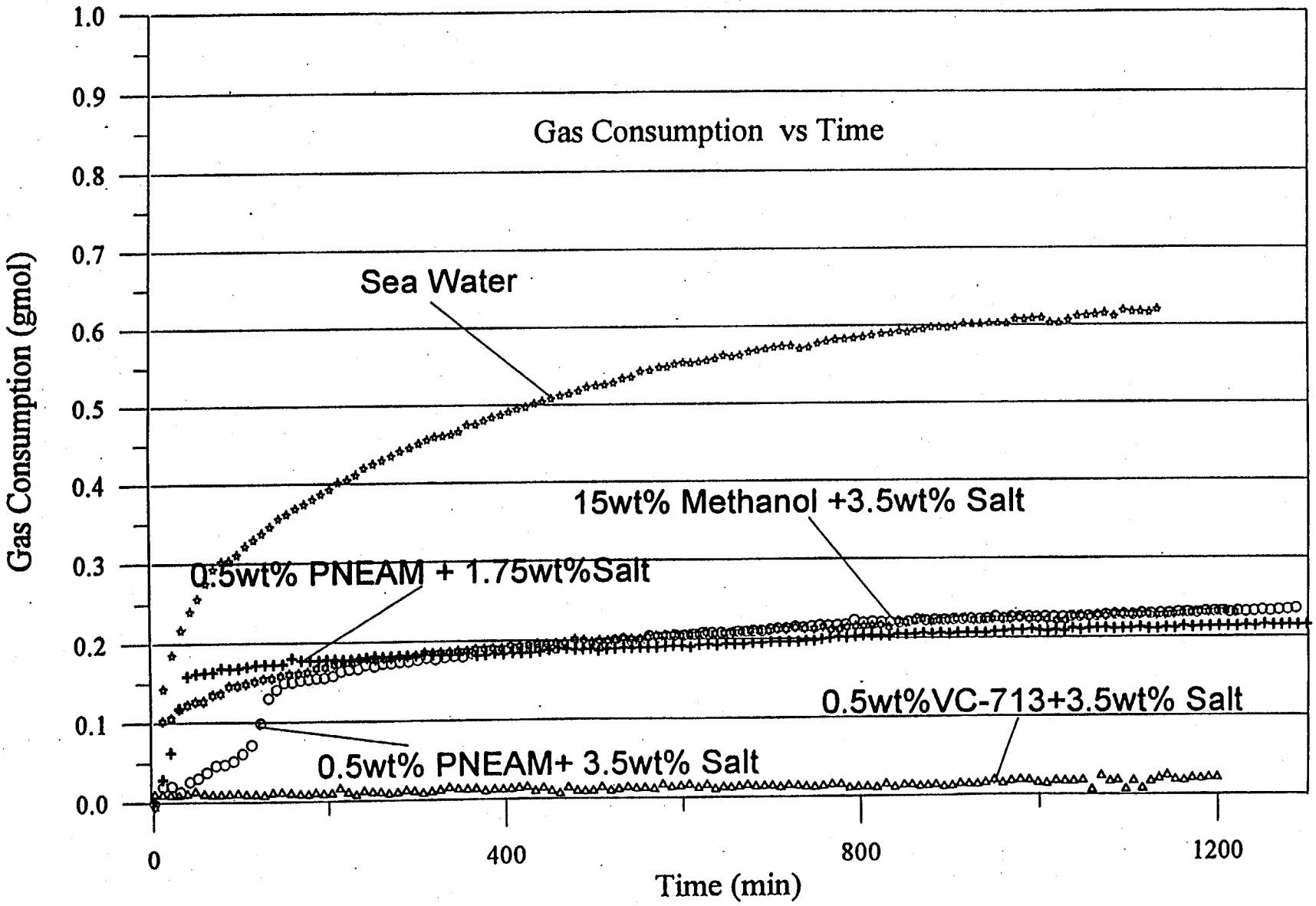

Figure 44. Increasing The Percentage of VC in Copolymer VP/VC, Improves Hydrate Inhibition Performance

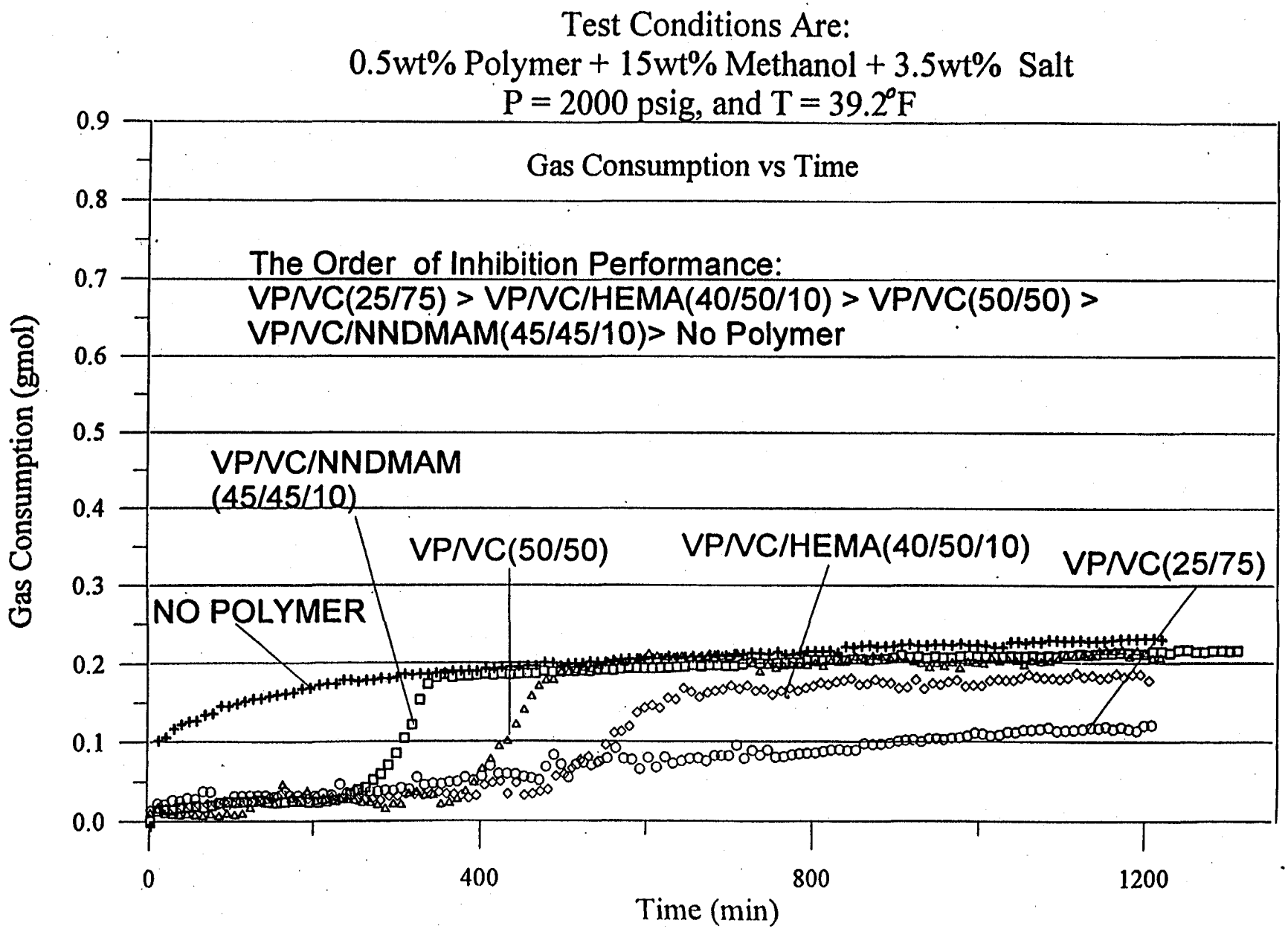

Figure 45.

Ethanol Does Not Work As Well As Methanol When Combined with VC-713

0.5wt%VC-713 + 3.5wt% Salt + X wt % Alcohol,
P = 2000 psig, and T = 39.2°F

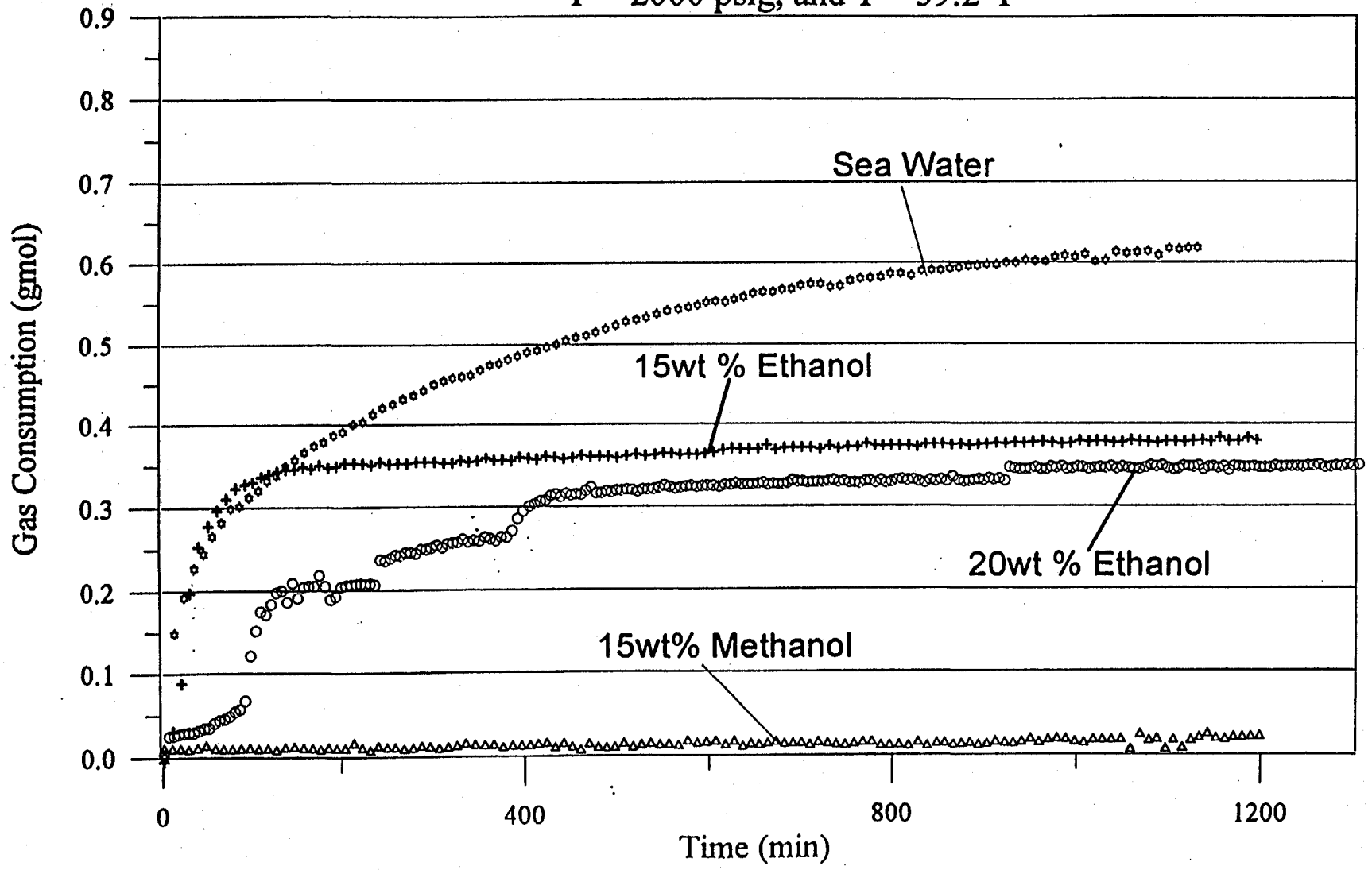

Figure 46.

Combining 0.5wt% VC-713 with 15wt% MEG Does Not Work as Well as Combining 0.5wt% VC-713 with 15 wt% MeOH in Sea Water at 2000 psig and 39.2°F

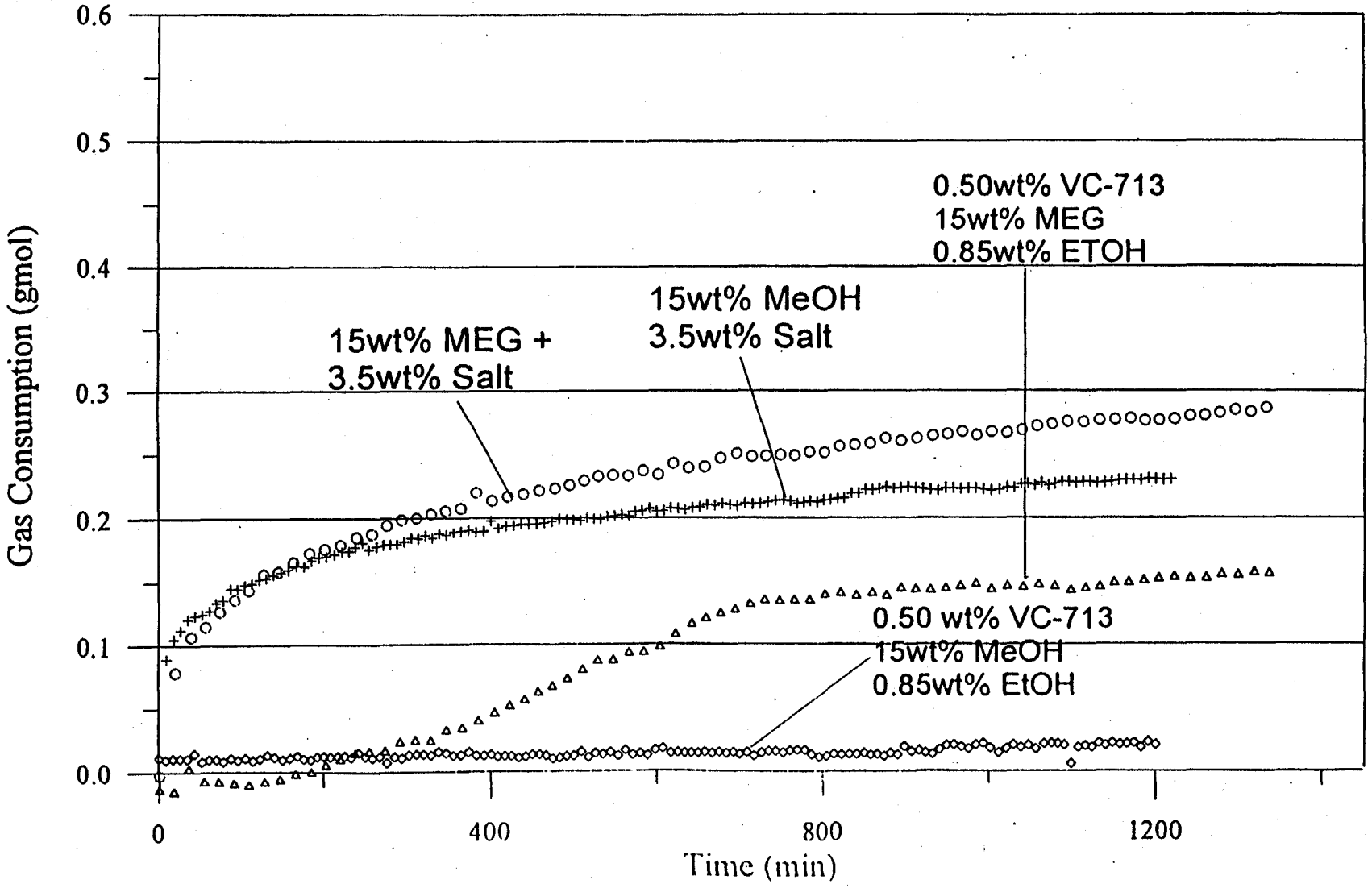

Figure 47:

Combining 0.75wt% VC-713 or 0.375wt% PVP(K-17)+0.375wt% PVCAP with 15 wt% MEG(Ethlyene Glycol) + 3.5wt% Salt Provides Good Hydrate Inhibition at 2000 psig and 39.2°F

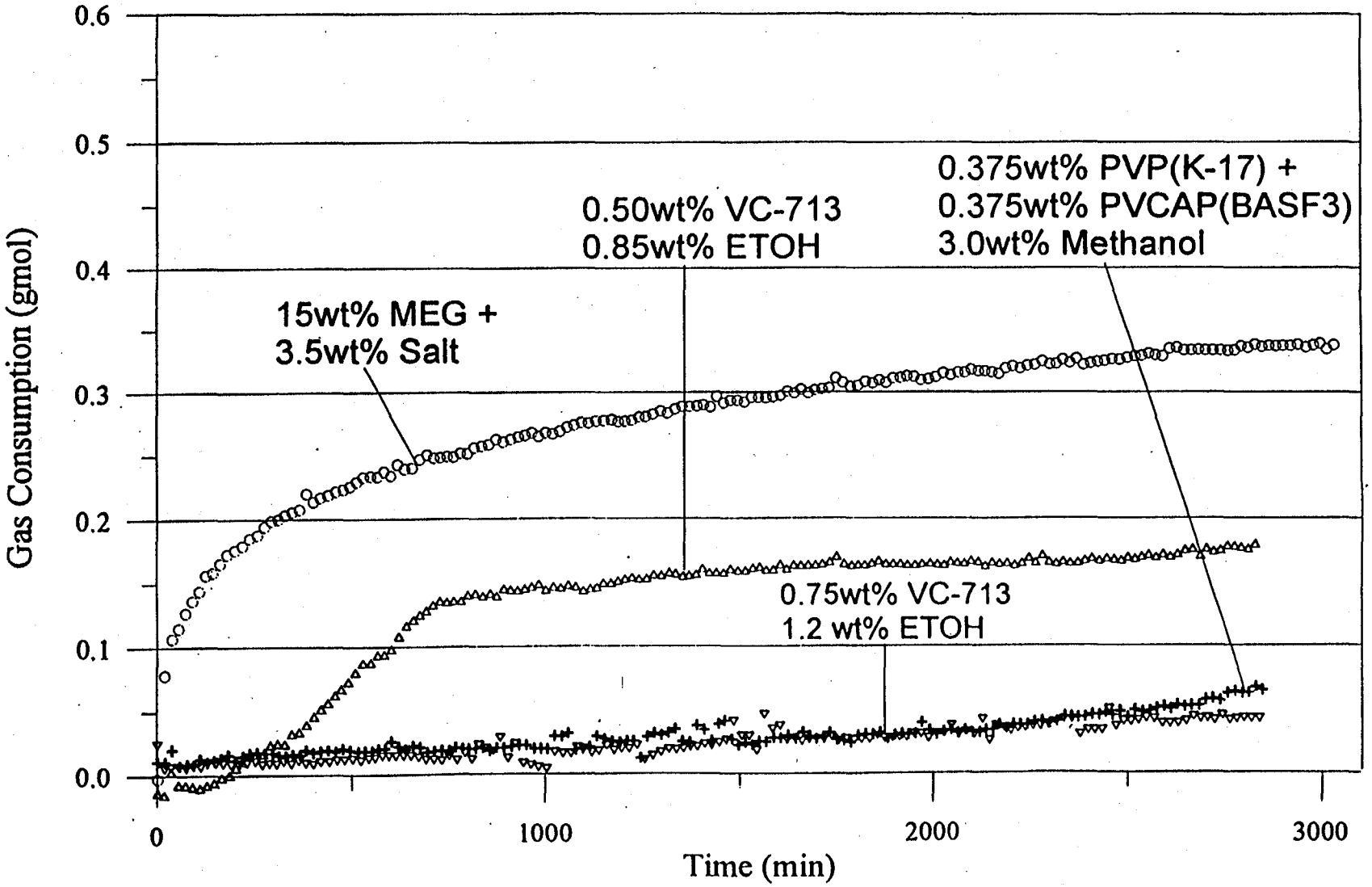

Figure 48.

Increasing The Concentration of MEG Can Improve Inhibition Performance When Combined with 0.375 wt%PVCAP(BASF3) + 0.375wt% PVP(K-17) + 3.0wt% MeOH at 1500 and 2000 psig and 39.2 °F

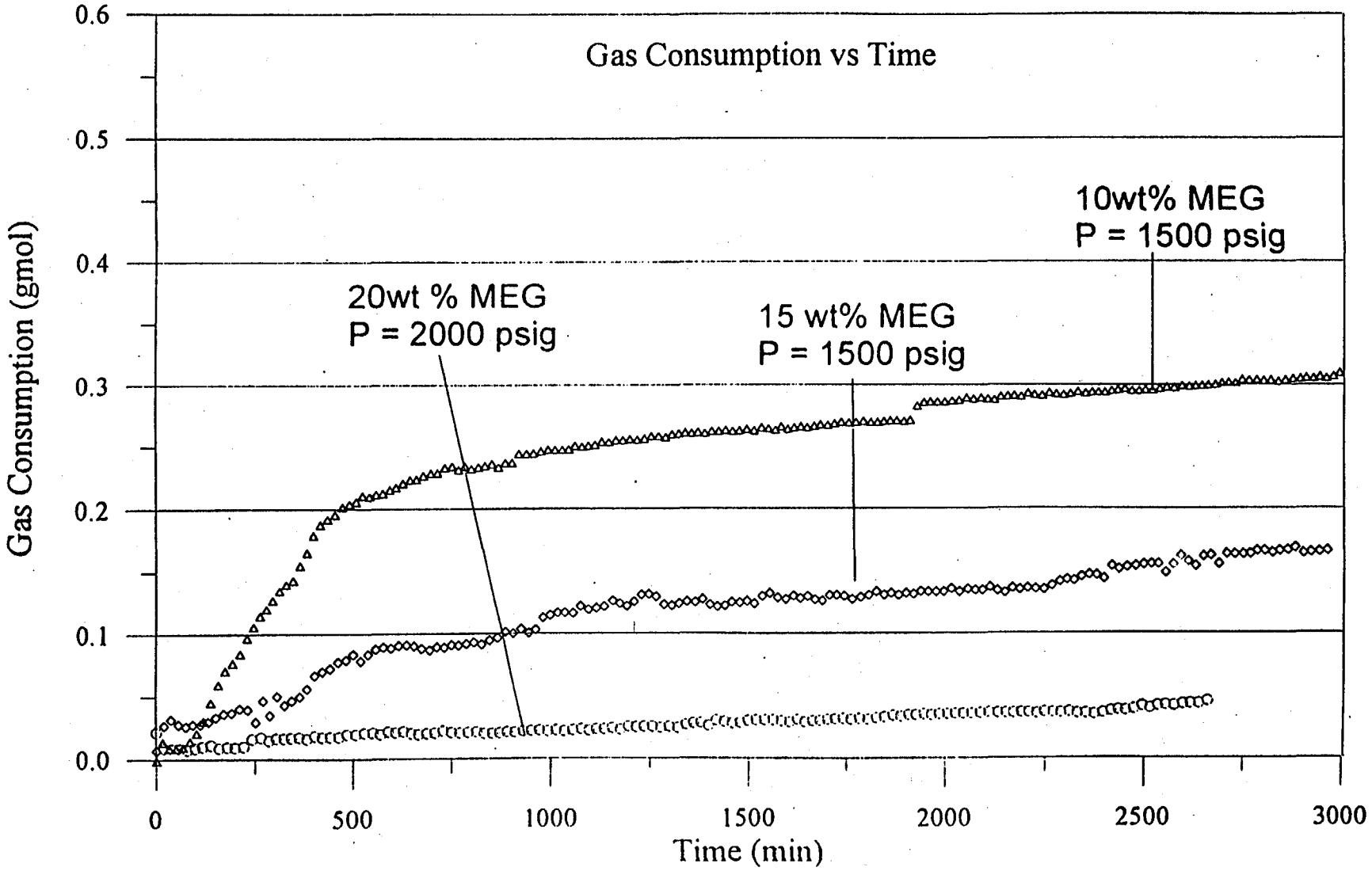

Figure 49.

0.75wt% VC-713 or 0.375wt% PVCAP + 0.375 wt% PVP(k-17) Provide Inhibition Perfomance in DI Water at 1000 psig and 39.2 °F

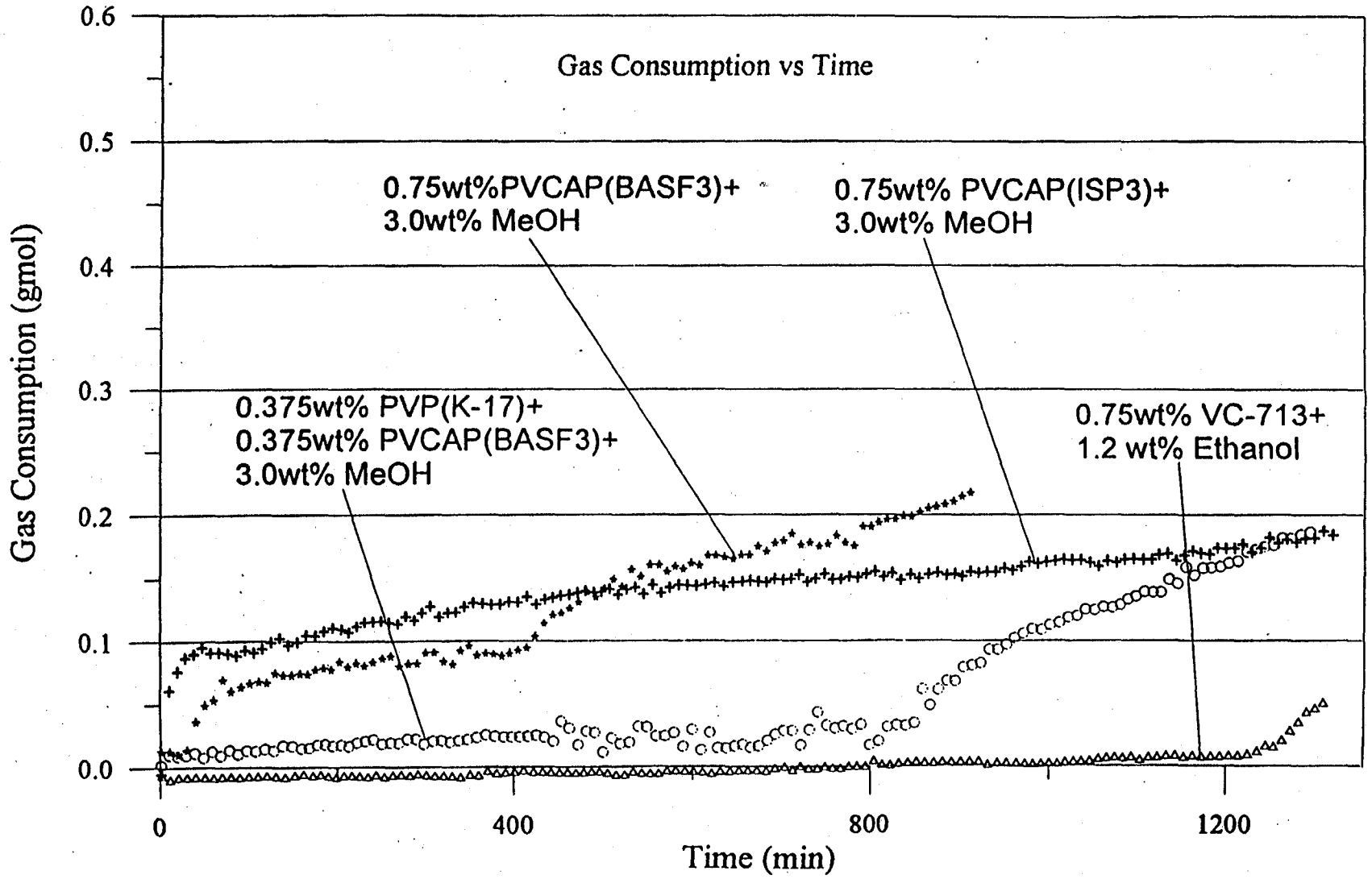

Figure 50.

High Molecular Weight PVCAP(ISP) Performs Better Than Low MW PVCAP(ISP) in DI Water at The Conditions of 0.75wt%PVCap + 3.0wt% Methanol, P = 1000 psig and T = 39.2°F

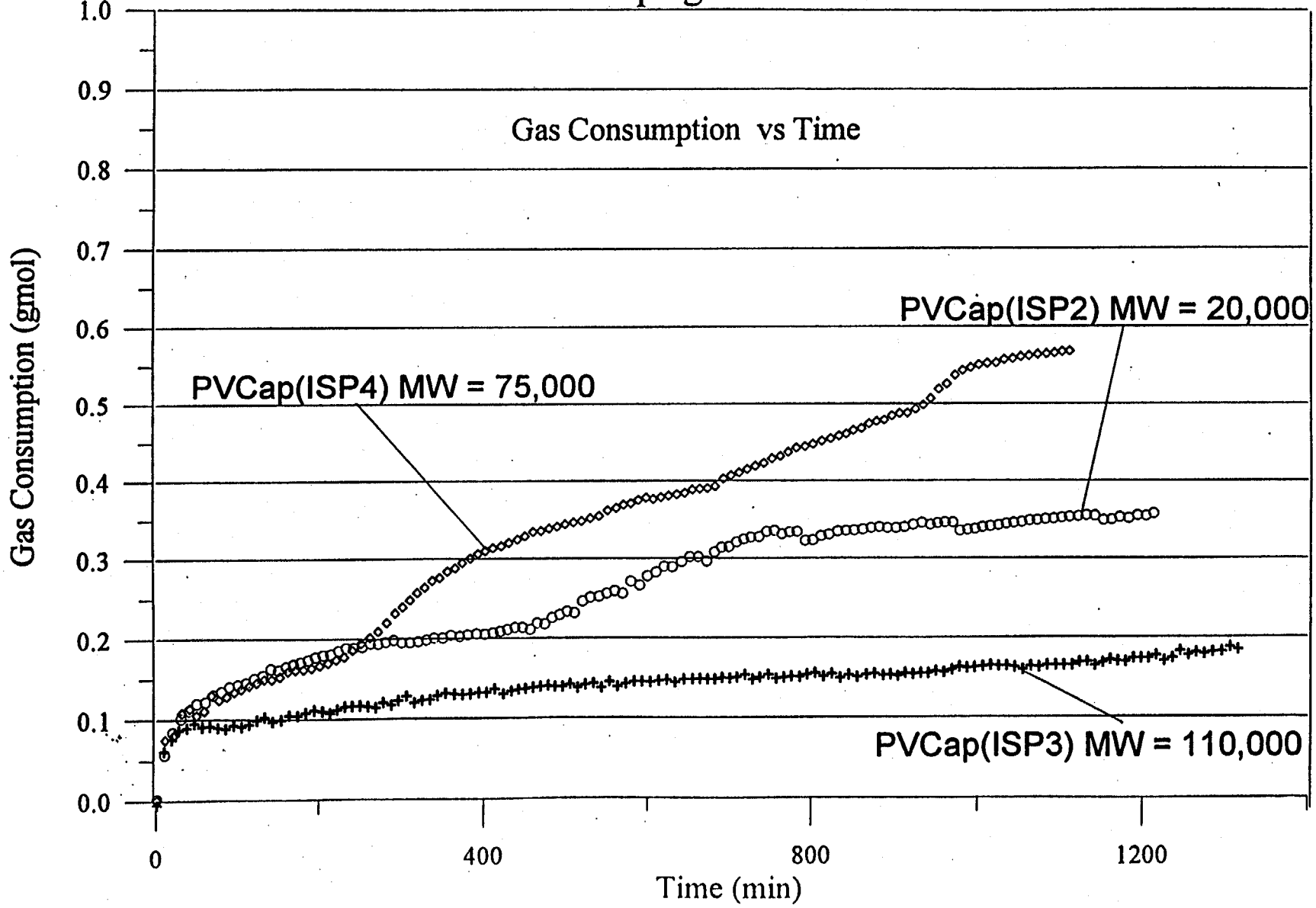

Figure 51.

Different MW VP/VC(25/75) Performs Similar in DI Water
at The conditions of 0.75wt%VP/VC(25/75)
P = 1000 psig and T = 39.2°F

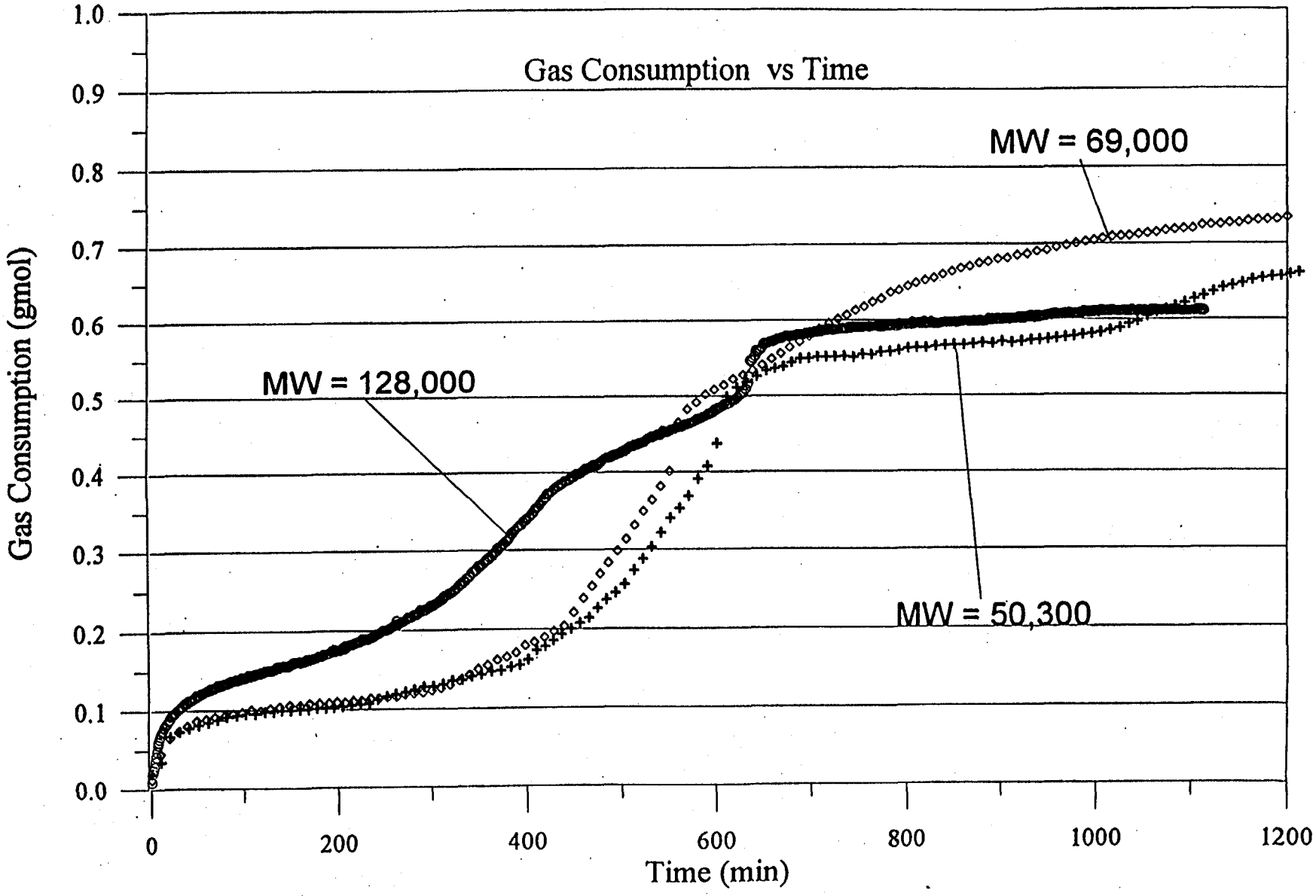

Figure 52.

Methanol Combined with Kinetic Inhibitors Improves Hydrate Inhibition in DI Water

0.5wt% Polymer +18.5wt% Methanol,
P = 2000 psig , and T = 39.2 °F

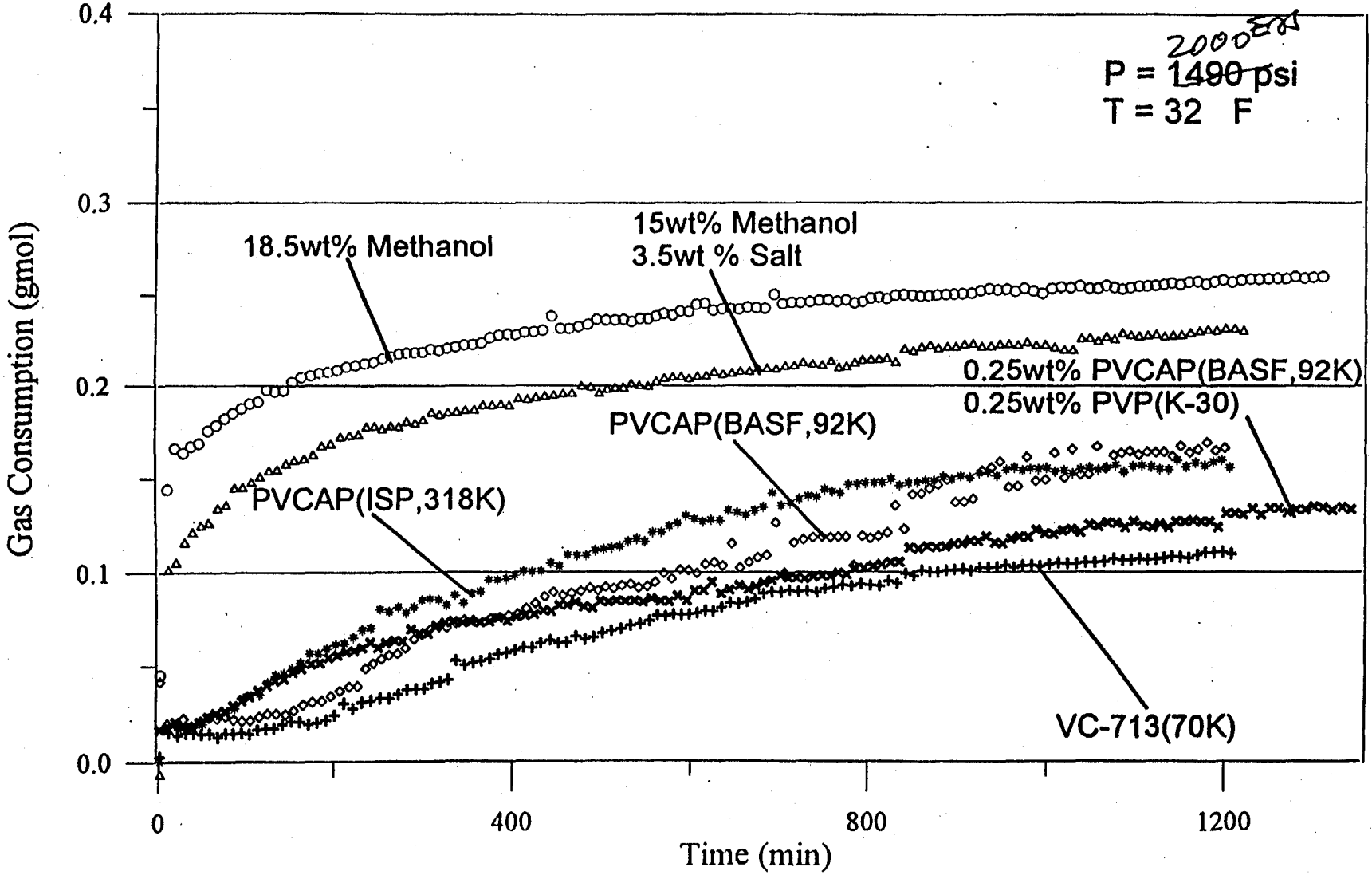

Figure 53:

Combing 0.75wt% Polymer with 15wt% Methanol Does Not Provide Good Hydrate Inhibition in DI Water at P = 2000 psig and T = 39.2 °F

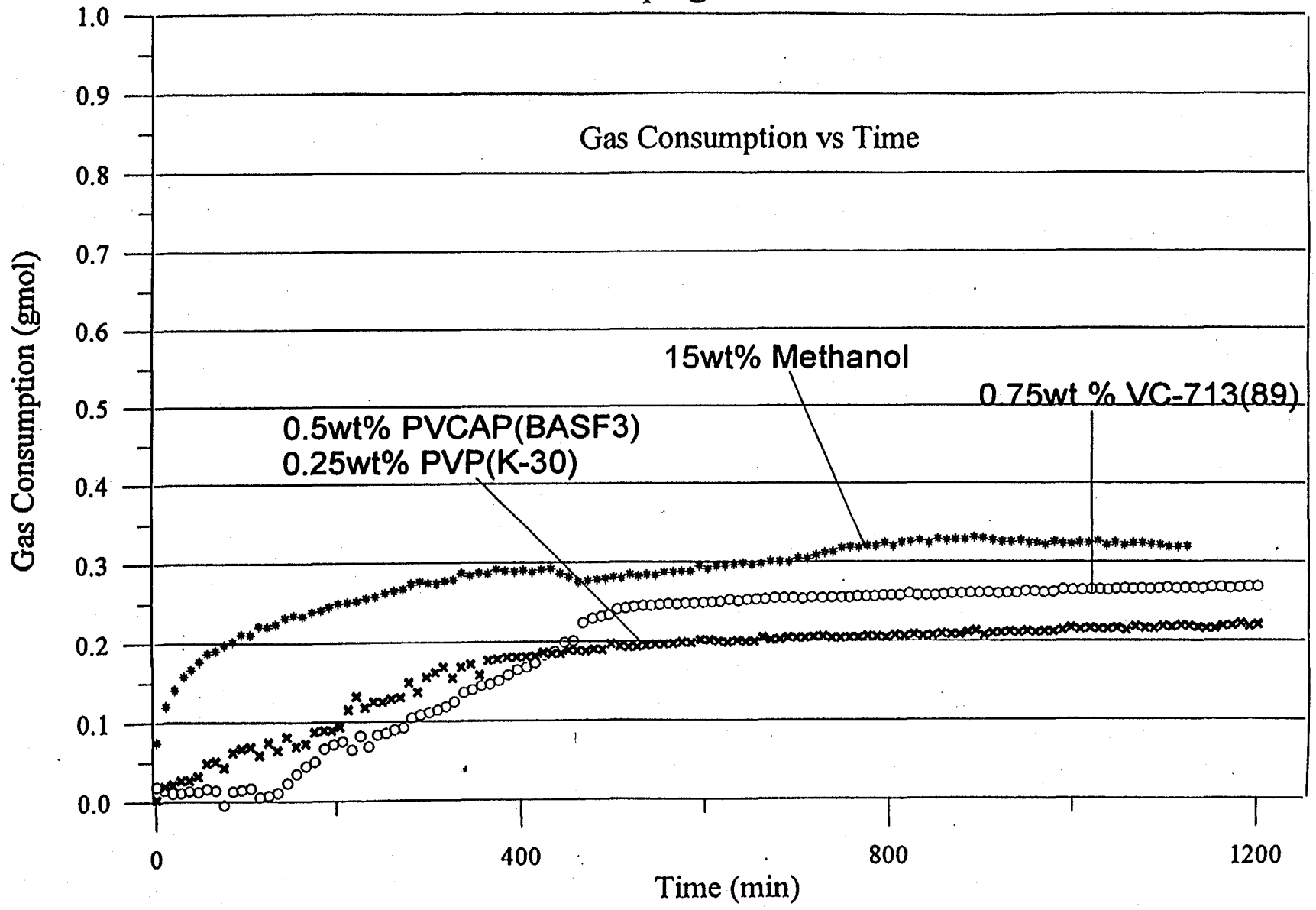

Figure 54.

Low Molecular Weight PVCAP(ISP) Performs Better Than High MW PVCAP(ISP) in Sea Water at The Conditions of 0.5wt%PVCap + 3.5wt% Sea Salt+2.0wt% Methanol P = 1000 psig and T = 39.2°F

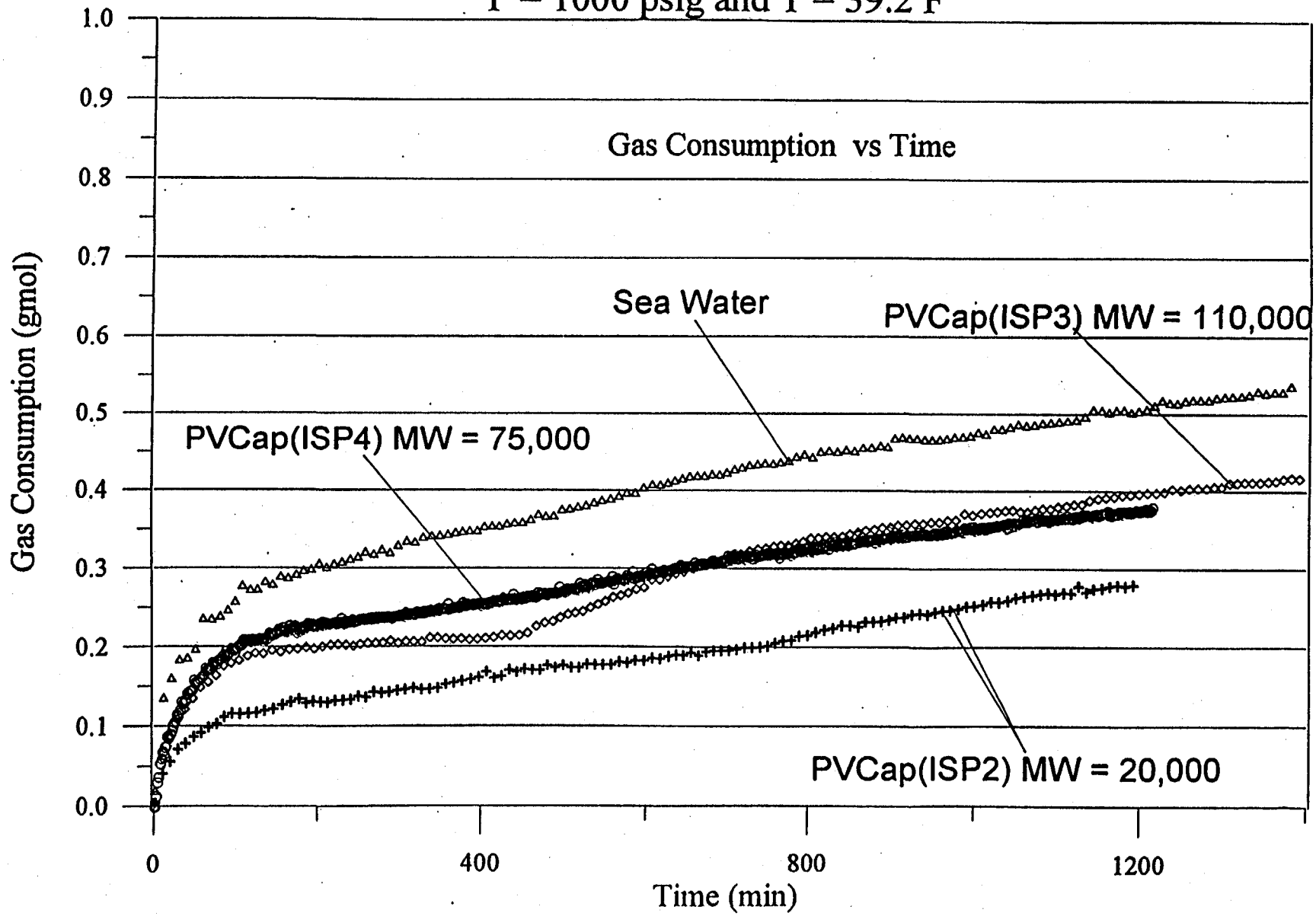

Figure 55.

Different MW VP/VC(25/75) Perform Similar at The Conditions of 0.5wt%VP/VC(25/75) + 3.5wt% Sea Salt + 2.0wt% Methanol P =1000 psig and T = 39.2°F

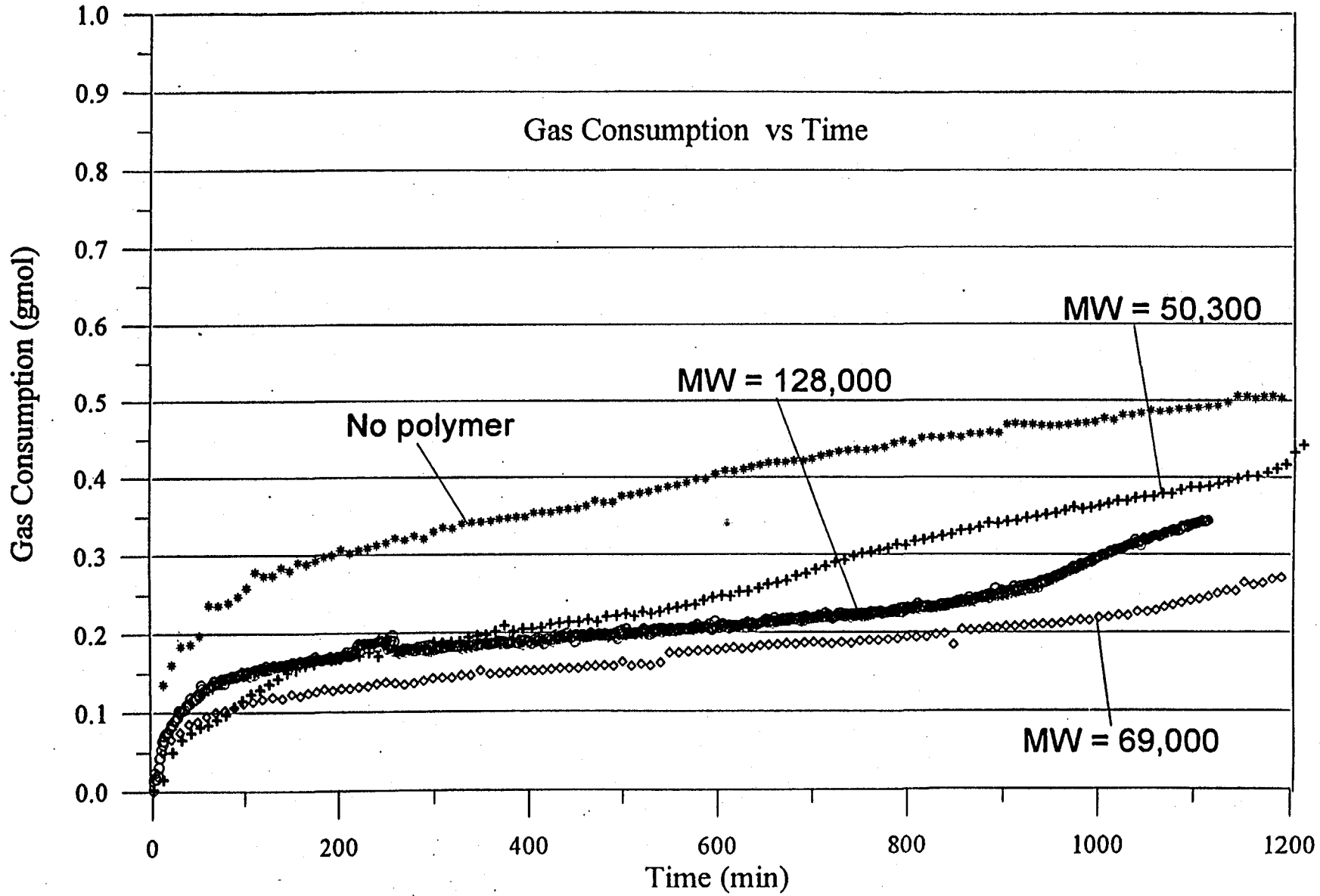

Figure 56.

Aged Solution Performs Worse Than Fresh Solution for 0.75wt%PVCap(BASF3) in DI Water at P = 1000 psig and T = 39.2°F

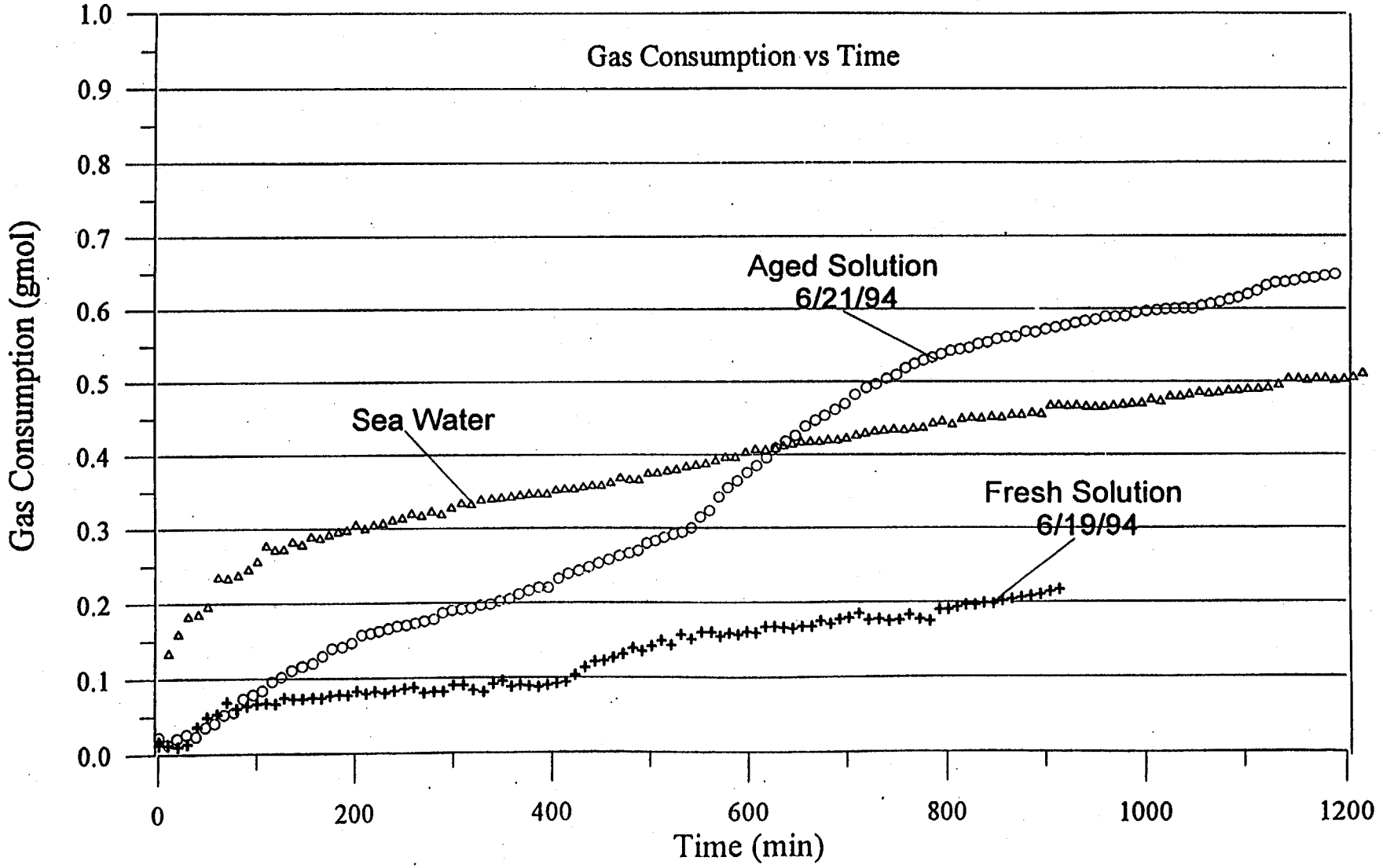

Figure 57.

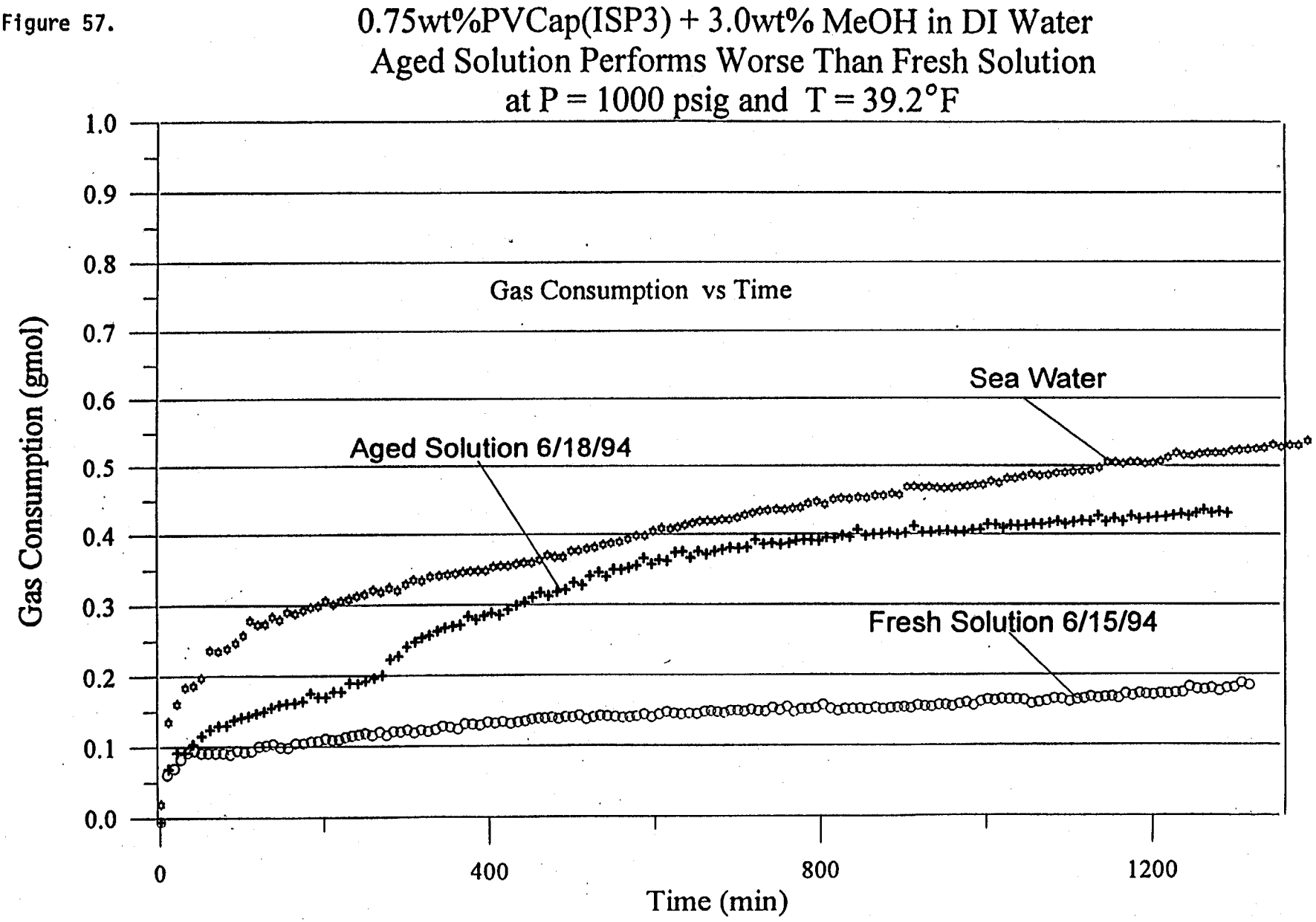
0.75wt%PVCap(ISP3) + 3.0wt% MeOH in DI Water
Aged Solution Performs Worse Than Fresh Solution
at P = 1000 psig and T = 39.2°F
Gas Consumption vs Time
Gas Consumption (gmol)
Time (min)
Sea Water
Aged Solution 6/18/94
Fresh Solution 6/15/94
1.0
0.9
0.8
0.7
0.6
0.5
0.4
0.3
0.2
0.1
0.0
0
400
800
1200

Figure 58.

The Aged Solution Performs Similar to The Fresh Solution for 0.5wt%PVCap(BASF3) + 3.5wt% Sea Salt at P = 1000 psig and T = 39.2°F

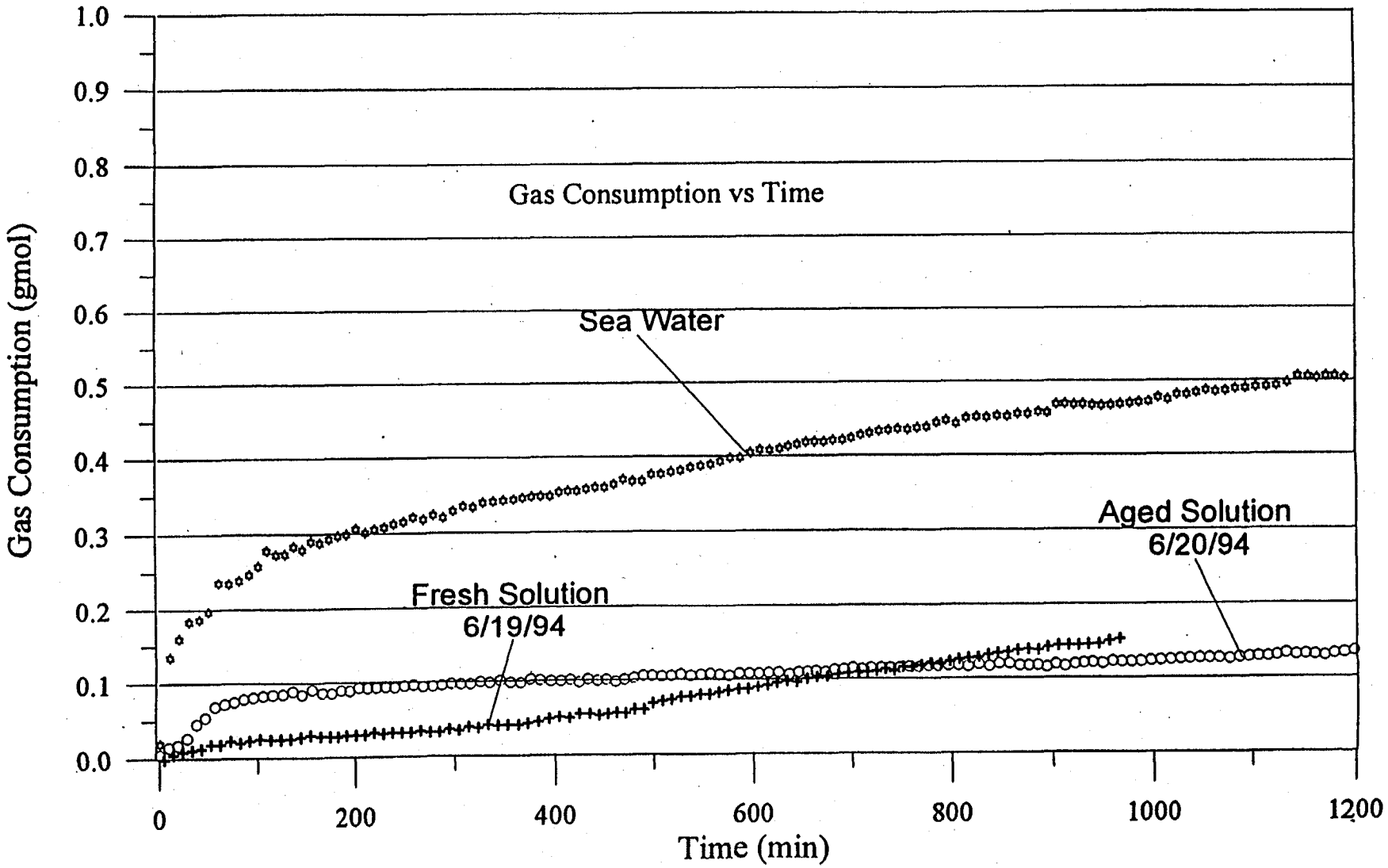

Figure 59.

Aged Solution Performs Similar to Fresh Solution for
0.5wt%PVCap(ISP3) + 3.5wt% Sea Salt +2.0wt%MeOH
at P = 1000 psig and T = 39.2°F

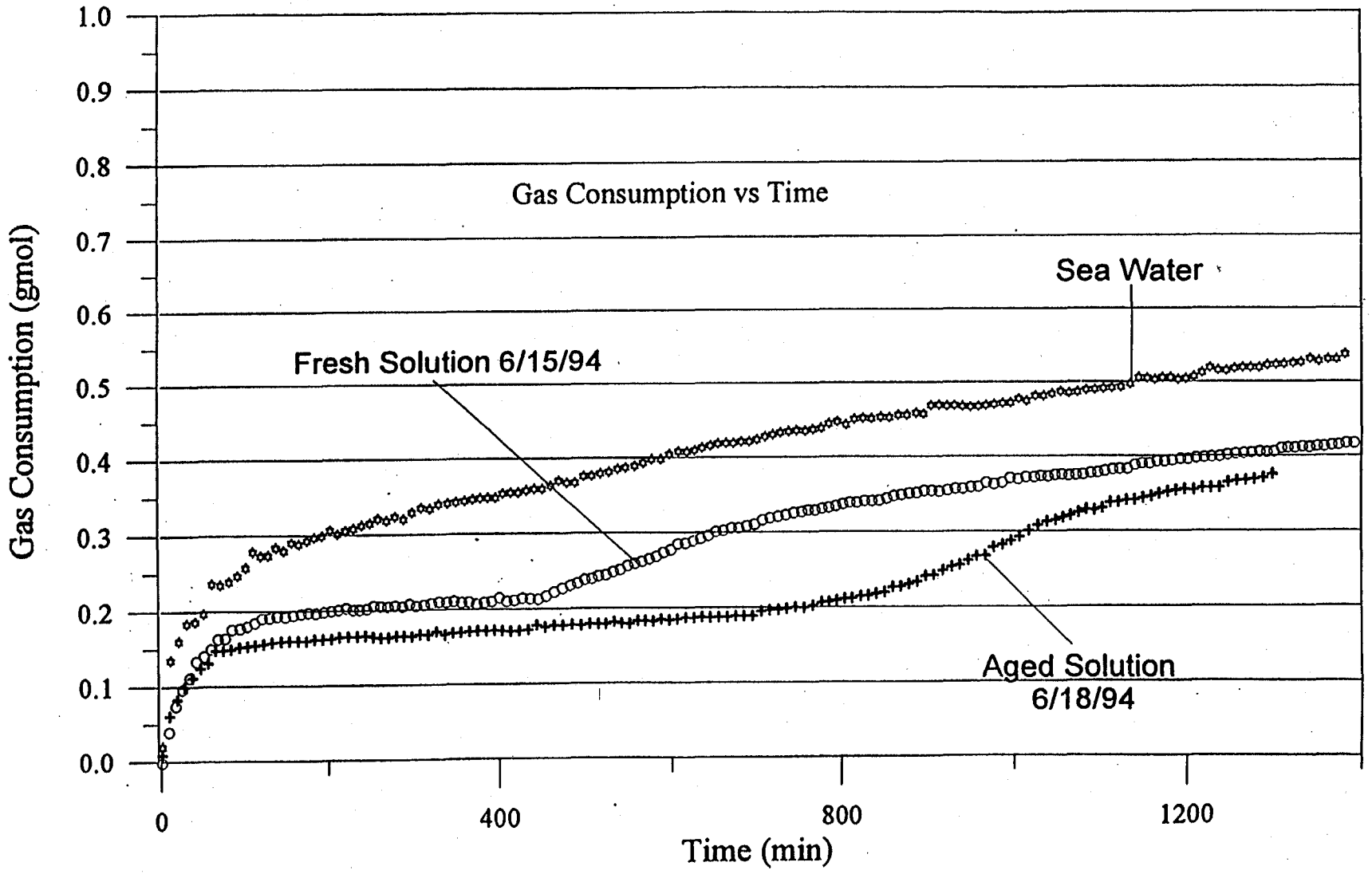

Figure 60.

Aged Solution Performs Similar to Fresh Solution for
0.75wt% PVCAP(BASF3) + 3.5wt% Salt + 3.0wt% Methanol at
P = 1500 psig and T = 39.2°F

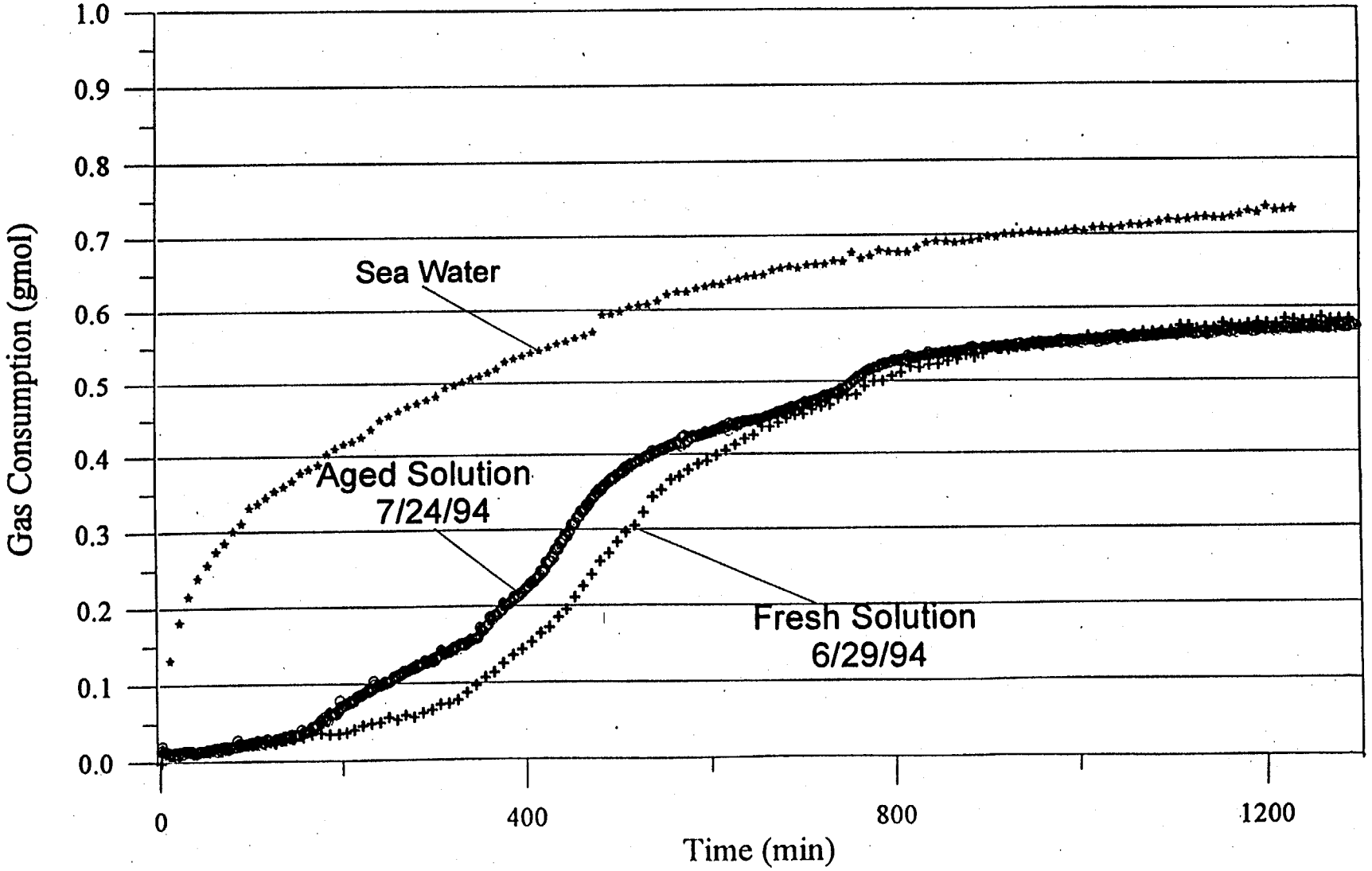

Figure 61.

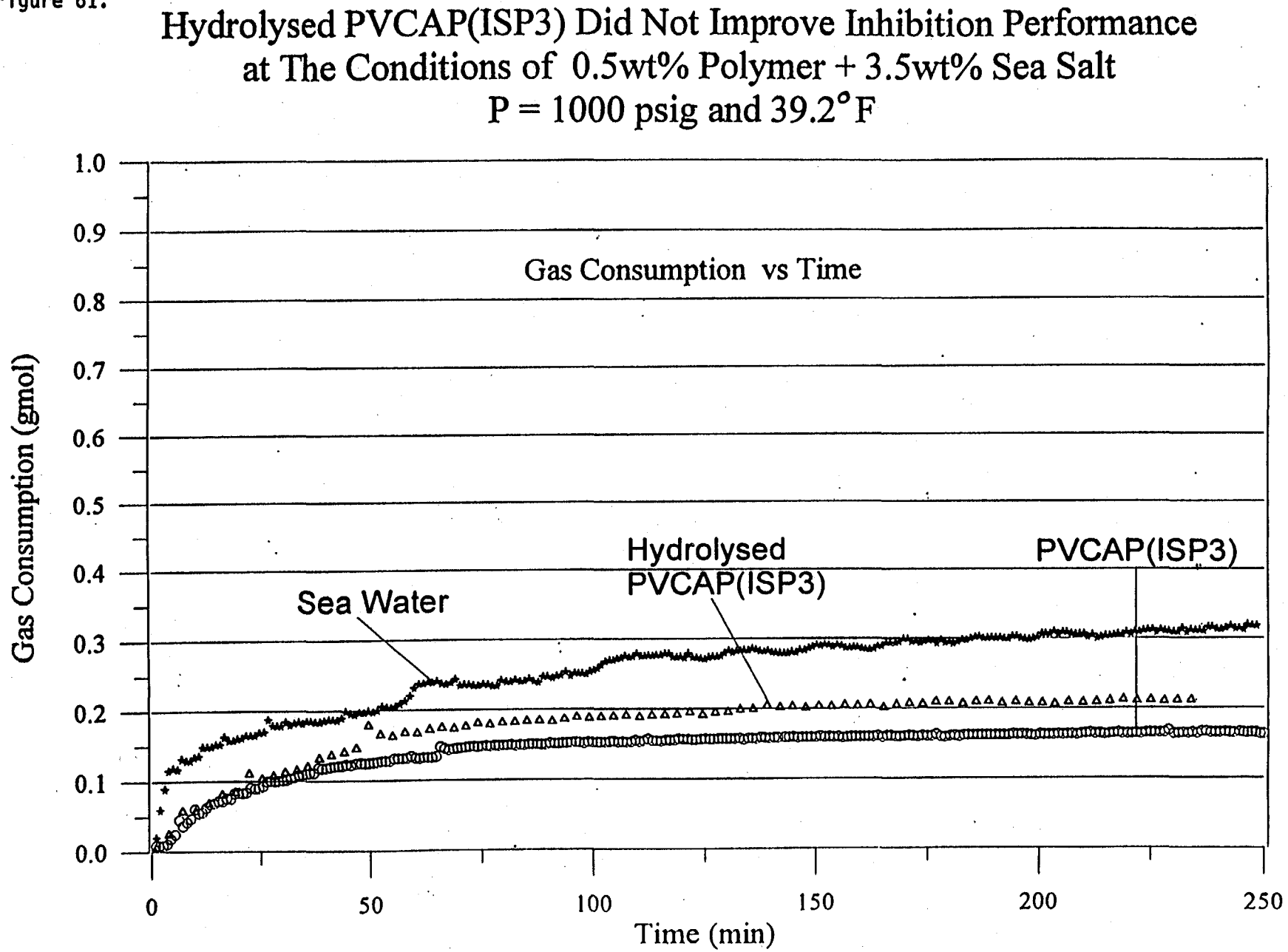
Hydrolysed PVCAP(ISP3) Did Not Improve Inhibition Performance
at The Conditions of 0.5wt% Polymer + 3.5wt% Sea Salt
P = 1000 psig and 39.2° F
Gas Consumption vs Time
Gas Consumption (gmol)
1.0
0.9
0.8
0.7
0.6
0.5
0.4
0.3
0.2
0.1
0.0
Sea Water
Hydrolysed
PVCAP(ISP3)
PVCAP(ISP3)
0
50
100
150
200
250
Time (min)

Figure 62.

Hydrolyzed VP/VC Does Not Improve Inhibition Performance at The Conditions of 0.5wt% VP/VC +3.5wt% Sea Salt, P = 1000 psig and T = 39.2 °F

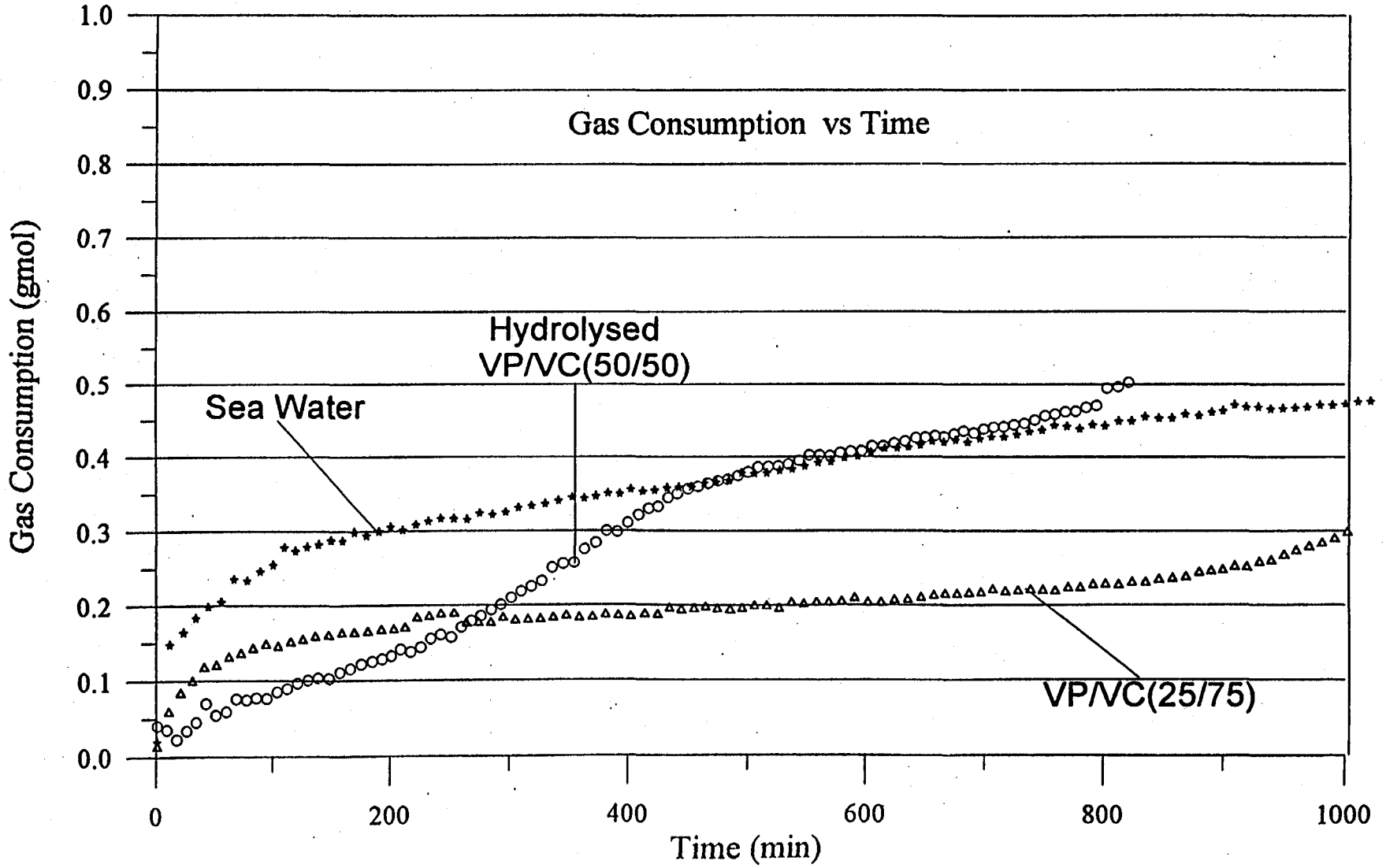

Figure 63.

Steel Balls in Cells Have Little Effect on The Gas Consumption
Test Conditions Are:
0.5 wt% PVCAP(BASF3) + 0.5wt% Ethanol + 3.5wt% Salt
120 Grams Solution, P = 1000 psig and T = 39.2°F

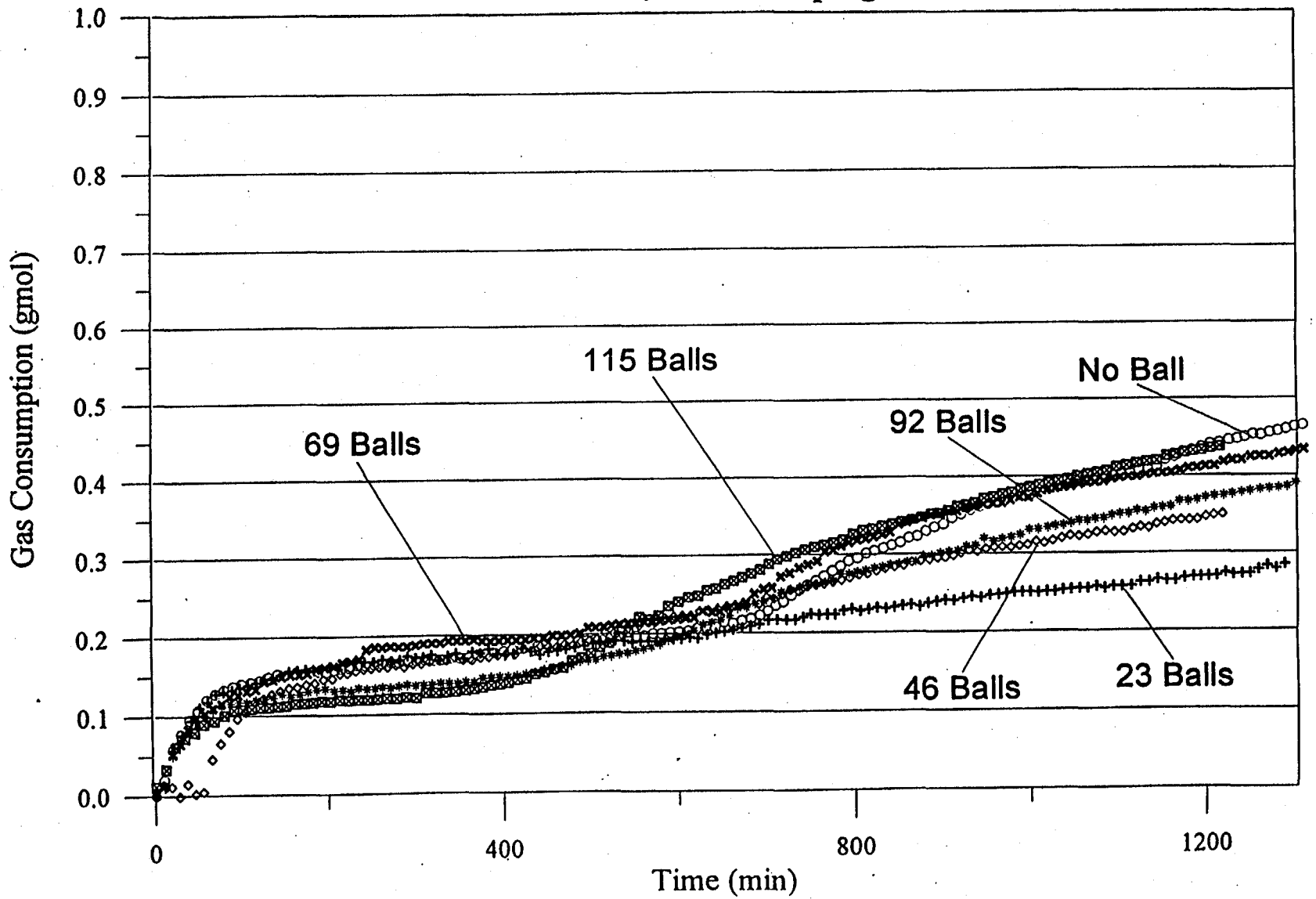

Figure 64.

Compare The Performances of Different Amount of Test Solution in Reactors. Test Conditions Are: 0.5 wt% PVCAP(BASF3) + 0.5wt% Ethanol + 3.5wt% Salt P = 1000 psig, and T = 39.2 °F

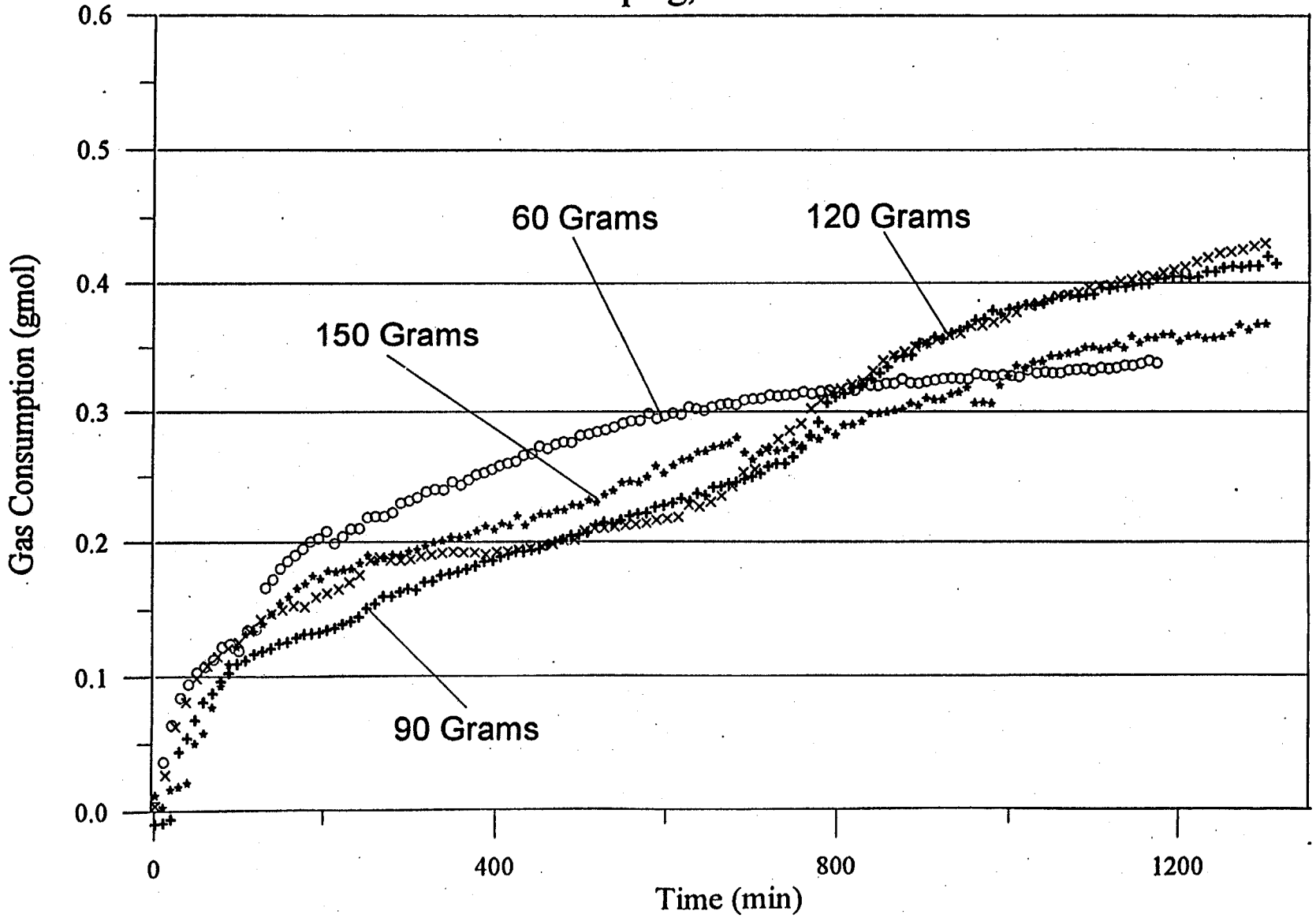

Figure 65.

Compare The Gas Consumption of Different Amount of Test Solution in Cell. Test Conditions Are: 0.5 wt% PVCAP(BASF3) + 0.5wt% Ethanol + 3.5wt% Salt P = 1000 psig and T = 39.2°F

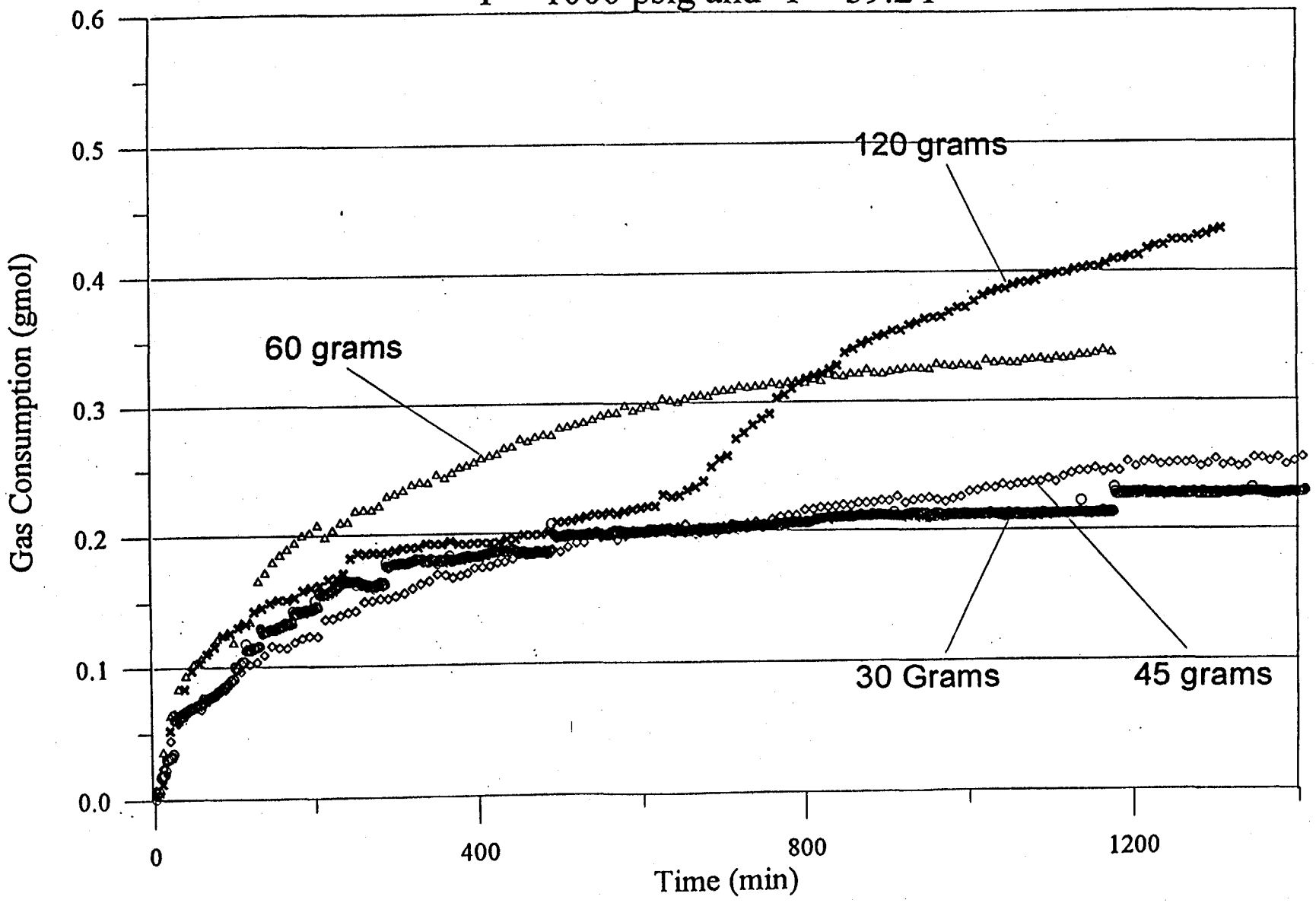

Figure 66.

1. The Gas Consumption Is Directly Proportional to The Amount of DI Water In the Cell
2. When Less Test Solution Is Used, Shorter Time Is Needed to Reach The Maximum Gas Consumption

Test Conditions Are: P = 1000 psig and T = 39.2 °F

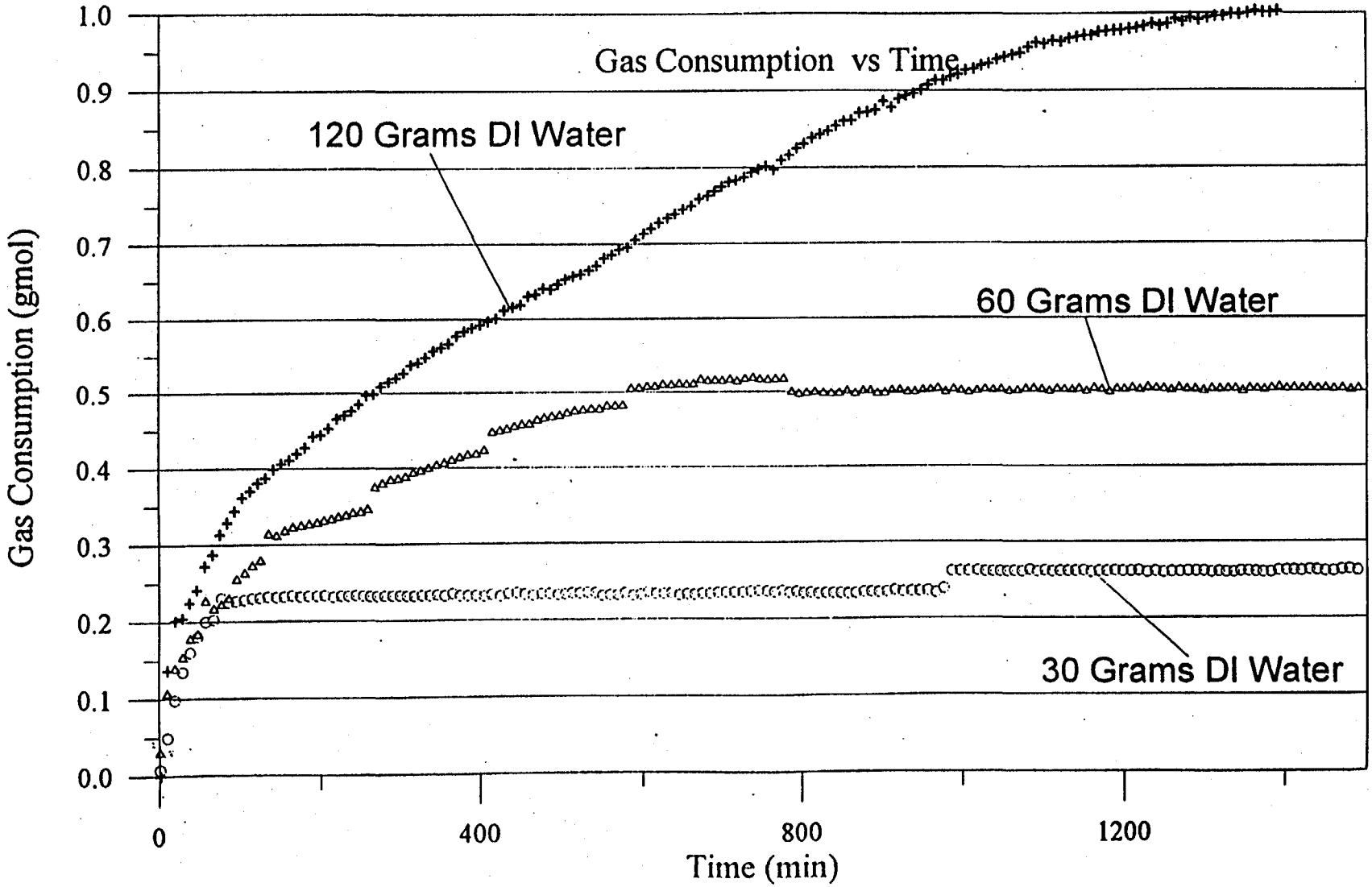

Figure 67. If The Test Solution in The Cell Is Reduced, The Induction Time Will Decrease

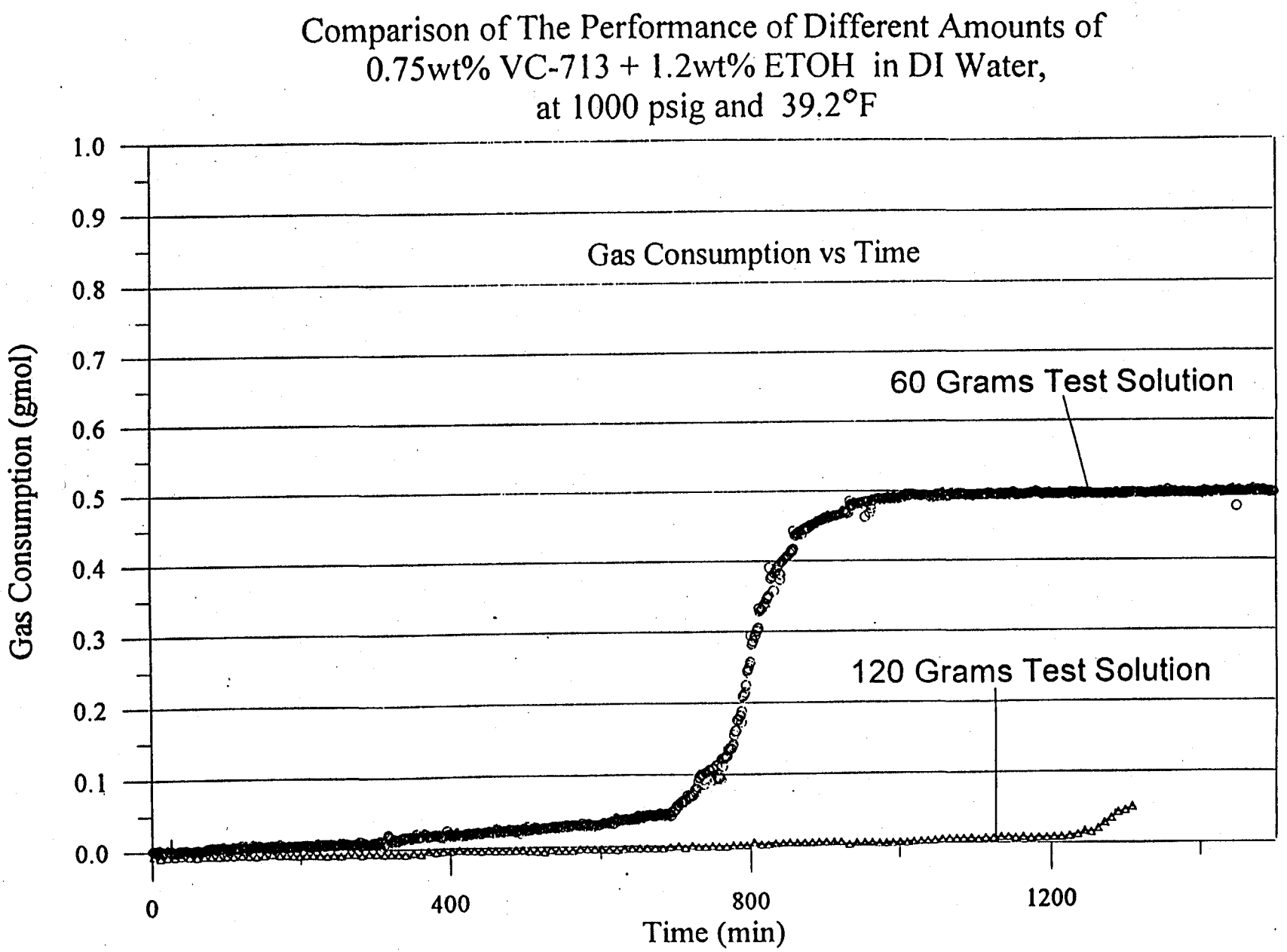

Figure 68.

If The Test Solution in The Cell Is Reduced,
The Induction Time Will Decrease

Comparison of The Performance of Different Amounts of
0.75wt%VC-713 + 3.5wt% Salt + 1.2wt%Ethanol + 1.8%Methanol
at 1500 psig and 39.2°F

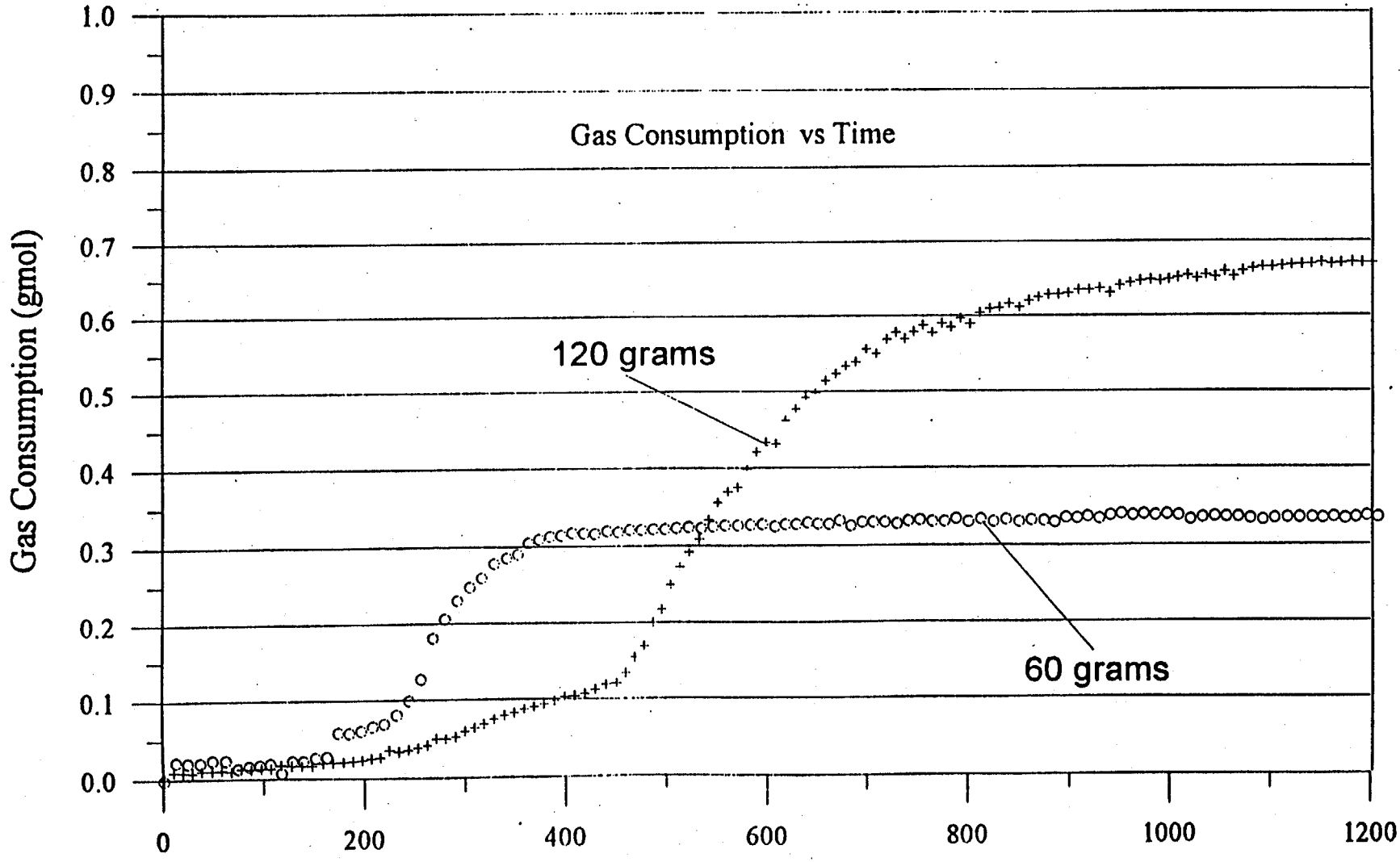

Figure 69.

When Less Test Solution is Used, Shorter Time Is Needed To Reach The Maximum Gas Consumption.

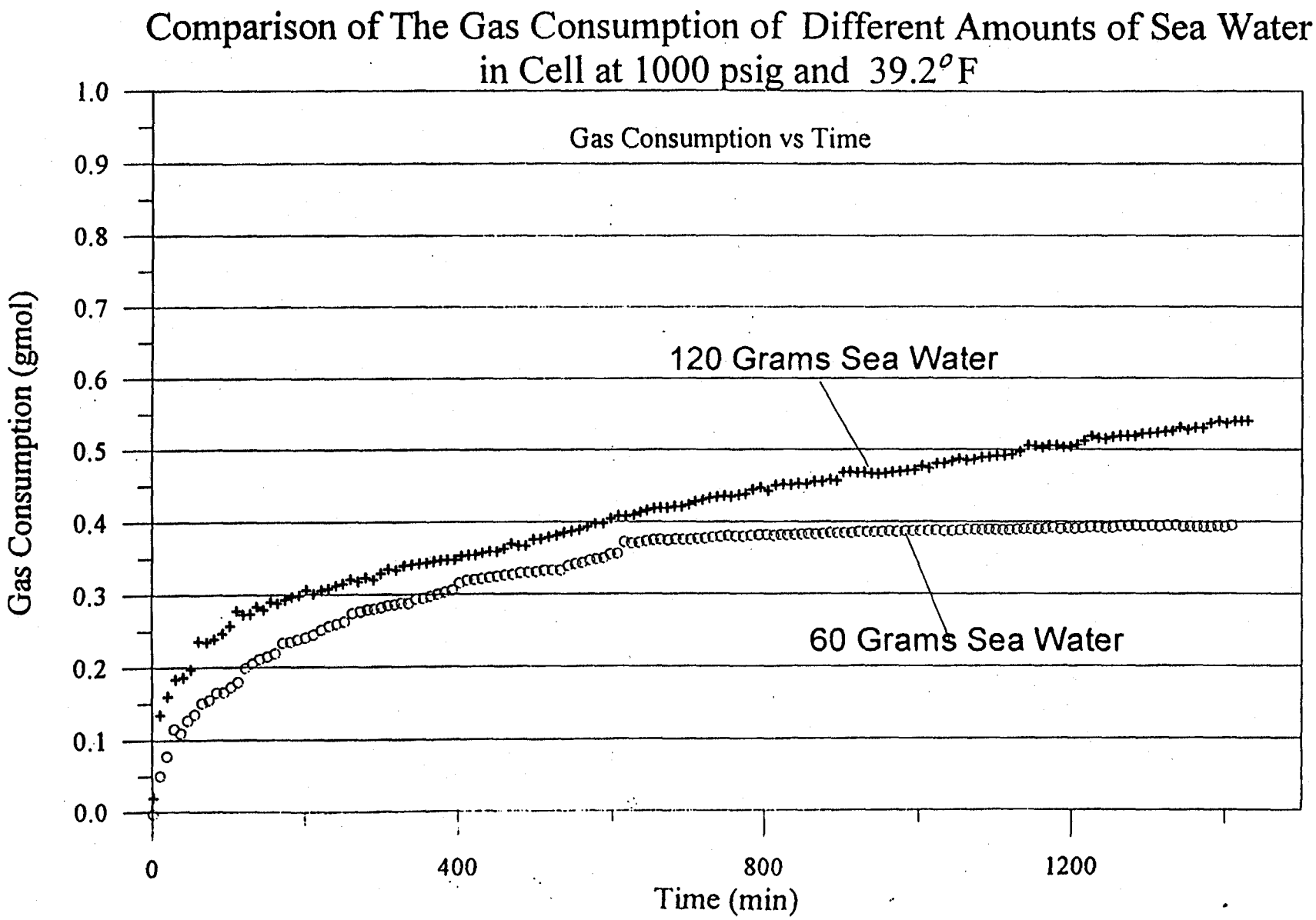

Figure 70. Reducing The Test Solution In The Cell Will Decrease Induction Time,

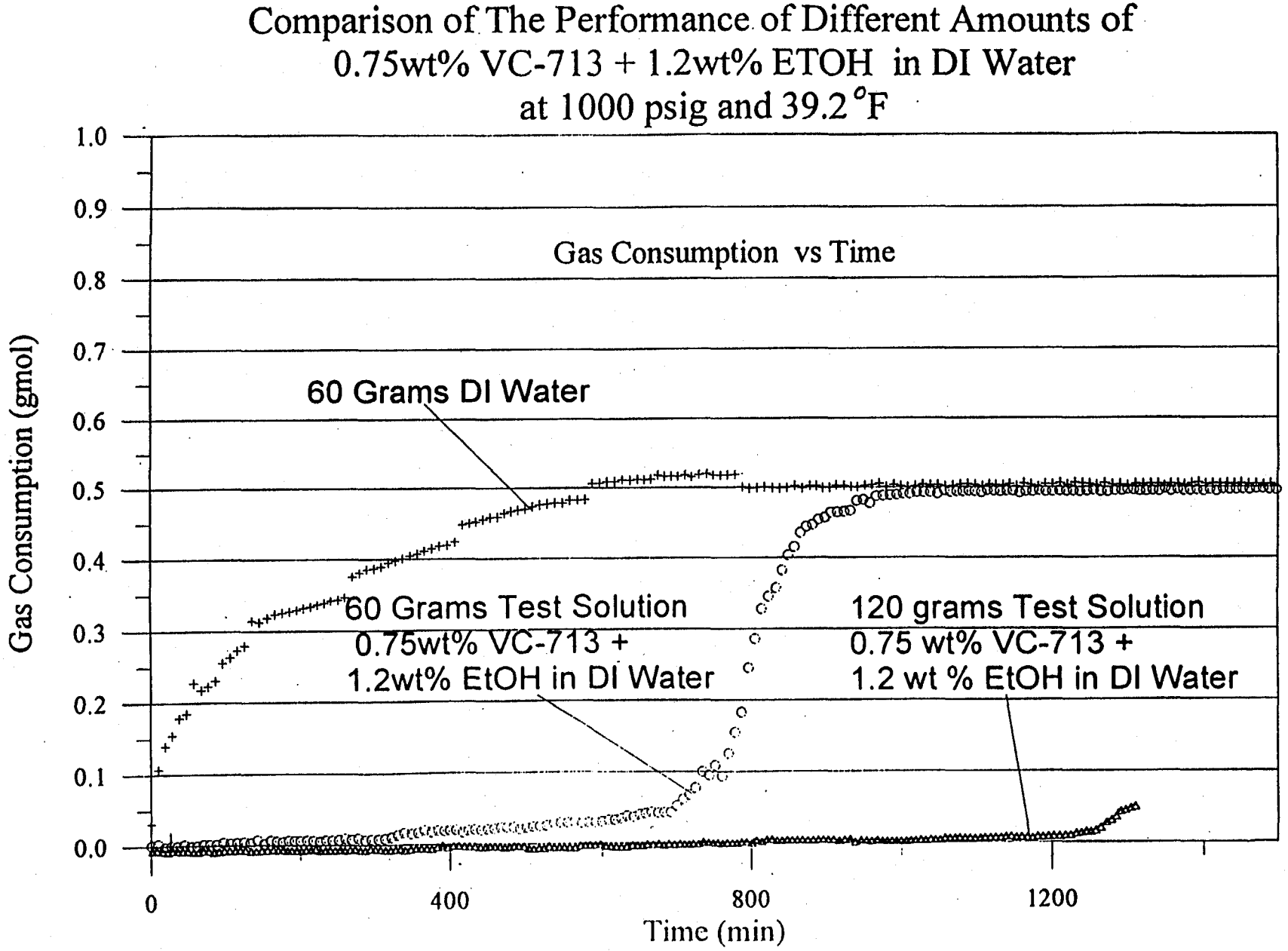

Figure 71.

Combining PVP(K-17) with PVCAP Gives Better Inhibition Performance Than Using PVCAP Alone

0.75wt%Polymer + 3.5wt% Salt +0 .75wt%Ethanol + 2.25%Methanol
at 1500 psig and 39.2°F and 60 Grams Test Solution

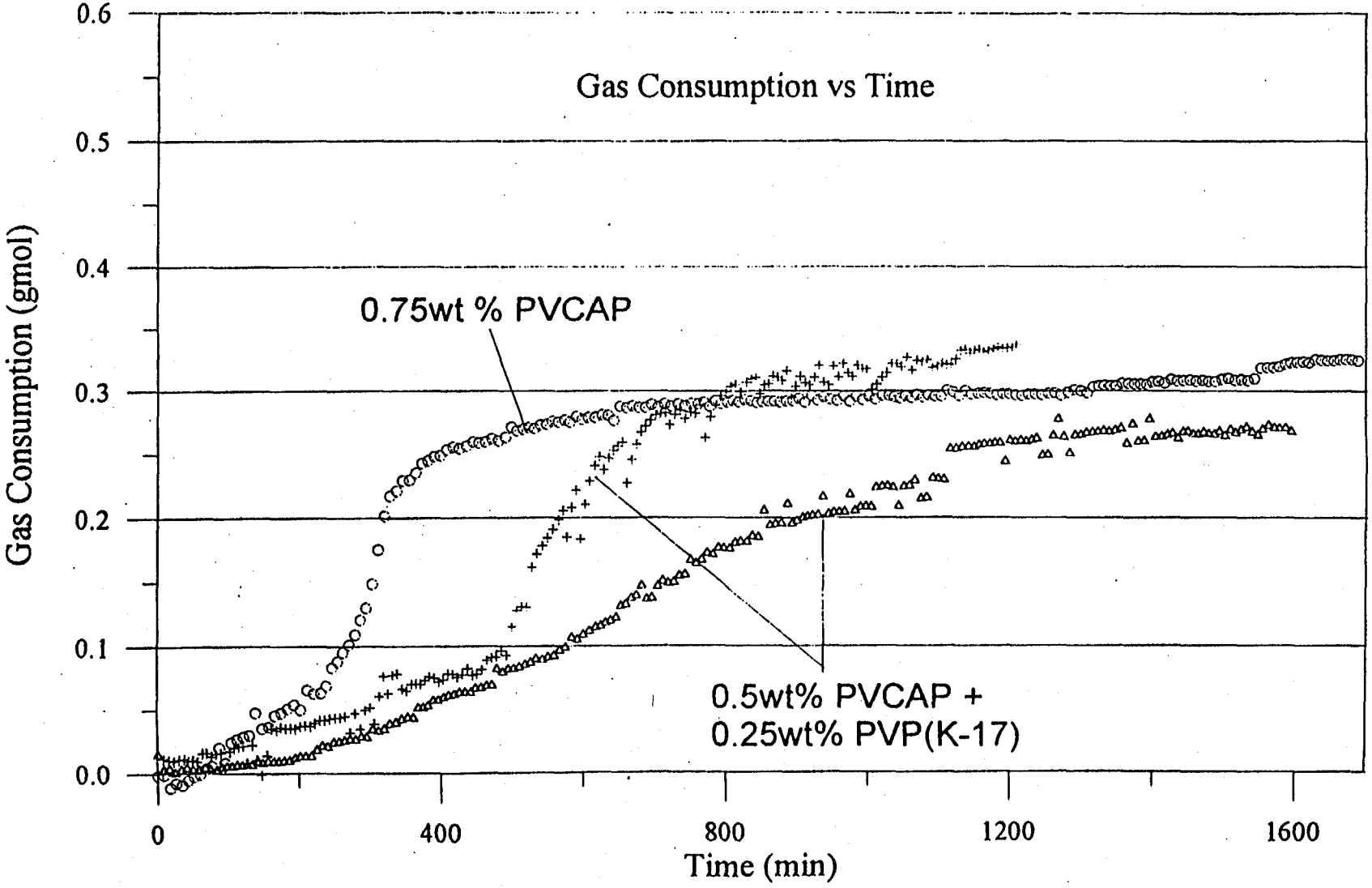

Figure 72.

Polymer Solution Did Not Change Its Inhibition Performance After Being Processed as Following : Agitated and Heated from 25°C to 90°C and Then Agitated and Cooled to 25°C, (The Cloud Point of The Solution is about 40°C)

0.75WT% VC-713 + 1.8wt% Methanol+1.2wt%Ethanol
(60grams Test Solution ,1000 psig and 39.2°F)

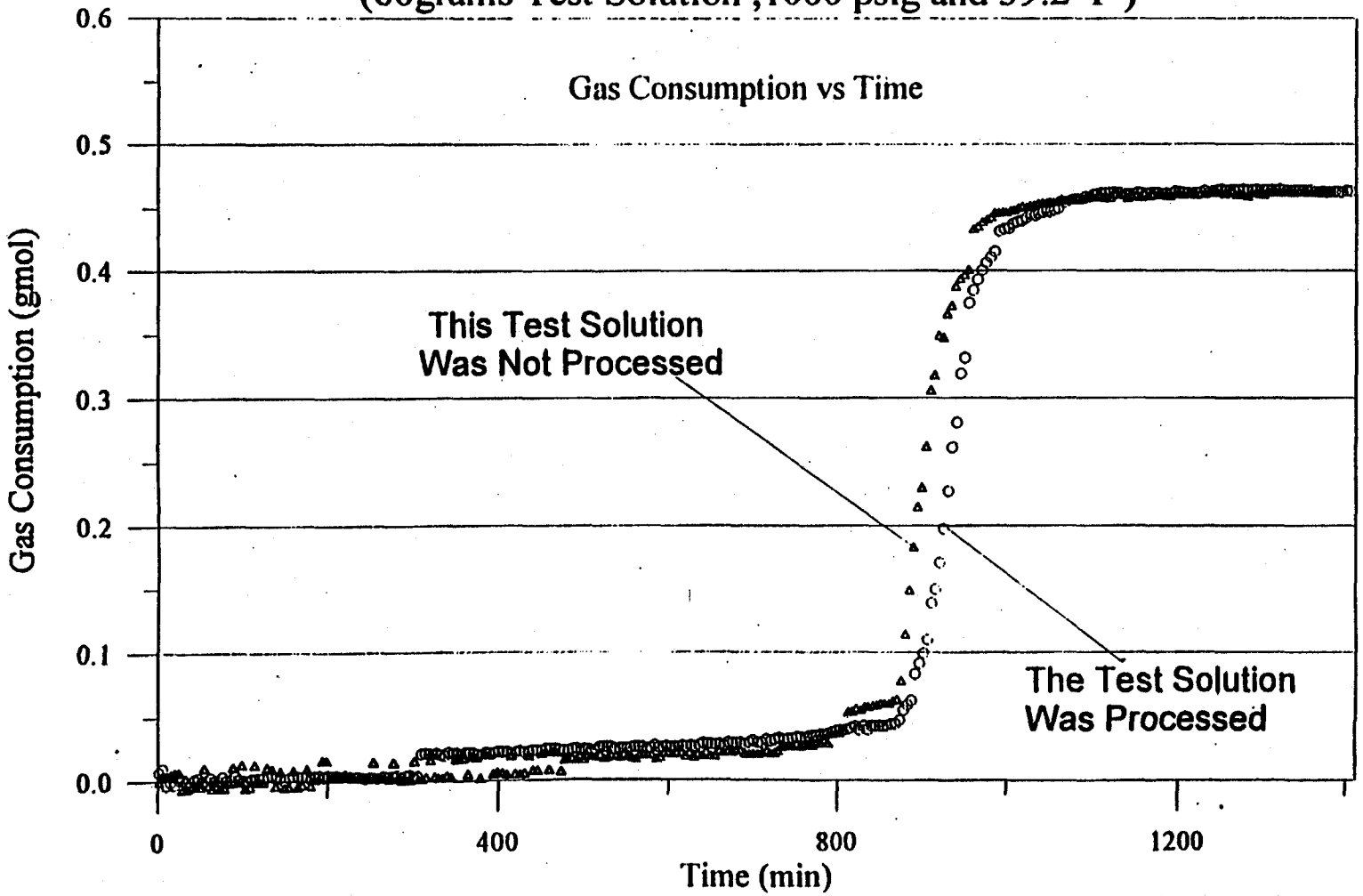

Figure 73. Phase Separation Processes Did Not Affect Polymer's Inhibition Performance

The Process is as Follows: Agitated and Heated from Ambient T (about 25°C) to 90°C, Then Agitated and Cooled to Ambient T. (The Processes Lasted about 3 Hours. The Cloud Point of The Solution Is about 30°C)

Test Conditions Are:

0.5wt% VC-713 + 3.5 wt% Salt + 0.75wt% EtOH + 1.25wt% MeOH

60grams Test Solution at 1000 psig and 39.2° F

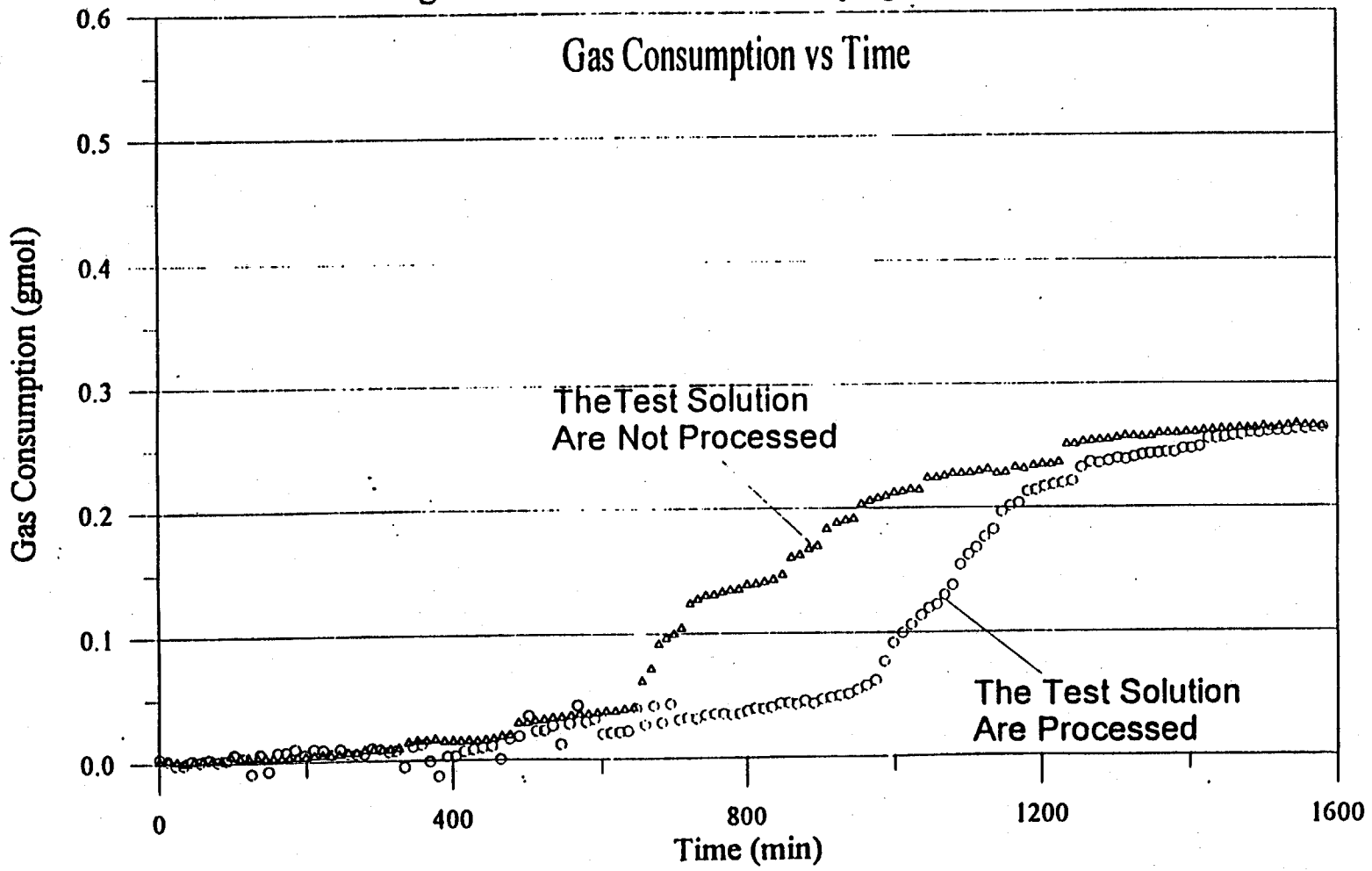

Figure 74.

When The Test Solution Was Processed as Following :
Agitated and Heated from Ambient T to 90°C, and Then Agitated and Cooled to Ambient T, Its Inhibition Performance Did Not Change
(The Cloud Point of The Solution Is about 45°C)

0.75wt% PVCAP(BASF3) + .75 wt% Ethanol + 2.25wt% Methanol
(60 grams Test Solution, 1000 psig and 39.2°F)

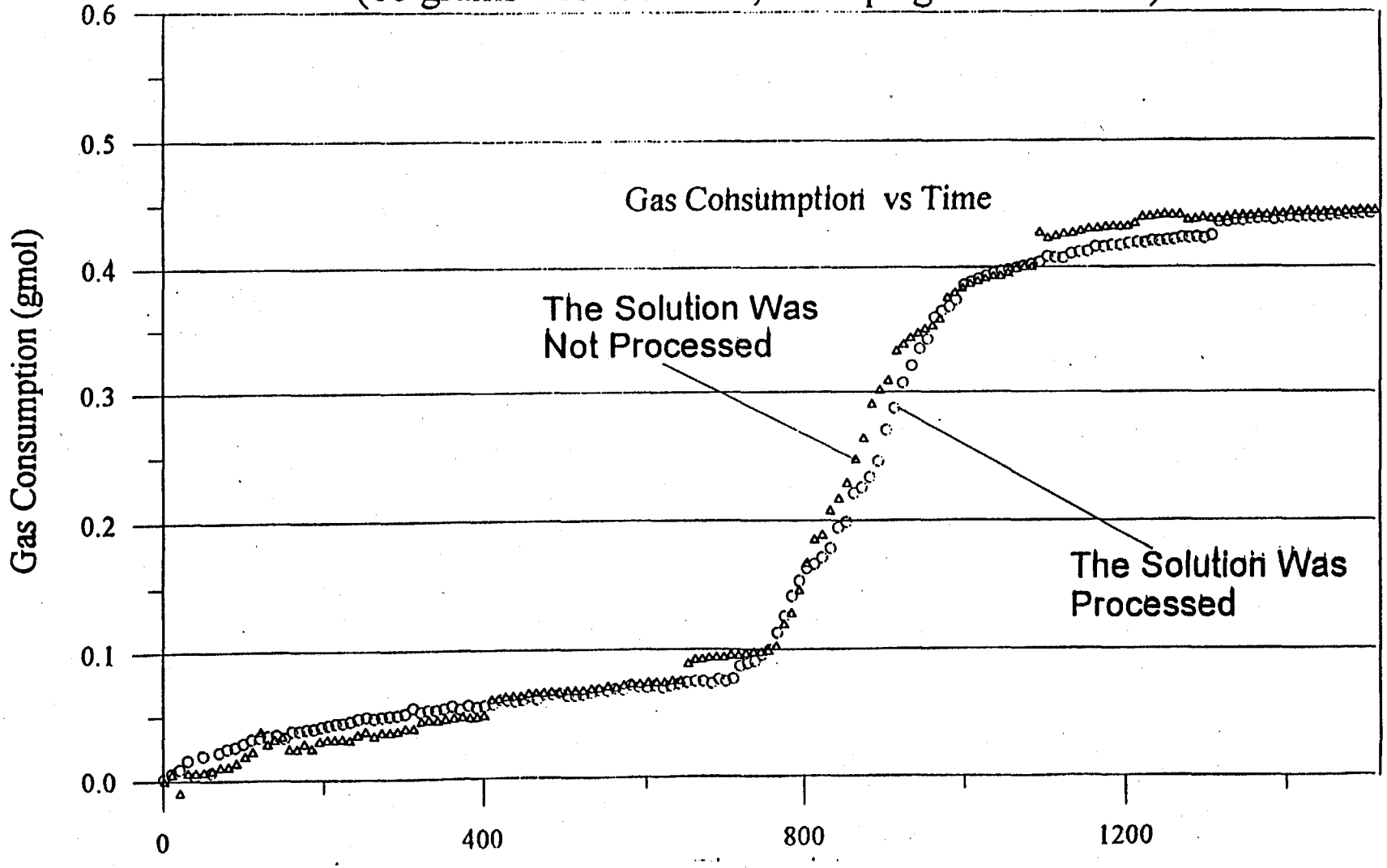

Figure 75 Polymer Solution Did Not Change Its Inhibition Performance After Being Processed As Following: Agitated and Heated from Amibent T to 90°C and Then Agitated and Cooled to Amibent T (The Cloud Point of The Solution Is about 40°C)

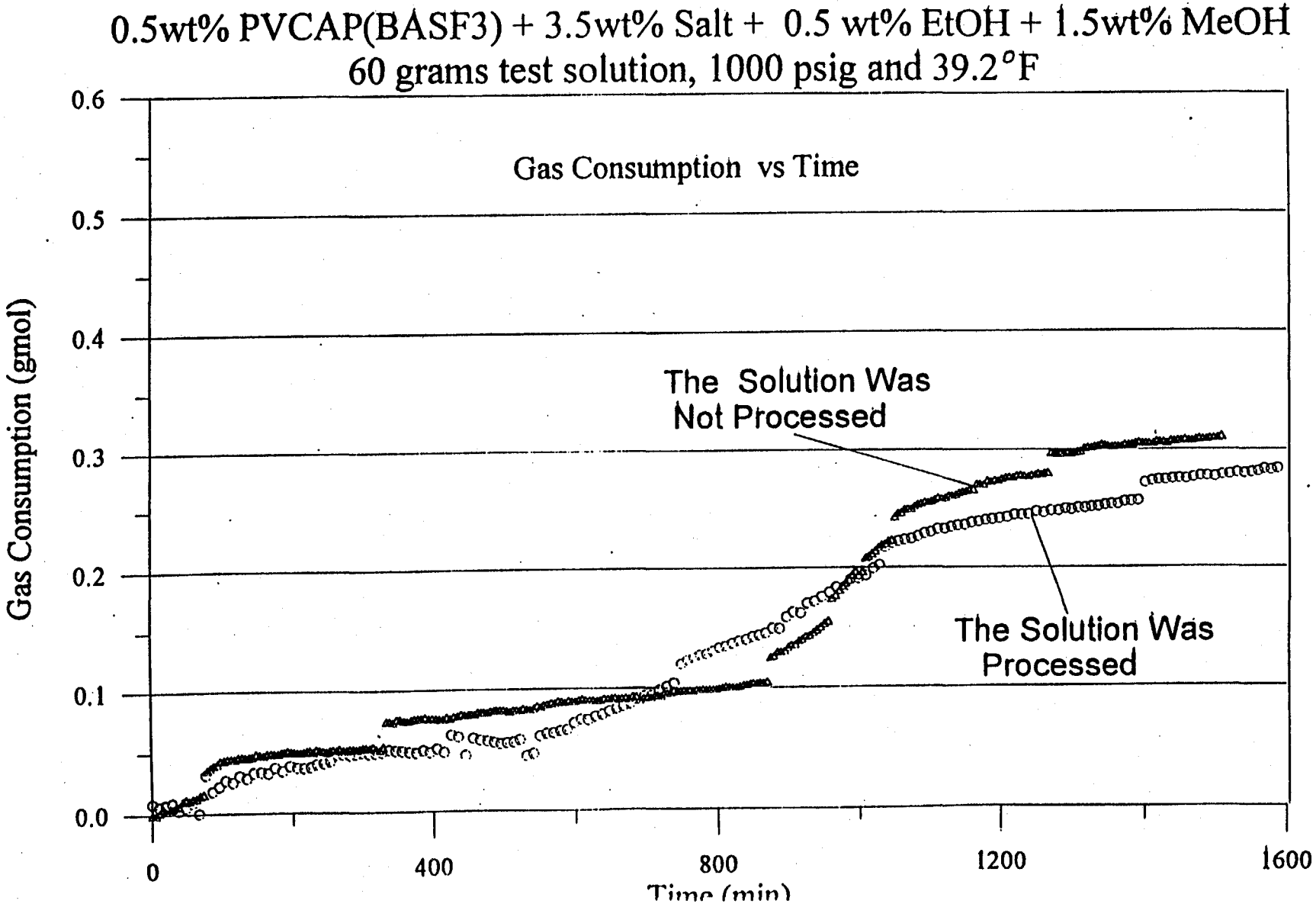

Figure 76.

If The Test Solution Contains Thermodynamic Inhibitors
The Maximum Gas Consumption Will Decrease

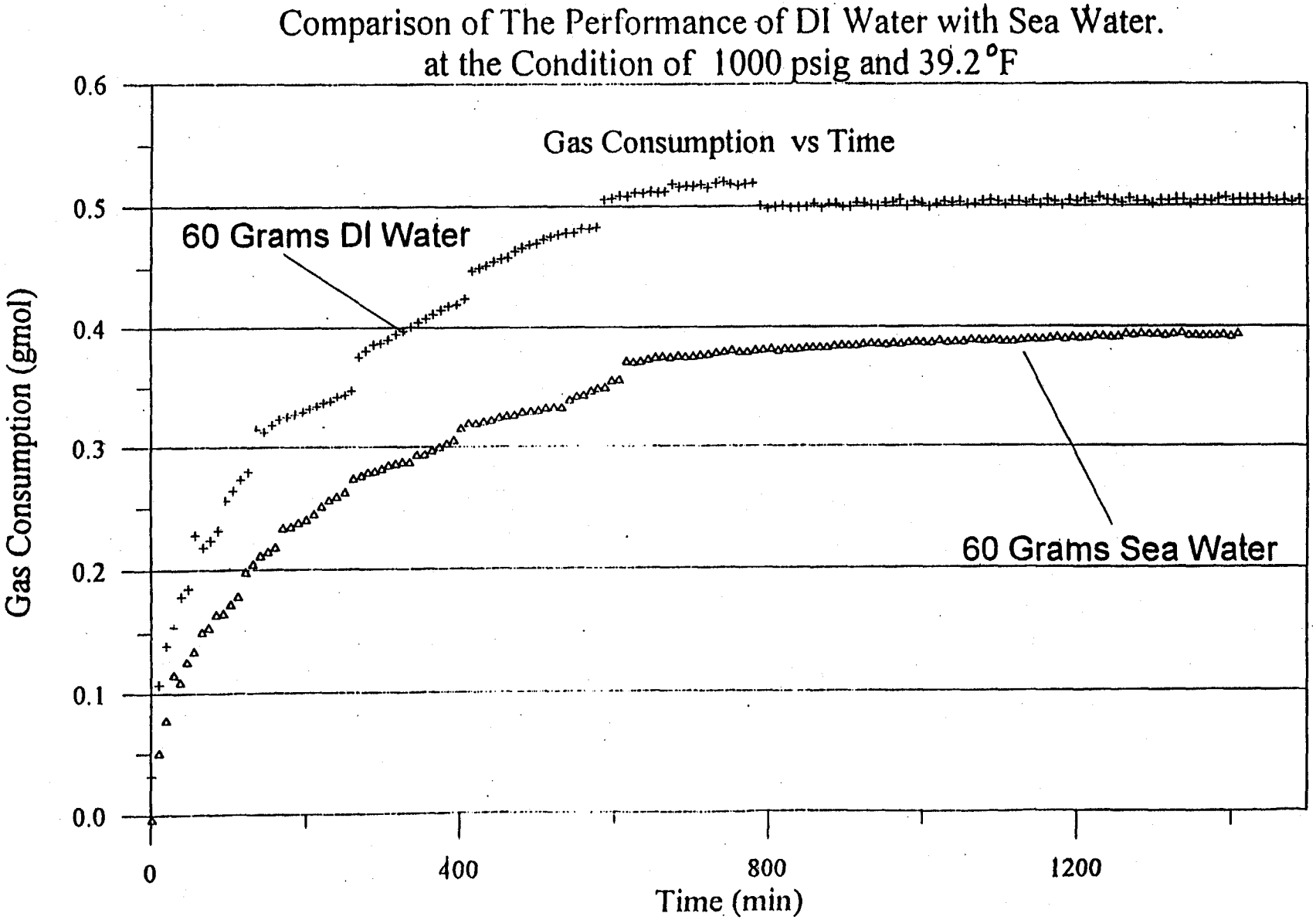

Figure 77.

The Solubilities of Green Canyon Gas in Pure MeOH and ETOH Are The Same at 1500 psig and 39.2 °F (120 grams Test Solution, 69 Balls)

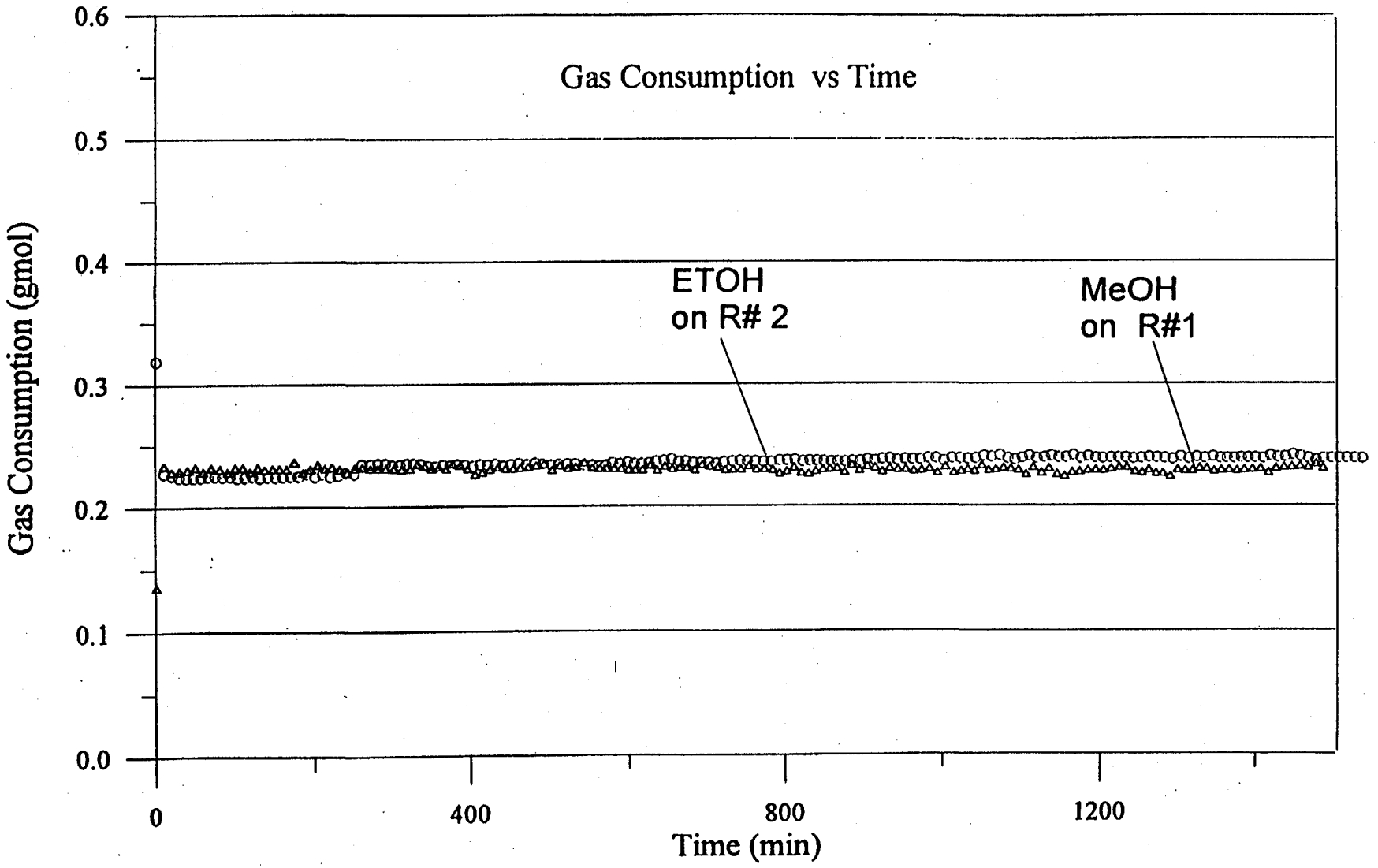

Figure 78.

When The Concentration of Polymer Is Increased,
The Gas Solubility in The Test Solution Is Slightly Increased.

Comparison of The Solubility of Different Concentration of Polymer
X wt%PVCAP(BASF4) + 30.0wt% Methanol in DI Water
(150 Grams Test Solution, at 1000 psig and 39.2°F)

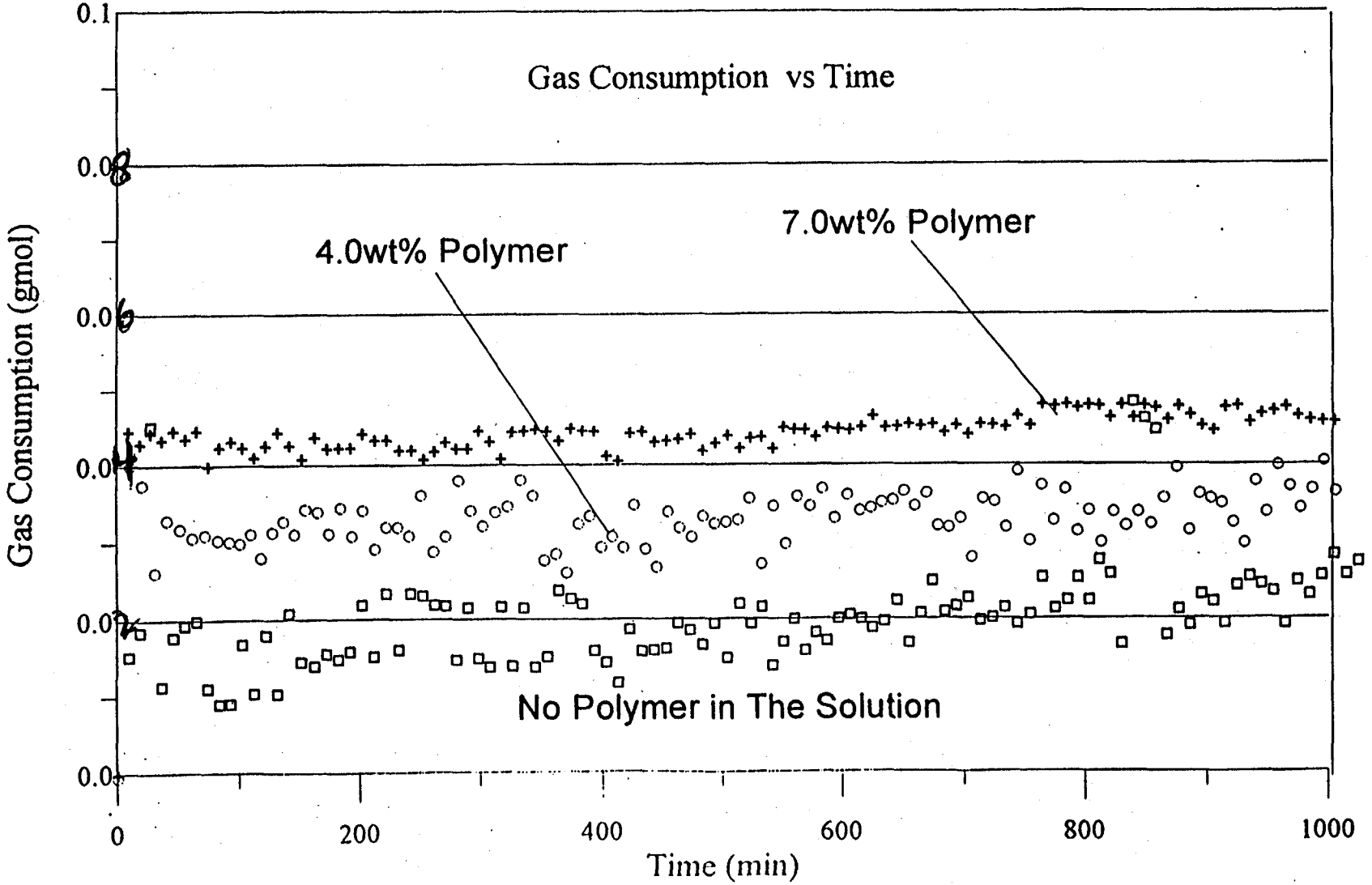

Figure 79.

When Pressure Is Increased from 1000 psig to 1500 psig,
The Gas Solubility in The Test Solution Is Slightly Increased.

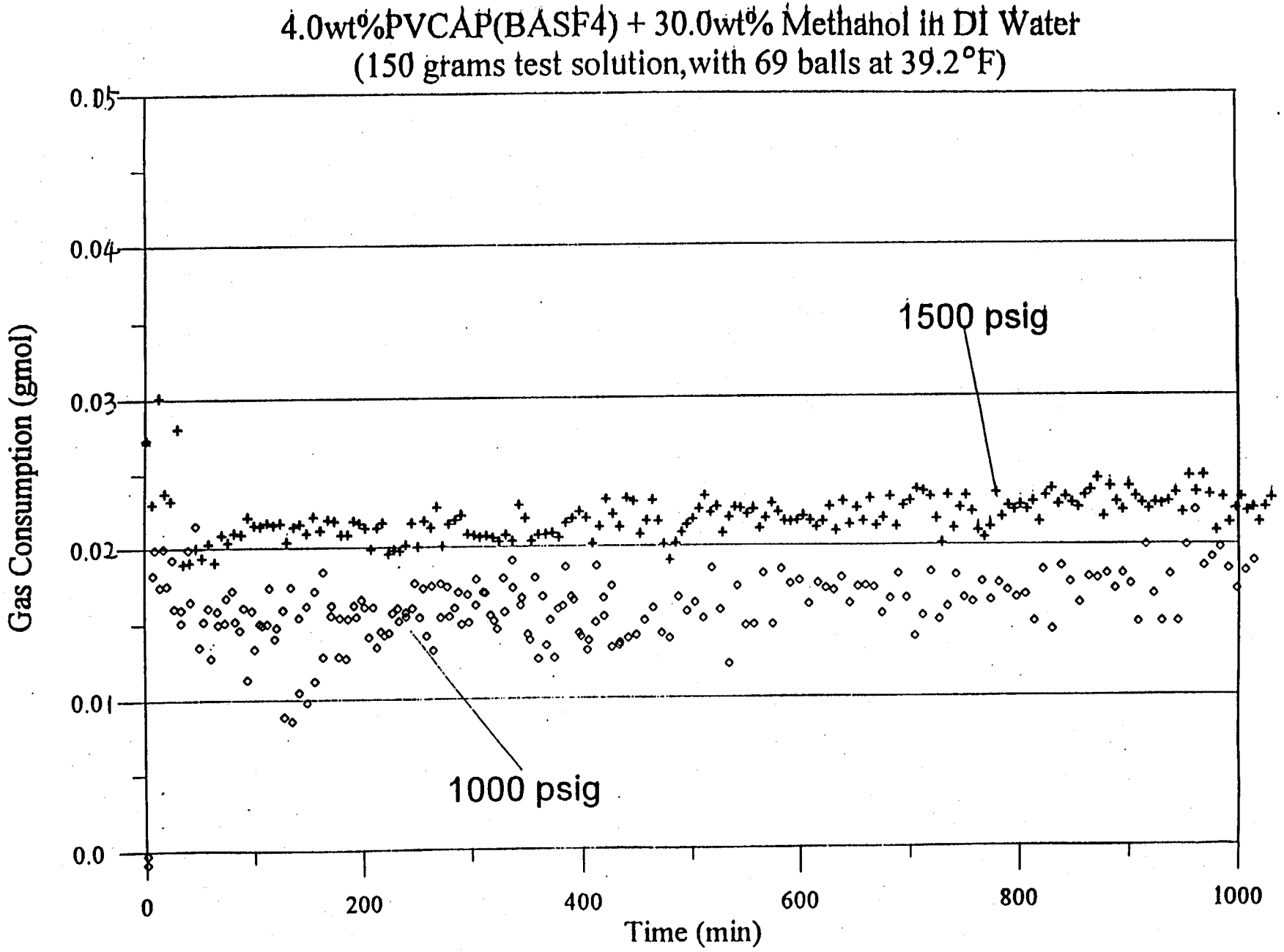

Figure 80.

Combining Different Salts with Polymer Provided Similar Hydrate Inhibition at The Conditions of 0.25 wt% PVCAP(BASF3) + 0.25wt% PVP(K-17) + 3.5wt% Salt + 2.0wt% MeOH, P = 1000 psig and T =39.2° F

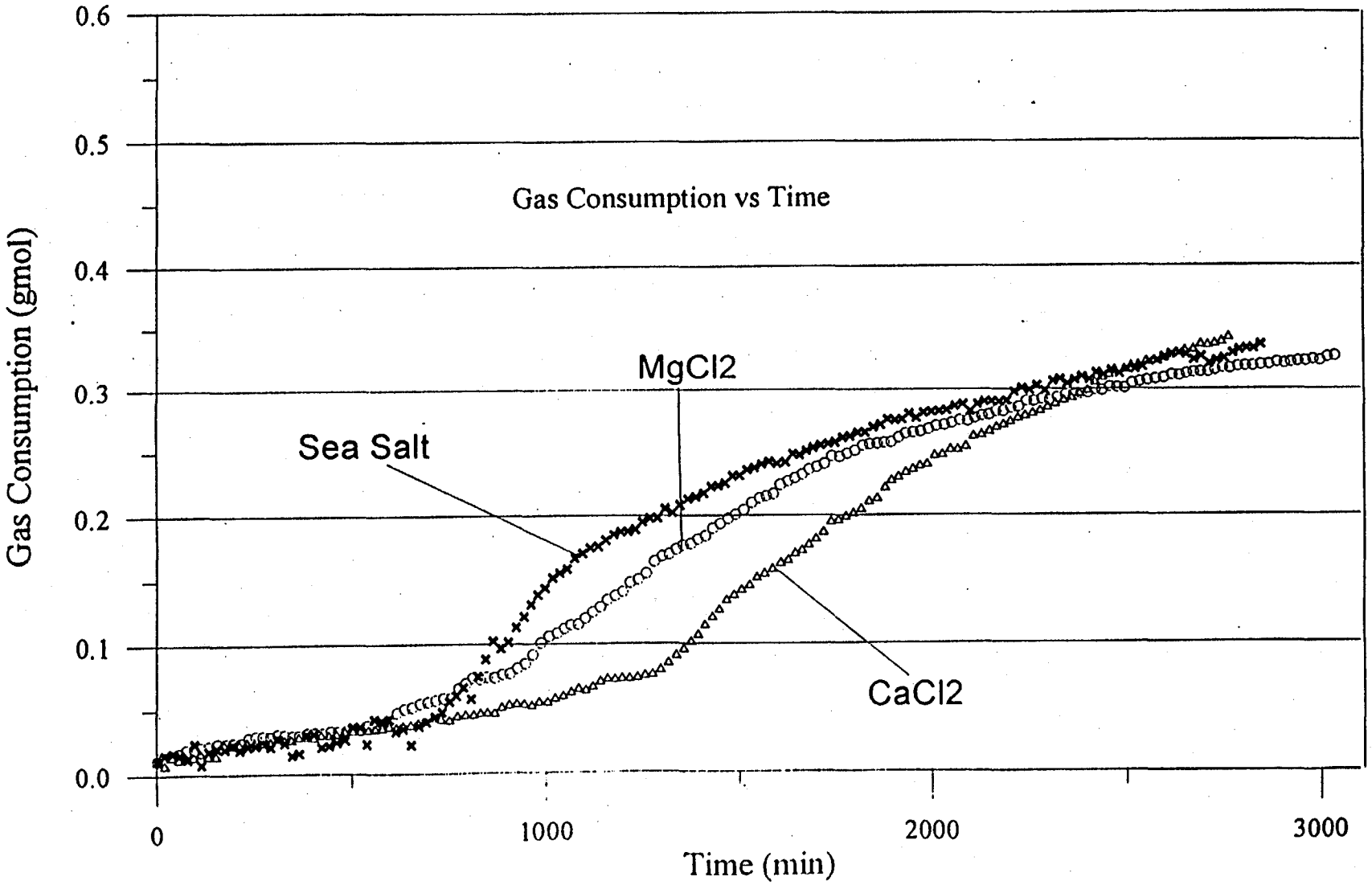

Filtering Apparatus

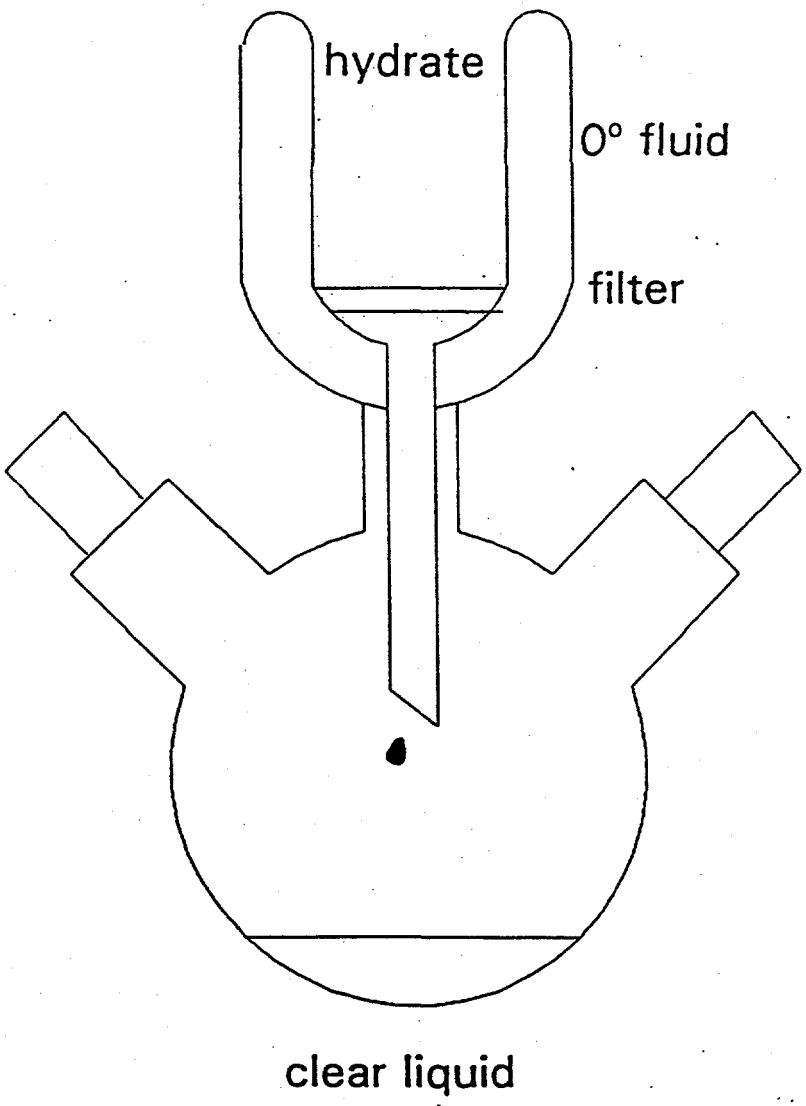

Figure 81. Hydrate filtering apparatus.

Figure 82.

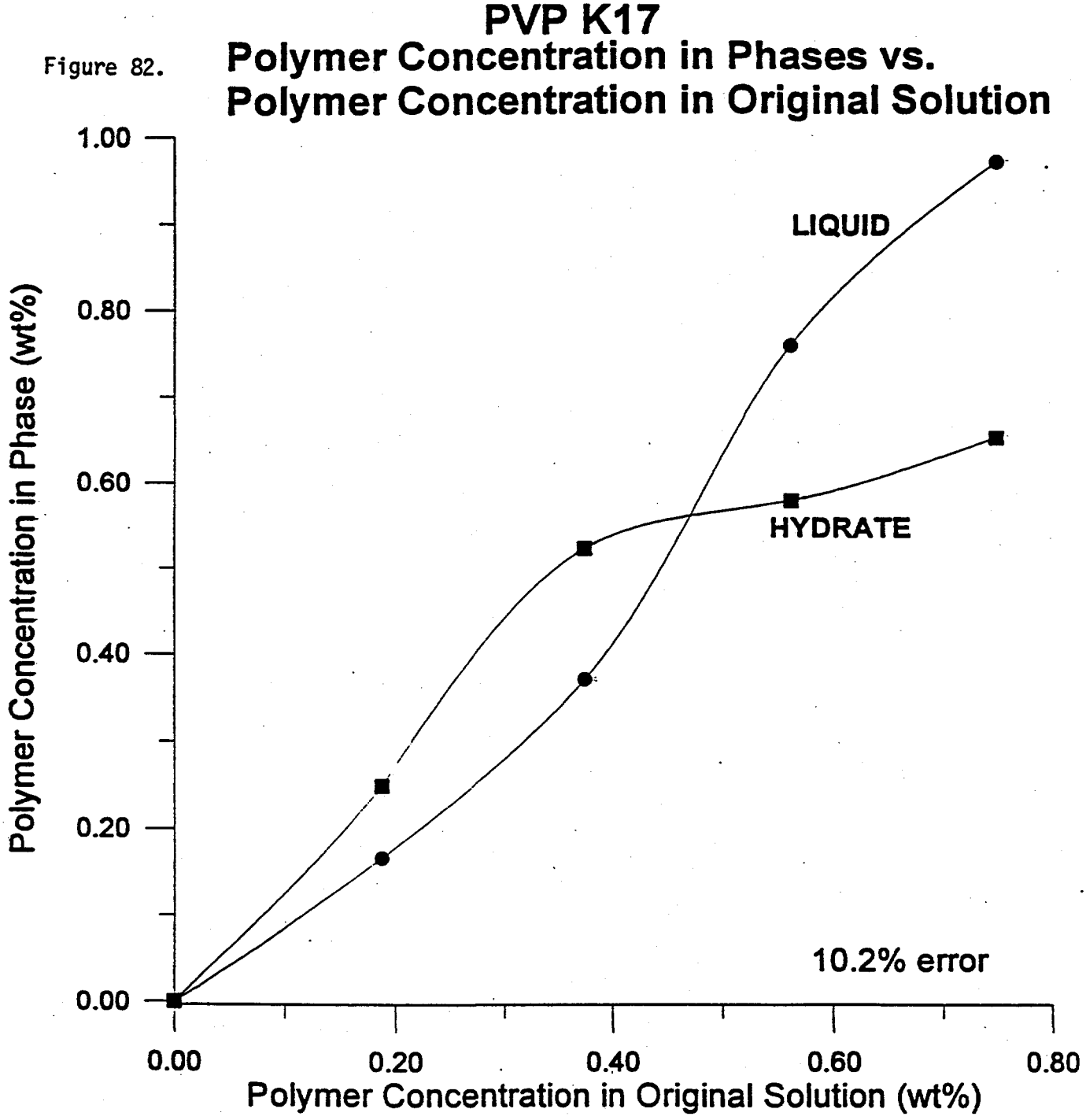
PVP K17
Polymer Concentration in Phases vs.
Polymer Concentration in Original Solution
1.00
0.80
0.60
0.40
0.20
0.00
Polymer Concentration in Phase (wt%)
LIQUID
HYDRATE
10.2% error
0.00
0.20
0.40
0.60
0.80
Polymer Concentration in Original Solution (wt%)

Figure 83.

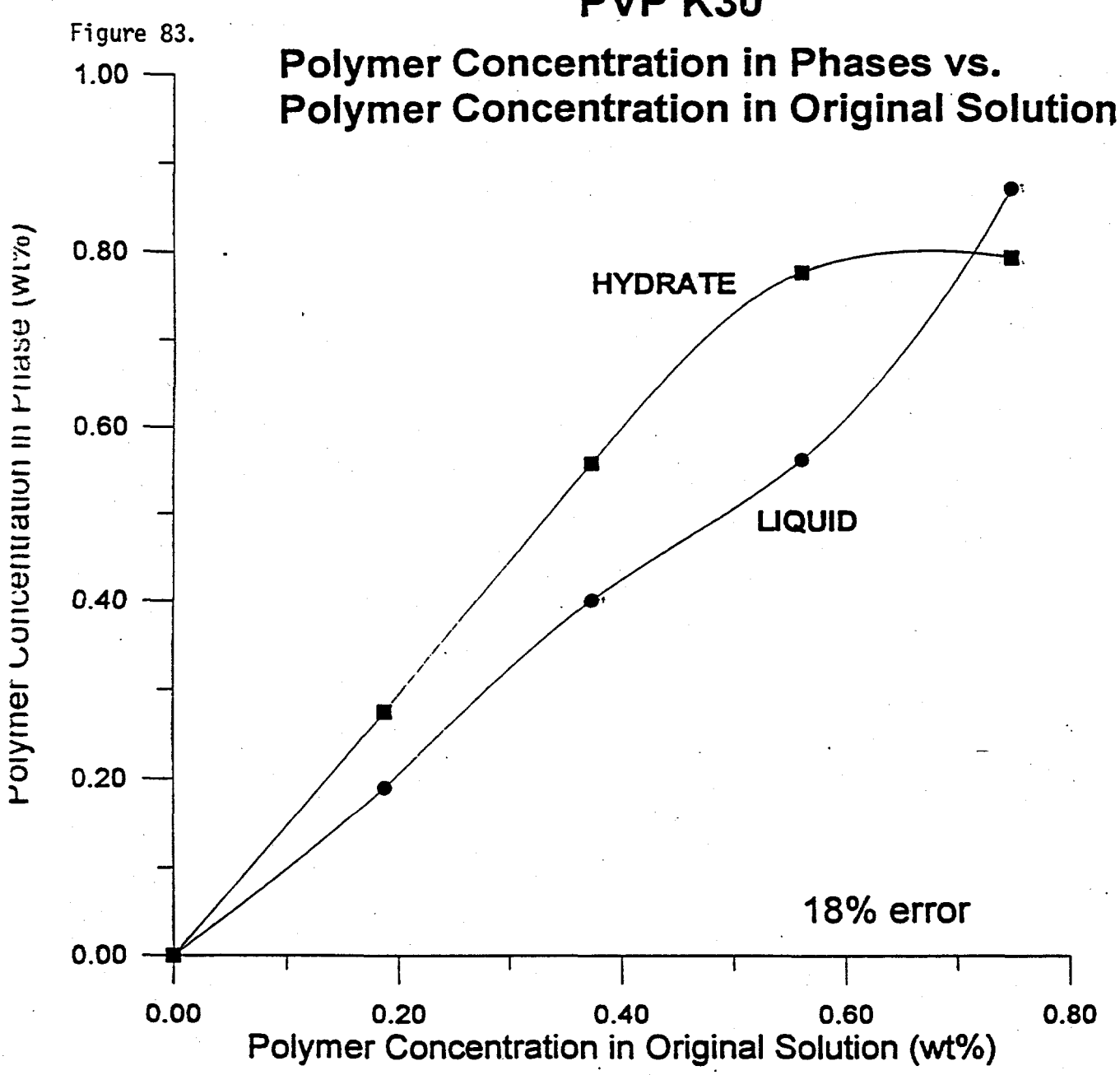
PVP K30
Polymer Concentration in Phases vs.
Polymer Concentration in Original Solution
Polymer Concentration in Phase (wt%)
1.00
0.80
0.60
0.40
0.20
0.00
HYDRATE
LIQUID
18% error
0.00
0.20
0.40
0.60
0.80
Polymer Concentration in Original Solution (wt%)

Figure 84.

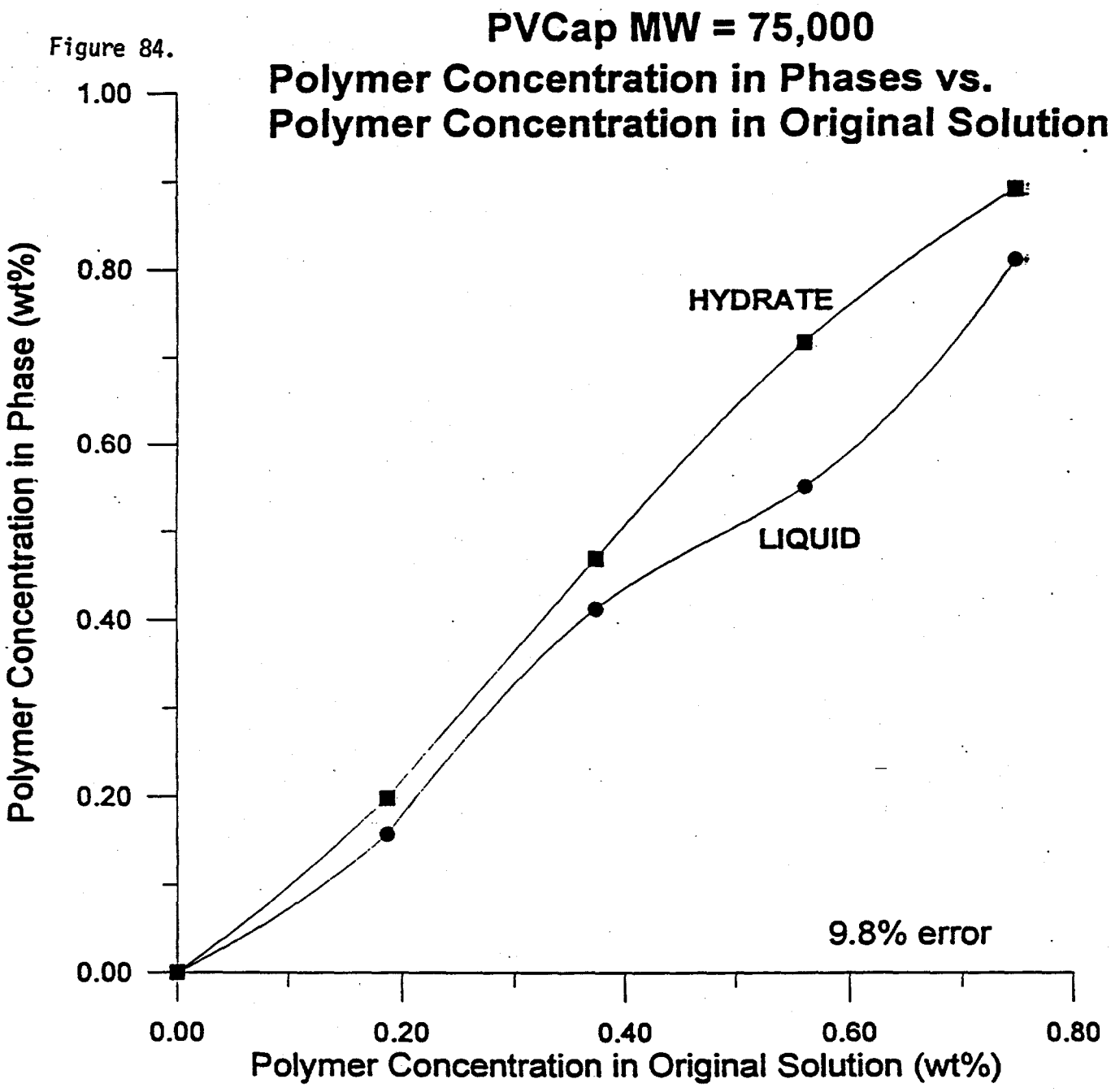
PVCap MW = 75,000
Polymer Concentration in Phases vs.
Polymer Concentration in Original Solution
Polymer Concentration in Phase (wt%)
1.00
0.80
0.60
0.40
0.20
0.00
HYDRATE
LIQUID
9.8% error
0.00
0.20
0.40
0.60
0.80
Polymer Concentration in Original Solution (wt%)

Figure 85.

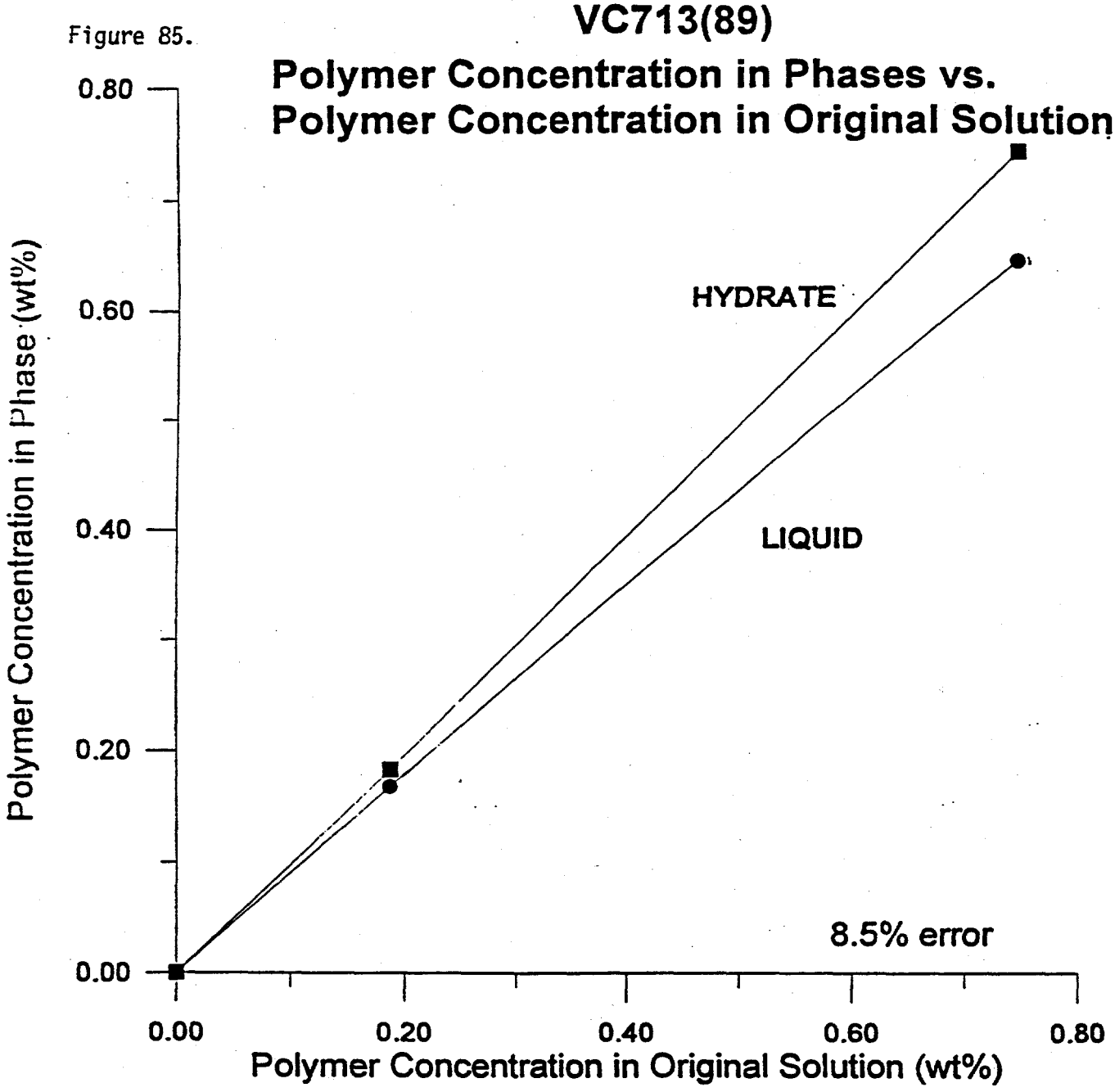
VC713(89)
Polymer Concentration in Phases vs.
Polymer Concentration in Original Solution
HYDRATE
LIQUID
8.5% error
Polymer Concentration in Phase (wt%)
0.00
0.20
0.40
0.60
0.80
Polymer Concentration in Original Solution (wt%)

Figure 86: FT-IR Spectrum of a blend of PVP-K90, PVCAP, and PMMA (std.) (1:1:1 molar).

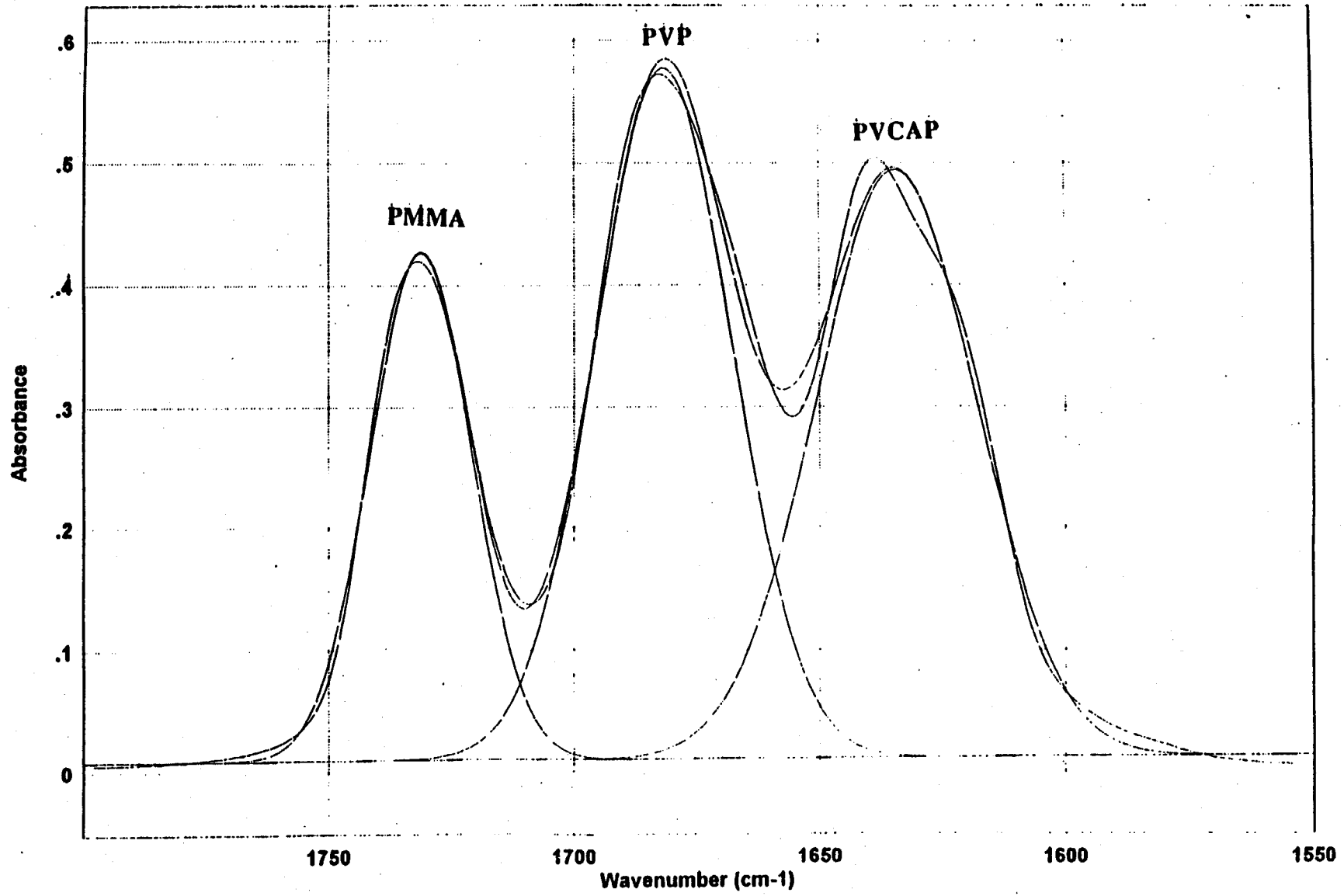

Figure 87: FT-IR Spectrum of PVP-K90/PVCAP in hydrate phase and PMMA std.

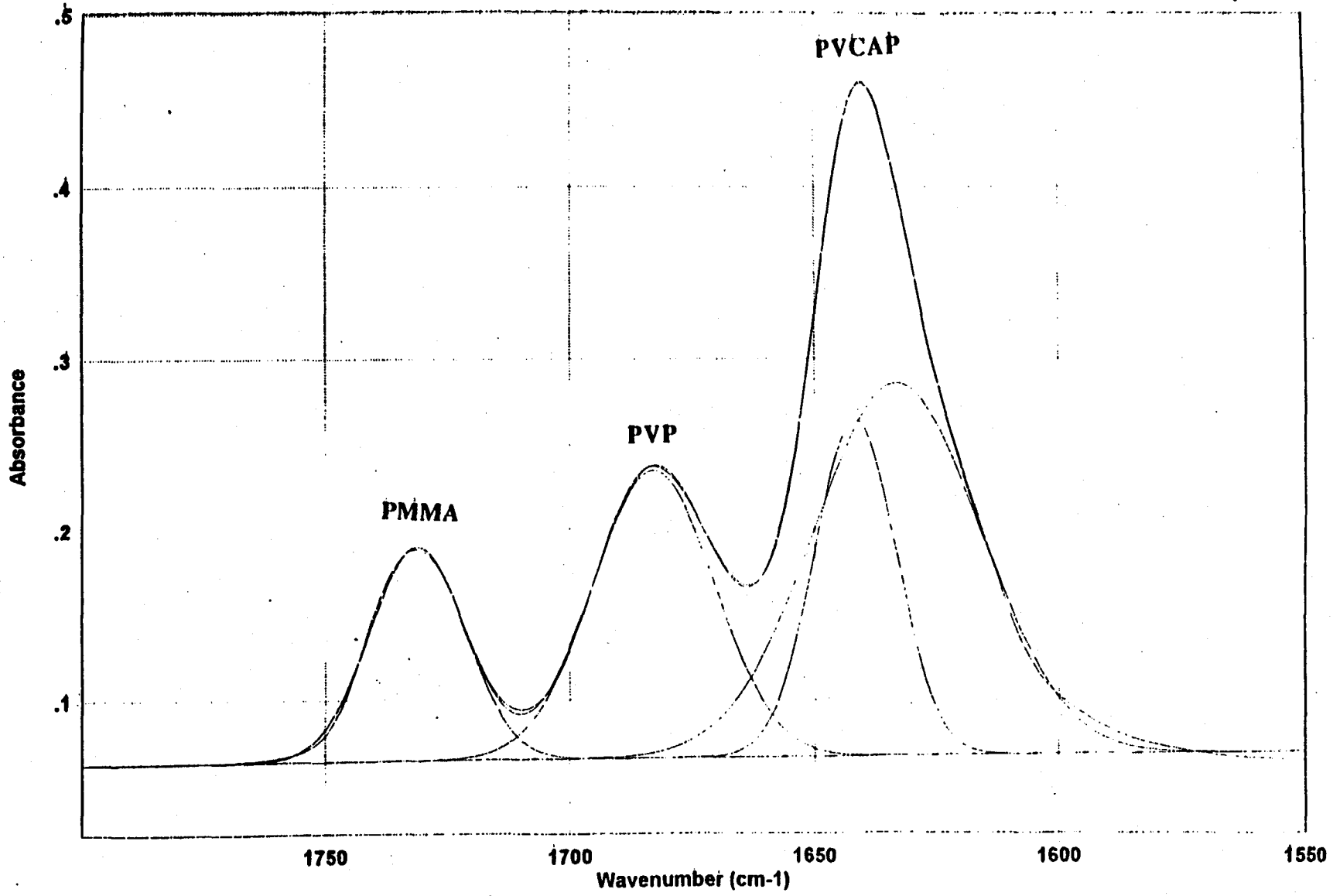

Figure 88: FT-IR Spectrum of PVP-K90/PVCAP in liquid phase and PMMA std.

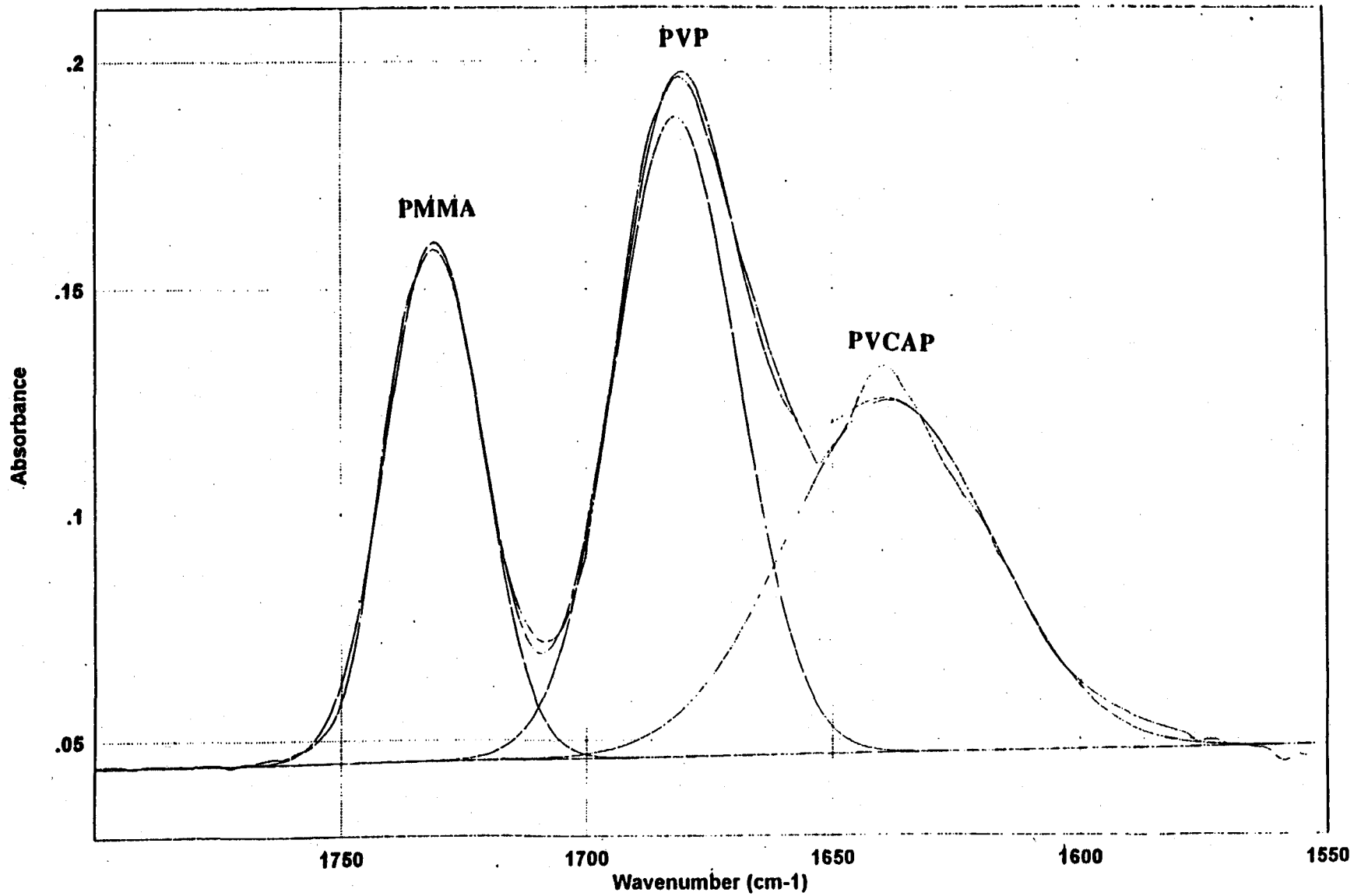

Figure 89.

PVP Polymer Series

Photon Corr. Spec. Data

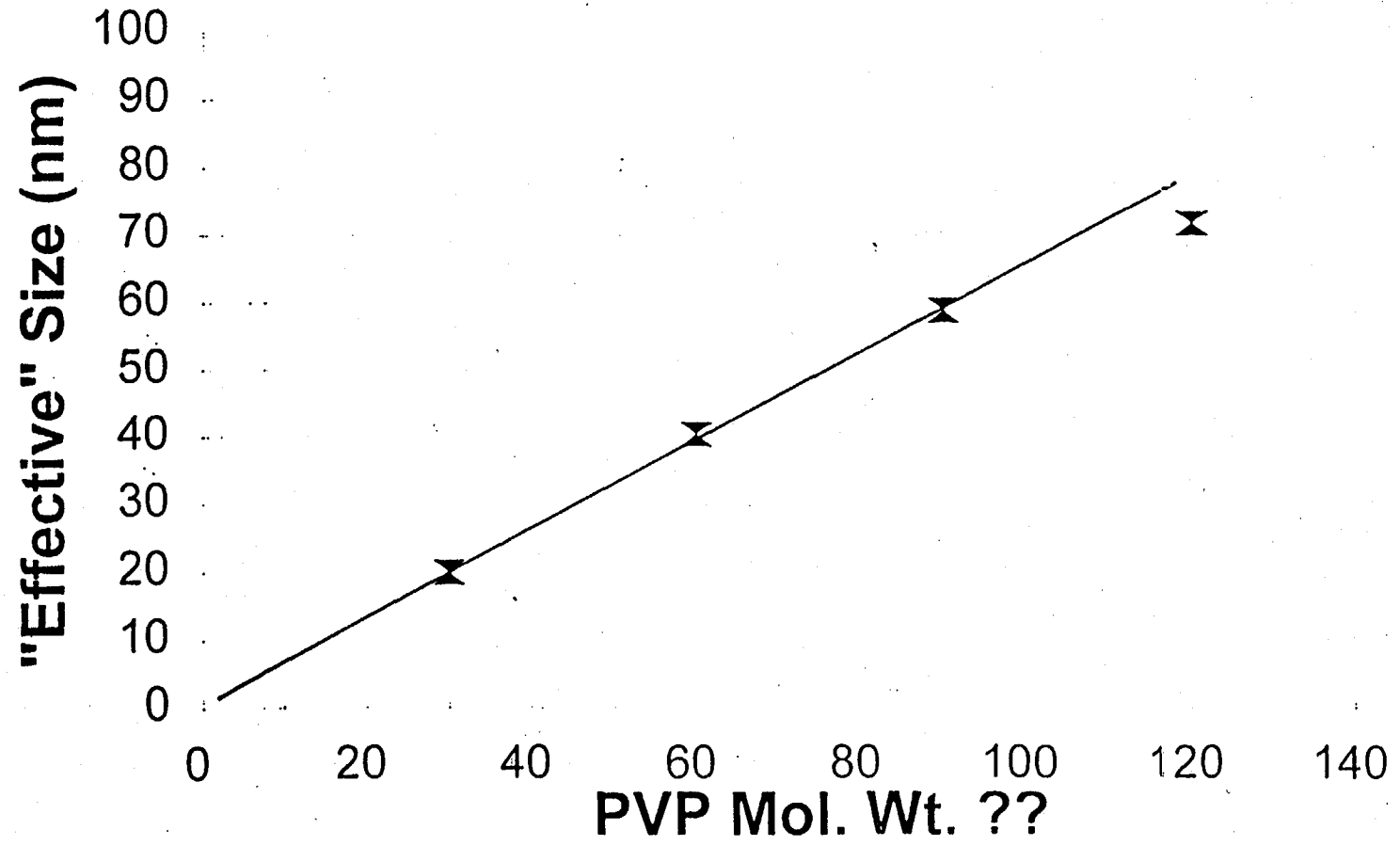

Figure 90.

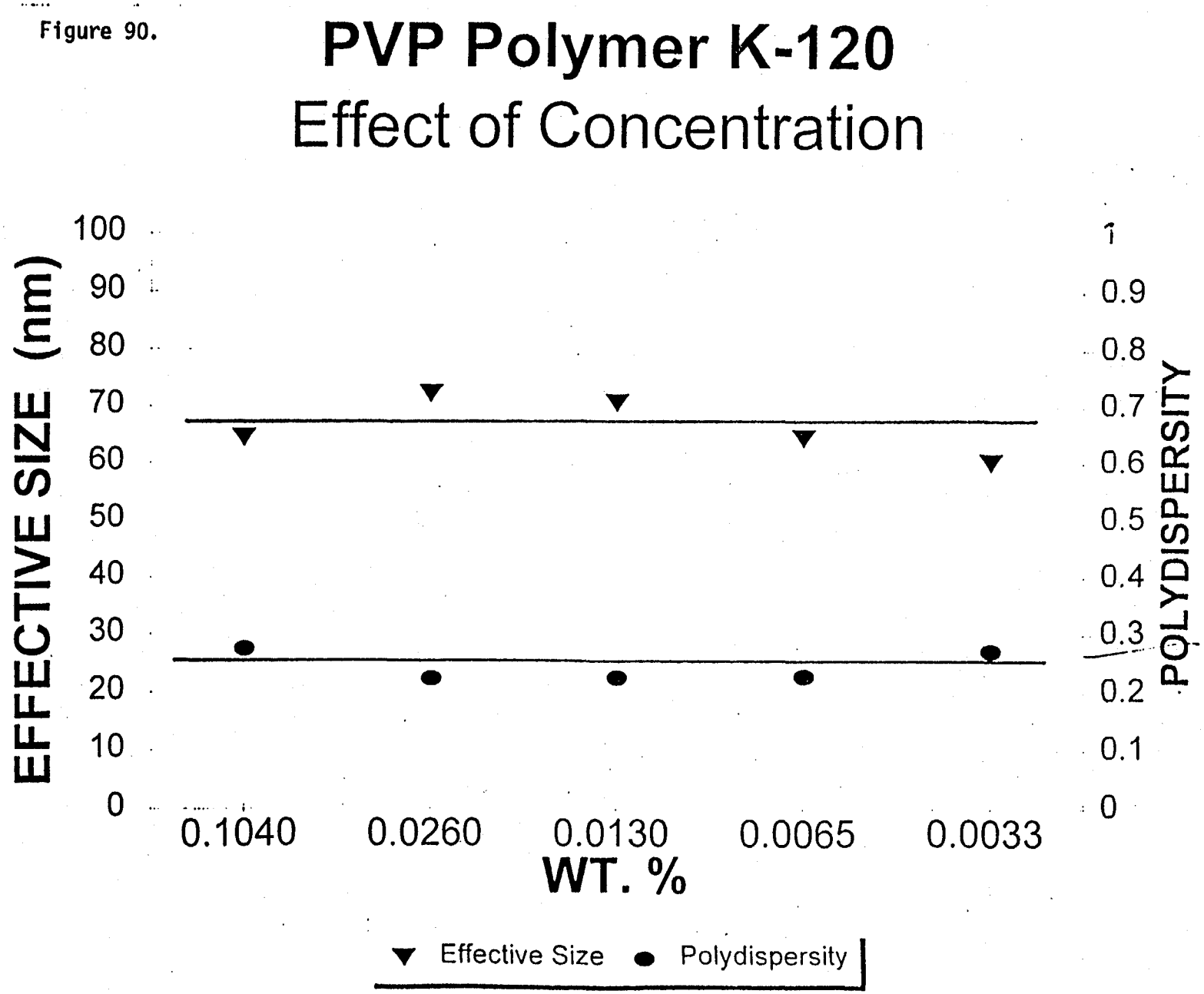
PVP Polymer K-120
Effect of Concentration
EFFECTIVE SIZE (nm)
100
90
80
70
60
50
40
30
20
10
0
1
0.9
0.8
0.7
0.6
0.5
0.4
0.3
0.2
0.1
0
POLYDISPERSITY
0.1040
0.0260
0.0130
0.0065
0.0033
WT. %
Effective Size
Polydispersity

Figure 91.

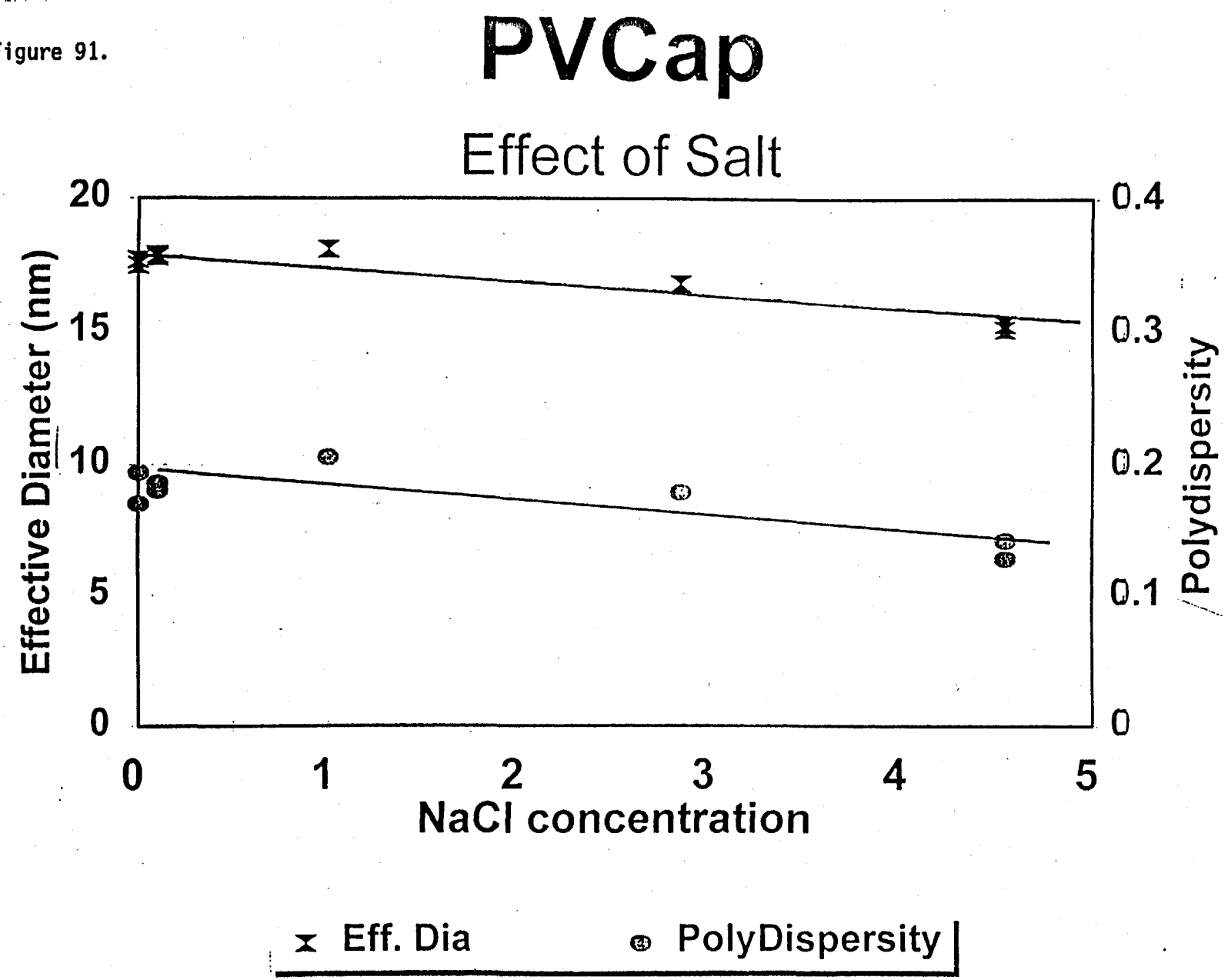
PVCap
Effect of Salt
Effective Diameter (nm)
Polydispersity
NaCl concentration
0
5
10
15
20
0
0.1
0.2
0.3
0.4
0
1
2
3
4
5
Eff. Dia
PolyDispersity

Figure 92.

VC-713 POLYMER

Effect of Salt on Effective Diameter

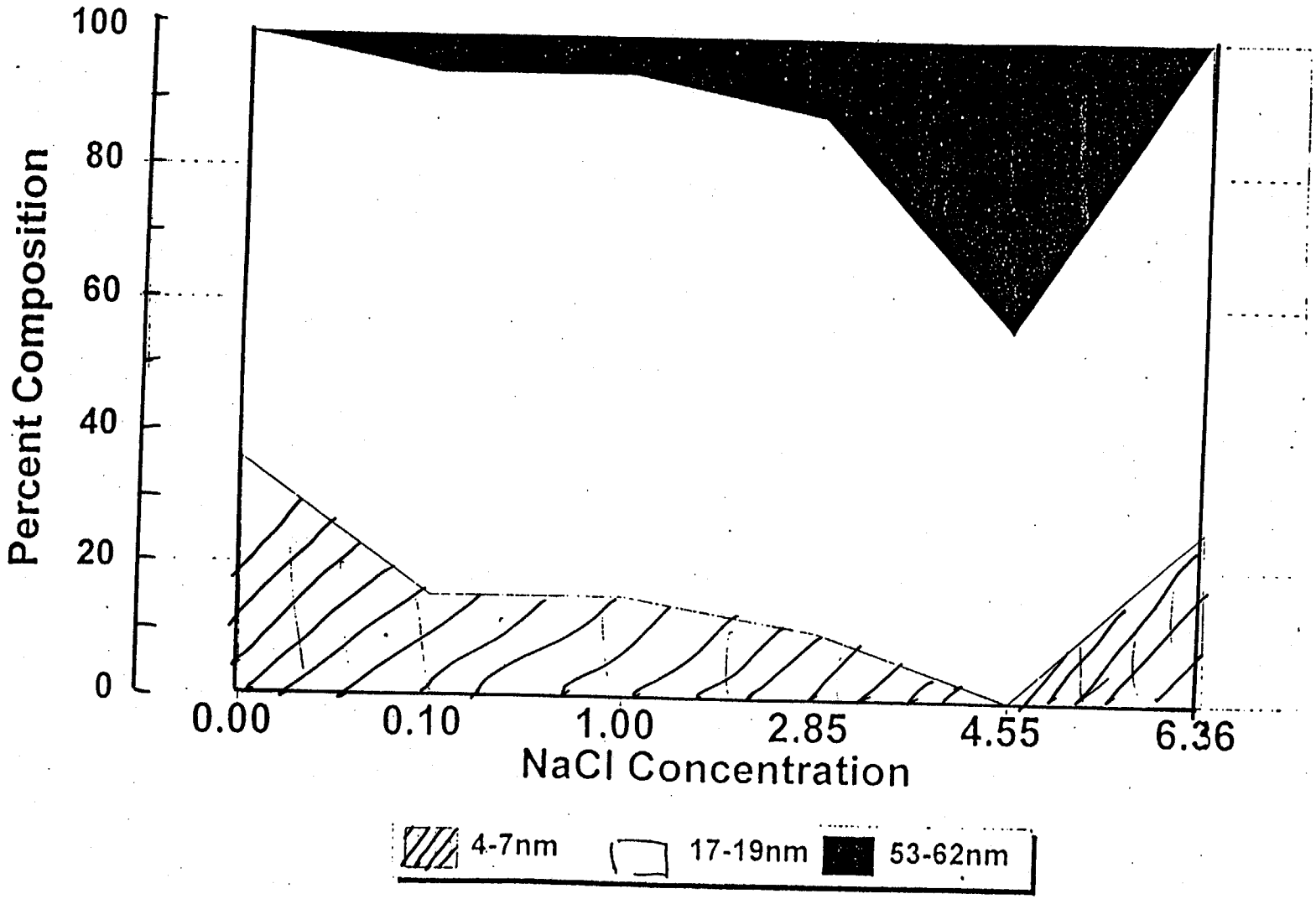

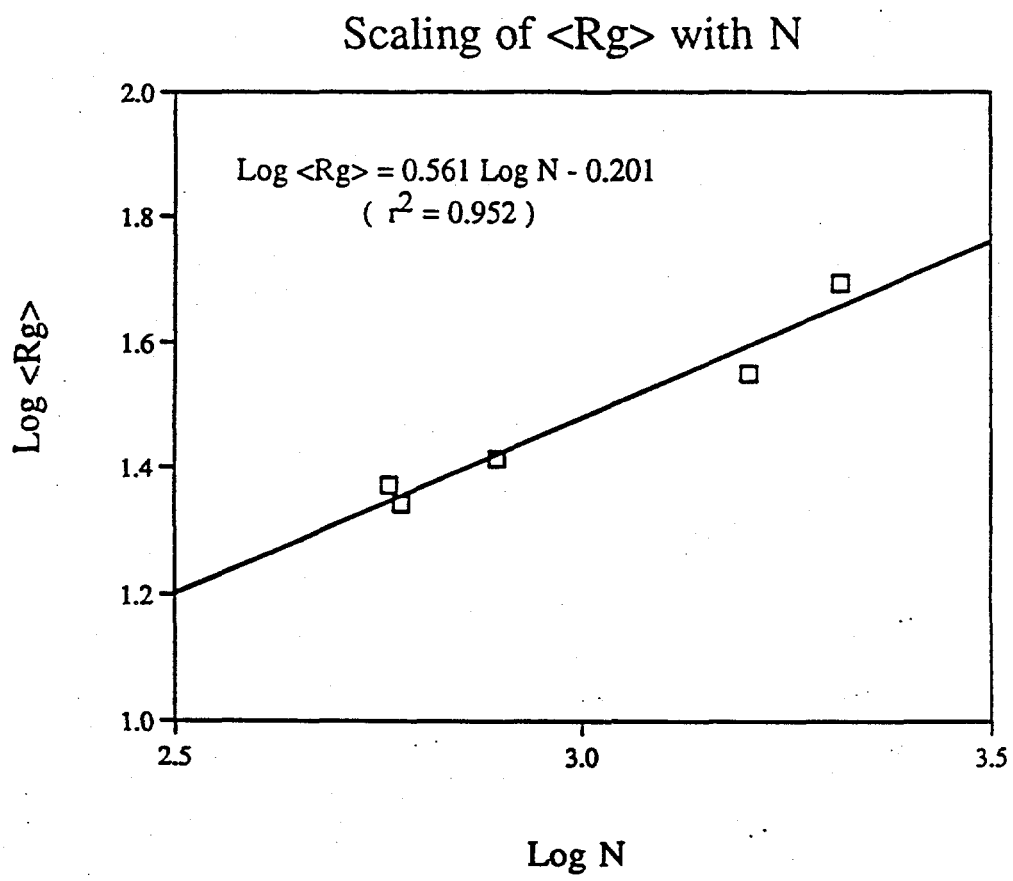

Figure 93. Low angle laser light scattering data for radius of gyration (size) to number of repeat units (molecular weight) for PVCAP.

Figure 94. **Comparison of the relative change in water structure by inhibitors (Kollmann forcefield)**

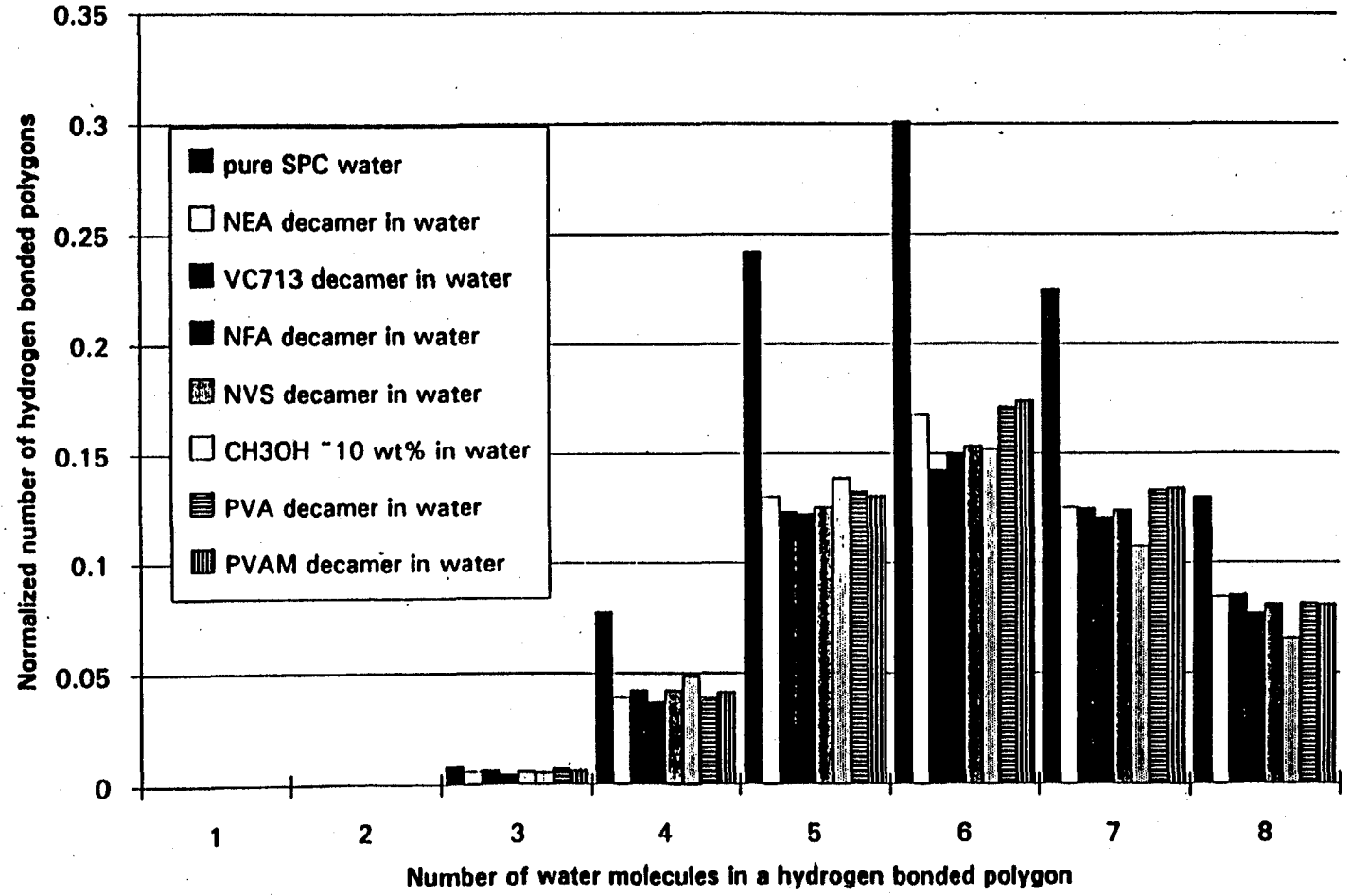

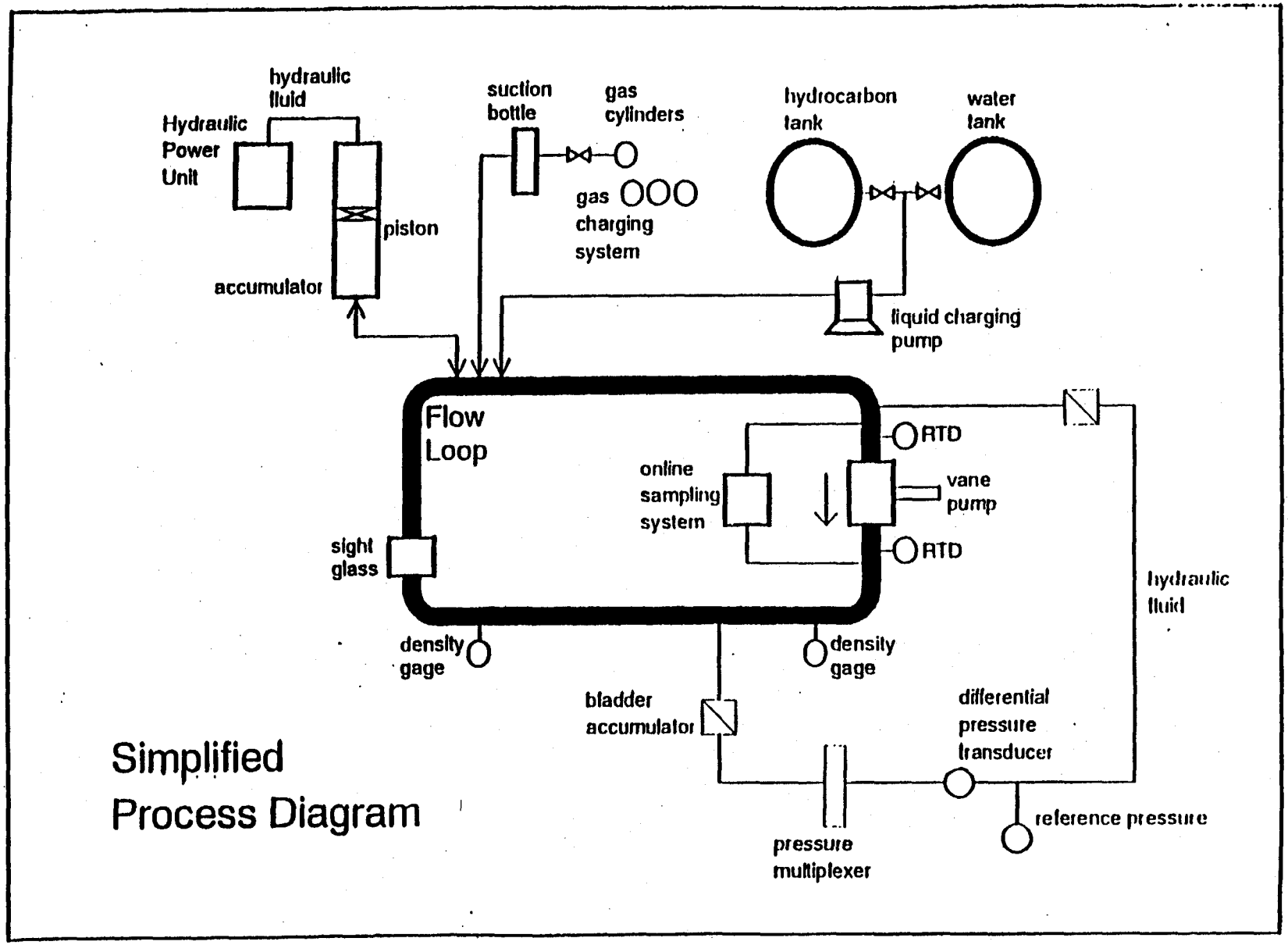

Figure 95. Schematic diagram of Exxon flow loop.

Figure 96.

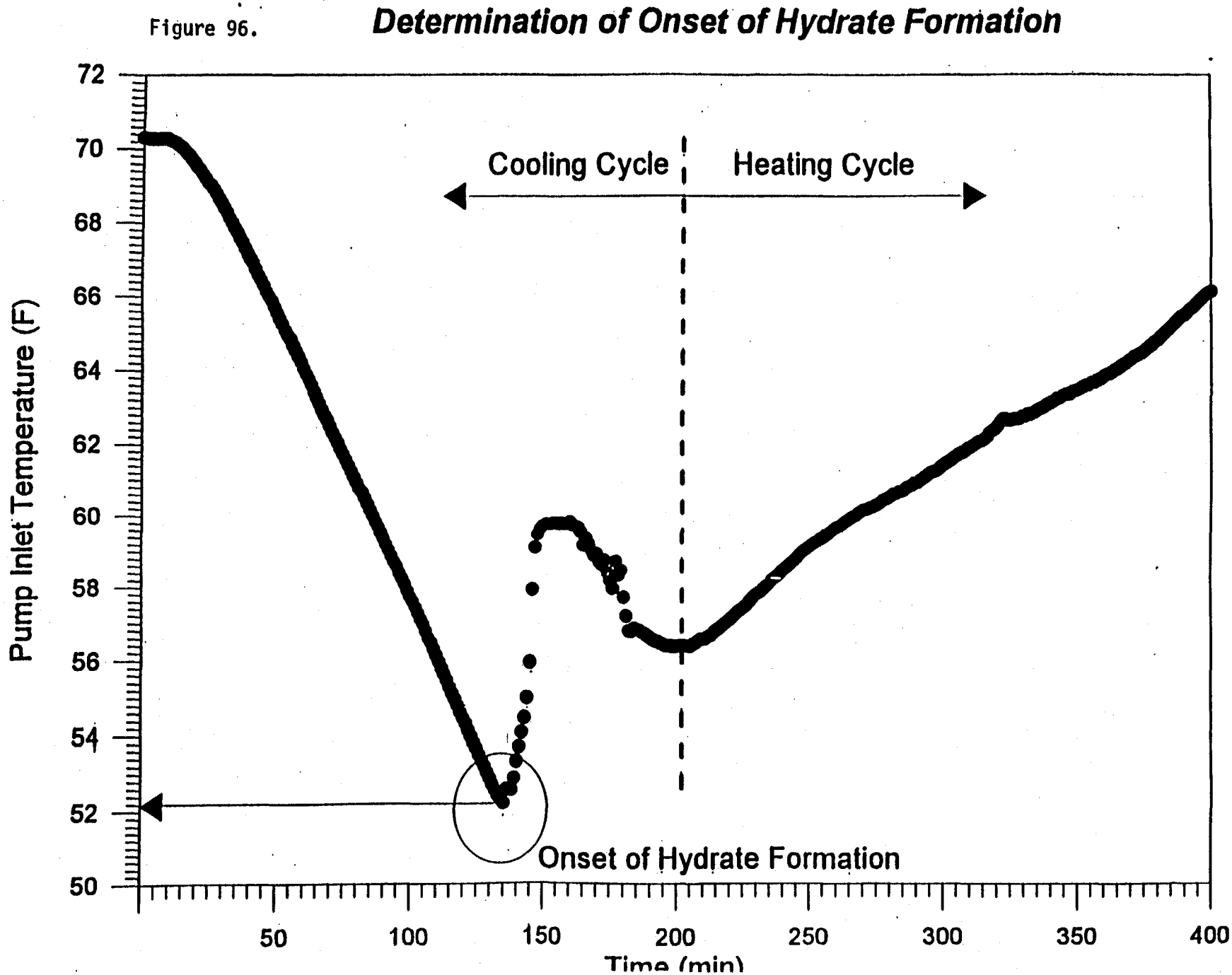
Determination of Onset of Hydrate Formation
Cooling Cycle
Heating Cycle
Onset of Hydrate Formation
Pump Inlet Temperature (F)
Time (min)
72
70
68
66
64
62
60
58
56
54
52
50
50
100
150
200
250
300
350
400

Figure 97. **Determination of Onset of Hydrate Formation**

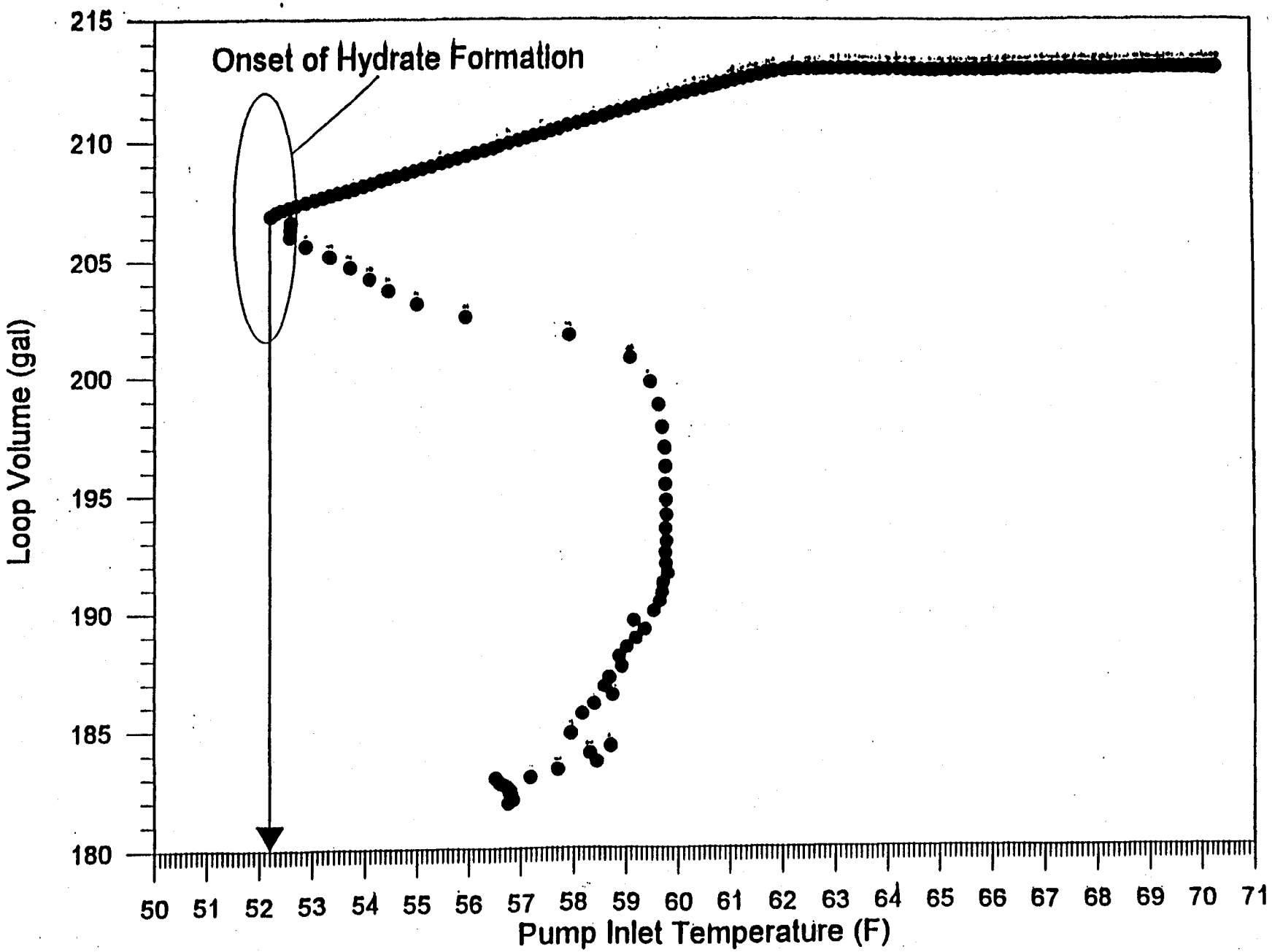

Figure 98. **Onset temperature is not a strong function of flow rate, but it is a strong function of PVCAP concentration**

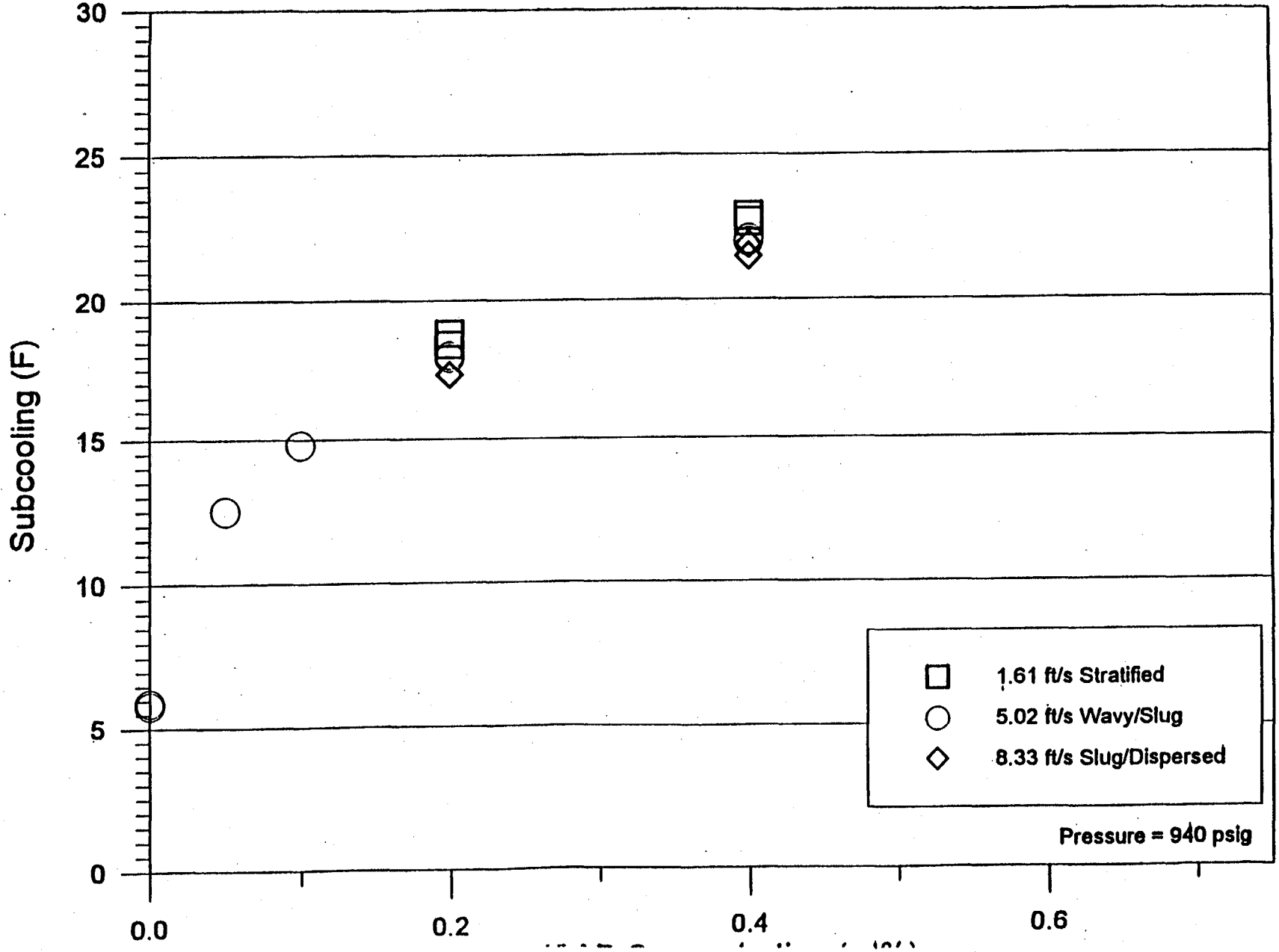

Figure 99. PVCAP and VC-713 have similar hydrate inhibition performance. Both inhibitors perform better than PVP.

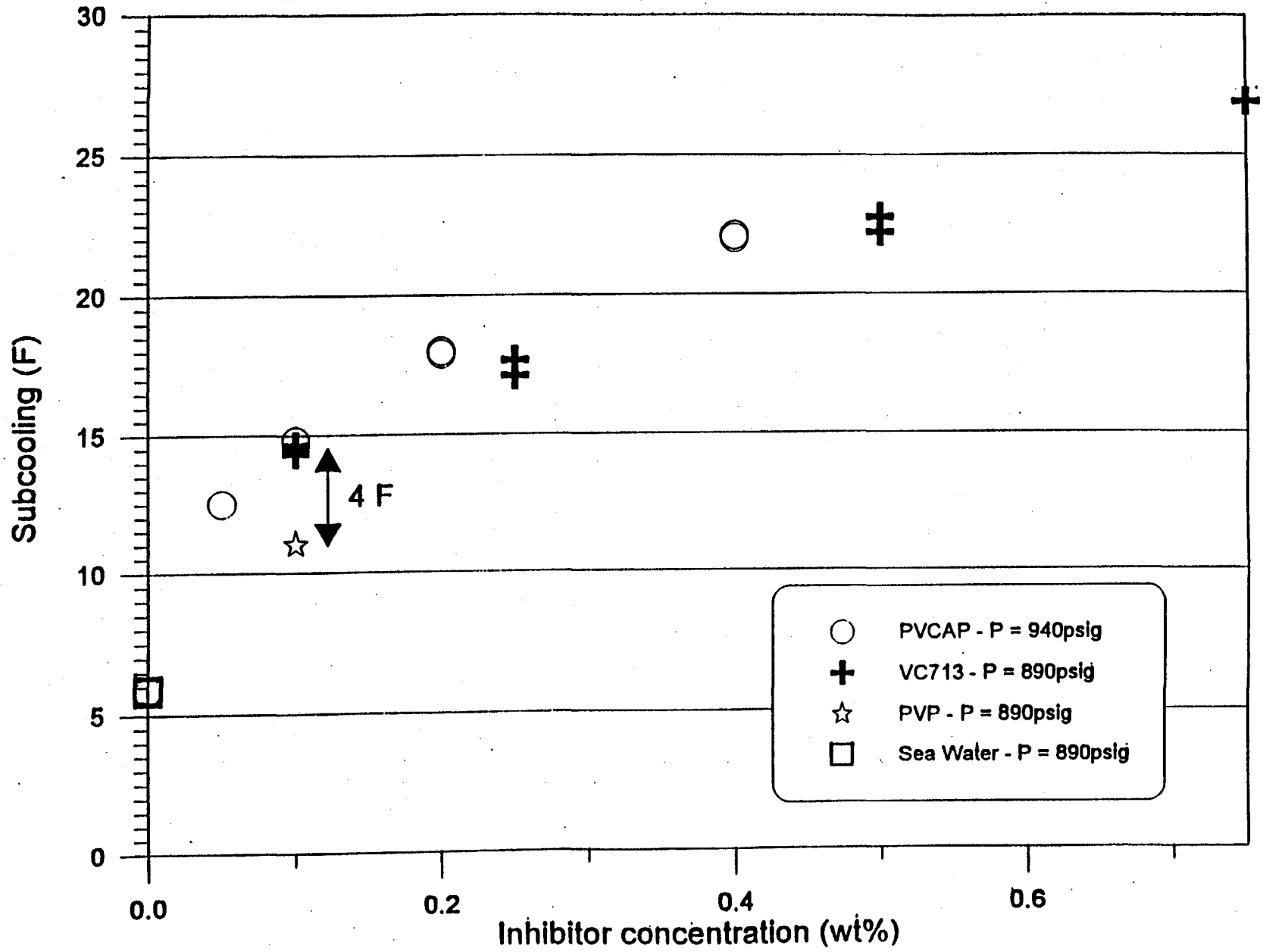

Figure 100.

HE-300 does not substantially increase the amount of subcooling observed over that for PVCAP.

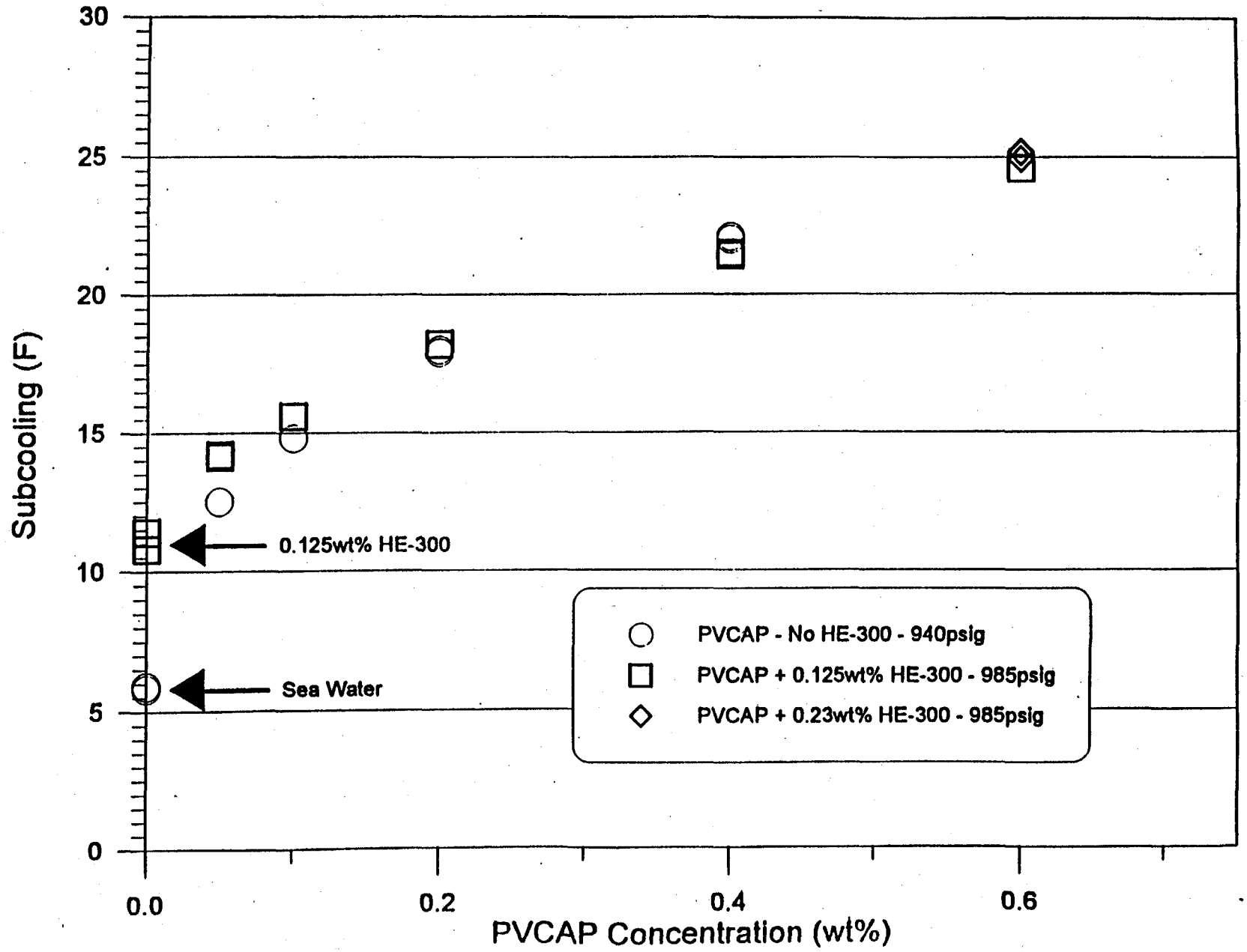

Figure 101. **Increasing the PVCAP concentration results in lower gas consumption.**

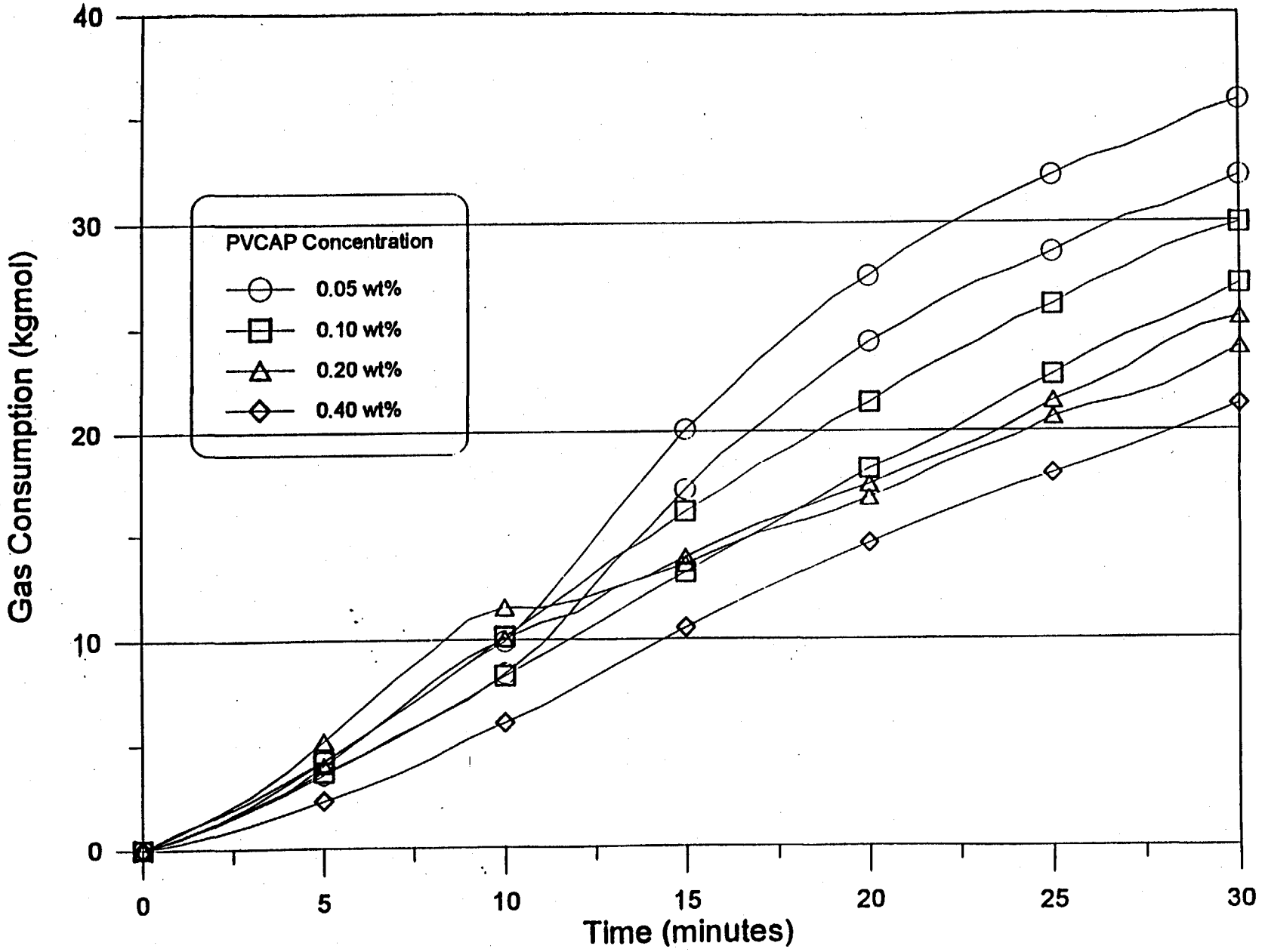

Figure 102. **0.125wt% HE-300 + 0.4wt% PVCAP Dramatically Lowers the Consumption Over PVCAP Alone - Effects are Nonlinear**

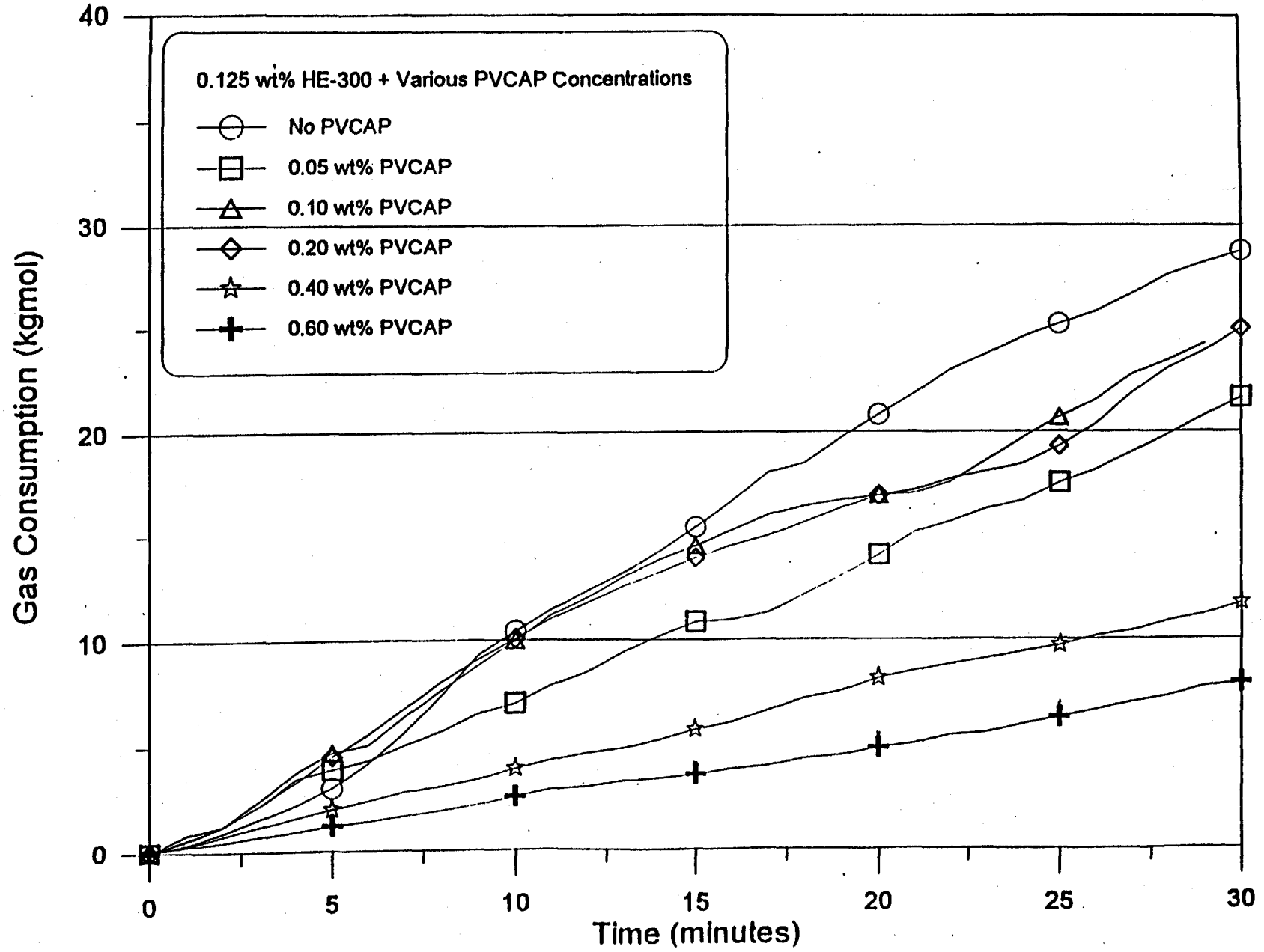

Fig. 103 Consortium Pipeline Tests and the Likelihood for Hydrate Formation.

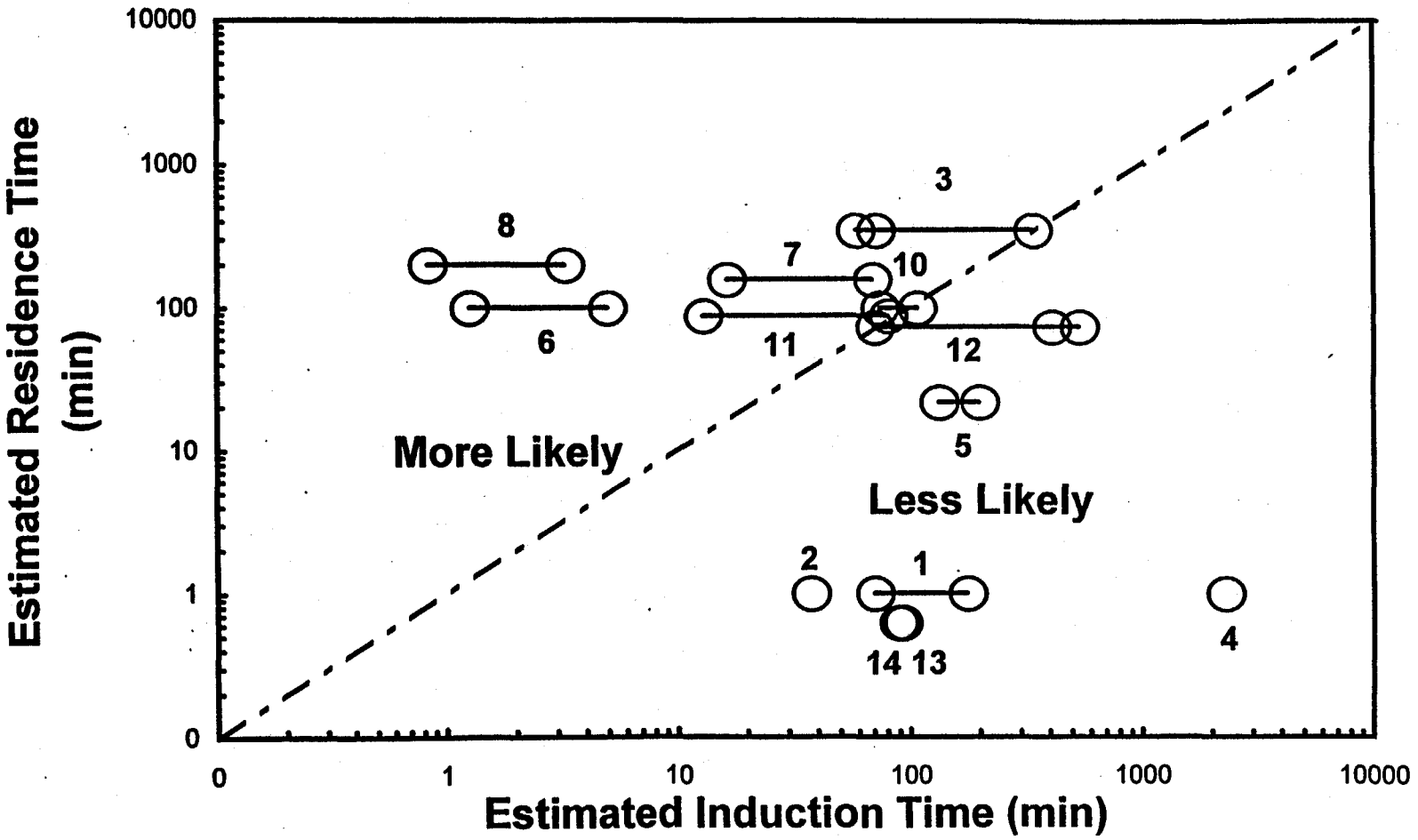

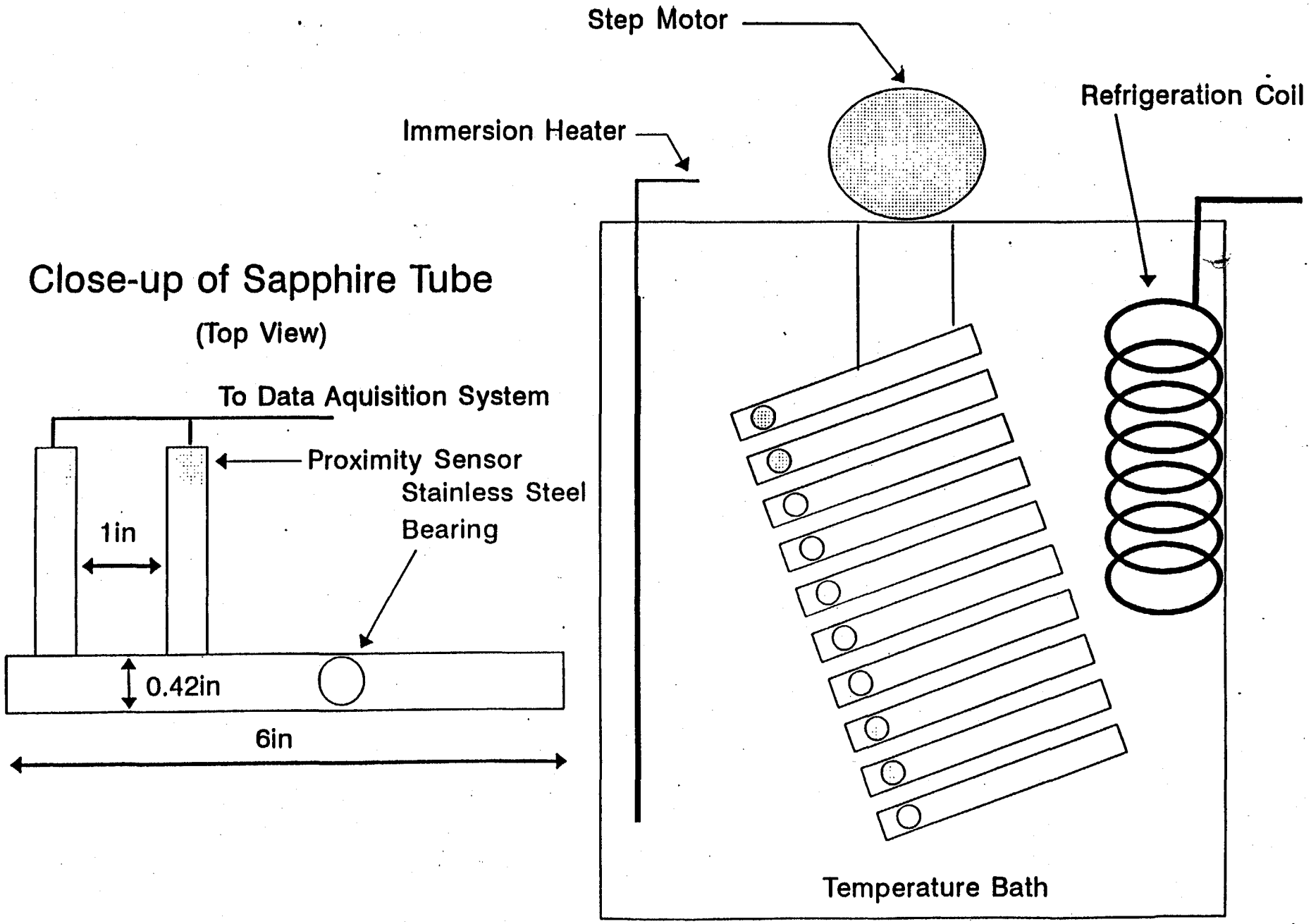

Figure 104. Schematic diagram of the sapphire screening apparatus.

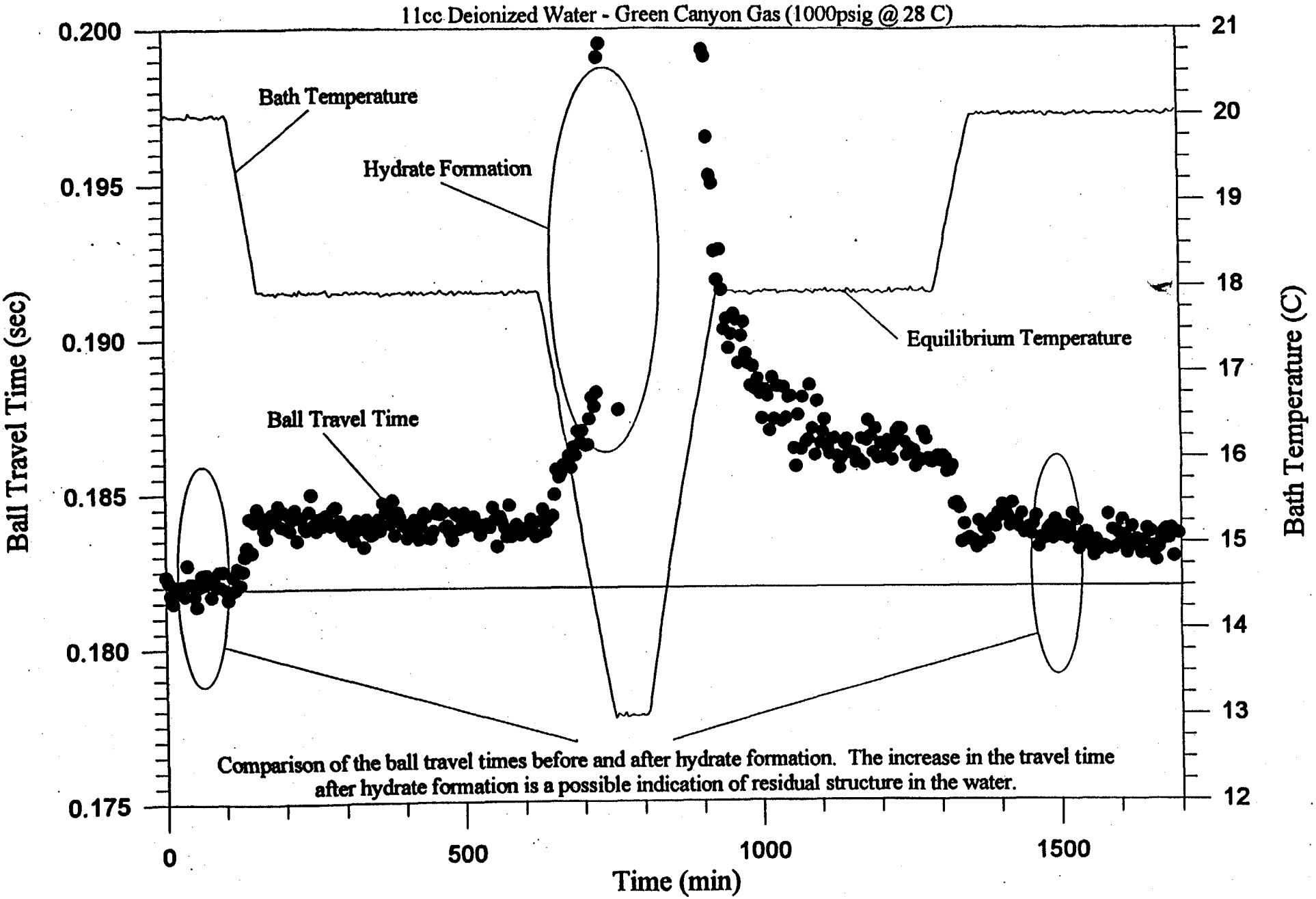

Figure 105. It may be possible to detect residual structure in the water after dissociating the hydrate.

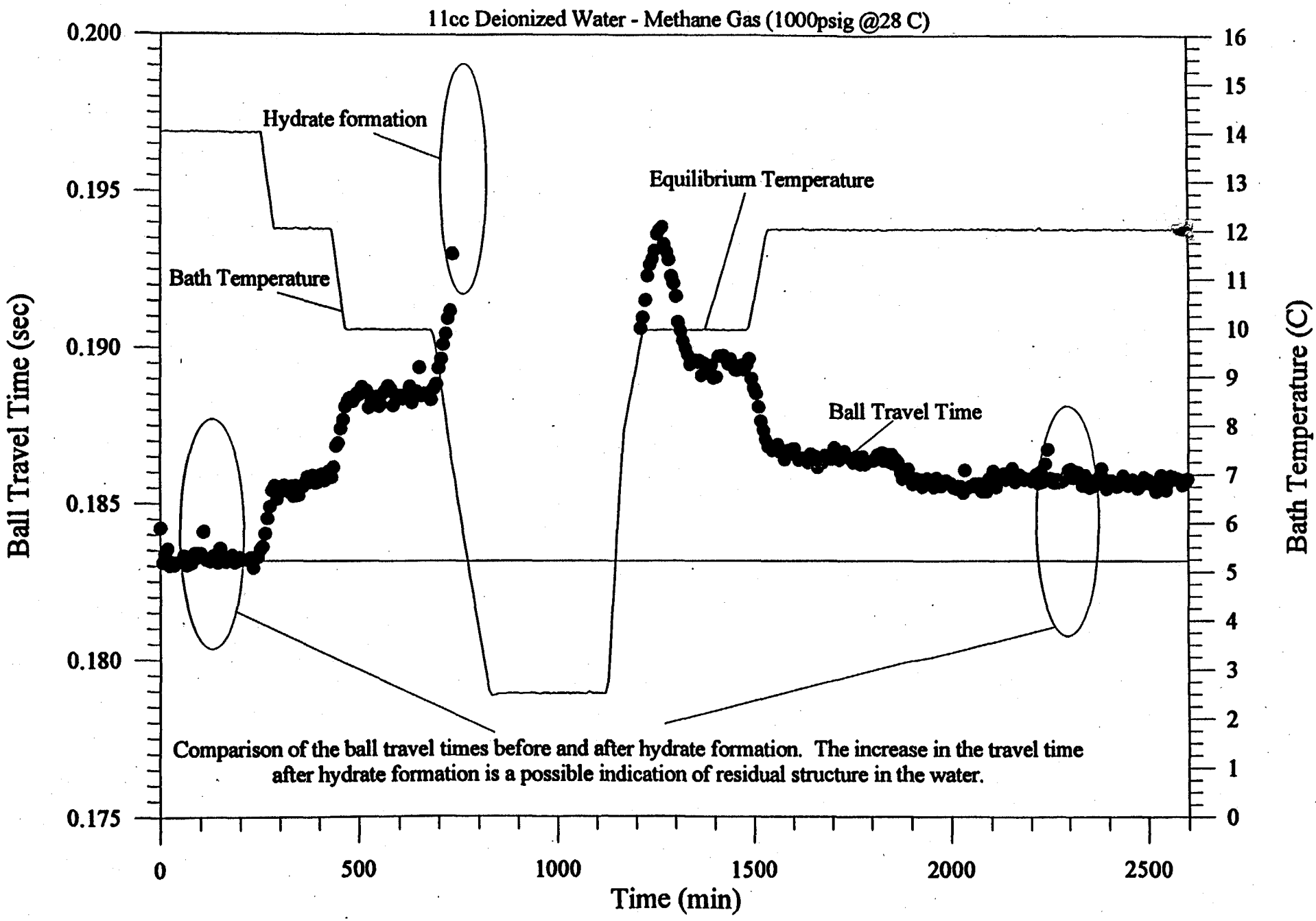
11cc Deionized Water - Methane Gas (1000psig @28 C)
Hydrate formation
Equilibrium Temperature
Bath Temperature
Ball Travel Time
Comparison of the ball travel times before and after hydrate formation. The increase in the travel time after hydrate formation is a possible indication of residual structure in the water.
Ball Travel Time (sec)
Bath Temperature (C)
Time (min)
0.200
0.195
0.190
0.185
0.180
0.175
16
15
14
13
12
11
10
9
8
7
6
5
4
3
2
1
0
0
500
1000
1500
2000
2500